

AD-A256 435



①

AFIT/GE/ENG/92J-04

**DEVELOPMENT OF AN ANALOG MIMO
QUANTITATIVE FEEDBACK THEORY (QFT)
CAD PACKAGE**

THESIS

Richard Robert Sating

AFIT/GE/ENG/92J-04

DTIC
ELECTE
OCT 27 1992
E D

Approved for public release; distribution unlimited

92-28138



92 10 1 1 1

AFIT GE ENG/92J-04

**DEVELOPMENT OF AN ANALOG
MIMO QUANTITATIVE FEEDBACK
THEORY (QFT) CAD PACKAGE**

THESIS

Presented to the Faculty of the School of Engineering
of the Air Force Institute of Technology

Air University

In Partial Fulfillment of the
Requirements for the Degree of
Master of Science in Electrical Engineering

Richard Robert Sating, B.S.E.E.

June, 1992

Available For	
1. <input checked="" type="checkbox"/> DTIC	<input checked="" type="checkbox"/>
2. <input type="checkbox"/> NTIS	<input type="checkbox"/>
3. <input type="checkbox"/> GPO	<input type="checkbox"/>
4. <input type="checkbox"/> Other	<input type="checkbox"/>
Availability Codes	
Dist	Availability or Special
A-1	

DTIC QUALITY INSPECTED 2

Approved for public release; distribution unlimited

Preface

The purpose of this thesis was to develop a CAD package to automate the development of multivariable controllers based on the Quantitative Feedback Theory design technique developed by Dr. Horowitz. During this thesis effort, I had the opportunity to gain experience in a newly emerging field of control theory while having the opportunity to develop a unique software package. Work performed using the CAD package has suggested that it will substantially reduce the difficulty and time required to design a QFT controller.

My sincere thanks go to my advisor Dr. Constantine Houpis for his advice, time, and tireless effort throughout my thesis effort and also to Dr. Horowitz and Dr. Lamont for their guidance and insight they provided while on my committee. I would also like to give special thanks to Capt. Jeff Bradley for putting my QFT CAD package to the test on his thesis project. The software could never have reached its present stage in the development process without knowledge gained through Capt. Bradley's work. Finally, I would like to thank my fellow classmates for their support and wish them the best of luck in their careers.

Richard Robert Sating

Table of Contents

Preface	ii
List of Symbols	ix
List of Figures	xvi
List of Tables	xx
Abstract	xxi
1 Introduction	1-1
1.1 Background	1-1
1.2 Research Objectives	1-2
1.3 Assumptions	1-2
1.4 Limitations	1-2
1.5 Scope	1-3
1.6 Requirements	1-3
1.7 Software engineering requirements	1-3
1.8 Approach	1-4
1.9 Summary	1-4
2 Basic Theory	2-1
2.1 Introduction: Overview of Multivariable Control Problem	2-1
2.2 The Plant P	2-2
2.3 Modeling of Uncertain Plants	2-3
2.4 Actuator and Sensor Models	2-4
2.5 Problem Specifications	2-4
2.5.1 Performance Specifications	2-5
2.5.2 Stability Specifications	2-8
2.6 Insertion of a Weighting Matrix	2-9
2.7 Polynomial Matrix Inverse	2-10

2.8	Improved Method	2-12
2.9	Formation of Templates	2-13
2.10	Bounds on Nichols Chart	2-15
2.10.1	Stability Bounds	2-15
2.10.2	Disturbance Bounds	2-16
2.10.3	Gamma Bounds	2-18
2.10.4	Tracking Bounds	2-18
2.10.5	Composite Bounds	2-21
2.11	Compensator Design	2-21
2.12	Prefilter Design	2-22
2.13	Simulation	2-24
2.14	Summary	2-25
3	Implementation	3-1
3.1	Introduction	3-1
3.2	Choice of Platform	3-1
3.3	Loading Plant Data	3-6
3.3.1	Plant Model Parameters	3-7
3.3.2	Structure of Plant Set Data	3-7
3.4	Loading of Sensor and Actuator Models	3-10
3.5	Dimension of Control Problem	3-10
3.6	Sensor Gain Matrix	3-10
3.7	Weighting Matrix	3-11
3.8	Formation of Effective Plant Models	3-12
3.9	Inverse of \underline{P}_e	3-14
3.10	Applying the Improved Method	3-16

3.11	Templates	3-16
3.12	Choice of Nominal Plant	3-17
3.13	Specifications	3-18
3.13.1	Stability Specifications	3-19
3.13.2	Performance Specifications	3-19
3.13.3	Gamma Bound Specifications	3-20
3.14	Generating Bounds	3-21
3.14.1	Stability Bounds	3-21
3.14.2	Disturbance Bounds	3-27
3.14.3	Gamma Bounds	3-31
3.14.4	Tracking Bounds	3-38
3.14.5	Composite Bounds	3-47
3.15	Compensator Design	3-49
3.16	Prefilter Design	3-52
3.17	Flowchart of MIMO QFT/CAD Package	3-54
3.18	Simulation	3-55
3.19	Summary	3-57
4	Results	4-1
4.1	Introduction	4-1
4.2	Validation of Thesis Results of Philip Arnold	4-1
4.3	Validation of Thesis Results of Robert Betzold	4-20
4.4	Summary	4-33
5	Chapter 5	5-1
5.1	Accomplishments	5-1
5.2	Conclusions	5-1
5.3	Recommended Areas of Further Study	5-2

Appendix A - Philip Arnold's Design	A-1
A.1 <u>P_e</u> Matrix Transfer Functions From CAD Package	A-1
A.1.1 Plant Case 1	A-1
A.1.2 Plant Case 2	A-3
A.1.3 Plant Case 3	A-5
A.1.4 Plant Case 4	A-7
A.1.5 Plant Case 5	A-9
A.1.6 Plant Case 6	A-11
A.1.7 Plant Case 7	A-13
A.1.8 Plant Case 8	A-15
A.1.9 Plant Case 9	A-17
A.1.10 Plant Case 10	A-19
A.1.11 Plant Case 11	A-21
A.1.12 Plant Case 12	A-23
A.1.13 Plant Case 13	A-25
A.1.14 Plant Case 14	A-27
A.1.15 Plant Case 15	A-29
A.1.16 Plant Case 16	A-31
A.1.17 Plant Case 17	A-33
A.1.18 Plant Case 18	A-35
A.1.19 Plant Case 19	A-37
A.1.20 Plant Case 20	A-39
A.1.21 Plant Case 21	A-41
A.1.22 Plant Case 22	A-43
A.1.23 Plant Case 23	A-45

A.1.24	Plant Case 24	A-47
A.2	<u>P_e</u> Determinants From CAD Package	A-49
A.3	<u>Q</u> Matrix from CAD Package	A-57
A.3.1	Plant Case 1	A-57
A.3.2	Plant Case 2	A-58
A.3.3	Plant Case 3	A-60
A.3.4	Plant Case 4	A-62
A.3.5	Plant Case 5	A-64
A.3.6	Plant Case 6	A-66
A.3.7	Plant Case 7	A-67
A.3.8	Plant Case 8	A-68
A.3.9	Plant Case 9	A-70
A.3.10	Plant Case 10	A-72
A.3.11	Plant Case 11	A-74
A.3.12	Plant Case 12	A-76
A.3.13	Plant Case 13	A-77
A.3.14	Plant Case 14	A-78
A.3.15	Plant Case 15	A-80
A.3.16	Plant Case 16	A-82
A.3.17	Plant Case 17	A-84
A.3.18	Plant Case 18	A-86
A.3.19	Plant Case 19	A-87
A.3.20	Plant Case 20	A-88
A.3.21	Plant Case 21	A-90
A.3.22	Plant Case 22	A-92

A.3.23	Plant Case 23	A-94
A.3.24	Plant Case 24	A-96
Appendix B - Robert Betzold's Design		B-1
B.1	<u>P_e</u> Matrix Transfer Functions From CAD Package	B-1
B.1.1	Plant Case 1	B-1
B.1.2	Plant Case 2	B-3
B.1.3	Plant Case 3	B-5
B.2	<u>P_e</u> Determinants From CAD Package	B-7
B.3	<u>Q</u> Matrix Transfer Functions From CAD Package	B-8
B.3.1	Plant Case 1	B-8
B.3.2	Plant Case 2	B-9
B.3.3	Plant Case 3	B-10
B.4	<u>Q</u> Matrix from CAD Package	B-11
B.4.1	Plant Case 1	B-11
B.4.2	Plant Case 2	B-12
B.4.3	Plant Case 3	B-13
Bibliography		BIB-1
Vita		VITA-1

List of Symbols

a_{ij}	2-12
a_{ij}'	2-19
A_x	3-35
A_y	3-35
AF	3-40
AF_{err}	3-43
\hat{AF}	3-41
AF_{opt}	3-41
AF_{req}	3-43
α_1	3-33
α_2	3-33
B_{D_u}	3-39
b_{ij}	2-12
b_{ij}'	2-19
b_{ij}	2-12
B_{O_r}	3-39
B_{R_L}	3-39
B_x	3-35
B_y	3-35
C_x	3-36
C_y	3-36
$c(t)_L$	2-5
$c(t)_U$	2-5
CL	2-7

d_{ij}	2-12
ΔM	3-45
$\Delta \hat{M}_{TB}$	3-45
$\Delta M_{TB_{max}}$	3-46
δ_R	2-18
δ_R'	2-18
δ_α	3-45
$\Delta \tau_{d_{ii}}$	3-42
$\Delta \tau_{r_i}$	2-19
$\Delta \tau_{r_i}'$	2-19
\underline{F}	2-1
f_{ij}	2-12
\underline{G}	2-1
ξ_i	2-12
ξ_m	3-19
γ	2-8, 3-19
γ_{12}	2-13, 3-20
γ_{21}	2-13, 3-20
H_{cl}	3-49
H_{cu}	3-49
H_{uu}	3-49
\underline{I}	2-24
J	2-3
k	3-31

\mathcal{L}	2-7
L_i	2-11
L_{10}	2-14, 2-17
LTI	2-3
M	3-21
$M_d(c)$	3-32
$M_b(c)$	3-32
M_c	3-16
M_{cu}	3-48
M_F	2-17, 3-28
M_F	2-18, 3-20
M_{F2}	3-20
M_{FB}	3-37
\hat{M}_{FB}	3-45
(\hat{M}_{FB})	3-46
M_i	3-16
M_{inv}	3-29
M_l	2-8, 2-12, 3-19
M_m	3-19
M_{nom}	3-26
$M_{nominal}$	3-18
m_o	2-17
M_p	2-25
M_{sp}	3-26

M_{cl}	3-48
M_t	3-26
M_{TB}	3-41
M_{TB_i}	3-44
M_{uu}	3-48
MIMO	2-1
NC	2-4
ω	2-7
ω_i	2-15
\underline{P}	2-2
\vec{p}_{ij}	2-10
PCONT	2-2
\underline{P}_e	2-1
$P_{c_{des}}$	3-12
\underline{P}_{e_i}	3-12
$\underline{P}_{e_{sum}}$	3-12
p_{ij}	3-12
\vec{p}_{ij}	3-14
param	3-8
Φ	2-17, 3-21
Φ_1	3-35
Φ_2	3-36
Φ_a	3-32
Φ_b	3-32

Φ_c	3-16
$\Phi_{D_{\max}}$	3-31
$\Phi_{D_{\min}}$	3-31
$\Phi_{G_{\max}}$	3-36
$\Phi_{G_{\min}}$	3-36
Φ_{GB}	3-37
$\Phi_{GB_{\max}}$	3-36
$\Phi_{GB_{\min}}$	3-37
Φ_i	3-16
Φ_{inv}	3-29
$\Phi_{M_m \max}$	3-23
$\Phi_{M_{\text{ref. max}}}$	3-23
Φ_{nom}	3-26
Φ_{nominal}	3-18
Φ_{SB}	3-26
$\Phi_{SB_{\max}}$	3-25
$\Phi_{SB_{\min}}$	3-25
Φ_t	3-26
Φ_{TF}	3-41
$\Phi_{\text{TEMPLATE}_{\max}}$	3-25
$\Phi_{\text{TEMPLATE}_{\min}}$	3-25
Ψ	3-35

\mathcal{L}	2-7
L_i	2-11
L_{io}	2-14, 2-17
LTI	2-3
M	3-21
$M_a(\varphi)$	3-32
$M_b(\varphi)$	3-32
M_c	3-16
M_{cu}	3-48
M_D	2-17, 3-28
M_{T1}	2-18, 3-20
M_{T2}	3-20
M_{GB_i}	3-37
\hat{M}_{TB}	3-45
$(\hat{M}_{TB})_i$	3-46
M_I	3-16
M_{inv}	3-29
M_l	2-8, 2-12, 3-19
M_m	3-19
M_{nom}	3-26
$M_{nominal}$	3-18
m_e	2-17
M_p	2-25
M_{SP}	3-26

M_{cl}	3-48
M_t	3-26
M_{TB}	3-41
M_{TB_1}	3-44
M_{uu}	3-48
MIMO	2-1
NC	2-4
ω	2-7
ω_i	2-15
\underline{P}	2-2
p_{ij}^*	2-10
PCONT	2-2
\underline{P}_e	2-1
$P_{e_{dec}}$	3-12
\underline{P}_{e_i}	3-12
$\underline{P}_{e_{sum}}$	3-12
p_{ij}	3-12
p_{ij}^*	3-14
param	3-8
ϕ	2-17, 3-21
Φ_1	3-35
Φ_2	3-36
ϕ_a	3-32
ϕ_b	3-32

Φ_c	3-16
$\Phi_{D_{max}}$	3-31
$\Phi_{D_{min}}$	3-31
$\Phi_{G_{max}}$	3-36
$\Phi_{G_{min}}$	3-36
Φ_{GB}	3-37
$\Phi_{GB_{max}}$	3-36
$\Phi_{GB_{min}}$	3-37
Φ_i	3-16
Φ_{inv}	3-29
$\Phi_{M_{m_{max}}}$	3-23
$\Phi_{M_{n_{max}}}$	3-23
Φ_{nom}	3-26
$\Phi_{nominal}$	3-18
Φ_{SB}	3-26
$\Phi_{SB_{max}}$	3-25
$\Phi_{SB_{min}}$	3-25
Φ_t	3-26
Φ_{TF}	3-41
$\Phi_{TEMPLATE_{max}}$	3-25
$\Phi_{TEMPLATE_{min}}$	3-25
Ψ	3-35

Q	2-10
q_{iio}	2-14
q_{ij}	2-10, 3-14
q_{ije}	2-13
QFT	2-1
ρ_1	3-35
RHP	2-18
s	2-7
Sp	2-8
$SISO$	2-3
\underline{I}	2-5
T_{ACT}	2-2
T_{ACT_i}	2-4
t_{d_i}	2-11
t_{ij}	2-5
t_P	2-25
T_R	2-20, 2-25
t_r	2-11
$t_{r_{10}}$	3-54
$T_{R_{max}}$	2-20
$T_{R_{tar}}$	2-20
TRU	2-7
t_s	2-25
$TSENS$	2-2
$TSENS_i$	2-4

τ_{d_u}	2-19
TB	3-41
URV	2-5
val	3-8
<u>W</u>	2-2
<u>W_i</u>	3-12
w _{ij}	3-11
WSENS _i	3-12

List of Figures

Fig. 2-1 A MIMO uncertain plant	2-1
Fig. 2-2 MIMO QFT controller block diagram	2-1
Fig. 2-3 Components of the Plant \underline{P}	2-2
Fig. 2-4 Formation of square effective plant	2-2
Fig. 2-5 Uncertainty in SISO plant transmission	2-3
Fig. 2-6 Compensated system	2-5
Fig. 2-7 CLTF Matrix Elements	2-5
Fig. 2-8 Time Domain Performance Specifications	2-6
Fig. 2-9 Frequency Domain Performance Specifications	2-6
Fig. 2-10 Stability Specifications	2-8
Fig. 2-11 MISO equivalents for 3 by 3 effective plant	2-11
Fig. 2-12 Sample template with numbered plant cases	2-14
Fig. 2-13 Template for bound	2-15
Fig. 2-14 Plotting of stability bounds	2-15
Fig. 2-15 Template with plant case 1	2-17
Fig. 2-16 Formation of disturbance bound	2-17
Fig. 2-17 Allocation for disturbance	2-19
Fig. 2-18 Transmission without prefilter	2-23
Fig. 2-19 Successful prefilter design	2-23
Fig. 3-1 Roots of high precision polynomial	3-3
Fig. 3-2 Roots of standard precision polynomial	3-3
Fig. 3-3 Effect of largest error term	3-5
Fig. 3-4 Plant parameter listing	3-7
Fig. 3-5 Plant model listing excerpt	3-8
Fig. 3-6 Factored form transfer function	3-9

Fig. 3-7 Plant transfer function Bode plots	3-9
Fig. 3-8 Listing of effective plant signs	3-13
Fig. 3-9 Listing of effective plant determinants	3-13
Fig. 3-10 Templates with nominal point emphasized	3-18
Fig. 3-11 Upper point of tangency with stability bound	3-24
Fig. 3-12 Template quantities of interest	3-25
Fig. 3-13 Stability bound range	3-25
Fig. 3-14 Test point on template	3-26
Fig. 3-15 Stability bound search test point on NC	3-26
Fig. 3-16 Lower point of tangency with stability bound	3-27
Fig. 3-17 Standard Nichols chart	3-28
Fig. 3-18 Inverse Nichols chart	3-28
Fig. 3-19 Closed gamma bound vector sum	3-32
Fig. 3-20 Open gamma bound vector sum	3-32
Fig. 3-21 Closed Gamma Bound on NC	3-33
Fig. 3-22 Open Gamma Bound on NC	3-33
Fig. 3-23 Closed gamma bound quantities of interest	3-34
Fig. 3-24 Open gamma bound quantities of interest	3-34
Fig. 3-25 Test point on template	3-37
Fig. 3-26 Gamma bound angle range	3-37
Fig. 3-27 Pair of bounds on NC	3-48
Fig. 3-28 Composite bound for bound pair	3-48
Fig. 3-29 Flowchart for MIMO QFT CAD Package	3-54
Fig. 4-1 Performance tolerances on the AFTI/F-16	4-2
Fig. 4-2 Templates for channel 1	4-4
Fig. 4-3 Templates for channel 2	4-4

Fig. 4-4 Template for q_{11} , 0.5 rad/sec	4-5
Fig. 4-5 Template for q_{11} , 4 rad/sec	4-5
Fig. 4-6 Template for q_{11} , 8 rad/sec	4-5
Fig. 4-7 Template for q_{22} , 0.5 rad/sec	4-5
Fig. 4-8 Template for q_{22} , 4 rad/sec	4-5
Fig. 4-9 Template for q_{22} , 8 rad/sec	4-5
Fig. 4-10 Bode plot of q_{11} for all plant cases	4-6
Fig. 4-11 Matlab Bode angle plot comparison	4-6
Fig. 4-12 Stability bounds for channel 2	4-7
Fig. 4-13 Allocated tracking bounds for channel 2	4-7
Fig. 4-14 Disturbance bounds for channel 2	4-8
Fig. 4-15 Gamma bounds for channel 2	4-8
Fig. 4-16 Channel 2 OLTF with composite bounds	4-9
Fig. 4-17 Channel 2 OLTF from Arnold's thesis	4-9
Fig. 4-18 Gamma bounds with OLTF for channel 2	4-11
Fig. 4-19 Bode plot of channel 2 open loop transmission	4-12
Fig. 4-20 Channel 2 nominal CLTF with filter bounds	4-12
Fig. 4-21 Stability bounds for channel 1	4-13
Fig. 4-22 Tracking bounds for channel 1	4-14
Fig. 4-23 Disturbance bounds for channel 1	4-14
Fig. 4-24 Channel 1 OLTF with composite bounds	4-16
Fig. 4-25 Channel 1 OLTF from Arnold's thesis	4-16
Fig. 4-26 Bode plot of channel 1 open loop transmission	4-17
Fig. 4-27 Channel 1 nominal CLTF with filter bounds	4-17
Fig. 4-28 Closed loop transmissions for Arnold	4-18
Fig. 4-29 Open loop transmissions for channel 1	4-19

Fig. 4-30 Open loop transmissions for channel 2	4-19
Fig. 4-31 (1,1) MISO loop from Betzold's thesis	4-20
Fig. 4-32 (2,1) SISO loop from Betzold's thesis	4-20
Fig. 4-33 Templates for Channel 1 of Betzold's thesis	4-21
Fig. 4-34 Templates for channel 2 of Betzold's thesis	4-21
Fig. 4-35 Stability bounds for channel 2	4-22
Fig. 4-36 Disturbance bounds for channel 2	4-23
Fig. 4-37 Channel 2 OLTF with gamma bounds	4-23
Fig. 4-38 Channel 2 OLTF with composite bounds	4-24
Fig. 4-39 Channel 2 OLTF from Betzold's thesis	4-24
Fig. 4-40 Stability bounds for channel 1	4-26
Fig. 4-41 Allocated tracking bounds for channel 1	4-26
Fig. 4-42 Channel 1 OLTF with composite bounds	4-27
Fig. 4-43 Channel 1 OLTF from Betzold's thesis	4-27
Fig. 4-44 OLTF with bounds - disturbance not allocated	4-28
Fig. 4-45 Open loop Bode plot for channel 1	4-28
Fig. 4-46 Channel 1 nominal CLTF with filter bounds	4-29
Fig. 4-47 Bode plots of closed loop transfer functions	4-29
Fig. 4-48 OLTF with re-designed compensator	4-31
Fig. 4-49 Nominal closed loop for new channel 1 design	4-31
Fig. 4-50 Closed loop Bode plots for re-designed system	4-32
Fig. 4-51 Open loop transmissions for channel 1	4-32
Fig. 4-52 Open loop transmissions for channel 2	4-33

List of Tables

Table 3-1 Coefficient form precision requirements	3-4
-------------------------------------------------------------	-----

Abstract

This thesis describes the development of an analog MIMO Quantitative Feedback Theory (QFT) CAD package for the automation of the multivariable control design process. The CAD package is capable of carrying a design from problem setup through the design process to a frequency domain analysis of the compensated MIMO system. The package automates the selection of the weighting matrix, formation of the square effective plants, the polynomial matrix inverse required to form the equivalent plants, generation of templates, selection of a nominal plant, generation of stability, tracking, disturbance, gamma, and composite bounds, loop shaping, design of the prefilter elements, and the frequency domain analysis of the completed design. Disturbance allocation is automatically performed while generating the tracking bounds. The package allows gain scheduling to be used in the weighting matrix. The improved method may be applied for the case of a 2×2 effective plant. The package is implemented using Mathematica for use on the Sun Workstations.

1 Introduction

1.1 Background

Quantitative Feedback Theory (QFT) was developed by Dr. Isaac Horowitz, professor emeritus at the University of California at Davis, as a frequency response control technique for the control of systems with uncertain plants and disturbance inputs. The first techniques were for a multiple-input single-output (MISO) continuous time system. In 1979 Quantitative Feedback Theory was further developed for use as a method of control for multiple-input multiple-output (MIMO) uncertain continuous time systems. First in 1961, then more intensely in 1986, Dr. Horowitz extended the QFT control technique to the control of discrete time plants.

The first analog QFT CAD package developed at AFIT, ICECAP-QFT, was developed in 1985 by Sandra Cole (9). Although the ICECAP-QFT CAD package was extended to handle digital control problems in 1990 by Professor Constantine H. Houptis, Professor Gary B. Lamont, and Dr. Robert Ewing, it was still limited in application to MISO control problems. A second QFT CAD package for both analog and digital systems has since been developed by Dr. Oded Yaniv at Tel-Aviv University in Israel (22). QFT CAD routines have also been developed by Bailey (4), Chait (8), and Thompson (27). However, like ICECAP-QFT, Dr. Yaniv's QFT CAD package and the CAD routines developed by Bailey, Chait, and Thompson are currently limited in application to the control of MISO uncertain systems. The need therefore exists for a MIMO QFT CAD package to automate the design process for the more difficult analog and discrete MIMO control system problem.

The need for automation of the design process was best illustrated by difficulties encountered by previous QFT thesis students. Each student was faced with the task of implementing the complex QFT design process for the problem at hand. The time involved in working through the details of the design process greatly increased the difficulty of each thesis and limited the difficulty of problems attempted. In addition, the details of the custom implementation and the manual techniques used increased the possibility of errors. These difficulties would be greatly reduced by the availability of a MIMO QFT CAD package. Industry and academia has repeatedly stressed the need for such a CAD package.

1.2 Research Objectives

The objective of this thesis is to develop a MIMO QFT CAD package as a tool to be used in future research and development work. As a tool, the CAD package will promote the use of the QFT control technique in future thesis work as well as in the engineering community by automating the design process. This thesis stresses the analog MIMO QFT design package.

1.3 Assumptions

Several assumptions are made regarding the design specifications and the system to be controlled:

- Plant uncertainty can be expressed by a set of linear-time-invariant (LTI) transfer functions
- Deterministic LTI transfer functions can be used to model sensor and actuator dynamics
- Performance specifications can be expressed by use of LTI transfer functions as upper and lower bounds
- Stability requirements are constant across all frequencies (it is not unreasonable to allow them to be a function of frequency)
- Each weighting matrix element may consist of a unique s-plane LTI transfer function for each plant case
- Effective $m \times m$ square plant matrix, P_e , exists
- Diagonal dominance achievability at infinite ω
- No outside disturbances present

1.4 Limitations

The MIMO QFT CAD package, as currently implemented, imposes several limitations:

- Diagonal prefilter matrix F
- Diagonal compensator matrix G
- QFT Method 2 design for 2×2 systems only
- Only continuous-time control system design is considered

1.5 Scope

The research conducted for this thesis covers several areas:

- Selection of a development environment from available programming languages and control packages
- Investigation of numerical precision requirements for successful implementation
- Investigation of previous QFT thesis work
- Investigation of previous QFT CAD packages
- Investigation of current QFT control techniques for control of MIMO systems
- Investigation of Air Force contractor plant data formats
- Implementation of current QFT control theory to the development of a continuous-time MIMO QFT CAD package
- Validation of MIMO QFT CAD package based on previous thesis work

1.6 Requirements

Several requirements have been imposed on the capabilities of the MIMO QFT CAD package:

- Loading of $p \times l$ plant matrix in contractor format
- Allow insertion of a $l \times m$ weighting matrix
- Allow insertion of a $m \times p$ sensor gain matrix
- Allow insertion of actuator and sensor dynamics
- Formation of $m \times m$ plant matrix inverse \mathbf{P}_e^{-1}
- Extensible to discrete-time control problems
- Extensible to the QFT Improved Method 2 design technique
- Addition of MISO QFT subroutines
- Allow transfer of completed design to MATRIXx

1.7 Software engineering requirements

- User interface

- Modular software
- Documentation

1.8 Approach

The first step in the thesis effort is the review of existing programming languages and control CAD packages from which a platform is chosen for the development effort. The development effort begins with the development of routines which accept the MIMO design data and transform the MIMO problem into a set of MISO equivalent problems. Software is then developed to carry out the QFT design procedure for the MISO equivalent problems. The final step in this thesis effort is the validation of the software implementation of the MIMO QFT CAD package by comparing results obtained from the CAD package to those obtained by previous thesis students for two MIMO analog design problems.

1.9 Summary

This thesis consists of five chapters. The first chapter introduces the thesis problem. The second chapter provides an overview of MIMO QFT theory as applied in this thesis. Chapter 3 discusses the method by which the MIMO QFT theory is applied during the development of the CAD package. In Chap. 4 the operation of the CAD package is validated by comparing results obtained from this package to those obtained in two previous thesis efforts. Conclusions and recommendations are then presented in Chap. 5.

2 Basic Theory

2.1 Introduction: Overview of Multivariable Control Problem

Quantitative Feedback Theory (QFT) is applied in this thesis investigation to the control of uncertain continuous time MIMO plants which are free from outside disturbances. The uncertain square plant \underline{P}_e shown in Fig. 2-1 has m inputs and m outputs. By use of a diagonal compensator \underline{G} and a diagonal prefilter \underline{F} in the feedback structure, shown in Fig. 2-2, it is desired that the closed loop system meet a set of stability and performance specifications defined for the problem. These specifications are discussed in detail in Sec. 2.5. If a compensator and prefilter can be designed which meet the stability and performance requirements for all controlled outputs and for all plant cases, then a robust control system design is achievable and the design is considered successful.

When using a diagonal compensator and prefilter, the closed loop system has m feedback paths. Each feedback path, with associated prefilter and compensator, is a channel of the QFT controller.

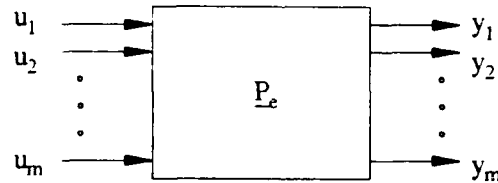


Fig. 2-1 A MIMO uncertain plant

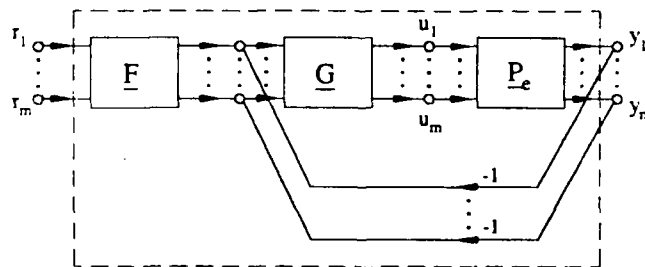


Fig. 2-2 MIMO QFT controller block diagram

2.2 The Plant \underline{P}

The plant model \underline{P} to be controlled is in general constituted by four component parts. A block diagram showing the placement of the $p \times l$ contractor plant model $\underline{P}_{\text{CONT}}$, the actuator dynamics $\underline{T}_{\text{ACT}}$, the sensor dynamics $\underline{T}_{\text{SENS}}$, and the $m \times p$ sensor gain matrix $\underline{W}_{\text{SENS}}$ is shown in Fig. 2-3. The plant \underline{P} of dimension $m \times l$ is, in general, not square.

For a plant model to be used in a QFT design, the plant must be square. The square plant \underline{P}_e of dimension $m \times m$ is formed from the non-square plant \underline{P} by use of the weighting matrix \underline{W} as shown in the block diagram in Fig. 2-4. Algebraically, the plant \underline{P} and the effective plant \underline{P}_e can be expressed, respectively, as follows:

$$\underline{P} = \underline{W}_{\text{SENS}} \cdot \underline{T}_{\text{SENS}} \cdot \underline{P}_{\text{CONT}} \cdot \underline{T}_{\text{ACT}} \quad (2-1)$$

$$\underline{P}_e = \underline{P} \cdot \underline{W} \quad (2-2)$$

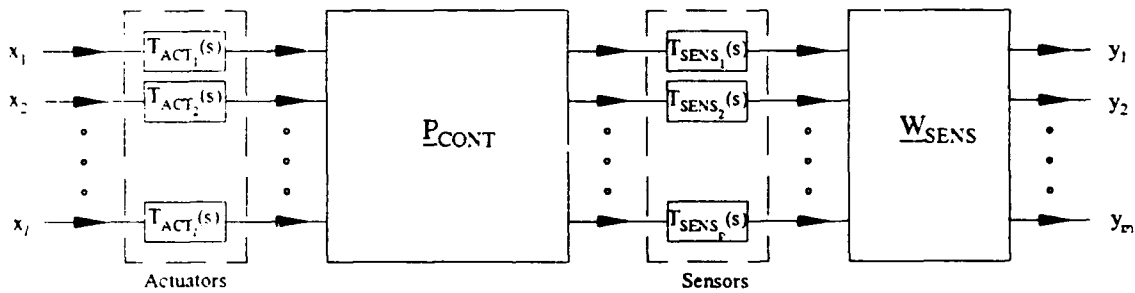


Fig. 2-3 Components of the Plant \underline{P}

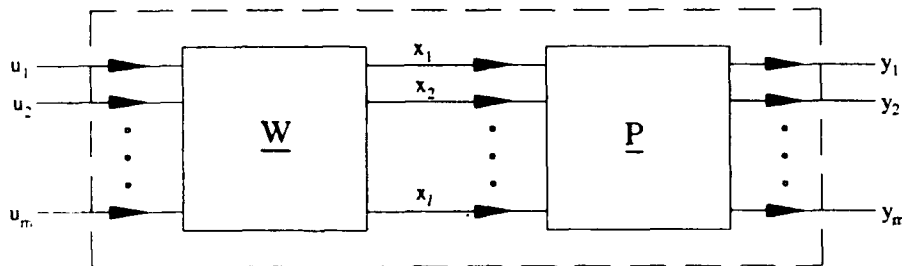


Fig. 2-4 Formation of square effective plant \underline{P}_e

2.3 Modeling of Uncertain Plants

Any real-world system to be controlled will inevitably be nonlinear, time varying, and uncertain to some extent. Most control techniques, however, are directly applied only to linear-time-invariant (LTI) systems (13). If a set of J LTI models can be obtained which effectively model the real world system, then some techniques can be applied to design a robust controller. By basing its design on such a set of LTI models, the QFT design technique produces a robust controller which will control the system in a desirable manner despite its real-world properties. This is so, even for a large class of uncertain nonlinear time varying plants (21:2-4).

An example of uncertainty in the transfer function for a single-input single-output (SISO) plant model at several frequencies is illustrated by the Nichols plot shown in Fig. 2-5. The scattering of the plant cases about the nominal plant case (heavy dot) is shown along with an outline enclosing the plotted plant cases. The range of plant cases is shown on the Nichols Chart (NC) for three different frequencies. The range

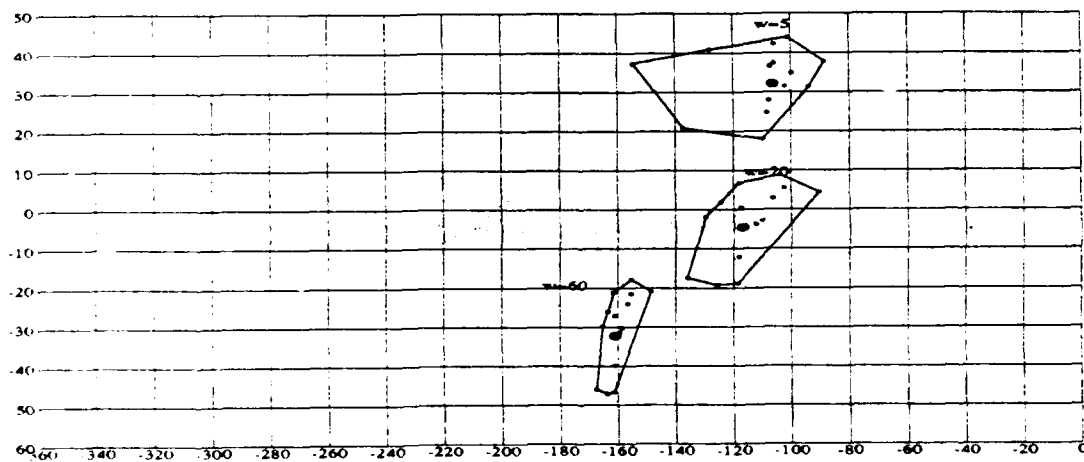


Fig. 2-5 Uncertainty in SISO plant transmission

The range of plant cases is shown on the Nichols Chart (NC) for three different frequencies. The range on the NC of possible plant transmissions at a given frequency defines the region of uncertainty at that frequency. For a QFT design, a sample set of plant cases taken over the range of plant uncertainty is used to model an uncertain plant. It is particularly important that the sample set include plant cases at the extremes of the region of uncertainty on the NC for each frequency of interest. This allows the QFT design procedure to take the full range of plant variation into account.

Uncertainty, nonlinearity, and time variance in a MIMO plant model are thus modeled by using a set of J LTI plant models. For a MIMO system, however, each plant case consists of an $m \times m$ matrix of transfer functions. The uncertain MIMO plant is therefore represented with a set of $m \times m$ transfer function matrices, one matrix for each plant case. As in the SISO case, the sample set should include plant cases at the extremes of plant variation on the NC.

2.4 Actuator and Sensor Models

Dynamics of the actuators and sensors used to control a system are in general, and for the purpose of this thesis, modeled by deterministic LTI transfer functions. The actuator transfer functions $T_{ACT_i}(s)$ model the dynamics involved in exerting the control effort required to apply an input to the plant. Likewise, the sensor transfer functions $T_{SENS_i}(s)$ represent the dynamics of the sensors used to measure the real-world plant outputs. The block diagram in Fig. 2-3 illustrates the use of actuators and sensors in the control of a real-world system. Each actuator and sensor is, in general, modeled by a unique transfer function.

2.5 Problem Specifications

Performance design specifications are placed on the controller design. Success of the design is judged mainly on the basis of satisfying these specifications. Other factors of importance which also may be considered include the order of the controller and prefilter transfer functions, the bandwidth, and, in digital systems, the sampling rate. However, for the purpose of this thesis, performance and stability specifications are emphasized.

2.5.1 Performance Specifications

Performance specifications for a compensated MIMO plant, shown in Fig. 2-6, can be given in either the frequency domain or the time domain. For example, consider the role of the elements of the compensated system control ratio matrix:

$$\underline{T}(s) = \begin{bmatrix} t_{11}(s) & t_{12}(s) \\ t_{21}(s) & t_{22}(s) \end{bmatrix} \quad (2-3)$$

where $t_{ij}(s)$ represents the control ratio between the i^{th} output and j^{th} input as illustrated in Fig. 2-7.

The set of plots shown in Figs. 2-8 and 2-9 illustrate the upper and lower performance bounds of the performance specifications in the time domain and frequency domain, respectively, for the compensated AFT/F-16 aircraft as defined in a previous QFT thesis investigating fault tolerance (2:4-26). The four plots in each figure are arranged in positions corresponding to the 2×2 closed loop transfer function matrix elements to which they apply.

For the off-diagonal transfer function elements, only an upper response bound is specified, since it is desired that the response of the off-diagonal MISO loops remain below a specified bound. For the purpose of this thesis effort, the bound must be specified in the frequency domain in the form of a transfer function.

Time domain performance specifications for the Lambda Unmanned Research Vehicle (URV) are shown in Fig. 2-8. Both upper and lower tracking bounds, $c(t)_U$ and $c(t)_L$ respectively, exist in the time

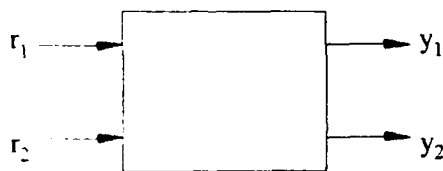


Fig. 2-6 Compensated system

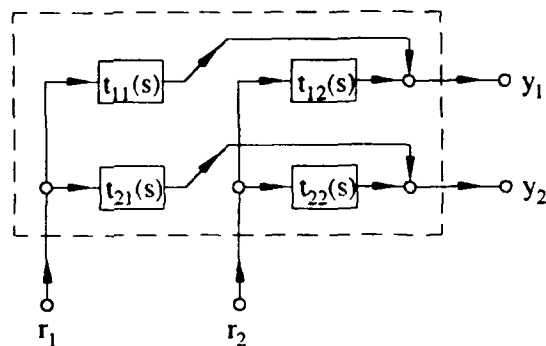


Fig. 2-7 CLTF Matrix Elements

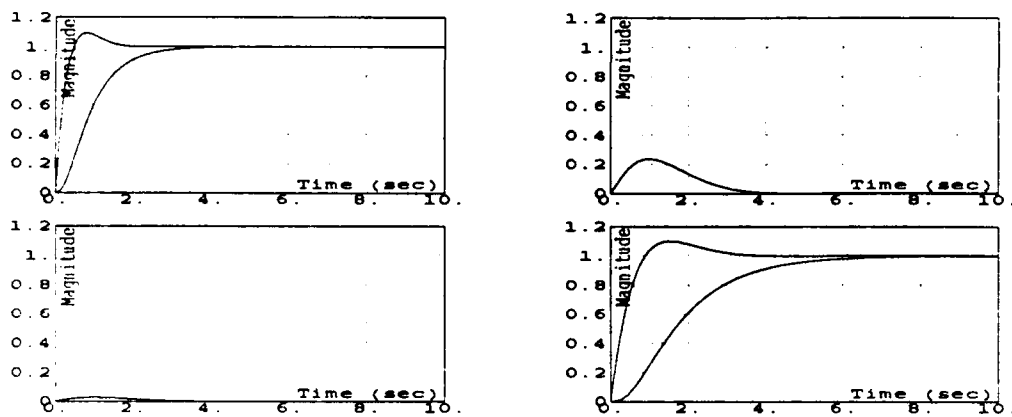


Fig. 2-8 Time Domain Performance Specifications

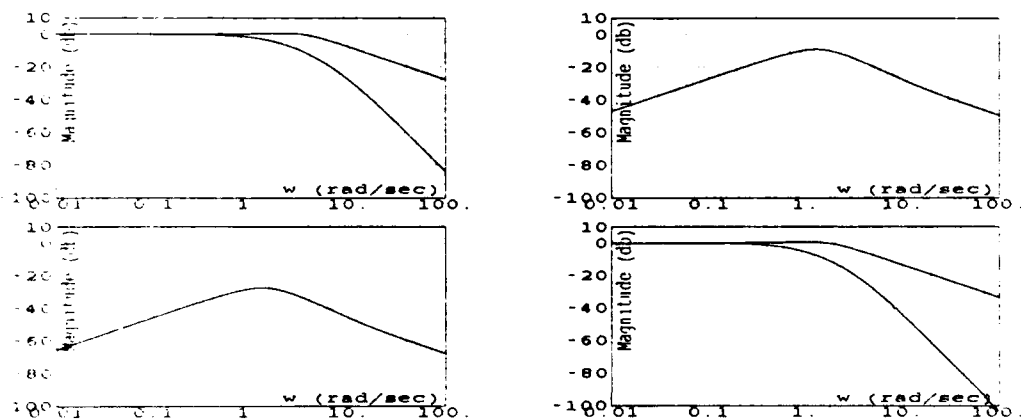


Fig. 2-9 Frequency Domain Performance Specifications

domain for the response of each diagonal $t_{ii}(s)$ transfer function element of $\underline{T}(s)$ to a step command applied to its respective command input (see Fig. 2-7). These upper and lower bounds constrain the step response magnitude to remain within a specified envelope. Only an upper bound exists in the time domain for each off-diagonal closed loop (CL) transfer function $t_{ij}(s)$, where $i \neq j$, for a step command input and for a diagonal \underline{F} . The upper bound constrains the magnitude of the undesired response due to coupling between channels to remain below a specified envelope.

The time domain and frequency domain specifications can be related by the Laplace transform. The complex frequency s times the Laplace transform of the time domain step response bounds yields the frequency domain bound transfer functions, i.e.,

$$T_{RU}(s) = s \left[\mathcal{L} [c(t)U] \right] \quad (2-4a)$$

$$T_{RL}(s) = s \left[\mathcal{L} [c(t)L] \right] \quad (2-4b)$$

The converse does not apply in general, however, because there is no specification for phase in the frequency domain.

Frequency domain specifications for the diagonal transfer functions include both upper and lower tracking bounds, T_{RU} and T_{RL} respectively. These specifications define the range of frequency response magnitudes permitted for the controlled output with respect to its corresponding command input. The purpose of these bounds is to desensitize the closed loop system to variation in the plant in its significant frequency range. There is a theorem, however, which states that any decrease in sensitivity achieved in any ω range must be paid for elsewhere in the frequency spectrum (17:1-9). This concept is expressed by the following equation:

$$\int_0^\infty \text{Log } S_P^T d\omega = 0 \quad (2-5)$$

where S_p is the sensitivity of the effective plant. A practical consequence of this is that the allowed variation should exceed the plant variation in higher (than the significant) ω range. This can be achieved if T_{RL} has an excess of poles over zeros greater than that of T_{RU} .

2.5.2 Stability Specifications

In addition to desirable performance, the QFT controller must provide an acceptable stability margin. The stability margin can be specified in terms of a phase margin γ , a gain margin g_m , or the corresponding M_L contour on the NC. The relationship between these three measures of stability, as applied in this thesis effort, is illustrated on the NC shown in Fig. 2-10. If any one of the three stability requirements are specified, the remaining two can be calculated. These calculations are discussed in Sec. 3.13.1.

The M_L contour is the stability specification used directly for the QFT design technique, placing an upper limit on the magnitude of the closed loop frequency response. The M_L contour on the NC forms a boundary which must not be violated by a plot of the open loop transmission transfer function for the compensated system for all J plants.

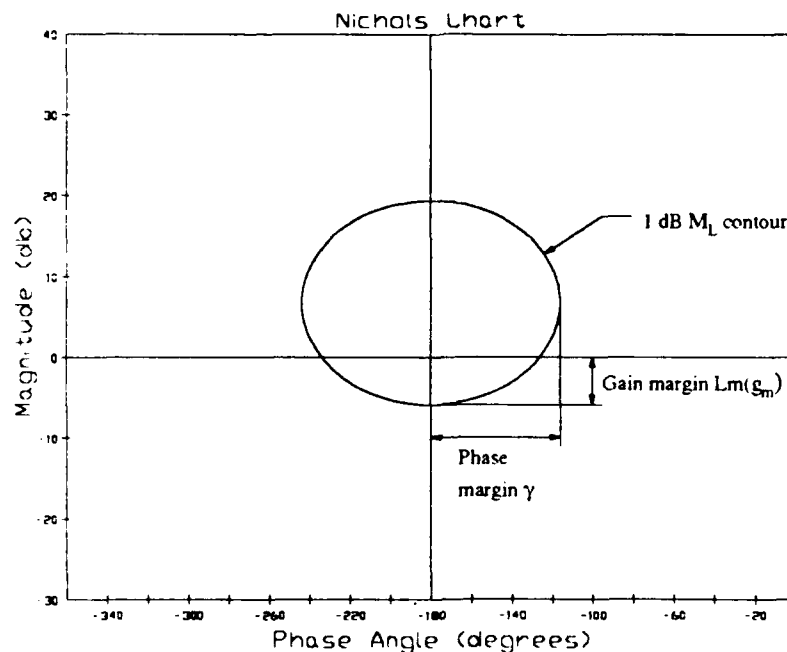


Fig. 2-10 Stability Specifications

2.6 Insertion of a Weighting Matrix

In cases where the $m \times l$ plant matrix is not a square matrix of the desired $m \times m$ dimensions, an $l \times m$ weighting matrix \underline{W} must be selected to form a square $m \times m$ effective plant \underline{P}_e . A block diagram illustrating the insertion of a weighting matrix is shown in Fig. 2-4.

For control of a multivariable system, one must apply at least as many inputs to the system as outputs to be controlled. When more plant inputs are available than required for control purposes, the designer has additional degrees of freedom in the blending of plant inputs used to control the system. The weighting matrix \underline{W} used to allocate the control effort to the plant inputs must be chosen such that all effective plants are full rank and the sign of the effective plants in the limit as $\omega \rightarrow \infty$ is the same for all plant cases (17:3-15). Once this requirement is satisfied, the designer seeks to obtain a minimum-phase effective plant. By applying the Binet-Cauchy theorem, the designer can determine whether a minimum-phase effective plant is achievable by the proper choice of the weighting matrix elements (17:5-17). If the condition of minimum-phase can be satisfied, the designer may further refine the choice of weighting matrix elements to minimize the control effort required and to minimize the range of uncertainty of the effective plant transfer function elements, as plotted on the NC.

In some multivariable control problems, the degree of uncertainty in the system to be controlled may render impossible a successful design (17:5-15). In these cases, the weighting matrix can be used to implement gain scheduling to reduce the uncertainty to a tolerable level. In an aircraft control problem, for example, measurements of variables such as altitude, Mach, angle of attack, and dynamic pressure may be available in addition to the defined outputs. Functions of these additional measurements may then be used in the weighting matrix of an aircraft flight control system to compensate for variation in plant dynamics over the flight envelope.

2.7 Polynomial Matrix Inverse

In order to begin the design of the QFT controller, the MIMO effective plant \underline{P}_e is transformed into a set of MISO equivalent plants. This transformation transforms the difficult MIMO design problem into a set of straightforward MISO design problems. The simplicity gained by use of this transformation is one of the major strengths of the QFT design process. The method of transforming the MIMO plant model into a set of the MISO equivalent plants is given below without proof. For more information see (17:Ch. 3).

First, the polynomial matrix inverse of the effective plant matrix is taken:

$$\underline{P}^{-1} = \{p_{ij}^*\} = \{1/q_{ij}\} \quad (2-6)$$

Next, the elements of \underline{P}^{-1} are inverted to form the \underline{Q} matrix:

$$\underline{Q} = \{q_{ij}\} = \{1/p_{ij}^*\} \quad (2-7)$$

The diagonal dominance condition is checked before the design process is continued. The diagonal dominance condition must be met by the elements of the \underline{Q} matrix in order for a QFT Method 1 design to be tractable (17:3-17). If the condition of diagonal dominance is not met, then a QFT Method 2 (improved method) design must be performed. If the result of the diagonal dominance test is unacceptable from the point of view of the designer, the choice of weighting matrix \underline{W} can be revised and the \underline{Q} matrix recomputed. QFT Methods 1 and 2 are discussed in Sec. 2.8, and the implementation of the diagonal dominance test is discussed in Sec. 3.9.

The role of the \underline{Q} matrix elements in the array of MISO equivalent plants is illustrated in Fig. 2-11. The MISO loops are decoupled except through the disturbance inputs. Each MISO loop has one command input and one disturbance input. The disturbance input is a function of the other controlled outputs. By the principle of superposition, the MISO loop transmission consists of both a tracking and a disturbance component. However, when using a diagonal prefilter, only the diagonal MISO loops have a transfer function component due to tracking:

$$t_{ii} = t_{r_i} + t_{d_i} \quad (2-8)$$

while the off-diagonal loops, with $f_{ij} = 0$ and $i \neq j$, have a transfer function component due to disturbance only:

$$t_{ij} = t_{d_{ij}} \text{ where } i \neq j. \quad (2-9)$$

Expressions for tracking and disturbance transfer function components can be derived from the signal flow graph of the (i,j) MISO loop:

$$(t_{r_i})_l = f_{ij} \left[\frac{g_i(q_{ii})_l}{1 + g_i(q_{ii})_l} \right] = f_{ij} \left[\frac{(L_i)_l}{1 + (L_i)_l} \right] \quad (2-10a)$$

$$(t_{d_{ij}})_l = \frac{(d_{ij})_l (q_{ii})_l}{1 + g_i(q_{ii})_l} = \frac{(d_{ij})_l (q_{ii})_l}{1 + (L_i)_l} \quad (2-10b)$$

where l is the index which specifies one of the J LTI plants, i.e., $l = 1, 2, \dots, J$, which the quantities L_i and q_{ii} are associated with, and where:

$$L_i = g_i q_{ii} \quad (2-11)$$

is defined as the loop transmission transfer function.

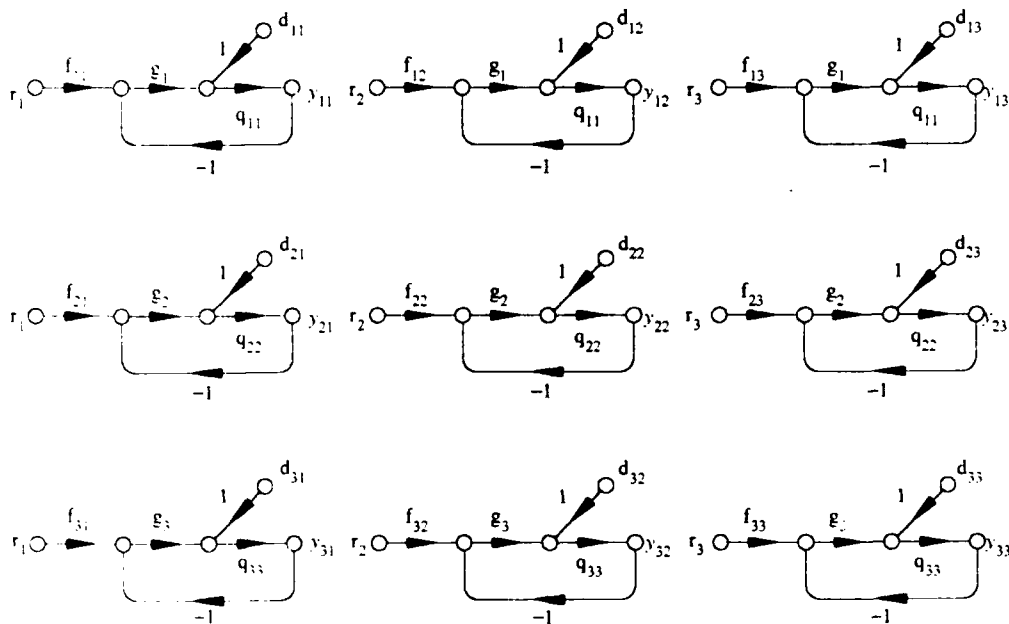


Fig. 2-11 MISO equivalents for 3 by 3 effective plant

The disturbance input, a function of all other controlled outputs, can be expressed by the equation:

$$d_{ij} = - \sum_{k \neq i} \frac{t_{kj}}{q_{ik}} \quad (2-12)$$

These MISO loops, each representing a closed loop transfer function element t_{ij} in terms of the compensator element g_i , the prefilter element f_{ij} , and effective plant q_{ij} are required to satisfy the performance and stability design specifications placed on the closed loop system.

For the diagonal MISO loops with upper and lower bounds:

$$a_{ii} \leq |t_{ii}|_l \leq b_{ii} \quad \text{for } l = 1, 2, \dots, J \quad (2-13)$$

For the off-diagonal MISO loops with an upper bound:

$$|t_{ij}|_l \leq b_{ij} \quad \text{for } l = 1, 2, \dots, J \quad (2-14)$$

For each row of MISO loops a stability margin is defined:

$$\left| \frac{g_i(q_{ii})_l}{1 + g_i(q_{ii})_l} \right| \leq M_L \quad \text{for } l = 1, 2, \dots, J \quad (2-15)$$

In order to design a compensator g_i for the MISO loops, the specifications are translated into bounds on the NC which must not be violated by the open loop MISO transmission $g_i q_{ii}$. In order for these bounds to take into account all plant cases, a set of templates, each outlining the range of plant uncertainty at a particular frequency, are used to generate the bounds. Template formation and the use of the templates as a tool for generating bounds on the NC is discussed in the following sections.

2.8 Improved Method

When using the QFT Method 1 design procedure, the compensators and prefilters are designed based on the $m \times m$ set of MISO loops in which the effective plants obtained from the Q matrix are used. When one of the m compensators g_i is designed successfully, the compensator exceeds the frequency domain performance specifications for some range of frequencies. In addition, correlation may exist between the uncertainty in the MISO loops in which g_i appears and the MISO loops for which the next compensator is to be designed. When the next compensator is designed, neither the improved performance due to g_i

nor correlation in the uncertainty in the MISO loops is taken into account. Failing to take this additional information into account leads to overdesign and may even preclude the possibility of a successful design (17:5-15). This is the price paid for transforming the difficult MIMO problem into a set of straightforward MISO problems (17:5-1).

The improved method, also known as QFT Method 2, takes into account the improved performance of the designed MISO loops and any correlation between the uncertainty in the designed MISO loops and the MISO loops in which the compensator to be designed next appears. The improved method requires the derivation of the effective q plant transfer function to be used in the row of MISO loops in which the next compensator to be designed appears, i.e. for a 2×2 system in which the compensator g_1 has been designed:

$$q_{22e} = \frac{q_{22} (1+L_1)}{1 - \gamma_{12} + L_1} \quad \text{where } L_1 = g_1 q_{11} \quad (2-16)$$

For a 2×2 system in which the compensator g_2 has been designed:

$$q_{11e} = \frac{q_{11} (1+L_2)}{1 - \gamma_{21} + L_2} \quad \text{where } L_2 = g_2 q_{22} \quad (2-17)$$

For a 2×2 system γ_{12} and γ_{21} are defined as:

$$\gamma_{12} = \gamma_{21} = \frac{p_{12} p_{21}}{p_{11} p_{22}} \quad (2-18)$$

In this thesis effort, and the current version of the CAD package, the improved method is addressed for a 2×2 MIMO problem only. For more information on the improved method, see (17:5-1).

2.9 Formation of Templates

A plant template outlines the range of uncertainty in the frequency domain transmission of a plant transfer function for a specific frequency, as plotted on the NC. The template is formed by first plotting the frequency domain transmission for each of the J plant cases, then enclosing the set of plant points with an outline. Figure 2-12 illustrates an example of a set of $J = 15$ numbered plant points and the template border assigned to them. The selection of the template border is to some extent a matter of engineering

judgment. The method by which the border is defined in the context of this thesis is discussed in detail in Sec. 3.11. It is important to note that the absolute location of the template points on the NC is unimportant; only the location of the plant cases relative to each other is required to define a template border. When performing a manual QFT design, the template borders are drawn on clear plastic and cut out for use on the NC. Plant templates must be generated for sufficient frequencies over the significant ω range. The template frequencies are the frequencies for which bounds on the MISO open loop transmission $g_i q_{ij}$ are generated and plotted on the NC. The bounds are then used for the design of the compensator g_i .

A nominal plant transfer function q_{ij0} is also defined. The identified nominal plant point on the template is used as the reference point upon which to execute the QFT design process. The bounds plotted on the NC are bounds on the nominal open loop transmission $L_{i0} = g_i q_{ij0}$. The nominal template point, while often one of the J plant points, in general need not be chosen from among the J plant points. The nominal template point need not even lie within the boundary of the template. The choice of nominal point has no effect on the template outline regardless of its location; the nominal point is a point of reference used when plotting the bounds. Nevertheless, the nominal plant is customarily chosen to be the lower left plant case of the templates whenever possible.

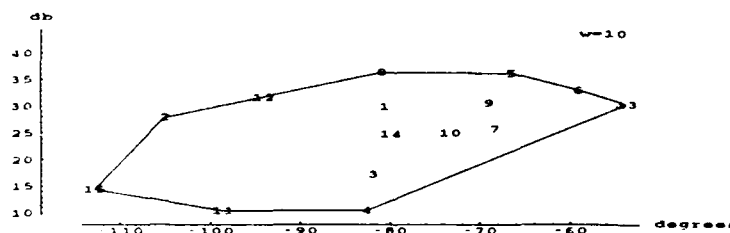


Fig. 2-12 Sample template with numbered plant cases

2.10 Bounds on Nichols Chart

For a given row i of MISO loops, bounds on the nominal open loop transmission $L_{io} = g_i q_{iio}$ are plotted on the NC, one set for each MISO loop in the row. For a template, generated for a given frequency $\omega = \omega_i$ (see Fig. 2-13), several bounds may be included in the set plotted on the NC. These bounds include a stability bound, a disturbance bound, a tracking bound, and a gamma bound (Sec. 2.10.3). Each set of bounds is replaced by a single composite bound before beginning a design. If a compensator g_i can be designed such that all the bounds are satisfied, then the stability and performance specs for that row of t_{ij} can be satisfied. The theory for each of these bounds is now discussed.

2.10.1 Stability Bounds

The stability bounds constrain the maximum closed loop transmission based on the open loop transfer function to have a bounded magnitude:

$$\left| \frac{g_i(q_{ii})l}{1 + g_i(q_{ii})l} \right| \leq M_L \quad \text{for } l = 1, 2, \dots, J \quad (2-19)$$

This specification is met by requiring that the open loop MISO transfer function, for all J plants, does not violate the M_L constant magnitude contour on the NC. This can be assured by plotting a bound on the NC, see Fig. 2-14, which the nominal open loop plant transmission $L_{io} = g_i q_{iio}$ must not violate. This bound can be plotted for a given frequency by plotting the path of the nominal point while traversing the M_L

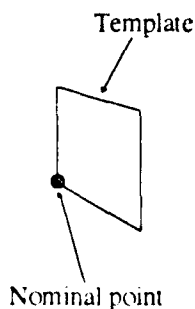


Fig. 2-13 Template for bound

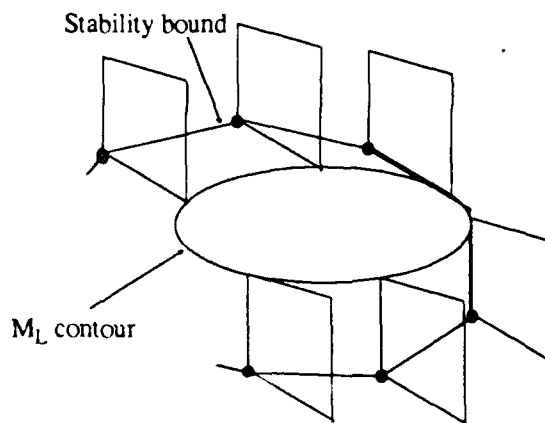


Fig. 2-14 Plotting of stability bounds

contour with the template generated for that frequency as shown in Fig. 2-14. Because the shape of the template plotted at each frequency is unique, the stability contour plotted for each frequency is also unique.

2.10.2 Disturbance Bounds

The responses of the off-diagonal MISO loops result from coupling and are considered undesirable components which are added to the commanded diagonal MISO loop response. Performance specifications require that the magnitude of the transmissions t_{ij} for these off-diagonal MISO loops remain below the bounds b_{ij} where $i \neq j$. From Eq. (2-9b) the upper bound implies the requirement:

$$|t_{ij}| = \left| d_{ij} \left[\frac{q_{ii}}{1 + g_i q_{ii}} \right] \right| \leq b_{ij} \quad \text{for } i \neq j \quad (2-20)$$

where the disturbance is a function of all other controlled outputs:

$$d_{ij} = - \sum_{k \neq i} \frac{t_{kj}}{q_{ik}} \quad (2-21)$$

Since the relative phases of t_{kj} and q_{ik} are not aprior known, one must use the specifications which dictate that $|d_{ij}|$ is less than an upper bound for each plant case l in the set of J plants:

$$(|d_{ij}|_{\max})_l = \sum_{k \neq i}^m \frac{b_{kj}}{|q_{ik}|_l} \quad (2-22)$$

The most extreme upper bound on $|d_{ij}|$ for all the J plant cases is then:

$$|d_{ij}|_{\max} = [(|d_{ij}|_{\max})_l]_{\max \text{ over } l} \quad (2-23)$$

Based on Eqs. (2-20) and (2-23) a lower bound can be placed on $|1 + L_i|$

$$|1 + L_i| \geq \frac{|q_{ii}| |d_{ij}|_{\max}}{b_{ij}} \quad (2-24)$$

By substituting $L_i = \frac{1}{m}$ Eq. (2-24) is transformed such that the disturbance bound is plotted on the

inverse NC:

$$\left| \frac{m}{1 + m} \right| \leq \frac{b_{ij}}{|q_{ii}| |d_{ij}|_{\max}} \quad (2-25)$$

Simplifying by using the symbol M_D to designate the inverse NC constant magnitude contour:

$$\left| \frac{\mathbf{m}}{1 + \mathbf{m}} \right| \leq M_D \quad \text{where } M_D = \frac{b_{ij}}{|q_{ij}| |d_{ij}|_{\max}} \quad (2-26)$$

In general, M_D is different for different plant cases since q_{ij} is different for different plant cases. From this point forward the inverse NC constant magnitude contour is referred to as the M_D contour.

Equation (2-26) is in the form of a unity feedback system for which disturbance bounds can be drawn by use of the templates on the inverse NC. The inverse NC, the NC turned upside down, is used because it allows a bound on L_{io} to be plotted on the NC given the restriction on $\mathbf{m} = (L_{io})^{-1}$ in Eq. (2-26). Assume for a moment that for plant case l , illustrated on the template in Fig. 2-15, Eq. (2-26) places the most severe restriction on \mathbf{m} (and on $L_{io} = \frac{1}{\mathbf{m}_o}$) at all phase angles of \mathbf{m}_o , i.e., results in the maximum value on the right-hand-side of Eq. (2-26). The disturbance bound can then be plotted as shown in Fig. 2-16, where the disturbance bound is traced by the nominal point as the M_D contour associated with plant case l is traversed such that the point on the template border corresponding to plant case l is in contact with the M_D contour at all times. This is so because it is assumed that for plant case l the most extreme bound exists on L_{io} at all NC phase angles at which the bound is plotted. In general, a different point on the template border results in the most severe restriction on L_{io} at each phase angle ϕ for which the bound is plotted. This issue is addressed in Sec. 3.14.2. For more information on the use of the inverse NC for plotting disturbance bounds, see (11:712).

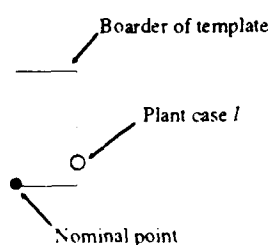


Fig. 2-15 Template with plant case l

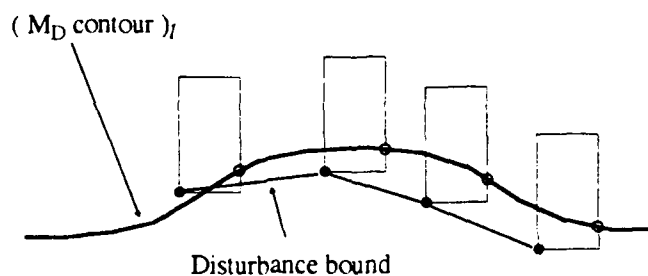


Fig. 2-16 Formation of disturbance bound

2.10.3 Gamma Bounds

Gamma bounds are a useful tool for improved method designs. Gamma bounds allow the designer to design the current compensator such that the next effective plant does not have right-half-plane (RHP) poles due to the current compensator design. Gamma bounds are not always mandatory. In the 2×2 case, if row 1 is designed first, a lower bound is placed on the denominator of q_{22} as defined by Eq. (2-16):

$$|1 - \gamma_{12} + L_1| \leq M_{\gamma_1} \quad (2-27)$$

This requirement is similar to that used for generating stability bounds. The method by which this requirement is used to form bounds on the NC is discussed in detail in Sec. 3.14.3.

2.10.4 Tracking Bounds

Tracking bounds are used to insure that the variation in closed loop frequency domain transmission $t_{ij} = t_{ji}$ for $i = j$ of the diagonal MISO loop does not exceed the variation δ_R permitted by the performance tolerances a_{ii} and b_{ii} where:

$$\delta_R = 20 \log \left(\frac{b_{ii}}{a_{ii}} \right) = 20 \log(b_{ii}) - 20 \log(a_{ii}) \quad (2-28)$$

The variation in the closed loop transmission results from uncertainty in both the response due to tracking and from the presence of the disturbance input:

$$t_{ij} = t_{r_i} + t_{d_{ij}} \quad (2-29)$$

where t_{r_i} and $t_{d_{ij}}$ are given by Eqs. (2-10a) and (2-10b).

A portion of the permitted variation δ_R of the total response t_{ij} is therefore allocated to the transmission due to disturbance $t_{d_{ij}}$ resulting in a reduced range of variation δ_R' for the transmission due to tracking t_{r_i} where:

$$\delta_R' = 20 \log \left(\frac{b_{ii}'}{a_{ii}'} \right) = 20 \log(b_{ii}') - 20 \log(a_{ii}') \quad (2-30)$$

Because the relationship between t_r and t_{d_u} is additive, the permitted variation is represented in terms of magnitude rather than log magnitude when allocating for disturbance:

$$\Delta\tau_{r_i} = 10^{(\delta_R/20)} = b_{ii} - a_{ii} \quad (2-31a)$$

$$\Delta\tau_{r_i}' = 10^{(\delta_R'/20)} = b_{ii}' - a_{ii}' \quad (2-31b)$$

By allocating the portion $2\tau_{d_u}$ to disturbance, the permitted variation in closed loop transmission t_r becomes $\Delta\tau_{r_i}'$, as shown in Fig. 2-17. The permitted closed loop variation in tracking is now:

$$\Delta\tau_{r_i}' = \Delta\tau_{r_i} - 2\tau_{d_u} \quad (2-32)$$

where:

$$\Delta\tau_{r_i} = b_{ii} - a_{ii} \quad (2-33)$$

The performance tolerances for the closed loop transmission t_r then become:

$$a_{ii}' = a_{ii} + \tau_{d_u} \quad (2-34a)$$

$$b_{ii}' = b_{ii} - \tau_{d_u} \quad (2-34b)$$

The requirement on the transmission due to tracking t_r becomes:

$$a_{ii}' \leq |t_r| \leq b_{ii}' \quad (2-35)$$

And the requirement on the transmission due to disturbance t_{d_u} becomes:

$$|t_{d_u}| \leq \tau_{d_u} \quad (2-36)$$

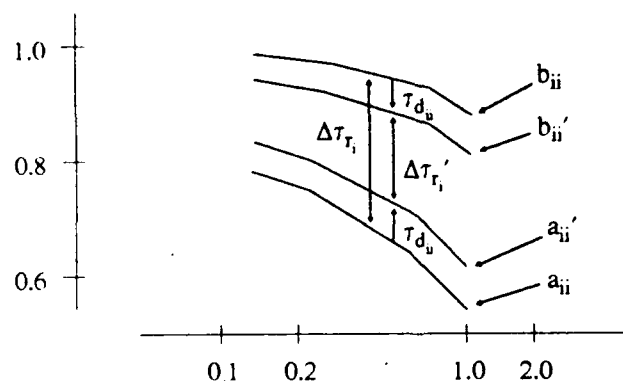


Fig. 2-17 Allocation for disturbance

With this disturbance allocation, tracking and disturbance requirements are placed on L_i based on Eqs. (2-34) and (2-35). The requirement on L_i which is satisfied at a point on the tracking bound for a given frequency $\omega = \omega_i$ and phase angle ϕ on the NC is:

$$\text{Lm}(T_{R_{\max}}) - \text{Lm}(T_{R_{\min}}) \leq \delta_R' \quad (2-37)$$

where $\delta_R' = \text{Lm}(\Delta\tau_{r_i}') = \text{Lm}(\Delta\tau_{r_i} - 2\tau_{d_{ij}})$ and where $T_{R_{\max}}$ and $T_{R_{\min}}$ are determined by maximizing and minimizing the transmission with unity gain prefilter T_R over the outline of the template:

$$T_R = \left| \frac{L_i}{1 + L_i} \right| \quad (2-38)$$

with the template placed with the nominal point on the tracking bound.

Based on Eq. (2-36) the method discussed in Sec. 2.10.2 is used to determine the point on the disturbance bound on L_i for the diagonal MISO loop at $\omega = \omega_i$ and at the phase angle ϕ on the NC. From Eq. (2-24) the constraint on L_i for $b_{ij} = \tau_{d_{ij}}$ is:

$$|1 + L_i| \geq \frac{|q_{ij}| |d_{ij}|_{\max}}{|\tau_{d_{ij}}|} \quad (2-39)$$

with $|d_{ij}|_{\max}$ defined by Eq. (2-23) with $i = j$. The constraint of Eq. (2-39), along with the template for $\omega = \omega_i$, is used to determine the location of the point on the disturbance bound.

The value of $\tau_{d_{ij}}$ is chosen such that Eqs. (2-37) and (2-39) place the same restriction on L_i ; this is the value of $\tau_{d_{ij}}$ for which the points on the tracking and disturbance bounds are identical at the phase angle ϕ on the NC and the value for which the least restrictive composite bound point on L_i will be generated. The method by which the CAD package determines this value of $\tau_{d_{ij}}$ is discussed in detail in Sec. 3.14.4. Composite bounds are discussed in Sec. 2.10.5.

In general the value of $\tau_{d_{ij}}$ is unique at each $\omega = \omega_i$ and for each NC angle ϕ at which the bound is plotted. Once a value of $\tau_{d_{ij}}$ is available at a given phase angle ϕ , δ_R' can be calculated and a point on the tracking bound can be plotted. To plot a point on the tracking bound, pick an angle for L_{i0} , say 0° . Place the template for the frequency of interest on the NC with the nominal point on the 0° axis. The

template is then moved up or down the 0° axis as needed until the difference between the largest ($T_{R_{max}}$) and smallest ($T_{R_{min}}$) closed loop transmissions is equal to the permitted variation in decibels:

$$Lm(T_{R_{max}}) - Lm(T_{R_{min}}) = \delta_R' \quad (2-40)$$

The position of the nominal point is then marked on the 0° axis. This procedure is repeated for a range of angles across the NC, using a unique $\tau_{d_{ij}}$ at each phase angle, and the bound contour is drawn through the set of points. By constraining the nominal loop transmission to be on or above the tracking bound, the actual variation in t_{ij} will be less than or equal to δ_R .

2.10.5 Composite Bounds

A set of composite bounds is often formed on the NC prior to compensator design. A composite bound is formed by plotting only the dominant portions of a set of bounds, for each frequency. If the open loop nominal transmission $L_{i0} = g_i q_{i0}$, where q_{i0} is the nominal plant, when plotted on the NC, does not violate the composite bound, then no bound from the original set of bounds is violated. For a successful compensator design, all bounds on L_{i0} must be satisfied for an entire row of MISO loops and for all frequencies of interest. One row of MISO loops for a 3×3 MIMO system, for example, would require a stability bound, a tracking bound, and two disturbance bounds to be plotted for each frequency of interest. For the case in which there are ten frequencies of interest, there would be a total of forty bound contours to plot. By plotting only ten composite bounds in place of forty, clutter is reduced substantially.

2.11 Compensator Design

A compensator is designed which satisfies all requirements placed on it by the MIMO QFT specifications once the bounds for the entire row of MISO loops are plotted on the NC. The bounds for the entire row MISO loops must be satisfied since the same g_i appears in all MISO loops in a given row. The bounds for all MISO loops in a given row can be plotted together on the NC since the same open loop transmission $L_i = g_i q_i$ appears in all MISO loops of a given row. The compensator is then designed based on the bounds as plotted on the NC.

The compensator is designed by properly shaping the open loop transmission such that all bounds are satisfied at the respective bound frequencies. The shaping is accompanied by adjustment of the compensator gain, and by adding poles and zeros as needed. Two main approaches exist for loop shaping. In the first approach, the initial open loop transfer function is taken to be q_{jio} , the nominal plant. The transfer function g_j is then designed by adding poles and zeros as needed, and adjusting the gain until a desirable loop shape is obtained on the NC (18:Sec. 3.8.2). For the second approach, the open loop gain L_{jo} is designed directly by beginning with a simple gain and then adding poles and zeros, and modifying the gain to obtain a desirable open loop shape on the NC. The equation $g_j = L_{jo} (q_{jio})^{-1}$ is then used to compute the compensator g_j (18:Sec. 3.8.1). The second approach is valid only for a minimum-phase, stable q_{jio} . The first approach usually gives a smaller order compensator, while the second approach gives the designer an indication of the degree to which the design can be optimized. The first approach is used here.

2.12 Prefilter Design

A compensator which satisfies all bounds on the NC guarantees that the range of variation in the closed loop transmission t_{ij} is acceptable for the corresponding MISO loop, but does not guarantee that the transmission lies entirely within the limits of the upper and lower tracking bounds b_{ij} and a_{ij} . A prefilter is therefore designed such that the bounds b_{ij} and a_{ij} are satisfied for all plant cases. The procedure below illustrates the method by which the prefilter is designed.

First, as for tracking bounds on the NC, a portion of the permitted range of variation of t_{ij} is allocated to the disturbance. The maximum and minimum limits on the range of variation of t_{ij} are therefore made more restrictive by the magnitude of the response due to disturbance $|t_{d_{ij}}|_{\max}$, as illustrated in Fig. 2-17 on page 2-19. The tolerances on t_{r_i} become:

$$b_{ij}' = b_{ij} - |t_{d_{ij}}|_{\max} \quad (2-41)$$

$$a_{ij}' = a_{ij} + |t_{d_{ij}}|_{\max} \quad (2-42)$$

Second, $T_{R_{\max}}$ and $T_{R_{\min}}$, the maximum and minimum values respectively of the diagonal MISO loop transmission magnitude T_R ($|t_{r_i}|$ with $f_{ij} = 1$), are determined at the template frequencies where T_R is:

$$T_R = \left| \frac{L_i}{1 + L_i} \right| \quad (2-43)$$

$T_{R_{\max}}$ and $T_{R_{\min}}$ are used to restrict the permitted range of variation about the nominal t_{r_i} such that a single nominal t_{r_i} can be plotted rather than requiring an array of J transmissions to be plotted on the Bode plot, one for each plant case. It is easier to work with a single transmission within a pair of bounds than to work with J transmissions within a pair of bounds.

The values $T_{R_{\max}}$ and $T_{R_{\min}}$ are obtained at each ω_i by placing the template for ω_i on the NC with the nominal point at the location of $L_{i0} = g_i q_{i0}$ for $\omega = \omega_i$. The template outline is then searched to determine the maximum and minimum closed loop transmissions $T_{R_{\max}}$ and $T_{R_{\min}}$.

Finally, the bounds on the nominal t_{r_i} are computed:

$$Lm(b_{ii}') - Lm(T_{R_{\max}}) \quad (2-44)$$

$$Lm(a_{ii}') - Lm(T_{R_{\min}}) \quad (2-45)$$

Once the prefilter bounds have been generated, a prefilter is synthesized such that the Bode plot of the nominal t_{r_i} lies between the prefilter bounds and satisfies $t_{r_i}(s) = 1$ in the limit as $s \rightarrow 0$. Examples of

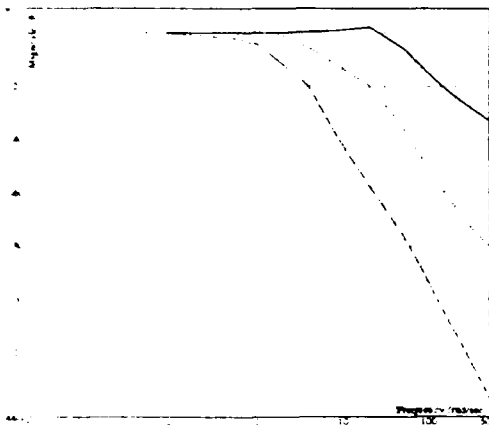


Fig. 2-18 Transmission without prefilter

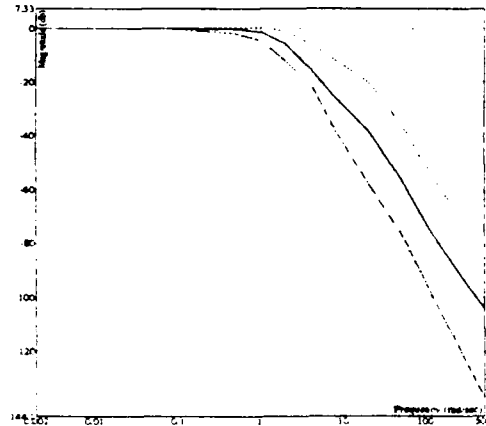


Fig. 2-19 Successful prefilter design

the Bode plot of t_i with prefilter bounds, both before and after the prefilter has been designed, are shown in Figs. 2-18 and 2-19.

2.13 Simulation

The completed QFT design must pass several levels of testing and validation. In past thesis work, tests were performed to validate that the closed loop system satisfied the design specifications in both the frequency and the time domains. Two tests were performed in the frequency domain. For the first frequency domain test, the M_L contour was plotted on the NC along with an array of open loop MISO loop transmissions $(L_i)_l = g_i(q_{il})l$ for row i of the MISO loops, one for each of the J plant cases ($l = 1, 2, \dots, J$) to validate that the M_L contour was not violated for row i of the MISO loops. If the M_L contour was not violated, then it was concluded that the stability specifications had been met for row i of the MISO loops. As an example, a plot of the open loop transmissions for channel 1 of a controller designed by Philip Arnold is shown in Fig. 4-29 on page 4-19.

For the second frequency domain test, an array of J Bode magnitude plots of each closed loop transfer function element was plotted along with the performance tolerances to validate that the performance specifications were satisfied in the frequency domain by the closed loop system. For each diagonal closed loop transmission t_{ii} , the J Bode magnitude plots were plotted along with the upper and lower tracking bounds a_{ii} and b_{ii} . For each off-diagonal closed loop transmission t_{ij} , the J Bode magnitude plots are plotted along with the upper bound b_{ij} . The $m \times m$ closed loop transfer function matrix \underline{T} , whose elements t_{ij} are the transmissions plotted on the Bode plots, is formed based on the equation:

$$\underline{T} = [\underline{I} + \underline{P}_e \underline{G}]^{-1} \underline{P}_e \underline{G} \underline{F} \quad (2-46)$$

where \underline{I} is the identity matrix, and \underline{P}_e , \underline{F} , and \underline{G} are the $m \times m$ effective plant matrix, diagonal prefilter matrix, and diagonal compensator matrix, respectively. These validation steps are important because they provide a method of validation independent from the MISO CAD routines used, the choice of plant templates, and the template border used.

The next simulation performed in previous thesis work involved setting up a System-Build model using MATRIXx and running a time domain simulation for each plant case. The results of these simulations were then used to validate that the figures of merit specifications, such as settling time t_s , time to peak t_p , rise time t_r , and peak response M_p were met. This simulation validated the robustness of the QFT design.

For the final simulation, nonlinear dynamics such as saturation and hysteresis were included in the System-Build model used in the time domain simulation. This simulation provided the most realistic evaluation of real-world performance.

2.14 Summary

This chapter presented a general overview of the MIMO QFT design procedure as it applies the development of the MIMO/QFT CAD package. The plant models and design specifications upon which the design is performed are introduced, along with a discussion of the tasks performed as the design proceeds from problem setup, through design, to simulation and testing. The discussion now shifts to the implementation of the QFT design procedures for the purpose of developing the MIMO/QFT CAD package.

3 Implementation

3.1 Introduction

This chapter presents a detailed discussion of the implementation of the QFT control theory presented in Chap. 2 and the development of the MIMO QFT CAD pack. Section 3.2 begins by discussing the choice of programming environment. Sections 3.3 through 3.6 discuss the setup of the control problem in preparation for the QFT design, including definition of plant models, sensor and actuator dynamics, and sensor gain matrix. Sections 3.7 through 3.9 discuss the transformation of the MIMO problem into a set of MISO equivalent problems. Section 3.10 discusses the implementation of the improved method. Sections 3.11 through 3.16 discuss the implementation of the MISO QFT design procedures, including definition of design specifications, generation of templates and bounds, and design of the compensator and prefilter for each channel of the control system. Finally, Sec. 3.18 discusses simulation and testing procedures implemented for the completed design.

3.2 Choice of Platform

Several platforms are considered for use in implementing the MIMO QFT CAD package. These packages are considered on the basis of their capabilities, numeric precision, portability, and cost. The packages considered include Matlab (), MATRIXx (20), Control-C (10), Mathematica (29), Macsyma (19), and the 'C' language (26).

The 'C' language is considered first. The greatest strengths of the 'C' language, as compared with the other alternatives, are the portability, availability, and increased speed gained by use of the compiler-based 'C' language. Also, the availability of Eispack (6), LINPACK (7), and ICECAP-QFT (9) routines as well as a numerical methods toolbox (23) for 'C' are helpful. The 'C' language also presents several drawbacks. First, numerical precision of the language is limited to the machine precision, unless extended by use of additional software. Second, the 'C' language, as a platform, does not offer an interactive mode. Third, the language does not free the developer from the details of implementing and using advanced data structures, such as a transfer function or a polynomial matrix. Finally, the 'C' language does not free the developer from managing the storage of the large amount of CAD data (pointer management).

MATRIXx is now considered. This package is specialized for engineering and control applications, with a variety of software tools available for solving control problems and has an interactive user interface. This strength comes at the expense of a number of weaknesses, however. First, numeric precision of all calculations are limited to 16 decimal digits of accuracy. Second, the language itself has many limitations, such as the 4096 character limit on the code used for a 'while' or a 'for' loop, and the lack of the logical 'and', 'or', and 'not' operators. Third, the types of data structures available are limited to those that can be expressed using a two dimensional matrix. Fourth, the availability of this package is limited due to its high price.

Matlab and Control-C are also considered. These packages, like MATRIXx, have a variety of tools useful for control applications and an interactive front end. They also, however, share the limitation of 16 decimal digits of accuracy for all calculations. Therefore, Matlab and Control-C are placed in the same category as MATRIXx.

Macsyma is also considered as a candidate. While this package is capable of working with and performing calculations on symbolic expressions, it has difficulty solving for the roots of a polynomial. Because this is a critical step in control system design, Macsyma is not considered further.

The remaining package considered is Mathematica. This package has many strengths. Its most distinguishing features include the use of symbolic arithmetic and the capability of performing calculations using arbitrary precision assigned by the user. In addition, Mathematica is equipped with an interactive user interface and an extensive, well refined, "free form" language executed by the command interpreter. This language allows for a wide variety of data structures of arbitrary size and dimension, including lists of matrices, arrays of transfer functions, and expressions in any number of variables (29:Sec. 1.8). The environment allows for selective hiding of information by use of local parameters, local variables, and local contexts (29:Sec. 2.6). Finally, Mathematica has the advantage of making any application written for it portable to many operating systems, including UNIX, VMS, and MS-DOS systems as well as the Macintosh. The low cost of Mathematica also is advantageous, placing a low financial demand on potential users of

the package. One weakness brought out in the review is that since Mathematica is not a compiler-based language, it can be slow. This problem can be overcome, however, since the MathLink facility provided with Mathematica allows a seamless interface to outside compiled software, including software written in 'C'. Another problem is the absence of control design tools offered by other packages such as Matlab and MATRIXx. Many of these tools are developed in this thesis for use in the CAD package, including routines for generating Bode and Nichols plots for a transfer function, and software for transforming a polynomial between coefficient form and factored form. Henceforth the CAD package developed in this thesis is referred to as MIMO/QFT CAD.

In making the final decision regarding the environment to be used, the numerical accuracy of the packages is considered a critical issue. In particular, the ability of the packages to accurately represent a high order polynomial in both coefficient and factored form is critical in MIMO QFT CAD design problems. A test case is used to illustrate this need for numerical accuracy.

A 50th order polynomial is entered in factored form, with the following set of roots each having at least 8 significant decimal digits of accuracy:

$$\text{roots} = \{ 1.0123456, 2.0123456, \dots, 50.0123456 \} \quad (3-1)$$

The factored form polynomial is expanded into coefficient form. The roots of the expanded polynomial are then obtained and plotted. The roots obtained from the polynomial in coefficient form represented with 50 digits of precision, plotted in Fig. 3-1 using Mathematica, are a close representation of the roots of the

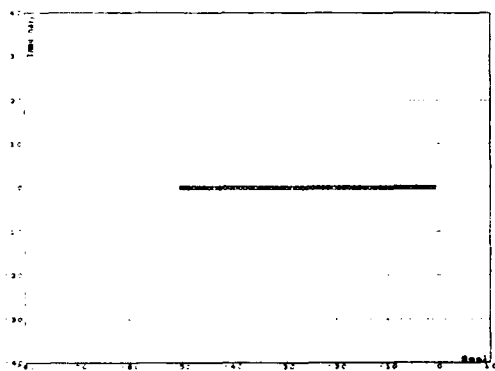


Fig. 3-1 Roots of high precision polynomial

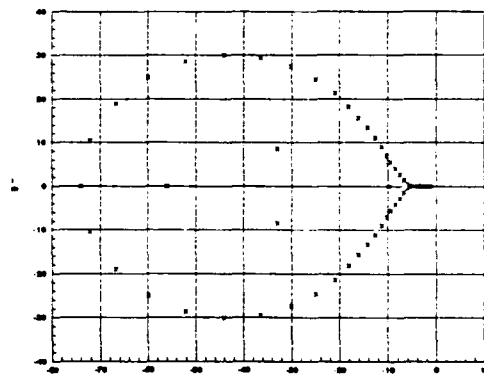


Fig. 3-2 Roots of standard precision polynomial

original factored form polynomial. With a 16 digit of precision representation, however, the root locations are displaced large distances from their original locations, shown as plotted by MATRIXx in Fig. 3-2.

The warping effect is accounted for by examining the polynomial in coefficient form expressed in terms of the factored form coefficients from which it is obtained.

In factored form, let:

$$p(s) = (s + r_1)(s + r_2)(s + r_3) \cdots (s + r_n) \quad (3-2)$$

Multiplying out the terms yields the coefficient form polynomial:

$$\begin{aligned} p(s) = & s^n + \left(\sum_{i=1}^n r_i \right) s^{n-1} + \left(\sum_{i \neq j} r_i r_j \right) s^{n-2} + \cdots \\ & + \left(\sum_{i=1}^n \prod_{j \neq i} r_j \right) s^1 + \left(\prod_{j=1}^n r_j \right) s^0 \end{aligned} \quad (3-3)$$

Each coefficient can now be examined to determine the number of digits required to represent it without error. Table 3-1 lists the number of digits required for each coefficient when using m digits of precision for each root. Using even one digit of precision in the roots of the 50th order polynomial, in coefficient form, in the example requires using 50 digits of precision to represent without rounding error the term resulting from $\prod_{j=1}^n r_j$. Note also that in this case only 1 or 2 digits of precision could be used to represent,

without rounding error, the term resulting from $\sum_{i=1}^n r_i$. The precision used for the roots in the example of

Coefficient	$\sum_{i=1}^n r_i$	$\sum_{i \neq j} r_i r_j$	$\sum_{i=1}^n \prod_{i \neq j} r_j$	$\prod_{j=1}^n r_j$
-------------	--------------------	---------------------------	-------------------------------------	---------------------

Table 3-1 Coefficient form precision requirements

Fig. 3-2 has $m = 8$ digits of precision and the machine precision is $n = 16$ digits. Therefore, the first

two non-unity coefficients $\sum_{i=1}^n r_i$ and $\sum_{i \neq j}^n r_i r_j$ are expressed without rounding error. The center of gravity

of the roots $\sum_{i=1}^n r_i$ therefore is not affected by rounding error. The product of roots, however, requiring

400 digits to be represented without rounding error is rounded to 16 digits of precision. For this example,

each rounded coefficient c_n is represented by a precise value a_n plus an error term e_n :

$$c_1 = a_1 + e_1 = \sum_{i=1}^n \prod_{j \neq i} r_j + e_1 \quad (3-4)$$

$$c_0 = a_0 + e_0 = \prod_{j=1}^n r_j + e_0 \quad (3-5)$$

In terms of the number of digits dropped, rounding error is most severe in the last term. The effect of the rounding error e_0 is analogous to the effect of turning up the gain in a unity feedback system with the polynomial as the denominator of the plant transfer function. This accounts for similarity between the pattern of migration of the roots and the migration of roots on a root locus plot:

The closed loop transmission of the system in the block diagram of Fig. 3-3 is:

$$\frac{e_0}{s^n + a_{n-1}s^{n-1} + \dots + (a_0 + e_0)} \quad (3-6)$$

Clearly, more than 16 digits of precision are needed to accurately represent the 50th order polynomial in coefficient form. Mathematica is the only package in which higher precision math can be used to solve this problem. The use of high precision math is most critical in the polynomial matrix inverse procedure,

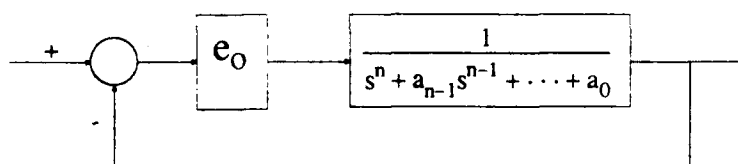


Fig. 3-3 Effect of largest error term

discussed in Sec. 3.9, where it is used to accurately compute the small difference of large numbers encountered during the matrix inverse and to accurately represent factored form polynomials which result from the matrix inverse.

A second feature critical to the development of the MIMO/QFT CAD package to be used by future thesis students is the availability of an interactive front end. No menu system can ever offer all the features that will be needed for future projects. Allowing the designer to stop the design process to make modifications to the CAD memory variables or to perform calculations using the CAD memory variables, allows any operations not performed inside the package to be handled outside the package using the Mathematica command line interface or by use of user-developed Mathematica programs. An interactive front end is available with MATRIXx, Matlab, Control-C, and Mathematica.

After considering the merits of the packages considered, Mathematica is chosen as the platform for the CAD package. This choice is motivated mainly by the numeric precision and symbolic capability available with Mathematica. The shortfall on execution speed associated with the interpreted execution is remedied by exporting computationally demanding tasks to 'C' subroutines, while the absence of control tools is addressed by developing the needed resources and adding them to the Mathematica development environment. These tools include a Nichols plot function, a Bode plot function, a generalized plot function, and polynomial manipulation functions.

3.3 Loading Plant Data

The first step in the design process is definition of the control problem. Loading the plant data has, in the past, been the most tedious and error-prone step in defining the problem. Automated loading of plant data in contractor format is implemented to eliminate these difficulties. Formats currently supported include:

- Genesis simulation format
- MATRIXx state space format
- Transfer function matrix loaded from memory

- Transfer function matrix loaded from console

3.3.1 Plant Model Parameters

Often, each plant model has associated with it a unique set of parameters. In an aircraft flight control problem, for example, each plant model may be associated with a particular flight condition. The flight condition could be defined, for example, by the vehicle altitude, Mach number, angle of attack, and weight. A distillation column, on the other hand, may have temperature and pressure as parameters.

The CAD package allows the designer to specify a set of parameters associated with the plant models. The parameter name, a memory variable name, a typical value, and a description are entered for each parameter. For example, the plant parameters for the Lambda URV are shown in Fig. 3-4 as listed by the CAD package (18:3-2). The designer may then specify the values of these parameters along with a comment to be stored along with each plant model when a plant model is loaded. An excerpt from a CAD package listing of plant models for the Lambda URV is shown as an example in Fig. 3-5. Nineteen plants were used to model the aircraft over the range of variation of the parameters shown in Fig. 3-4.

3.3.2 Structure of Plant Set Data

The set of plant matrices is stored in a list along with the associated plant parameter variable names defined in Fig. 3-4, the plant parameter values, and a comment string. In the excerpt of the listing of plant models in Fig. 3-5, four plant parameters, the associated values of the parameters, and a plant comment

Current List of Flight Condition Variables		
Variable	Nominal Value	Description
-----	-----	-----
Xcg	20	Center of gravity X-position (% of MAC)
U	100	Forward airspeed (kts)
q	15	Dynamic pressure (lbs/sq_ft)
w	200	Weight (lbs)

Fig. 3-4 Plant parameter listing

are shown for the first three flight conditions of the Lambda URV as stored in the plant set data structure.

Each plant matrix is stored in the form of a transfer function matrix in s.

The plant list, a 4th order structure, is illustrated below using Mathematica syntax:

```
{ { comment1, { { param11, val11 }, ..., { paramm1, valm1 } }, plant1 },
... { commentn, { { param1n, val1n }, ..., { parammn, valmn } }, plantn } } (3-7)
```

The form of the plant parameter list, a 2nd order structure, is illustrated below:

```
{ { paramName1, paramVarName1, paramTypical1, paramDescrip1 },
... { paramNamep, paramVarNamep, paramTypicalp, paramDescripp } } (3-8)
```

Once a plant has been loaded the transfer function elements can be displayed in factored form or plotted on a Bode plot. An example of the listing of the factored form transfer function of the (1,1) plant matrix element for plant case 1 is shown in Fig. 3-6. A Bode plot of the transfer functions for all plant cases is shown in Fig. 3-7. Alternatively, the Bode plot for any one of the plant cases could be plotted.

Current List of Plant Models			
Plant	Comments	Parameter	Value
-----	-----	-----	-----
#1	SSLAT1	Xcg	21.8
		U	110
		q	35.05
		W	181
#2	SSLAT2	Xcg	21.8
		U	110
		q	35.05
		W	215
#3	SSLAT3	Xcg	21.8
		U	110
		q	40.08
		W	181

Fig. 3-5 Plant model listing excerpt

Plant Case: 1 Element: {1, 1}	
Roots of Numerator	Roots of Denominator
-----	-----
0	0.01410828486
-0.9516270805 + 3.844813704 I	-0.9733554679 + 3.9181016 I
-0.9516270805 - 3.844813704 I	-0.9733554679 - 3.9181016 I
	-6.749157971

Fig. 3-6 Factored form transfer function

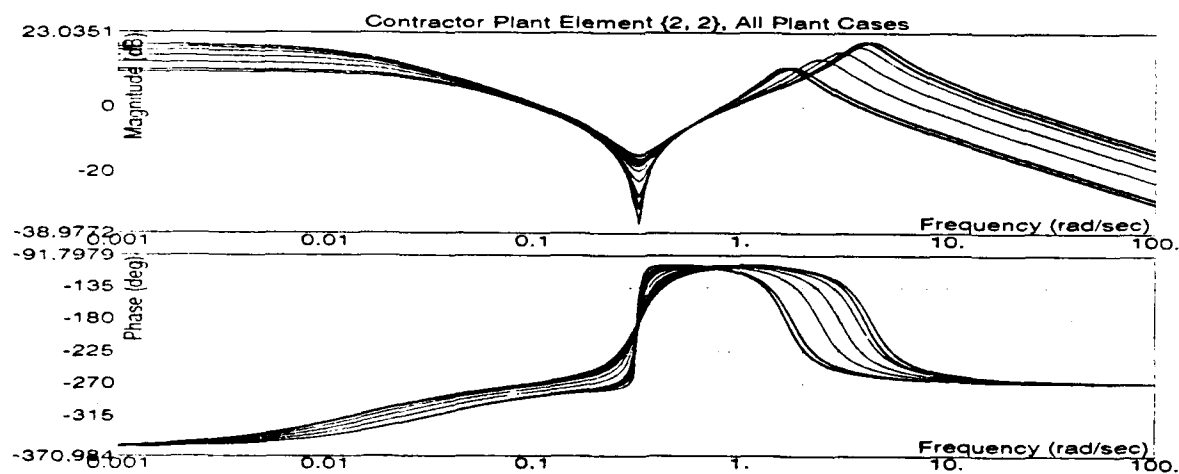


Fig. 3-7 Plant transfer function Bode plots

3.4 Loading of Sensor and Actuator Models

Dynamics of the sensors and actuators are specified in the frequency domain in the form of LTI transfer functions at the console in either coefficient or factored form. A unique LTI transfer function may be specified for the actuator used to drive each contractor plant input and for the sensor used to measure each plant output. The actuator transfer functions are stored as a list:

$$\text{actdyn} = \{ T_{\text{ACT}_1}, T_{\text{ACT}_2}, \dots, T_{\text{ACT}_l} \} \quad (3-9)$$

The sensor transfer functions are also stored as a list:

$$\text{sensdyn} = \{ T_{\text{SENS}_1}, T_{\text{SENS}_2}, \dots, T_{\text{SENS}_l} \} \quad (3-10)$$

It is assumed that there is no uncertainty in the actuator and sensor models and that LTI models can be used for the purposes of the QFT design. (If there is uncertainty then the actuators and sensors should be merged with the plant.)

3.5 Dimension of Control Problem

The dimension m of the control problem is the number of outputs that are to be controlled by the QFT controller. The dimension of the control problem determines the dimensions of the $m \times m$ square effective plant matrix, prefilter matrix, and compensator matrix, and must be defined before defining the sensor gain matrix, the weighting matrix, or the design specifications.

3.6 Sensor Gain Matrix

In some instances, a subset of plant outputs or a linear combination of plant outputs are to be controlled. In these cases, the designer can specify the appropriate sensor gain matrix $\underline{W}_{\text{SENS}}$. A block diagram illustrating the placement of the sensor gain matrix when forming the plant \underline{P} is shown in Fig. 2-3.

An entry is accepted at the console for each matrix element, one element at a time, in the format of a coefficient form or factored form polynomial where the coefficients, poles, zeros, and gain can be constants or any function of plant parameters defined in Fig. 3-4. Constants may be entered as elements of the sensor gain matrix $\underline{W}_{\text{SENS}}$ by specifying transfer functions with no poles or zeros but with the desired gain. Each

function entered for a transfer function is required to give a real number when evaluated at the "typical values" of the plant parameters. Each function entered for a pole or zero is required to give a real or a complex number when evaluated at the "typical values" of the plant parameters. If complex, the pole or zero is included in the transfer function as a complex conjugate pair. If a pole, zero, coefficient, or a gain gives a symbolic expression or cannot be evaluated, the designer is required to re-enter the expression. The "typical values" are thus required for each plant parameter for the purpose of validating that the elements of \underline{W}_{SENS} evaluate to gains or to transfer functions in s for the plant parameters of each plant case.

3.7 Weighting Matrix

A block diagram illustrating the insertion of the weighting matrix \underline{W} to form the effective plant \underline{P}_e is shown in Fig. 2-4. The elements of \underline{W} are defined by the designer in the same manner as for \underline{W}_{SENS} . The weighting matrix must result in an effective plant \underline{P}_e which is full rank and for which the diagonal elements are the same sign for all plant cases as $\omega \rightarrow \infty$. It is also desirable that the determinant of the effective plant be minimum-phase (17:Sec. 5-8). The first step in selecting the $l \times m$ weighting matrix for an $m \times l$ plant \underline{P} with more inputs than outputs to be controlled (l inputs and m outputs) is application of the Binet-Cauchy theorem to determine whether a minimum-phase plant can be achieved by a proper choice of weighting matrix elements. By the Binet-Cauchy theorem, a sufficient condition for the existence of a minimum-phase \underline{P}_e is that the determinant of some $m \times m$ submatrix of the elements of \underline{P} be minimum-phase (17:5-19). If such a submatrix can be identified from the $l!/l-m)! m!$ possible choices, then a minimum-phase effective plant is achievable. The CAD package presents, for inspection, a set of plant inputs which results in a minimum-phase \underline{P}_e . The designer then applies engineering judgment in choosing the weighting matrix elements. The weighting matrix selection procedure is an area of research in itself. For more information, consult (15).

The CAD program stores the weighting matrix elements in a two dimensional matrix:

$$wmatrix = [w_{11}, w_{12}, \dots, w_{1l}] \dots [w_{m1}, w_{m2}, \dots, w_{ml}] \quad (3-11)$$

3.8 Formation of Effective Plant Models

The effective plant transfer function matrices are formed, one for each plant case, after the weighting matrix, actuators, sensors, and sensor gain matrix are defined. For each of the J plant cases, the weighting matrix and sensor gain matrix, whose elements may be functions of plant parameters, are evaluated using the plant parameter values associated with each plant model.

Therefore, for each plant case i :

$$\underline{W}_i = [\underline{W}(\text{param}_1, \text{param}_2, \dots, \text{param}_p)] \begin{cases} \text{param}_1 = \text{paramVal}_1 \\ \text{param}_2 = \text{paramVal}_2 \\ \vdots \\ \text{param}_p = \text{paramVal}_p \end{cases} \quad (3-12a)$$

$$\underline{W}_{\text{SENS}_i} = [\underline{W}_{\text{SENS}}(\text{param}_1, \text{param}_2, \dots, \text{param}_p)] \begin{cases} \text{param}_1 = \text{paramVal}_1 \\ \text{param}_2 = \text{paramVal}_2 \\ \vdots \\ \text{param}_p = \text{paramVal}_p \end{cases} \quad (3-12b)$$

The effective plant is then formed from its component parts:

$$\underline{P}_{e_i} = \underline{P}_i \cdot \underline{W}_i = (\underline{W}_{\text{SENS}_i} \cdot \underline{T}_{\text{SENS}} \cdot \underline{P}_{\text{CONT}_i} \cdot \underline{T}_{\text{ACT}}) \cdot \underline{W}_i \quad (3-13)$$

When the effective plant is formed, a common denominator is factored out of each of the components: $\underline{W}_{\text{SENS}}$, $\underline{T}_{\text{SENS}}$, $\underline{P}_{\text{CONT}}$, $\underline{T}_{\text{ACT}}$, and \underline{W} . The resulting effective plant \underline{P}_e is thus obtained in the form of a numerator matrix $\underline{P}_{e_{\text{num}}}$ of transfer functions in s and a common denominator transfer function $P_{e_{\text{den}}}$, i.e.,

$$\underline{P}_e = \left(\frac{1}{P_{e_{\text{den}}}} \right) \cdot \underline{P}_{e_{\text{num}}} = [p_{ij}] \quad (3-14)$$

For each plant case i this equation is expressed as:

$$\underline{P}_{e_i} = \frac{1}{(P_{e_{\text{den}}})_i} \cdot (\underline{P}_{e_{\text{num}}})_i = [p_{ij}]_i \quad (3-15)$$

and where each element of $\underline{P}_{e_{\text{num}}}$ is a polynomial in factored form.

By factoring out a common denominator, the numerical difficulty of the matrix inverse required to form \underline{Q} is reduced by requiring a polynomial matrix inverse rather than a transfer function matrix inverse.

Once a weighting matrix is chosen, the sign of the m diagonal elements of \underline{P}_e must be checked as $\omega \rightarrow \infty$ for all plant cases. The CAD package allows the sign of all plant cases to be examined for $\omega \rightarrow \infty$.

in table form, as shown in Fig. 3-8. The sign of the effective plant elements can also be seen on the Bode angle plot for each plant transfer function element, provided the plot reaches a sufficiently high frequency. The default frequency range used by the CAD package is always sufficiently high.

Next, \underline{P}_e must be checked to insure that it is full rank. The CAD package allows the designer to list the determinant of \underline{P}_e , one plant case at a time, as shown in Fig. 3-9. A non-zero determinant for each plant case is indicative of full rank. The numerator of the determinant, because it becomes the numerator

High Frequency Signs of Diagonal Transfer Functions		
Plant Case	Channel 1	Channel 2
#1	+	-
#2	+	-
#3	+	-
#4	+	-
#5	+	-
#6	+	-

Fig. 3-8 Listing of effective plant signs

Determinant of Effective Plant Matrix		Plant Case: 1
Roots of Numerator of Det[Pe]		Roots of Denominator of Det[Pe]
-----		-----
0		0.01410828486
-0.1518880702		-0.9733554679 + 3.9181016 I
		-0.9733554679 - 3.9181016 I
		-6.199628022
		-6.749157886
		-9. + 6.244997998 I
		-9. - 6.244997998 I
		-50.
		-50.
Factored form gain multiplier: -2.4346665		

Fig. 3-9 Listing of effective plant determinants

of the equivalent plants q_{ij} , is examined since it determines the minimum- or non-minimum-phase character of the system (17:5-11).

If any of the above criteria are found to be unacceptable, the weighting matrix is revised, \underline{P}_e recomputed, and the tests applied once again. This iterative procedure may be repeated until an acceptable weighting matrix is obtained or the design process is aborted.

3.9 Inverse of \underline{P}_e

Once a satisfactory weighting matrix is determined, and \underline{P}_e is derived, the polynomial matrix inverse can then be performed from which the effective plants q_{ij} are obtained. Recalling that the effective plant is factored into a polynomial numerator matrix and a common denominator; i.e.,

$$\underline{P}_e = \left(\frac{1}{P_{e_{den}}} \right) \cdot \underline{P}_{e_{num}} \quad (3-16)$$

The inverse is performed using the Mathematica Inverse function:

$$\underline{P}_e^{-1} = \frac{\text{adj} \underline{P}_e}{\det \underline{P}_e} = [p_{ij}^*] = P_{e_{den}} \cdot \underline{P}_{e_{num}}^{-1} \quad (3-17)$$

The effective plants are then formed by inverting the elements p_{ij}^* :

$$Q = \frac{\det \underline{P}_e}{\text{adj} \underline{P}_e} = [q_{ij}] = \left\{ \frac{1}{p_{ij}^*} \right\} \quad (3-18)$$

The matrix elements are then tested to validate that the condition of diagonal dominance is satisfied:

(17:5-1)

1. For $m = 2$, must satisfy for all plant cases as $\omega \rightarrow \infty$ the equation:

$$|p_{11} p_{22}| > |p_{12} p_{21}| \quad (3-19)$$

2. For $m = 3$, must satisfy for all plant cases as $\omega \rightarrow \infty$ the equation:

$$\begin{aligned} |p_{11}^* p_{22}^* p_{33}^*| &> |p_{11}^* p_{23}^* p_{32}^*| + |p_{12}^* p_{21}^* p_{33}^*| + |p_{12}^* p_{23}^* p_{31}^*| \\ &+ |p_{13}^* p_{22}^* p_{31}^*| + |p_{13}^* p_{21}^* p_{32}^*| \end{aligned} \quad (3-20)$$

Essentially, these tests validate that the sign of the determinant of \underline{P}_c does not change over the plant cases. If diagonal dominance holds for all plant cases, then the first method design can be attempted. If, however, diagonal dominance does not hold for a plant case, then the QFT Method 2 (improved method) design must be attempted. If the results of this test are not satisfactory from the point of view of the designer, then the choice of weighting matrix \underline{W} is modified, and the \underline{Q} matrix recomputed. Iterative modification of the weighting matrix may be continued until a satisfactory \underline{Q} matrix is obtained or until the design is aborted.

Additional tools for examining the effective plants q_{ij} of the \underline{Q} matrix set include a Bode plot function and a transfer function display subroutine. The Bode plot for a \underline{Q} matrix element can be displayed for a specified plant case or for all plant cases together. Also, the CAD package allows the \underline{Q} matrix transfer function elements to be displayed in factored form for any selected plant case. The Bode plot for the entire plant set is particularly useful for displaying the variation in effective plant transmission as an aid in selecting template frequencies.

Before the effective plants q_{ij} are used for controller design, however, it is best to cancel equal or nearly equal pole-zero pairs from all \underline{Q} matrix transfer functions. In general, transfer functions of the \underline{Q} matrix returned by the polynomial matrix inverse procedure are high order compared to those of the effective plant \underline{P}_c from which they are computed.

The CAD package has a function which performs automatic cancellation, canceling pole-zero pairs based on a user specified ratio of the distance between the pole-zero pair to the distance of the zero from the origin:

$$\text{ratio} > \frac{|s_{\text{pole}} - s_{\text{zero}}|}{|s_{\text{zero}}|} \quad (3-21)$$

Since pole-zero pairs are cancelled in both the right-half and left-half planes, the designer must be sure to select a ratio small enough such that only nearly identical RHP pole-zero pairs introduced by the polynomial matrix inverse procedure are cancelled. Physically meaningful RHP pole-zero pairs must not be cancelled.

3.10 Applying the Improved Method

The improved method (QFT Method 2) can be applied for a 2x2 MIMO system using the MIMO QFT CAD package once one of the two loop transmissions has been designed. The improved method implementation uses Eqs. (2-16), (2-17), and (2-18) to form a new set of effective plants. An improved method plant is generated for each plant case, replacing the effective plant obtained from the polynomial matrix inverse procedure. Once the effective plants are replaced by the improved method effective plants, the design procedure for QFT Method 2 proceeds in the same manner as for a QFT Method 1 design. The designer proceeds with generating templates and bounds on the NC, and designs the compensator and prefilter based on the improved method effective plants.

3.11 Templates

Before the plant templates are generated, the CAD package requires the designer to specify the template frequencies. The specified frequencies are stored in a list:

$$flist = [freq_1, freq_2, \dots, freq_n] \quad (3-22)$$

Plant templates are generated, one for each template frequency, to outline the range of uncertainty in the transmission of the effective plant q_{ji} (or the effective plant q_{jic} when the improved method is used). Several steps are required to generate a template. First, the log magnitude and angle in degrees are evaluated for each of the plant cases and are placed in a list of template point locations. Next, the magnitude and angle of the center of the distribution of plant cases on the NC is calculated:

$$M_c = \frac{1}{J} \sum_{i=1}^J M_i \quad (3-23)$$

$$\phi_c = \frac{1}{J} \sum_{i=1}^J \phi_i \quad (3-24)$$

The polar angle of each plant case with respect to the center of the distribution is then calculated, and the list of J plant cases sorted based on the polar angle. A set of line segments are now drawn around the

outline without zig-zagging back and forth across the template. For the final step, all plant cases which can be enclosed in the interior of the template by a line segment connecting the two adjacent template points are dropped from the outline. This procedure is analogous to placing a rubber band around a set of nails, representing the template points, and retaining only the outermost plant points grabbed by the rubber band. For a more detailed discussion of the procedure for generating the convex template outline, with all interior angles less than 180° , see (1:43).

Formation of a convex template outline is but one approach to generating a template. An alternative approach used by Yaniv (22), the grid method, generates an array of plant points over the range of variation of plant transfer function parameters. This approach was not chosen for the MIMO/QFT CAD package due to the fact that the ranges of variation of plant transfer function parameters and correlation among plant transfer function parameters which vary is unknown in many control problems. In aircraft flight control problems, for example, unstructured uncertainty in the plant matrix is not easily modeled in terms of variation of plant transfer function parameters. Only a set of representative plant matrices may be available over the range of uncertainty of the aircraft. In addition to grid method another alternative approach was developed by Bailey (4) but was not used for the MIMO/QFT CAD package because it also requires the range and correlation of variation of plant transfer function parameters be known. Formation of the convex template outline is therefore used to generate templates for the MIMO/QFT CAD package.

3.12 Choice of Nominal Plant

In addition to generating the templates, a nominal plant transmission is chosen. In general the nominal plant need not be chosen from the set of plant cases. For an analog QFT design, however, the package requires the designer to choose from the set of J effective plants. While any plant case can be chosen as the nominal, an accepted practice is to select the plant case at the lower left corner of the templates whenever possible.

The package allows the designer to display a plot of the numbered plant cases for a user specified template frequency. The designer chooses a nominal plant from the set of plant cases. A chart of the

templates is then displayed with the nominal point emphasized, as shown in Fig. 3-10. If the choice of nominal point is not satisfactory, another nominal point may be selected.

Once a nominal plant case is chosen, the template is shifted such that the nominal plant case is located at (0deg,0dB) on the NC:

$$M_i = M_i - M_{\text{nominal}} \quad \text{for all } i \text{ in } J \quad (3-25a)$$

$$\phi_i = \phi_i - \phi_{\text{nominal}} \quad \text{for all } i \text{ in } J \quad (3-25b)$$

This can be done because only the location of the plants relative to each other is of importance when generating bounds. The template can then be shifted on the NC such that the nominal plant is at a desired location simply by adding the coordinates of the desired location to all plant cases. In this way, the template can be conveniently placed at any desired location on the NC.

3.13 Specifications

The design specifications must be defined before bounds are generated and any compensator or prefilter elements are designed. Specifications for gamma bounds are optional, and may be defined when using the improved method.

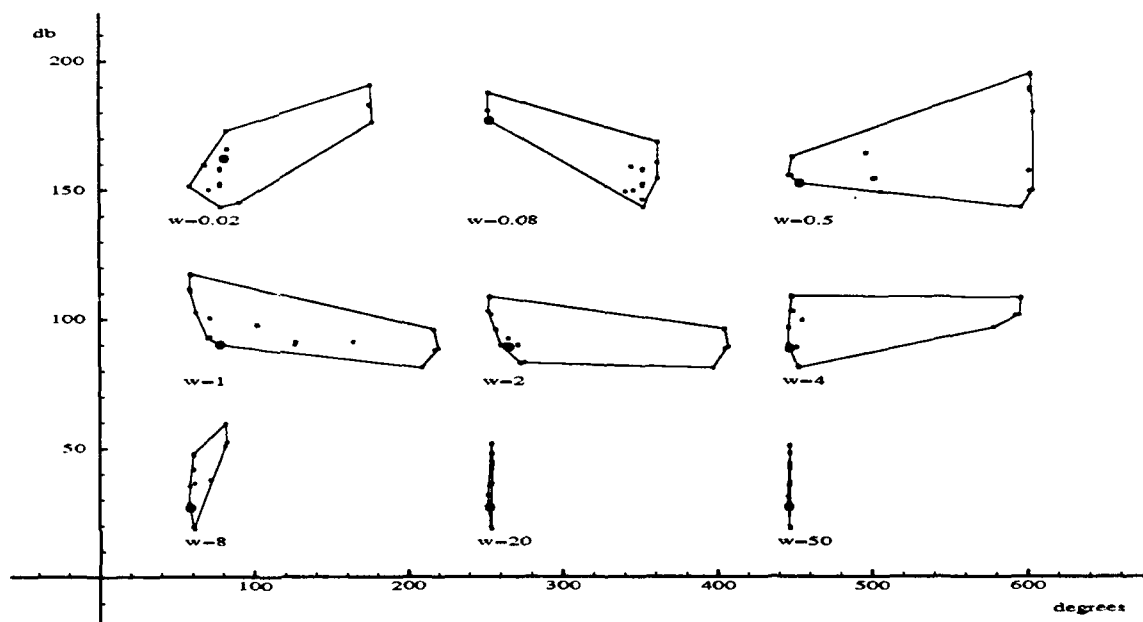


Fig. 3-10 Templates with nominal point emphasized

3.13.1 Stability Specifications

A stability margin must be specified for each row of MISO loops. As discussed in Sec. 2.5.2, the CAD package allows the stability margin to be specified in terms of the gain margin g_m , the phase margin angle γ , or the corresponding M_L contour. Any one of these three specifications can be determined from any of the others. This is illustrated graphically on the NC shown in Fig. 2-10. Only the M_L contour stability specification is stored in memory.

If g_m or γ are given, then M_L in dB can be computed using the equations:

$$M_L = 20 \log_{10} \left(\frac{1}{\sqrt{1 - \cos^2(\gamma - 180^\circ)}} \right) \quad (3-26)$$

$$M_L = 20 \log_{10} \left(\frac{10^{-g_m/20}}{1 + 10^{-g_m/20}} \right) \quad (3-27)$$

Conversely, if M_L is given in decibels:

$$g_m = \left(\frac{1 - M_m^2}{1 - M_m^{-1}} \right) \quad (3-28)$$

$$\gamma = 180^\circ - \cos^{-1} \left(\sqrt{1 - M_m^2} \right) \quad (3-29)$$

where the closed loop magnitude associated with the M_L contour is:

$$M_m = 10^{(M_L/20)} \quad (3-30)$$

Equations (3-26) and (3-29) are derived in Sec. 3.14.1 in which plotting of stability bounds is discussed.

3.13.2 Performance Specifications

Performance tolerances must be defined for each input-output response relationship. These tolerances are specified in the frequency domain, and are defined in transfer function form at the console. An array of Bode magnitude plots can then be plotted for the performance tolerances. The transfer functions are then stored, as entered, using the following structure:

$$\begin{aligned} \text{pspecs} = & \{ \{ \{ b_{11}, a_{11} \}, \dots, \{ b_{1m} \} \}, \\ & \{ \{ b_{m1} \}, \dots, \{ b_{mm}, a_{mm} \} \} \} \end{aligned} \quad (3-31)$$

3.13.3 Gamma Bound Specifications

The gamma specifications are optional, and may be defined when using the improved method. Gamma bounds provide insight into the loop shaping procedure which allows the designer to avoid unnecessarily introducing new right-half-plane poles into the equivalent plants of remaining channels. Placing additional restrictions on the compensator currently being designed may substantially reduce the difficulty of performance bounds on loop transmissions yet to be designed. The improved method requires the derivation of the effective q plant transfer function, i.e. for a 2×2 system in which the compensator for channel 1 has been designed:

$$q_{22e} = \frac{q_{22}(1+L_1)}{1 - \gamma_{12} + L_1} \quad (3-32)$$

By proper design of the compensator g_1 , new RHP poles are not introduced in q_{22e} . In order to plot the gamma bound for channel 1, a minimum value is specified for the magnitude of the denominator of Eq. (3-32).

$$M_{\gamma_1} \leq |1 - \gamma_{12} + L_1| \quad (3-33)$$

For the case in which the compensator for channel 2 is designed first, the requirement on channel 2 is:

$$M_{\gamma_2} \leq |1 - \gamma_{21} + L_2| \quad (3-34)$$

For a 2×2 system γ_{12} and γ_{21} are defined as:

$$\gamma_{12} = \gamma_{21} = \frac{p_{12} p_{21}}{p_{11} p_{22}} \quad (3-35)$$

The minimum value for each channel is stored in a list of the form:

$$\text{gspecs} = \{ \text{gspecs}_1, \dots, \text{gspecs}_m \} \quad (3-36)$$

At the present time, the CAD package can generate gamma bounds only for a 2×2 MIMO problem.

3.14 Generating Bounds

This section provides a detailed discussion of the methods used by the MIMO/QFT CAD package to generate stability, disturbance, gamma, and tracking bounds plotted on the NC. Methods for generating bounds have also been developed by during previous research efforts. Those interested in alternative approaches to generating bounds may consult Cole (9) and Bailey (4).

3.14.1 Stability Bounds

A stability bound is plotted for each template. Stability bounds constrain the maximum closed-loop transmission with unity gain prefilter to have a bounded magnitude:

$$\left| \frac{g_i(q_{ii})_l}{1 + g_i(q_{ii})_l} \right| \leq M_L \quad \text{for } l = 1, 2, \dots, J \quad (3-37)$$

The bound is plotted for a given frequency by plotting the path of the nominal point while traversing the M_L contour with the template generated for that frequency tangent to the M_L contour at all times. To do this, the software must be able to determine the point of tangency on the outline of the template and the location of the template, when tangent to the M_L contour at that point, as the M_L contour is traversed. To accomplish this task, an equation is derived which gives the NC magnitude M to which a template point at the NC phase angle ϕ must be shifted to be in contact with the M_L contour (13). The use of this equation to plot points on the stability bound is then discussed.

For a given point along the outline of the template, at a given angle ϕ on the NC, an equation can be derived for the open loop transmission magnitude M required for this point to be in contact with the M_L contour (13). The derivation begins with the requirement that the magnitude of the closed loop transmission be equal to the magnitude M_m associated with the M_L contour for the open loop transmission L where $M_m = 10^{M_L/20}$ and M_L is given in decibels:

$$M_m = \left| \frac{L}{1 + L} \right| \quad (3-38)$$

Taking the magnitude of the numerator and denominator, with $L = M e^{j\phi}$ yields:

$$\begin{aligned}
M_m &= \frac{M}{|1 + M \cos(\varphi) + jM \sin(\varphi)|} \\
&= \frac{M}{\sqrt{(1 + M \cos(\varphi))^2 + (M \sin(\varphi))^2}}
\end{aligned} \tag{3-39}$$

Squaring both sides and multiplying both sides by the denominator yields:

$$M_m^2 \left[(1 + M \cos(\varphi))^2 + (M \sin(\varphi))^2 \right] = M^2 \tag{3-40}$$

Multiplying out the left side and using the identity $\sin^2(\varphi) + \cos^2(\varphi) = 1$ yields:

$$M_m^2 \left[1 + 2 M \cos(\varphi) + M^2 \sin^2(\varphi) \right] = M^2 \tag{3-41}$$

Subtracting M^2 from both sides and multiplying out terms yields a quadratic equation in M :

$$(M_m^2 - 1) M^2 + [2 M_m^2 \cos(\varphi)] M + M_m^2 = 0 \tag{3-42}$$

The quadratic equation has two solutions for the open loop transmission magnitude M :

$$\begin{aligned}
M &= \frac{-2 \cos(\varphi) M_m^2 \pm \sqrt{4 \cos^2(\varphi) M_m^4 - 4 M_m^2 (M_m^2 - 1)}}{2 (M_m^2 - 1)} \\
&= \frac{-\cos(\varphi) \pm \sqrt{\cos^2(\varphi) - (1 - M_m^2)}}{(1 - M_m^2)}
\end{aligned} \tag{3-43}$$

In addition, an equation must be derived for the range of angles for which real solutions for Eq. (3-43) exist. This range is then used to determine the range of angles over which the stability bound exists. A real solution for Eq. (3-43) exists when:

$$\cos^2(\varphi) - (1 - M_m^2) \geq 0 \tag{3-44}$$

The equation below can be solved for the angles which bound the range of real solutions:

$$\cos^2(\varphi) - (1 - M_m^2) = 0 \tag{3-45}$$

The solution to this equation, for a given M_m , yields two values for $\cos(\varphi)$, thus rearranging and taking the square root of both sides:

$$\cos(\varphi) = \pm \sqrt{1 - M_m^2} \tag{3-46}$$

The solution with the negative sign is chosen since the M_L contour exists for some range of phase angles between -270° and -90° on the NC, in which $\cos(\phi)$ is negative:

$$\cos(\phi) = -\sqrt{1 - M_m^2} \quad (3-47)$$

Since $\cos(\phi) = \cos(-\phi)$ taking the inverse cosine yields two solutions for ϕ :

$$\phi = \pm \cos^{-1} \left(-\sqrt{1 - M_m^2} \right) \quad (3-48)$$

The two solutions for ϕ bound the range of angles over which the M_L contour exists on the NC once reflected into the $(-360^\circ, 0^\circ)$ angle range by adding $\pm k 360^\circ$ where k is an integer. The inverse cosine function in Mathematica, however, returns only one of these two solutions, an angle between 0° and $+180^\circ$, which is:

$$\phi = +\cos^{-1} \left(-\sqrt{1 - M_m^2} \right) \quad (3-49)$$

The angle range for which the M_L contour exists, therefore, is:

$$\phi_{M_m \min} \leq \phi \leq \phi_{M_m \max} \quad (3-50)$$

Where:

$$\phi_{M_m \min} = +\cos^{-1} \left(-\sqrt{1 - M_m^2} \right) - 360^\circ \quad (3-51a)$$

$$\phi_{M_m \max} = -\cos^{-1} \left(-\sqrt{1 - M_m^2} \right) \quad (3-51b)$$

Equation (3-51b), which gives the phase angle of the right edge of the M_L contour, is used to derive an expression for the phase margin angle γ associated with the M_L contour. Using the fact that $\gamma = 180^\circ + \phi_{M_m \max}$ where $-180^\circ < \phi_{M_m \max} < -90^\circ$ as seen in Fig. 2-10 on page 2-8:

$$\gamma = 180^\circ - \cos^{-1} \left(\sqrt{1 - M_m^2} \right) \quad (3-52)$$

Solving Eq. (3-52) for M_m and using the fact that $M_L = 20 \log_{10}(M_m)$ yields an expression for the M_L contour associated with the phase margin stability specification γ :

$$M_L = 20 \log_{10} \left(\frac{1}{\sqrt{1 - \cos^2(\gamma - 180^\circ)}} \right) \quad (3-53)$$

Equations (3-52) and (3-53) are given as Eqs. (3-29) and (3-26) respectively in Sec. 3.12.1 which lists the equations used by the CAD package to convert among the various stability specifications. The application of Eqs. (3-43) and (3-50) to plotting the stability bound is now discussed.

A template with the nominal point at a fixed NC angle, when tangent to the M_L contour, can be tangent at only one point on the outline of the template. Because the point of tangency is unknown a-priori, Eq. (3-43) for M cannot be used directly to determine the position at which the template is tangent to the M_L contour. Equation (3-43) is used, however, to search for the point of tangency. The location of the points of tangency on the template when tangent above and tangent below the M_L contour are addressed separately.

To locate the point of tangency above the M_L contour, the entire outline of the template is searched. The point on the template which requires the largest open loop gain to bring the template into contact with the M_L contour is the point of tangency, as illustrated in Fig. 3-11. Note that any increase in open loop gain causes the template to lose contact with the M_L contour. The search routine, by applying Eq. (3-43) around the outline of the template, locates this point of tangency by searching for the point which requires the largest M to contact the M_L contour.

Before the CAD package begins the search, the range of angles in Eq. (3-50) over which the M_L contour exists is calculated using Eqs. (3-51a) and (3-51b). This range is used first to calculate the range of angles over which the stability contour exists, and second, to eliminate from the search any portion of the outline of the template which is to the right or left of the M_L contour on the NC and therefore cannot

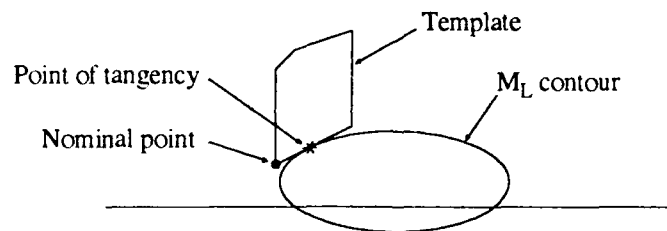


Fig. 3-11 Upper point of tangency with stability bound

come into contact with it by moving the template up or down. The range of angles occupied by the stability contour is calculated as follows:

$$\Phi_{SB_{max}} = \Phi_{M_{max}} - \Phi_{TEMPLATE_{min}} \quad (3-54a)$$

$$\Phi_{SB_{min}} = \Phi_{M_{min}} - \Phi_{TEMPLATE_{max}} \quad (3-54b)$$

The angles $\Phi_{TEMPLATE_{min}}$ and $\Phi_{TEMPLATE_{max}}$ are illustrated on the template shown in Fig. 3-12 and the angles $\Phi_{SB_{min}}$, $\Phi_{SB_{max}}$, $\Phi_{M_{min}}$ and $\Phi_{M_{max}}$ are illustrated on the NC in Fig. 3-13. The stability bound is then plotted, beginning with an angle just less than $\Phi_{SB_{max}}$, in two degree intervals, until the end of the stability bound angle range $\Phi_{SB_{min}}$ is reached. A graphical illustration of the stability bound angle range is shown in Fig. 3-13.

The maximum value of M is found by applying a binary search to each line segment of the template outline, one at a time, and retaining the overall maximum value found. An 8 iteration binary search is performed on each line segment by applying Eq. (3-43) at 8 test points along the segment. The final test point of the 8 iteration binary search comes to within $1/512$ of the segment length of the true location of the maximum M. An 8 iteration binary search was selected so the search would come to within less than one degree of the true location of the maximum M even for a template segment which traverses 360° of the NC. The greater of the values of M obtained at the indexed endpoint of the segment and at the last test point of the binary search is taken to be the maximum value for M over the entire segment. For more information on binary search, see reference (28).

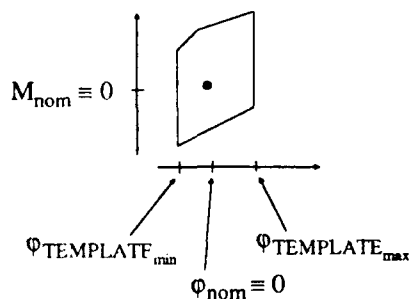


Fig. 3-12 Template quantities of interest

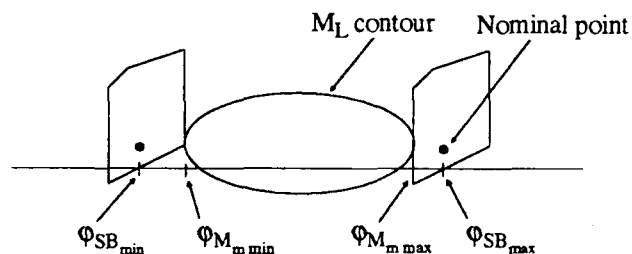


Fig. 3-13 Stability bound range

During the binary search, Eq. (3-43) is applied at test points on each template segment. The following discussion illustrates the method by which this is done, using as an example the arbitrary test point (ϕ_t, M_t) located on a template segment as shown in Fig. 3-14. Recall that the template is shifted such that the nominal point is at $(\phi_{nom}, M_{nom}) = (0, 0)$ as shown in Fig. 3-14. It is the shifted template that is available in memory when generating the stability bound. For a stability bound point at angle ϕ_{SB} on the NC, see Fig. 3-15, the search iteration shifts the template such that the nominal point is located at (ϕ_{SB}, M_{SB_i}) . The value M_{SB_i} is the NC magnitude to which the nominal must be shifted for the test point to be in contact with the upper portion of the M_L contour (see Fig. 3-15). The test point is shifted along with the nominal point to $(\phi_t + \phi_{SB}, M_t + M_{SB_i})$. The location to which the test point is shifted can then be calculated by applying Eq. (3-43) with $\phi = \phi_t + \phi_{SB}$. Two solutions are returned for the open loop transmission magnitude M required at the test point to be in contact with the M_L contour. The larger solution for M is taken, where $M = M_t + M_{SB}$, since the template must be in contact with the upper portion of the M_L contour during this search. The location to which the nominal point must be shifted, the quantity the search seeks to maximize, is then calculated from:

$$M_{SB_i} = M - M_t \quad (3-55)$$

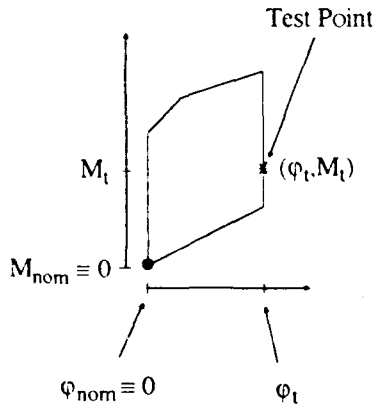


Fig. 3-14 Test point on template

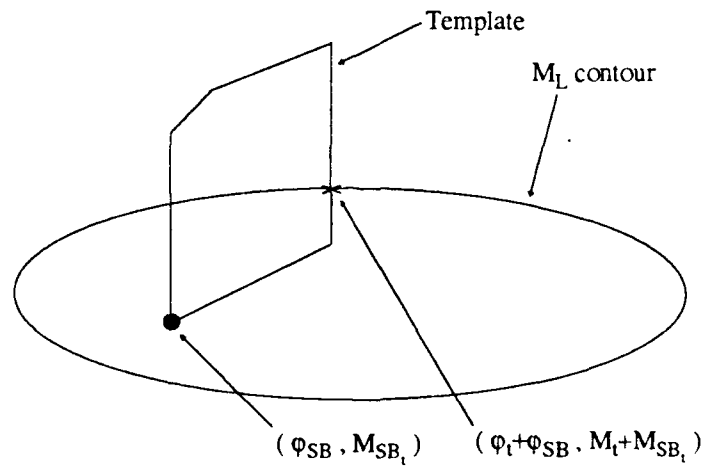


Fig. 3-15 Stability bound search test point on NC

If the test point happens to be the point of tangency, having the maximum possible M_{SB_i} associated with it, then $M_{SB} = M_{SB_i}$ is achieved and a stability bound point is plotted at (ϕ_{SB}, M_{SB}) .

To locate the point of tangency at which the template is tangent to and below the M_L contour, the entire outline of the template is searched again. The point on the template which requires the lowest open loop gain to bring the template into contact with the M_L contour at that point is the point of tangency, as illustrated in Fig. 3-16. The search routine, by applying Eq. (3-43) around the outline of the template, locates this point of tangency by searching for the minimum value of M . The search routine is performed using exactly the same procedure as that used to locate a point on the upper stability bound contour, except that a minimum value of M_{SB_i} is determined.

3.14.2 Disturbance Bounds

Disturbance bound are plotted for each template, one for each off-diagonal MISO loop in row i of the MISO loops for which the compensator is designed. By satisfying the disturbance bound on the NC the open loop transmission L_i obeys the constraint at each template frequency:

$$|t_{ij}| = |d_{ij}| \left| \frac{q_{ij}}{1 + L_i} \right| \leq b_{ij} \quad \text{for } i \neq j \quad (3-56)$$

where:

$$d_{ij} = - \sum_{k \neq i} \frac{t_{kj}}{q_{ik}} \quad (3-57)$$

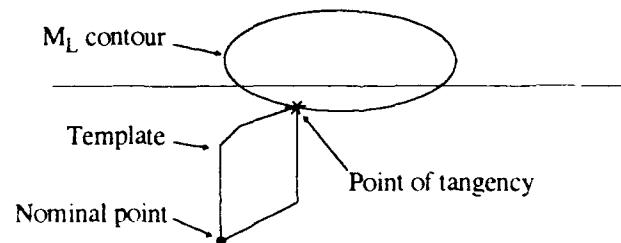


Fig. 3-16 Lower point of tangency with stability bound

The specifications and the plant uncertainty dictate the magnitude of the disturbance $|d_{ij}|$. This upper bound on the maximum disturbance magnitude for each plant case l in the set of J plants is given by:

$$(|d_{ij}|_{\max})_l = \sum_{k \neq i} \frac{b_{kj}}{|q_{ijk}|_l} \quad (3-58)$$

The most extreme upper bound on $|d_{ij}|$ for all the J plant cases is then:

$$|d_{ij}|_{\max} = [(|d_{ij}|_{\max})_l]_{\max \text{ over } l} \quad (3-59)$$

Based on Eqs. (3-56) and (3-59) a lower bound is placed on $|1 + L_i|$, i.e.:

$$|1 + L_i| \geq \frac{|d_{ij}|_{\max} |q_{ii}|}{b_{ij}} \quad (3-60)$$

By making the substitution $L_i = \frac{1}{m}$ as in Sec. 2.10.2, the above equation is transformed such that bounds can be plotted on the inverse NC. Thus, Eq. (2-24) is repeated below:

$$\left| \frac{m}{1+m} \right| \leq \frac{b_{ij}}{|q_{ii}| |d_{ij}|_{\max}} \quad (3-61)$$

Simplifying by using the symbol M_D to designate the inverse NC constant magnitude contour:

$$\left| \frac{m}{1+m} \right| \leq M_D \quad \text{where } M_D = \frac{b_{ij}}{|q_{ii}| |d_{ij}|_{\max}} \quad (3-62)$$

In general, M_D is different for different plant cases since q_{ii} is different for different plant cases. Equation (3-62) can be utilized to determine the disturbance bounds for m as shown in Fig. 3-17. Since

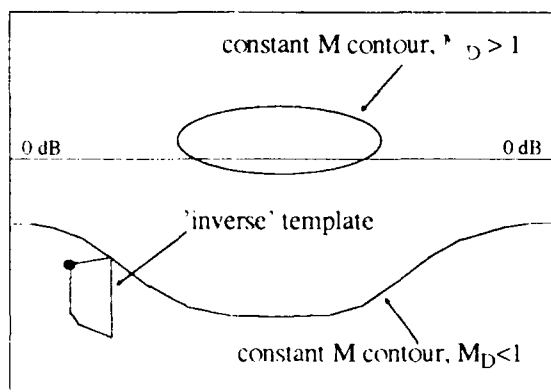


Fig. 3-17 Standard Nichols chart

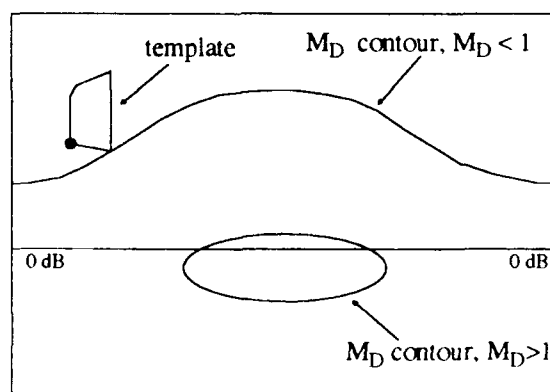


Fig. 3-18 Inverse Nichols chart

the disturbance bounds are desired for L_{i0} then from this point forward the inverse NC is utilized whose constant magnitude contour is referred to as the M_D contour.

Equation (3-62) is used to plot bounds on L_{i0} on the inverse NC as shown in Fig. 3-18. To accomplish this task, an equation is derived which gives the location of the constant magnitude contour in dB on the inverse NC for a specified phase angle of L_{i0} and value of M_D (13). Based on the equation for the location of the constant magnitude contour, a search is implemented to locate the template point on the outline of the template for which the most extreme disturbance bound point results. The quantity M_D is re-evaluated based on q_{ii} for each template point examined by the search routine. The search algorithm therefore takes into account correlation between the right-hand-side and left-hand-side of Eq. (3-61) due to correlation between q_{ii} and $m = \frac{1}{L_i} = \frac{1}{g; q_{ii}}$.

The algorithm used to search the template outline when plotting disturbance bounds is identical to that used when plotting stability bounds. However, for a given point along the outline of the template, at a given angle on the NC, a different equation is used to determine the open loop transmission magnitude required for the test point to be in contact with the M_D contour of the inverse NC.

The first equation derived gives the location of the constant magnitude contour in dB on the inverse NC for a specified value of M_D and phase angle of m (13). The derivation begins with the requirement on m :

$$\left| \frac{m}{1+m} \right| \leq M_D \quad (3-63)$$

Taking the magnitude of the left-hand-side, with $m = M_{inv} e^{j\phi_{inv}}$ yields:

$$\begin{aligned} M_D &= \frac{M_{inv}}{\sqrt{1 + M_{inv} \cos(\phi_{inv}) + jM_{inv} \sin(\phi_{inv})}} \\ &= \frac{M_{inv}}{\sqrt{[1 + M_{inv} \cos(\phi_{inv})]^2 + [M_{inv} \sin(\phi_{inv})]^2}} \end{aligned} \quad (3-64)$$

Squaring both sides and multiplying both sides by the denominator yields:

$$M_D^2 \left[(1 + M_{inv} \cos(\varphi_{inv}))^2 + (M_{inv} \sin(\varphi_{inv}))^2 \right] = M_{inv}^2 \quad (3-65)$$

Multiplying out the left-hand-side, and substituting $\sin^2(\varphi) + \cos^2(\varphi) = 1$ yields:

$$M_D^2 \left[1 + 2 M_{inv} \cos(\varphi_{inv}) + M_{inv}^2 \sin^2(\varphi_{inv}) \right] = M_{inv}^2 \quad (3-66)$$

Subtracting M_{inv}^2 from both sides and multiplying out terms yields a quadratic equation in M_{inv} :

$$(M_D^2 - 1) M_{inv}^2 + [2 M_D^2 \cos(\varphi_{inv})] M_{inv} + M_D^2 = 0 \quad (3-67)$$

The solutions to the quadratic equation is now written as:

$$\begin{aligned} M_{inv} &= \frac{-2 \cos(\varphi_{inv}) M_D^2 \pm \sqrt{4 \cos^2(\varphi_{inv}) M_D^4 - 4 M_D^2 (M_D^2 - 1)}}{2 (M_D^2 - 1)} \\ &= \frac{-\cos(\varphi_{inv}) \pm \sqrt{\cos^2(\varphi_{inv}) - (1 - M_D^2)}}{(1 - M_D^2)} \end{aligned} \quad (3-68)$$

Note, however, that this requirement applies to $\mathbf{m} = (\mathbf{g}_i \mathbf{q}_{ii})^{-1}$, not to $\mathbf{L}_i = \mathbf{g}_i \mathbf{q}_{ii}$, as desired. By making the substitution $M = M_{inv}^{-1}$ and $\varphi = -\varphi_{inv}$, the solution is now written to apply to $\mathbf{g}_i \mathbf{q}_{ii}$, where $\mathbf{g}_i \mathbf{q}_{ii} = M e^{i\varphi}$.

$$M = \frac{(1 - M_D^2)}{-\cos(\varphi) \pm \sqrt{\cos^2(\varphi) - (1 - M_D^2)}} \quad (3-69)$$

Two cases are now considered: those for which $M_D > 1$, and those for which $M_D < 1$.

For the case of $M_D < 1$, one solution to Eq. (3-69) exists for a template point at the NC phase angle φ corresponding to the NC magnitude required for the template point to contact the M_D contour which runs across the NC. A disturbance bound generated using an M_D contour with $M_D < 1$ is an open contour running across the entire angle range of the NC. Choosing the positive sign in the denominator of Eq. (3-69) results in a positive gain M , which is the desired solution:

$$M = \frac{(1 - M_D^2)}{-\cos(\varphi) + \sqrt{\cos^2(\varphi) - (1 - M_D^2)}} \quad \text{for } M_D < 1 \quad (3-70)$$

For the case of $M_D > 1$, two solutions exist over a limited range of angles on the NC. This case is analogous to the pair of solutions obtained when using Eq. (3-43) to plot stability bounds. The derivation of the range of angles for which the solution exists is carried out using exactly the same steps used to obtain the range for the M_L contour, given by Eqs. (3-50) and (3-51). The range derived for the M_D contour is shown below:

$$\phi_{D_{\min}} \leq \phi \leq \phi_{D_{\max}} \quad (3-71)$$

Where:

$$\phi_{D_{\min}} = +\cos^{-1}\left(-\sqrt{1-M_D^2}\right) - 360^\circ \quad (3-72a)$$

$$\phi_{D_{\max}} = -\cos^{-1}\left(-\sqrt{1-M_D^2}\right) \quad (3-72b)$$

A disturbance bound generated using an M_D contour, with $M_D > 1$, is a closed contour on the NC. Both solutions of Eq. (3-69) for M exist provided the angle lies in the range of the M_D contour:

$$M = \frac{(1 - M_D^2)}{-\cos(\phi) \pm \sqrt{\cos^2(\phi) - (1 - M_D^2)}} \quad \text{for } M_D > 1 \quad (3-73)$$

The case of $M_D = 1$ is not considered, since a small value can be subtracted from M_D allowing it to be handled as if $M_D < 1$.

3.14.3 Gamma Bounds

Gamma bounds are generated based on Eq. (3-74), one for each template, and one for each row of MISO loops, other than the current row, yet to be designed (13). Recall that it is desired that the denominator of the effective plant, to be calculated by applying the improved method, not become smaller than a specified minimum value despite plant uncertainty, i.e.:

$$|1 + g_i q_{ji} - \gamma_{ij}| \geq k \quad (3-74)$$

Equation (3-74) is the requirement associated with row j of the MISO loops when gamma bounds on L_i are generated. The constraint this inequality places on the open loop transmission $L_i = g_i q_{ji} = M e^{j\phi}$ is illustrated on the polar plots shown in Figs. 3-19 and 3-20. The polar plots illustrate vector addition of

the quantities $1-\gamma_{ij}$ and several \mathbf{L}_i vectors along with a circle of radius k centered at the origin. The circle bounds the forbidden region which must not enclose the vector sum $1 + \mathbf{g}_{ij} \mathbf{q}_{ij} - \gamma_{ij}$.

In Fig. 3-19, the case for which a closed gamma bound is generated, it can be seen that for a limited range of phase angles $\varphi_a \leq \varphi \leq \varphi_b$ a range of unacceptable transmission magnitudes $M_a(\varphi) \leq M \leq M_b(\varphi)$ places the vector sum $1 - \gamma_{ij} + M e^{j\varphi}$ inside the forbidden region. The corresponding locus of $\mathbf{L} = M e^{j\varphi}$ for which the circle of radius k is violated is enclosed by the closed gamma bound on the NC in Fig. 3-21. An equation for $M_a(\varphi)$ and $M_b(\varphi)$ is derived in this section (13).

In Fig. 3-20, the case for which a gamma bound exists across the NC, it can be seen that for a range of unacceptable transmission magnitudes $0 \leq M \leq M_b(\varphi)$ at a given phase angle φ for which the vector $\mathbf{L} = M e^{j\varphi}$ enters the forbidden region of the polar plot. For each phase angle φ , the transmission magnitude M must be large enough that the vector sum $1 - \gamma_{ij} + M e^{j\varphi}$ reaches outside the forbidden region on the polar plot. For this case an open gamma bound exists on the NC shown in Fig. 3-22 bounding from above the locus of unacceptable transmission magnitudes. An equation for $M_b(\varphi)$ is derived in this section (13).

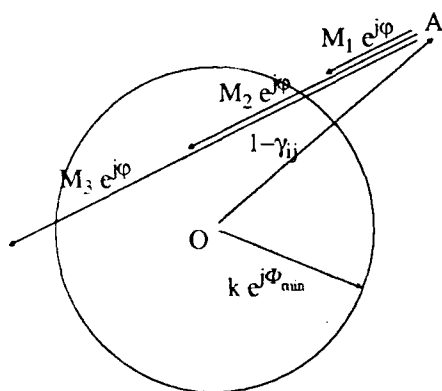


Fig. 3-19 Closed gamma bound vector sum

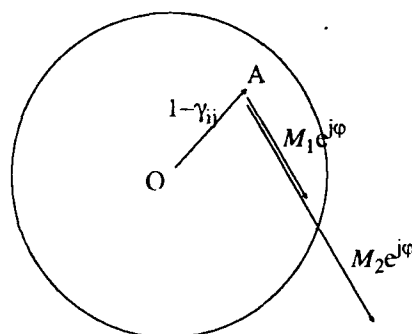


Fig. 3-20 Open gamma bound vector sum

The examples in Figs. 3-19 and 3-20 illustrate the process by which a gamma bound is generated for a single plant transmission. This process is now extended to address the fact that a region of plant uncertainty exists as defined by the template. Initially, it is assumed that gamma is fixed. The process of computing gamma bounds is then generalized to account for the fact that gamma varies among the plant cases.

Assuming for a moment that γ_{ij} is fixed, the range limits of the transmission magnitude $M_a(\varphi)$ and $M_b(\varphi)$ are derived in terms of the transmission phase angle φ beginning with the inequality:

$$|1 - \gamma_{ij} + g_i q_{ij}| \geq k \quad (3-75)$$

The bound on $g_i q_{ij}$ exists where the inequality is about to be violated:

$$|1 - \gamma_{ij} + g_i q_{ij}| = k \quad (3-76)$$

Substituting $1 - \gamma_{ij} = \alpha_1 + j\alpha_2$ and $g_i q_{ij} = M e^{j\varphi}$ yields:

$$|\alpha_1 + j\alpha_2 + M [\cos(\varphi) + j\sin(\varphi)]| = k \quad (3-77)$$

Taking the magnitude and squaring both sides:

$$[\alpha_1 + M \cos(\varphi)]^2 + [\alpha_2 + M \sin(\varphi)]^2 = k^2 \quad (3-78)$$

Multiplying out the equation and collecting like terms in M yields the quadratic equation:

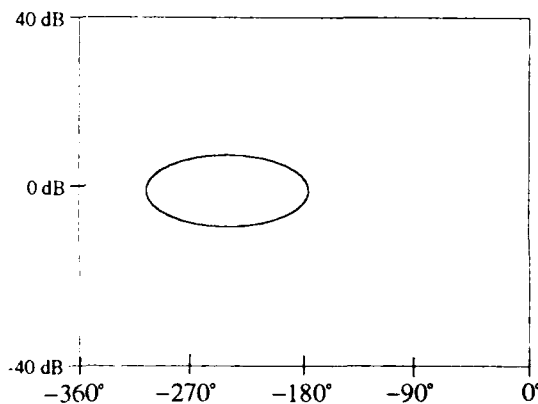


Fig. 3-21 Closed Gamma Bound on NC

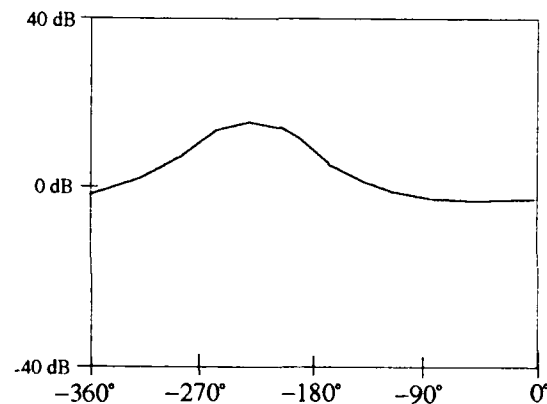


Fig. 3-22 Open Gamma Bound on NC

$$M^2 + 2 [\alpha_1 \cos(\varphi) + \alpha_2 \sin(\varphi)] M + (\alpha_1^2 + \alpha_2^2 - k^2) = 0 \quad (3-79)$$

Solving the quadratic equation for M yields the range limits $M_a(\varphi)$ and $M_b(\varphi)$:

$$M_a(\varphi) = -[\alpha_1 \cos(\varphi) + \alpha_2 \sin(\varphi)] - \sqrt{[\alpha_1 \cos(\varphi) + \alpha_2 \sin(\varphi)]^2 - (\alpha_1^2 + \alpha_2^2 - k^2)} \quad (3-80a)$$

$$M_b(\varphi) = -[\alpha_1 \cos(\varphi) + \alpha_2 \sin(\varphi)] + \sqrt{[\alpha_1 \cos(\varphi) + \alpha_2 \sin(\varphi)]^2 - (\alpha_1^2 + \alpha_2^2 - k^2)} \quad (3-80a)$$

Solutions exist for angles at which the discriminant is non-negative:

$$[\alpha_1 \cos(\varphi) + \alpha_2 \sin(\varphi)]^2 - (\alpha_1^2 + \alpha_2^2 - k^2) \geq 0 \quad (3-81)$$

Since this transcendental equation cannot be solved for φ , an iterative search is used to determine the range for which solutions exist.

Refer to Fig. 3-23 during the following discussion. The vector $\mathbf{L} = M\mathbf{e}^{j\varphi}$, provided it has a sufficiently large magnitude $M > M_1$, is tangent to the circle of radius k at point B when the angle between the vector $M\mathbf{e}^{j\varphi}$ and the radius vector drawn to point B is 90° . This fact is used by a binary search which searches the outline of the circle of radius k to locate the point of tangency at point B. Once the point of tangency

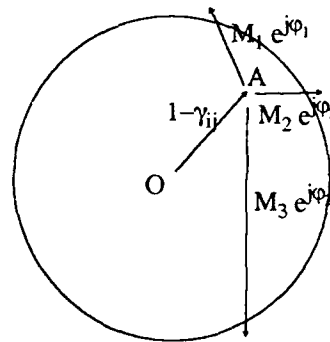
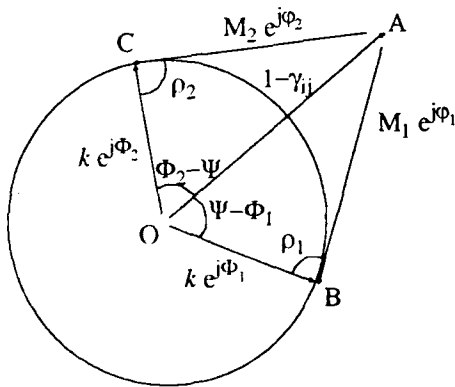


Fig. 3-23 Closed gamma bound quantities of interest Fig. 3-24 Open gamma bound quantities of interest

is located, basic geometry is applied to calculate ϕ_1 and ϕ_2 . The implementation of the binary search and the method by which ϕ_1 and ϕ_2 are calculated are now discussed.

Let:

$$\alpha_1 + j\alpha_2 = 1 - \gamma_{ij} \quad (3-82)$$

The coordinates of point A on the polar plot are:

$$A_x = \alpha_1 \quad (3-83a)$$

$$A_y = \alpha_2 \quad (3-83b)$$

The polar angle of the vector OA is:

$$\Psi = \arg(\alpha_1 + j\alpha_2) \quad (3-84)$$

Given a trial polar angle Φ_1 of the vector OB, the coordinates of B are computed:

$$B_x = k \cos(\Phi_1) \quad (3-85a)$$

$$B_y = k \sin(\Phi_1) \quad (3-85b)$$

The polar angle ϕ_1 of vector AB, the first angle needed to compute the angle range of the gamma bound, is given by:

$$\phi_1 = \arg[(B_x - A_x) + j(B_y - A_y)] \quad (3-86)$$

The angle ϕ_2 , the second angle needed, is now computed from ϕ_1 using basic geometry. The fact that the sum of interior angles of a triangle is 180° yields the equation:

$$(\Psi - \Phi_1) + (\rho_1) + (180^\circ - \Psi + \phi_1) = 180^\circ \quad (3-87)$$

where Ψ , Φ_1 , ρ_1 , and ϕ_1 are angles shown in Fig. 3-23. Solving for ρ_1 yields the angle at B between the radius vector OB and the open loop transmission vector AB:

$$\rho_1 = \Phi_1 - \phi_1 \quad (3-88)$$

This is the angle which is 90° when point B is a point of tangency. The binary search, using 15 iterations, locates the angle Φ_1 for which $\rho_1 \approx 90^\circ$ to within $45 \cdot 2^{-15}$ degrees.

Recognizing that the triangles AOC and AOB are similar triangles, the angles AOC and AOB are taken to be equal. Therefore Φ_2 is computed directly without iteration:

$$\Phi_2 - \Psi = \Psi - \Phi_1 \quad (3-89)$$

Solving for Φ_2 yields:

$$\Phi_2 = 2\Psi - \Phi_1 \quad (3-90)$$

The coordinates of C are then computed:

$$C_x = k \cos(\Phi_2) \quad (3-91a)$$

$$C_y = k \sin(\Phi_2) \quad (3-91b)$$

Followed by the angle ϕ_2 :

$$\phi_2 = \arg[(C_x - A_x) + j(C_y - A_y)] \quad (3-92)$$

The angles ϕ_1 and ϕ_2 are then shifted into the range $(-360, 0^\circ)$ by adding integer multiples of $\pm 360^\circ$ as needed. The range is initially taken to be:

$$(\phi_{G_{\min}}, \phi_{G_{\max}}) = [\min(\phi_1, \phi_2), \max(\phi_1, \phi_2)] \quad (3-93)$$

The range of angles is then checked to be sure $\phi_{G_{\max}} - \phi_{G_{\min}} < 180^\circ$ as required by inspection for any point outside the circle of radius k on the polar plot. If this inequality does not hold, then the angle range should include the 0° (or the 360°) point; the order of the angle limits are reversed. The reversal is corrected by adding 360° to what is improperly taken to be the minimum angle in the angle range, making it the maximum angle and including 0° in the angle range:

$$(\phi_{G_{\min}}, \phi_{G_{\max}}) = [\max(\phi_1, \phi_2), \min(\phi_1, \phi_2) + 360^\circ] \quad (3-94)$$

Using Eqs. (3-80a) and (3-80b) along with the algorithm for determining $\phi_{G_{\min}}$ and $\phi_{G_{\max}}$, the mechanism now exists for plotting the gamma bound on the NC using the existing template outline search routines.

When plotting a gamma bound on the NC the range of angles over which the gamma bound is plotted, as shown in Fig. 3-26, is calculated analogous to the angle range of the stability bound:

$$\phi_{GB_{\max}} = \phi_{G_{\max}} - \phi_{\text{TEMPLATE}_{\min}} \quad (3-95a)$$

$$\varphi_{GB_{min}} = \varphi_{G_{min}} - \varphi_{TEMPLATE_{max}} \quad (3-95b)$$

Let a test point on the outline of the template be located at (φ_t, M_t) and the template nominal located at $(0, 0)$, as shown in Fig. 3-25. When using the template to plot a point on the gamma bound, the template must be shifted such that the nominal point is located at the angle φ_{GB} at which the point on the bound is to be plotted. The test point, shifted along with the template, is shifted to the NC angle:

$$\varphi = \varphi_t + \varphi_{GB} \quad (3-96)$$

For the case of $||-\gamma_{ij}| > k$ two points are plotted on the gamma bound at each NC angle φ_{GB} at which the gamma bound is plotted. Equations (3-80a) and (3-80b) are applied with $\varphi = \varphi_t + \varphi_{GB}$ to determine the limits $M_a(\varphi)$ and $M_b(\varphi)$ on the transmission magnitude M at the test point. These limits are then related back to the nominal point:

$$M_{GB_i} = M - M_t \quad (3-97)$$

The most restrictive limits on the nominal open loop transmission magnitude, the NC magnitudes at which the points on the gamma bound are plotted at $\varphi = \varphi_{GB}$, are found by searching the template outline for the test points which result in the most restrictive values of M_{GB_i} . Using this procedure, the gamma bound is plotted on the NC across the range of angles for which it exists.

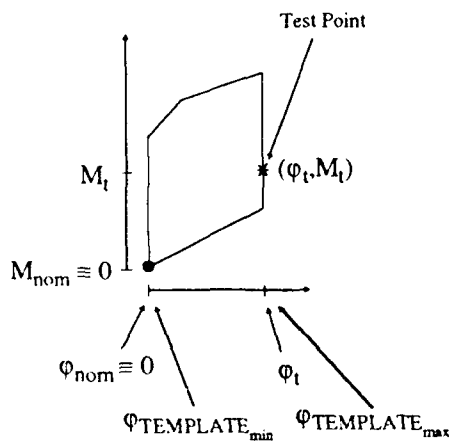


Fig. 3-25 Test point on template

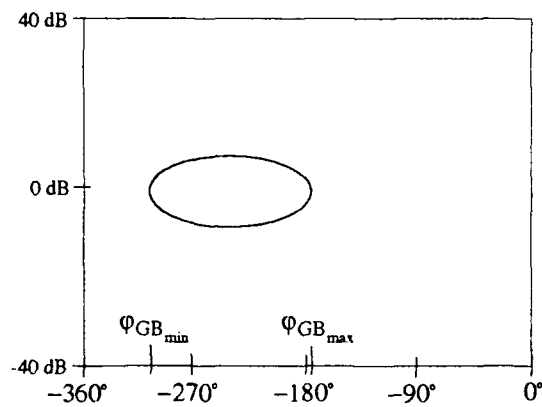


Fig. 3-26 Gamma bound angle range

An additional consideration which must be taken into account is the fact that a different gamma exists for each plant case. This variation is handled by the CAD package by generating a gamma bound for each value of γ_{ij} , one for each of the J plant cases. The value of γ_{ij} is held constant when generating each gamma bound. A composite bound is then formed from the set of J gamma bounds. The composite gamma bound is plotted on the NC in place of the J gamma bounds from which it was formed. The method by which a composite bound is formed is covered in Sec. 3.14.5.

3.14.4 Tracking Bounds

Tracking bounds are plotted across the NC using a procedure much different from those used to plot the stability, disturbance, and gamma bounds. Tracking bounds are used to insure that the variation in closed loop transmission t_{ii} of the diagonal MISO loop does not exceed the variation δ_R permitted by the performance specifications. The variation in the closed loop transmission results from both uncertainty in the response due to tracking and from the presence of the disturbance input:

$$t_{ii} = t_{r_i} + t_{d_{ii}} \quad (3-98)$$

where t_{r_i} and $t_{d_{ii}}$ are given by Eqs. (2-10a) and (2-10b).

As discussed in Sec. 2.10.2, a portion of the permitted variation δ_R of the total response t_{ii} is allocated to the transmission due to disturbance $t_{d_{ii}}$ resulting in a reduced range of variation δ_R' for the transmission due to tracking t_{r_i} . By allocating the portion $2\tau_{d_{ii}}$ to disturbance, the permitted variation in closed loop transmission t_{r_i} becomes $\Delta\tau_{r_i}'$, as shown by Fig. 2-17 and by the equation:

$$\Delta\tau_{r_i}' = \Delta\tau_{r_i} - 2\tau_{d_{ii}} \quad (3-99)$$

Once a portion of $\Delta\tau_{r_i}$ has been allocated to disturbance, the following specifications given in Sec. 2.10.2 must be met by the transmissions t_{r_i} and $t_{d_{ii}}$ of the diagonal MISO loop, respectively:

$$a_{ii}' \leq |t_{r_i}| \leq b_{ii}' \quad (3-100)$$

$$|t_{d_{ii}}| \leq \tau_{d_{ii}} \quad (3-101)$$

The portion $2\tau_{d_{ii}}$ allocated to disturbance must now be determined. The normal procedure has been to pick a trial value of $\tau_{d_{ii}}$, say 10% of the total permitted variation $\Delta\tau_{r_i}$. If for that value it is determined that adequate allocation is made for disturbance, that is, the specifications in Eqs. (3-100) and (3-101) are met at $\omega = \omega_i$, then the value $\tau_{d_{ii}}$ is maintained fixed as the tracking bound is plotted across a range of angles on the NC. Often, the same value of $\tau_{d_{ii}}$ is used at all ω_i for which performance bounds are plotted on the NC. In the MIMO/QFT CAD package, however, a unique optimized value of $\tau_{d_{ii}}$ is used at each phase angle on the NC and at each ω_i for which a point on the tracking bound is plotted (13).

The CAD package optimizes $\tau_{d_{ii}}$ such that the restrictions on \mathbf{L}_i due to Eqs. (3-100) and (3-101) are minimized. Based on the specification of Eq. (3-101) Eq. (3-60) is rewritten with $i = j$ and $b_{ij} = \tau_{d_{ii}}$ to obtain the disturbance requirement on \mathbf{L}_i for $\omega = \omega_i$:

$$\|1 + \mathbf{L}_i\| \geq \frac{|\mathbf{d}_{ii}|_{\max} |\mathbf{q}_{ii}|}{|\tau_{d_{ii}}|} \quad (3-102)$$

Based on the specification of Eq. (3-100) the tracking requirement on \mathbf{L}_i is written:

$$\text{Lm}(\mathbf{T}_{R_{\max}}) - \text{Lm}(\mathbf{T}_{R_{\min}}) \leq \delta_R' \quad (3-103)$$

where $\delta_R' = \text{Lm}(\Delta\tau_{r_i}) = \text{Lm}(\Delta\tau_{r_i} - 2\tau_{d_{ii}})$ and where $\mathbf{T}_{R_{\max}}$ and $\mathbf{T}_{R_{\min}}$ are determined by maximizing and minimizing the transmission with unity gain prefilter \mathbf{T}_R over the outline of the template:

$$\mathbf{T}_R = \left\| \frac{\mathbf{L}_i}{1 + \mathbf{L}_i} \right\| \quad (3-104)$$

with the template placed on the NC with the nominal point at the location of the nominal open loop transmission \mathbf{L}_{i0} at $\omega = \omega_i$.

The restrictions of Eqs. (3-102) and (3-103), which are functions of the choice of $\tau_{d_{ii}}$, are competing restrictions. As $\tau_{d_{ii}}$ is decreased (increased), Eq. (3-102) becomes more (less) restrictive while Eq. (3-103) becomes less (more) restrictive. Therefore, by choosing $\tau_{d_{ii}}$ such that Eqs. (3-102) and (3-103) place equally restrictive limits on \mathbf{L}_i , i.e., $\underline{\mathbf{B}}_{D_{ii}}(j\omega_i, \varphi) = \underline{\mathbf{B}}_{R_{ii}}(j\omega_i, \varphi) = \underline{\mathbf{B}}_{O_{ii}}(j\omega_i, \varphi)$, the overall restriction due to both Eqs.

(3-102) and (3-103) acting together is minimized. In general, the value of $\tau_{d_{ii}}$ is unique at each phase angle and at each ω_i for which tracking bounds are plotted. A disturbance bound is not plotted on the NC for the diagonal MISO loop since the disturbance and tracking bounds are evaluated, using this procedure, to be identical. The procedure for determining the optimal $2 \tau_{d_{ii}}$ is now discussed.

In order to allocate for disturbance, a value for $\tau_{d_{ii}}$ is required. The CAD package determines $\tau_{d_{ii}}$ indirectly, by first determining an allocation factor AF, which is the ratio of the range of variation allocated to disturbance $2 \tau_{d_{ii}}$ to the total range of variation $\Delta\tau_{r_i} = b_{ii} - a_{ii}$. AF is therefore defined as:

$$AF = \frac{2 \tau_{d_{ii}}}{b_{ii} - a_{ii}} \quad (3-105)$$

Once a value for AF has been determined, $\tau_{d_{ii}}$ is calculated:

$$\tau_{d_{ii}} = \frac{1}{2} AF \Delta\tau_{r_i} \quad (3-106)$$

The required portion of $\Delta\tau_{r_i}$ can now be allocated to disturbance, yielding:

$$\Delta\tau_{r_i}' = \Delta\tau_{r_i} - 2 \tau_{d_{ii}} \quad (3-107)$$

Expressed in decibels:

$$\delta_R' = Lm(\Delta\tau_{r_i}') \quad (3-108)$$

Once δ_R' is determined, the location of a tracking bound (TB) point on the NC can be determined. The template is placed on the NC such that the nominal point is at the NC phase angle ϕ_{TB} at which the point on the tracking bound is to be plotted. The template is then shifted up or down as needed such that the required δ_R' is obtained:

$$\delta_R' = Lm(T_{R_{max}}) - Lm(T_{R_{min}}) \quad (3-109)$$

where T_R is the closed loop transmission with unity gain prefilter:

$$T_R = \left| \frac{L_i}{1 + L_i} \right| \quad (3-110)$$

The location of the nominal template point when Eq. (3-109) is satisfied is a point on the tracking bound.

AF is optimized such that, when the open loop transmission at ω_i is in contact with the tracking bound point plotted for ω_i , the largest expected $|t_{dii}|$ is equal to the amount τ_{dii} set aside for disturbance. For the optimized AF, denoted AF_{opt} , just the required portion of $\Delta\tau_{ri}$ has been set aside for disturbance, no more, no less. When $AF = AF_{opt}$, Eqs. (3-102) and (3-103) are both satisfied as equalities, as desired. The optimized value of AF is valid only at a specific ω_i and for a tracking bound (TB) point at a specific phase angle ϕ_{TB} on the NC. The iterative method by which the MIMO/QFT CAD package determines AF_{opt} is now discussed, as it applies to the plotting of a TB point for $\omega = \omega_i$ at the phase angle ϕ_{TB} on the NC.

Step 1: The iterative procedure begins with an assumed initial value for AF. The optimized value AF_{opt} obtained for the last plotted TB point is used as the estimate \hat{AF} of AF_{opt} for the first search iteration performed for each TB point.

Step 2: $\Delta\tau_{ri}'$ and δ_R' are computed based on the estimate \hat{AF} :

$$\Delta\tau_{ri}' = (1 - \hat{AF})(b_{ii} - a_{ii}) \quad (3-111)$$

$$\delta_R' = \text{Ln}(\Delta\tau_{ri}') \quad (3-112)$$

Step 3: Using the template for $\omega = \omega_i$ a gradient search routine, with step size control, is used to determine the NC magnitude M_{TB} the template nominal point must be shifted to on the NC at phase angle ϕ_{TB} such that the uncertainty in closed loop transmission is equal to δ_R' in dB. The complex open loop transmission at the TB point is then:

$$\mathbf{L}_i = \mathbf{g}_i \mathbf{q}_{ii} = M_{TB} e^{j\phi_{TB}} \quad (3-113)$$

For the open loop transmission in Eq. (3-113) the condition of Eq. (3-103) is satisfied as an equality. The gradient search method used to determine M_{TB} is discussed in detail later in this section.

Step 4: The complex transmission of the compensator \mathbf{g}_i required for the open loop gain to be at the point (ϕ_{TB}, M_{TB}) on the NC is calculated:

$$g_i = \frac{M_{TB} e^{j\phi_{TB}}}{q_{ii}} \quad (3-114)$$

Step 5: From Eq. (2-26) $|t_{d_u}|_{\max}$ at $\omega = \omega_i$ can be determined based on the compensator g_i value of Eq. (3-114), from step 4, by applying a binary search to the line segments of the template outline using the equation:

$$|t_{d_u}| = \left| \frac{|d_{ii}|_{\max} q_{ii}}{1 + g_i q_{ii}} \right| \quad (3-115)$$

where q_{ii} is the complex transmission of the effective plant associated with each test point examined on the template outline by the binary search. The search used to determine $|t_{d_u}|_{\max}$ is avoided by recognizing that $T_{R_{\max}}$, see Eqs. (3-109) and (3-110), is available as an intermediate result of the search used in step 3. $|t_{d_u}|_{\max}$ is then calculated:

$$|t_{d_u}|_{\max} = \left(\frac{|d_{ii}|_{\max}}{|g_i|} \right) T_{R_{\max}} \quad (3-116)$$

where

$$T_{R_{\max}} = \left| \frac{L_i}{1 + L_i} \right|_{\max} = \left| \frac{g_i q_{ii}}{1 + g_i q_{ii}} \right|_{\max} \quad (3-117)$$

and from Eq. (2-19) the maximum value of $|d_{ii}|$ for each plant case l is:

$$(|d_{ii}|_{\max})_l = \left| \sum_{k \neq i} \frac{b_{ki}}{q_{ikl}} \right| \quad (3-118)$$

The value $|d_{ii}|_{\max}$ required to calculate $|t_{d_u}|_{\max}$ using Eq. (3-116) is then obtained by maximizing Eq. (3-118) over the J plant cases:

$$|d_{ii}|_{\max} = [(|d_{ii}|_{\max})_l]_{\text{MAX over } l} \quad (3-119)$$

Step 6: The CAD package utilizes the value of $T_{R_{\max}}$ in Eq. (3-117) and $|t_{d_u}|_{\max}$ in Eq. (3-119) to determine if the trial allocation factor $\hat{A}F$ results in:

$$|t_{d_u}|_{\max} = \tau_{d_u} \pm \Delta \tau_{d_u} \quad (3-120)$$

where $\Delta \tau_{d_u}$ is an acceptable error tolerance.

If Eq. (3-120) is satisfied, then the requirement of Eq. (3-102) is satisfied as an equality when the right hand side, maximized over the template outline, is equal to $lt_{d_{ii}}|_{\max}$. This is seen by rearranging Eq. (3-102) in the form of Eq. (3-115):

$$\frac{ld_{ii}|_{\max} |q_{ji}|}{1 + L_i} \leq \tau_{d_{ii}} \quad (3-121)$$

If the requirement of Eq. (3-121) is satisfied, then the estimate \hat{AF} has converged to the optimal allocation factor AF_{opt} and the iterative procedure terminates. If the requirement of Eq. (3-121) is not satisfied, then the estimate \hat{AF} is revised and the iterative procedure repeated, beginning with step 2. The following additional steps are performed to revise \hat{AF} .

Step 7: The allocation factor AF_{req} required to accommodate $lt_{d_{ii}}|_{\max}$, determined in step 5, is calculated:

$$AF_{req} = \frac{2 lt_{d_{ii}}|_{\max}}{b_{ji} - a_{ji}} \quad (3-122)$$

Step 8: The difference between AF_{req} and \hat{AF} is computed as a measure of the error (deviation from optimal) in the trial value \hat{AF} :

$$AF_{err} = \hat{AF} - AF_{req} \quad (3-123)$$

By examining Eqs. (3-105) and (3-122) it is seen that the error term AF_{err} is zero when $lt_{d_{ii}}|_{\max} = \tau_{d_{ii}}$. By revising \hat{AF} such that AF_{err} is made much smaller (hopefully zero) during the next iteration, the goal $lt_{d_{ii}}|_{\max} \approx \tau_{d_{ii}}$ will eventually be achieved. The CAD package uses a gradient step to make this revision. To implement the gradient step, the slope of AF_{err} as a function of \hat{AF} is determined. To compute the slope, values AF_{err1} and AF_{err2} corresponding to two closely spaced trial values \hat{AF}_1 and \hat{AF}_2 are required. The slope is then computed and the gradient step used to revise \hat{AF} . The following additional steps describe how the gradient step is implemented:

Step 9: \hat{AF} and AF_{err} from steps 2 to 6 are used as AF_{err1} and \hat{AF}_1 :

$$\hat{AF}_1 = \hat{AF} \quad (3-124)$$

$$AF_{err1} = AF_{err} \quad (3-125)$$

Step 10: A value for \hat{AF}_2 is computed by adding a small increment to \hat{AF}_1 :

$$\hat{AF}_2 = \hat{AF}_1 + 0.02 \quad (3-126)$$

Step 11: Steps 2 through 8 are repeated with $\hat{AF} = \hat{AF}_2$ to obtain $AF_{err2} = AF_{err}$.

Step 12: The slope of AF_{err} as a function of \hat{AF} is computed:

$$\frac{\partial AF_{err}}{\partial \hat{AF}} \approx \frac{AF_{err1} - AF_{err2}}{\hat{AF}_1 - \hat{AF}_2} \quad (3-127)$$

Step 13: The gradient step is taken to compute the revised \hat{AF} :

$$\hat{AF} = \hat{AF}_1 + (0 - AF_{err1}) \left(\frac{\partial AF_{err}}{\partial \hat{AF}} \right)^{-1} \quad (3-128)$$

For robustness, a step size control is used for the gradient step which is identical to that used for the search implemented for determining M_{TB} in step 3. The step size control is discussed later in this section.

Step 14: The iterative procedure is executed again beginning with step 2 using the revised \hat{AF} .

The iterative method, which is implemented based on the steps outlined above, returns the optimized AF and the associated M_{TB} obtained in step 3, which is the location of the point on the tracking bound at angle ϕ_{TB} for $AF = AF_{opt}$ on the NC. The entire iterative procedure is again applied when plotting the next point along the tracking bound on the NC, using AF_{opt} from the previous TB point as the initial estimate in step 1 of the search procedure. Because the optimal AF often does not change much between points for a tracking bound plotted at 2° or 5° increments using AF_{opt} of the previous bound point as the initial \hat{AF} , reduces the number of iterations required for \hat{AF} to converge to AF_{opt} . By repeating the iterative procedure for the range of angles of the NC, the complete tracking bound is generated.

For step 3, a gradient search enhanced by step size control is used to determine M_{TB} for a given δ_R' and $\omega = \omega_k$. To determine M_{TB} the template is placed on the NC and moved up or down as needed such that the uncertainty of the closed loop transmission magnitude exactly matches δ_R' , i.e. Eq. (3-109) is satisfied. With the template nominal point placed at (ϕ_{TB}, M_{TB_i}) , where M_{TB_i} is a trial value of the NC

magnitude, the actual uncertainty in the closed loop transmission magnitude δ_t is determined by searching the template outline for the maximum closed loop transmission magnitude $T_{R_{\max}}$ and the minimum closed loop transmission magnitude $T_{R_{\min}}$. The values of $T_{R_{\min}}$ or $T_{R_{\max}}$ are determined by using a binary search to find the minimum or maximum magnitude respectively of the closed loop transmission T_R for each line segment of the template outline using Eq. (3-110) at each point along the segment examined by the search. The overall minimum or maximum transmission is then $T_{R_{\min}}$ or $T_{R_{\max}}$, respectively.

The value of δ_t in dB for the trial template position is then calculated:

$$\delta_t = Lm(T_{R_{\max}}) - Lm(T_{R_{\min}}) \quad (3-129)$$

By evaluating δ_t at two closely spaced values of M_{TB_i} on the NC, a gradient of δ_t as a function of M_{TB_i} near the trial template position is estimated as follows:

$$\frac{\partial \delta_t}{\partial M_{TB_i}} \approx \frac{\delta_{t_2} - \delta_{t_1}}{M_{TB_{i,1}} - M_{TB_{i,2}}} \quad (3-130)$$

where δ_{t_1} and δ_{t_2} are the uncertainties in closed loop transmission for the template placed with the nominal point located at $(M_{TB_{i,1}}, \phi_{TB})$ and $(M_{TB_{i,2}}, \phi_{TB})$ respectively and where $M_{TB_{i,1}}$ and $M_{TB_{i,2}}$ are separated by a small distance ΔM :

$$M_{TB_{i,2}} = M_{TB_{i,1}} + \Delta M \quad (3-131)$$

An estimate of the value of M_{TB} at which $\delta_t = \delta_R'$ is then calculated:

$$\hat{M}_{TB} = M_{TB_{i,1}} + (\delta_R - \delta_{t_1}) \left(\frac{\partial \delta_t}{\partial M_{TB_i}} \right)^{-1} \quad (3-132)$$

where $M_{TB_{i,1}} = (\hat{M}_{TB})_{i-1}$ is the estimate of M_{TB} from the previous search iteration.

The excursion $\Delta \hat{M}_{TB}$ from the previous estimate $(\hat{M}_{TB})_{i-1}$ is then calculated:

$$\Delta \hat{M}_{TB} = \hat{M}_{TB} - (\hat{M}_{TB})_{i-1} \quad (3-133)$$

If \hat{M}_{TB} is within the acceptable range $(\hat{M}_{TB})_{i-1} \pm \Delta M_{TB_{\max}}$ imposed by the step size control of the previous estimate $(\hat{M}_{TB})_{i-1}$, δ_t is determined at the test point $M_{TB_i} = \hat{M}_{TB}$. If \hat{M}_{TB} is outside the acceptable

range, i.e. $|\Delta\hat{M}_{TB}| > \Delta M_{TB_{max}}$, the excursion from $(\hat{M}_{TB})_{i-1}$ to the test point M_{TB_i} where δ_i is determined is made only to the limit of the acceptable step size range:

$$M_{TB_i} = (\hat{M}_{TB})_{i-1} + \Delta M_{TB_{max}} \quad \text{for } \Delta\hat{M}_{TB} > 0 \quad (3-134a)$$

$$M_{TB_i} = (\hat{M}_{TB})_{i-1} - \Delta M_{TB_{max}} \quad \text{for } \Delta\hat{M}_{TB} < 0 \quad (3-134b)$$

The step size control therefore imposes a hard limit on the size of each step of the search procedure to prevent jumping too far from the region in which the gradient of Eq. (3-127) is valid. If the value of δ_i for the test point M_{TB_i} is closer to δ_R' than that obtained using the previous best estimate $(\hat{M}_{TB})_{i-1}$, M_{TB_i} is accepted as the current best estimate:

$$(\hat{M}_{TB})_{i-1} = (M_{TB})_i \quad (3-135a)$$

$$(\hat{M}_{TB})_i = M_{TB_i} \quad (3-135b)$$

If the difference between δ_i and δ_R' is within an acceptable tolerance, the search terminates. Otherwise, another search iteration is performed, with a reduced step size limit $\Delta M_{TB_{max}}$ imposed. The search is continued until successful or until aborted.

The search is aborted if more than a preset number of search iterations are executed without converging to the desired solution for M_{TB} at which $\delta_i \approx \delta_R'$, or if the size of the gradient step exceeds the step size limit $\Delta M_{TB_{max}}$ by a factor greater than 100. A large gradient step results when the search becomes trapped at a local minimum or at a local maximum where the gradient is small. The inverse of the gradient used in Eq. (3-100) then becomes large, as does the distance from $(\hat{M}_{TB})_i$ to the estimate \hat{M}_{TB} . When the search is aborted, when trapped in a local maximum or minimum, the gradient search must be restarted from a new test point. A suitable test point is found by evaluating δ_i based on gradually increasing the value of \hat{M}_{TB} from the value $(\hat{M}_{TB})_i$ at which the search had become trapped until a value of \hat{M}_{TB} is found for which δ_i overshoots the goal δ_R' . Several "step-back" iterations are then performed to reduce the amount of overshoot while maintaining the overshoot condition. Then, for either abort condition, the step size limit $\Delta M_{TB_{max}}$ is reset to an initial value, and the search begun again.

The CAD program begins plotting the tracking bound at the 0° axis by calling a binary search subroutine with a large search range to obtain a rough initial estimate for M_{TB} to be used by the gradient search procedure. The gradient search procedure is then used to obtain a refined solution for M_{TB} , which is then plotted as a bound point on the NC. The gradient search is used, with the previous M_{TB} as an initial estimate, to find M_{TB} at each successive angle on the NC. A list of the M_{TB} values and associated NC phase angles is retained in memory to be plotted on the NC during loop shaping.

The gradient search method for plotting tracking bounds was previously implemented for generating tracking bounds in a thesis by Sandra Cole (9). An alternative approach to the gradient search is to develop an equation which can be used to directly calculate the NC magnitude to which the template must be shifted for a given $\delta R'$. Direct calculation does not eliminate the need for search routines, however, because the equation for the NC magnitude requires the template points at which the minimum and maximum transmissions occur, $T_{R_{max}}$ and $T_{R_{min}}$ respectively, be known. These points are not known a-priori and therefore must be located using a search routine. Furthermore, the location of $T_{R_{max}}$ and $T_{R_{min}}$ on the template outline change when the template is moved to a new position on the NC, requiring an iterative process be used to locate the final NC magnitude to which the template must be shifted. Direct calculation was implemented by Yaniv (22) to plot tracking bounds. The gradient search method was chosen due to its association with the graphical method of locating tracking bounds presented in (17) and (11) and used in previous AFIT thesis work.

3.14.5 Composite Bounds

A set of composite bounds is formed based on any or all of the tracking, stability, disturbance, and gamma bounds. The composite bound for a given frequency is formed by retaining the most restrictive portion of the bounds for the given frequency from which the composite bound is formed. The procedure used to generate the composite bound hides the line segment of any bound whose endpoints lie entirely within the forbidden regions of other bounds. For a tracking bound, which is a single contour running across the NC, the forbidden region is the area on the NC below this bound. Thus the tracking bound is

classified as an "upper bound", as shown in Fig. 3-27. A stability bound is classified as a "closed bound", as shown in Fig. 3-27, in the context of this discussion since it encloses a forbidden region on the NC. Disturbance and gamma bounds are likewise classified using the above criteria.

As a first step in forming a composite bound, the bounds from which the composite bound is formed are placed in a list. The bounds, as stored in this list, may have one of two possible structures, depending on the classification of the bound. Each upper bound is represented in the form of a list, sorted by angle, of angle-magnitude coordinate pairs at which upper bound points are plotted over the range of angles $(-360^\circ, 0^\circ)$:

$$\{ \{ \phi_1, M_{uu1} \}, \{ \phi_2, M_{uu2} \}, \dots, \{ \phi_n, M_{uun} \} \} \quad (3-136)$$

Each closed bound is represented in the form of a list, sorted by angle, with one entry for each angle at which bound points are plotted on the NC. Each entry contains the angle ϕ at which the closed bound points are plotted, as well as the upper limit M_{cu} and lower limit M_{cl} of the forbidden region at that angle. The structure used to represent the closed bound is:

$$\{ \{ \phi_1, M_{cu1}, M_{cl1} \}, \{ \phi_2, M_{cu2}, M_{cl2} \}, \dots, \{ \phi_n, M_{cun}, M_{cln} \} \} \quad (3-137)$$

In this form, a pair of bounds is compared and all hidden points identified in linear time. A point on a bound is marked as hidden if it lies in the forbidden region of any other bound (see Fig. 3-28). For

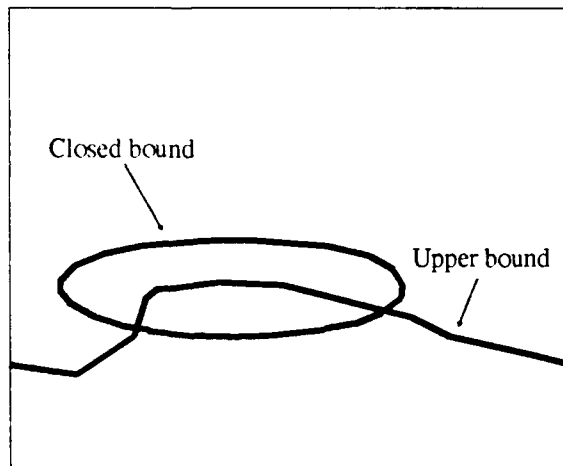


Fig. 3-27 Pair of bounds on NC

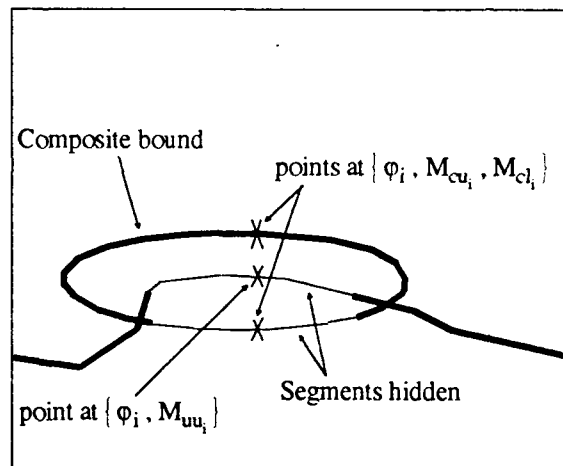


Fig. 3-28 Composite bound for bound pair

example the points $\{\phi_i, M_{uu_i}\}$ of the upper bound and the lower point of the closed bound point pair $\{\phi_i, M_{cu_i}, M_{cl_i}\}$ are hidden points as shown in Fig. 3-28. Each bound must therefore be compared with every other bound in the list of bounds to identify the hidden points.

A separate structure is used to flag bound points as hidden. For an upper bound it has the structure is:

$$\{ \{ \phi_1, H_{uu_1} \}, \{ \phi_2, H_{uu_2} \}, \dots, \{ \phi_n, H_{uu_n} \} \} \quad (3-138)$$

For a closed bound it has the structure is:

$$\{ \{ \phi_1, H_{cu_1}, H_{cl_1} \}, \{ \phi_2, H_{cu_2}, H_{cl_2} \}, \dots, \{ \phi_n, H_{cu_n}, H_{cl_n} \} \} \quad (3-139)$$

The flags H_{uu_i} , H_{cu_i} and H_{cl_i} are logical variables indicating a point is hidden. When a flag is set to "True", the bound point is displayed as part of the composite bound. When a flag is set to "False", the point is hidden. All flags are initially set to "True" before comparing bounds, and are set to "False" as hidden points are identified. Once a bound is compared with all other bounds, and the flags are set accordingly, all line segments for which one or both endpoints are not marked as hidden are included in the set of line segments used for the composite bound. For example in Fig. 3-28 only the upper point of the closed bound at phase angle ϕ_i is not flagged as hidden. Therefore, the flags H_{cl_i} and H_{uu_i} are set to "False" while the flag H_{cu_i} is set to "True".

Each bound, in turn, is compared with all other bounds and additional composite bound line segments collected. The final collection of line segments becomes the composite boundary on the NC. A line segment included on the composite bound may extend into a forbidden region, resulting in rough breaks at the points of intersection. This is the price paid for the simplicity of this method of generating a composite bound.

3.15 Compensator Design

The compensator is designed to satisfy design specifications for the entire row of MISO loops in which the compensator is used. In the 3×3 set of MISO equivalents shown in Fig. 2-11, it is seen that the same

compensator g_i and effective plant q_{ij} are shared by all MISO loops of a given row. This fact implies that the same set of stability bounds may be used for all MISO loops of the row in which the compensator is to be used. Since the nominal loop transmission $L_{io} = g_i q_{iio}$ is the same for all MISO loops in a given row, bounds for all MISO loops including stability and tracking bounds for the diagonal MISO loop, disturbance bounds for the off-diagonal MISO loop, and gamma bounds may all be plotted together on the NC. The nominal loop transmission L_{io} is synthesized for an entire row of MISO loops based on the stability, disturbance, tracking, and gamma bounds plotted together on the NC. Alternatively, a single composite bound may be used in place of the individual bounds at each bound frequency. The use of composite bounds may reduce by a factor of four or more the number of bounds displayed on the NC, reducing the difficulty in keeping track of the bounds that apply at a given frequency.

The CAD package sets the starting open loop transmission function that is used to start the synthesis (or loop shaping) process to $L_{io} = q_{iio}$ so that the compensator is initially taken to be $g_i = 1$. To assist in this loop shaping the CAD package makes a Bode plot of L_{io} , a Nichols plot of L_{io} with bounds, and a factored form listing of the compensator g_i available to the designer. On both plots, the bound frequencies are marked on the loop transmission using colored markers. On the NC, all bounds are plotted in color to match the color of the markers on the loop transmission. The designer must be sure the colored markers do not violate bounds of matching color. The Bode plot must be used to read off the frequencies associated with the colored markers, since the colored markers are used in place of frequency labels on the plot of L_{io} on the NC. The Bode plot ~~is~~ also useful for noting the frequency associated with features of interest on loop transmission, since this information is not readily obtained from the plot of L_{io} on the NC. The Bode plot thus allows better placement of poles and zeros when designing the compensator.

The designer is given the option of labeling L_{io} with numeric bound frequencies rather than with colored markers. The designer is also given the option to include numeric frequency labels along the bounds plotted on the NC. Frequency labels are useful when the NC is to be displayed on a monochrome monitor or when a hardcopy is generated on a postscript printer.

Assuming q_{iio} is identified as L_{io} , the CAD package allows the designer to add, delete, or modify the poles and zeros of L_{io} and g_i . The poles and zeros of L_{io} associated with q_{iio} cannot be modified and remain fixed. After any change to the poles and zeros, the gain is automatically adjusted such that the loop transmission is relatively unaffected at frequencies much less than that associated with the modified pole or zero. This allows the designer to "bend" the loop transmission on the NC at successively higher frequencies until an acceptable loop shape is obtained. In addition, the gain can be independently modified, as needed, by the designer. An updated listing, in factored form, of the poles, zeros, and gain of $g_i = L_{io}/q_{iio}$ is displayed after any of these changes are made.

Both real and complex poles and zeros may be added to L_{io} . Complex poles and zeros are displayed as a natural frequency and a zeta. The designer can add poles and zeros in the form displayed or as a complex number. The natural frequency of a complex pole or zero relates directly to the location at which the loop transmission bends, while the value of zeta determines how sharply the loop is bent. The rectangular coordinates of a complex pole or zero do not relate this information directly. Therefore rectangular coordinates are not used as the format in which complex poles and zeros are displayed.

The designer may terminate the loop shaping process by saving the compensator $g_i = L_{io}/q_{iio}$ used to obtain L_{io} or may abort the design changes before returning to the CAD package menu system. If saved, the compensator can be further modified by again executing the "Design Compensator" option. Once the designer has obtained a satisfactory compensator design, and the design has been saved, the prefilter is designed.

Alternatives exist to the approach used by the MIMO QFT/CAD package. Automatic loop shaping routines were developed by Thompson (27), and loop gain-phase shaping routines based on the Bode integral theorem were developed by Bailey (3). In addition, a method of optimizing the loop transmission based on a cost function was developed by Yaniv (22). The approach used by the MIMO/QFT CAD package, requiring the designer to choose the poles, zeros, and gain of the compensator, was chosen due

to the simplicity of implementation. Nevertheless, the MIMO/QFT CAD package may be enhanced in the future to include routines which automate the loop shaping process.

3.16 Prefilter Design

The proper design of the compensator g_i of the loop transmission function L_{i0} guarantees that the variation in closed loop transmission due to uncertainty for the channel is acceptable, but does not guarantee that the transmission is within the upper and lower tracking bound specifications a_{ii}' and b_{ii}' . The prefilter f_{ii} is therefore required to shift the closed loop MISO loop transmission t_r , such that it satisfies the upper and lower tracking bound specifications a_{ii}' and b_{ii}' shown in Fig. 2-17 on page 2-19 over the range of plant uncertainty. When using the CAD package, a set of filter bounds on the nominal T_R are generated and plotted on the Bode plot, along with the nominal T_R where:

$$T_R = \frac{L_i}{1 + L_i} \quad (3-140)$$

The prefilter is then designed by adding, deleting or modifying the poles and zeros and by adjusting the gain of the prefilter such that the nominal T_R satisfies the filter bounds. Figures 2-17 and 2-18 illustrate Bode plots of the nominal closed loop transmission both before and after successful prefilter design.

Several steps are required to generate the filter bounds. First, since only a_{ii} and b_{ii} are available to the prefilter design program a portion of the permitted range of variation of T_R is allocated to the disturbance to obtain the values a_{ii}' and b_{ii}' required to generate the prefilter bounds. The portion allocated to disturbance is unique at each frequency at which a point on the prefilter bounds is plotted. With the compensator design in hand, the maximum transmission due to disturbance $|t_{d_{ii}}|_{\max}$ is determined from $T_{R_{\max}}$ at each template frequency $\omega = \omega_i$ based on g_i using the same procedure used in step 5 of the tracking bound algorithm. Because the phase of $t_{d_{ii}}$ is unknown, the worst case is assumed; the maximum and minimum limits on the range of variation of T_R must each be reduced by the magnitude of the disturbance, as illustrated in Fig. 2-17 on page 2-19. The restricted tolerances become:

$$b_{ii}' = b_{ii} - |t_{d_{ii}}|_{\max} \quad (3-141a)$$

$$a_{ii}' = a_{ii} + |t_{d_i}|_{\max} \quad (3-141b)$$

Before the filter bounds are generated, $T_{R_{\max}}$ and $T_{R_{\min}}$, the maximum and minimum values of $|T_R|$ over the range of plant uncertainty, are obtained at each template frequency ω_i (11:727). These quantities are obtained at each ω_i by placing the template for ω_i on the NC with the nominal point at the location of ω_i on the loop transmission $L_{i0} = g_i q_{i0}$. The search subroutines used when generating the tracking bounds are then used to search the outline of the template for the maximum and minimum closed loop transmissions $T_{R_{\max}}$ and $T_{R_{\min}}$. These values are used to restrict the permitted range of variation about the nominal T_R by the amount of variation in T_R which occurs over the range of the template relative to the nominal transmission. By restricting the bounds about the nominal T_R , the single nominal T_R can be plotted rather than requiring an array of J transmissions to be plotted, one for each plant case. It is easier to work with a single transmission within a pair of bounds than to work with J transmissions within a pair of bounds.

The upper and lower filter bounds on the nominal T_R are (11:727):

$$Lm(b_{ii}') = Lm(T_{R_{\max}}) \quad (3-142a)$$

$$Lm(a_{ii}') = Lm(T_{R_{\min}}) \quad (3-142b)$$

The filter bounds are plotted on the Bode plot along with the nominal closed loop transmission T_R . Note that these bounds, as computed, cover only the range of frequencies covered by the templates. The CAD package is able to extend this frequency range one decade higher and one decade lower based on the values of $T_{R_{\min}}$ and $T_{R_{\max}}$ obtained by minimizing or maximizing $|T_R|$ over the plant cases and based on the value $|t_{d_i}|_{\max}$ obtained by maximizing $|t_{d_i}|$ over the plant cases. Templates on the NC are not used to compute these values since no templates are generated in the frequency range into which the bounds are to be extended. The assumption made here is that the loop transmission is far enough away from the $(-180^\circ, 0dB)$ point such that the constant magnitude contours on the NC are fairly straight in the vicinity of the template, if it had been generated. Little is gained by searching template segments since the segment endpoints contact the most extreme constant magnitude contours, if straight.

Once the nominal T_R and the filter bounds are plotted on the Bode plot, the prefilter $f_{ij} = t_{r_{io}}/T_R$ is designed using the same procedure for adding, deleting, and modifying poles and zeros and for modifying the gain used to design the compensator $g_i = L_{i0}/q_{iio}$ where $t_{r_{io}}$ is the nominal MISO loop closed loop transfer function t_{r_i} . Once the prefilter design is complete, the designer may either save or abort changes made to the prefilter. If the design is saved, the design process is continued on yet another row of MISO loops, until all compensators and prefilters have been designed. The completed design can then be tested.

3.17 Flowchart of MIMO QFT/CAD Package

The development of the various phases of the MIMO QFT/CAD package are presented in previous sections of this chapter. Figure 3-29 is a flowchart representing these various phases of the CAD package.

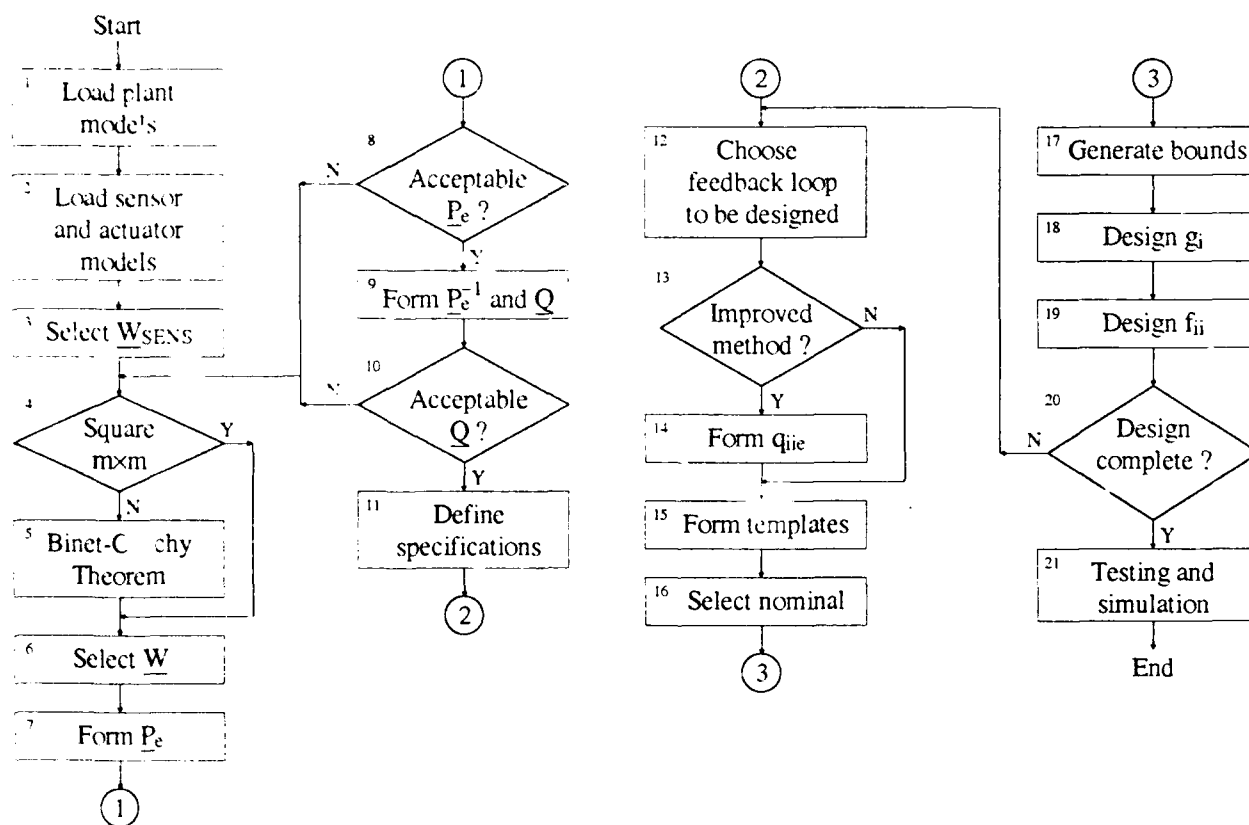


Fig. 3-29 Flowchart for MIMO QFT CAD Package

3.18 Simulation

The CAD package provides two methods of validating that the completed MIMO design meets the stability and performance specifications. The first method (25) allows the designer to validate that the stability specifications have been satisfied in the frequency domain by plotting on the NC an array of the J open loop MISO loop transmissions $(L_i)_l = g_i(q_{ii})_l$ for a given row of MISO loops i for all plant cases $l = 1, 2, \dots, J$ along with the M_L contour (this is none in block 18 in Fig. 3-29). If no open loop transmission violates the M_L contour, then the stability specifications have been satisfied for row i of the MISO loops of Fig. 2-11 on page 2-11. Figure 4-29 on page 4-19 shows the array of open loop transmissions for the first row of MISO loops in Arnold's thesis.

The second method of validation allows the designer to validate that the performance specifications placed on the closed loop system have been met by plotting an $m \times m$ array of Bode magnitude plots, one Bode plot for each transfer function in the $m \times m$ transfer function matrix $\underline{T} = \{t_{ij}\}$ for the closed loop system (this is done in block 19 of Fig. 3-29). The set of closed loop transfer functions $(t_{ij})_l$ for the J plant cases $l = 1, 2, \dots, J$ are plotted on the (i,j) Bode plot along with the performance tolerances a_{ij} for $i \neq j$ and b_{ij} for all i and j , as shown in Fig. 4-29 for the design of Arnold's thesis. Any violation of the performance tolerances by the closed loop transmissions are evident by inspection of the Bode plots. The designer can thus note the frequency and channel for which a violation occurs, modify the compensator and prefilter designs, and re-evaluate the frequency response of the closed loop system until satisfied with the results.

The $m \times m$ matrix of closed loop transfer functions \underline{T}_l for plant case l used to generate the set of Bode plots shown in Fig. 4-28 on page 4-18 is computed for each of the J plant cases $l = 1, 2, \dots, J$ using the equation:

$$\underline{T}_l = \{ (t_{ij})_l \} = [\underline{I} + (\underline{P}_e)_l \underline{G}]^{-1} (\underline{P}_e)_l \underline{G} \underline{F} \quad (3-143)$$

Where \underline{I} is the identity matrix, $(\underline{P}_e)_l$ is the $m \times m$ plant matrix for plant case l , \underline{G} is the diagonal compensator matrix, and \underline{F} is the diagonal prefilter matrix. The $m \times m$ matrix \underline{T} of transfer functions in s

is evaluated by direct use of Eq. (3-143) where \underline{I} , (\underline{P}_e) , \underline{G} , and \underline{F} are $m \times m$ matrices of transfer functions using the symbolic capability of Mathematica. For large systems where $m > 2$ the transfer function elements of \underline{T} may be very high order. For this reason, the log magnitude of the transfer function elements is evaluated at the complex frequency of each point plotted on the Bode plots by making the assignment $s \rightarrow j\omega$. High precision numbers must be used when \underline{T} is calculated using Eq. (3-143) and to evaluate \underline{T} as $s \rightarrow j\omega$ to overcome the errors in computing the small difference of large numbers encountered when evaluating the magnitude of high order polynomials in coefficient form. Using high precision allows a smooth, continuous Bode magnitude plot to be generated rather than a jagged, noisy plot. Direct evaluation of \underline{T} as $s \rightarrow j\omega$ is used because it allows Bode magnitude plots to be generated for arbitrarily high order transfer functions without the need to transform the high order transfer function elements of \underline{T} to factored form as required to use the Bode plot function.

To evaluate the performance of the design in the time domain (this is done in block 21 of Fig. 3-29), with nonlinearities introduced, the completed design is exported to MATRIXx. The CAD package allows the designer to store the plant models, compensator matrix, and prefilter matrix in the form of a MATRIXx command file. The command file, when executed during a MATRIXx session, creates the plant models, compensator matrix, and prefilter matrix in state space form. The designer may then create a System_Build model, inserting nonlinear elements if desired, and perform the necessary simulations.

Several alternatives to MATRIXx exist for time domain simulation. Other CAD packages on which simulation may be performed include Matlab (Fig. 4-11 Matlab Bode angle plot comparison), Control-C (10), and EASY5 (12). The packages Matlab, Control-C, EASY5, and MATRIXx all allow nonlinear simulation to be carried out in an object-oriented environment. MATRIXx was chosen as the CAD package to which the finished design is exported because previous QFT thesis work was done using MATRIXx. The CAD package may be enhanced in the future to allow transfer of the completed design to Matlab, Control-C, and EASY5.

3.19 Summary

Chapter 3 discussed the implementation of the MIMO QFT/CAD package. Algorithms used for implementing the CAD package are presented in detail, including the derivation of equations unique to the MIMO QFT/CAD package software. The software as developed in this chapter is tested by redoing two MIMO QFT designs done by prior thesis students. Results of this testing are presented in Chap. 4.

4 Results

4.1 Introduction

This chapter is intended to provide validation of the validity of the MIMO QFT CAD package presented in this thesis. This validation is accomplished by redoing two MIMO QFT designs done by two prior AFIT/ENG M.S. thesis students. In accomplishing this validation the following points must be kept in mind:

- (1) Prior AFIT MIMO QFT designs did not have available specially designed QFT CAD packages.
- (2) The control CAD packages available in the past did not have the degree of accuracy and the CAD tools necessary to perform the required MIMO QFT mathematical manipulations.

As is shown in this chapter, the MIMO QFT CAD package developed in this thesis, which is designed to be used on more powerful computers than were available in the past, provides the necessary degree of accuracy and facilitates the QFT design of MIMO control systems.

Sections 4.2 and 4.3 provide a comparison of the designs accomplished by Arnold (2) and Betzold (5), respectively. Further, in conjunction with this comparison, the validation of the MIMO QFT CAD package of this thesis is accomplished along with a demonstration of its increased degree of accuracy through a re-design of the channel 1 compensator and prefilter from Arnold's thesis.

4.2 Validation of Thesis Results of Philip Arnold

In Philip Arnold's thesis (2), MIMO QFT theory was applied to the design of an analog fault tolerant two channel flight control system for the AFTI/F-16. It was desired that the aircraft performance and stability conform to design specifications despite the possibility of any of six possible failure modes in any of four flight conditions. There were therefore 24 plant cases. The failure modes include the normal aircraft and five combinations of control surface failures in which control authority to the failed surface has been lost.

The pitch rate and roll rate of the normal aircraft were to be controlled using four control surfaces. A 4×2 weighting matrix, given in the thesis, was used to divide control authority of the two channels among the four control surfaces. In addition, the transfer function elements of the 2×4 basic aircraft transfer

function matrix were given for each flight condition. Failure modes were modeled by setting to zero transfer function elements associated with any failed surface. The 2×2 effective plant \underline{P}_e for that mode was then formed by utilizing a weighting matrix. A diagonal prefilter \underline{F} and a diagonal compensator \underline{G} were used to control the system.

The validation process began by generating the set of 24 effective plants. The effective plants are each formed as in Arnold's thesis from the weighting matrix and basic aircraft transfer function matrices associated with the 24 combinations of flight conditions and failure modes. The effective plant transfer functions are listed in Appendix A. Next, the equivalent plant transfer functions for the MISO loops are formed using the CAD package. Common factors are then cancelled using a ratio of 0.0001 as discussed in Sec. 3.9. The equivalent plants obtained are listed in Appendix B.

Next, design specifications used for the design are defined. The 4 dB M_L contour on the NC is used as the stability specification for both the pitch rate and roll rate channels. The requirement $1 - \gamma_{ij} + L_{20} > 0.05$ is used to generate gamma bounds for L_{i0} when g_j has been designed and L_{j0} is known

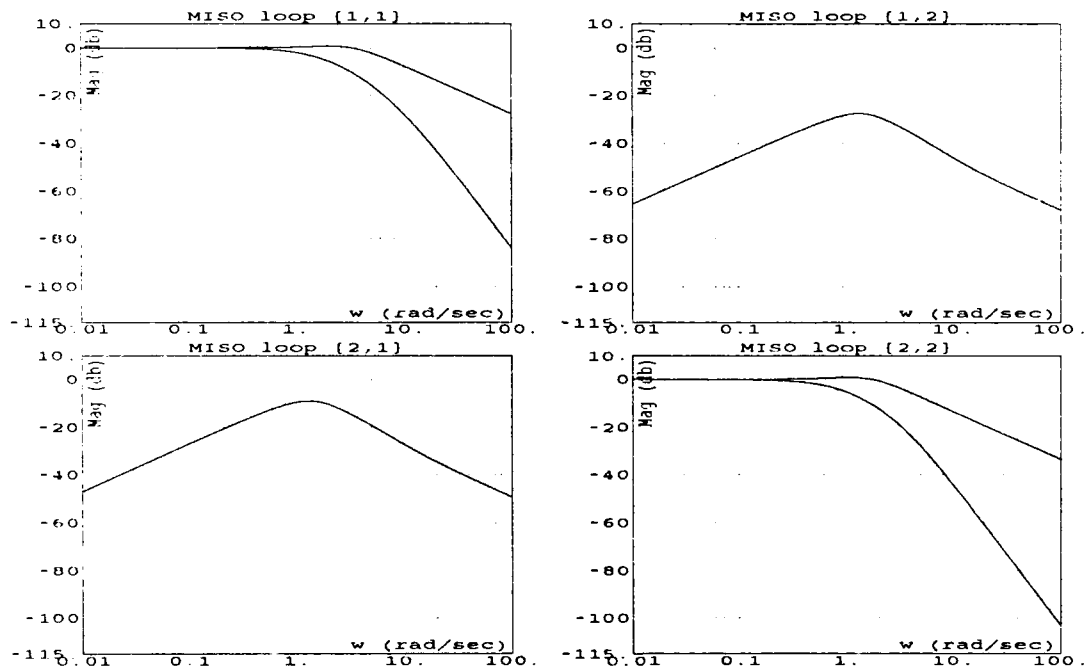


Fig. 4-1 Performance tolerances on the AFTI/F-16

as discussed in Sec. 3.14.3. The tolerances on pitch rate and roll rate responses in the frequency domain are shown in Fig. 4-1. The QFT design process can now begin.

Template frequencies are selected and entered into the CAD package based on those used by Arnold and based on resonances in the open loop system. Sets of templates for channels 1 and 2 are then generated, one template in each set for each template frequency. Plant cases #10 and #22 are chosen as the nominal plant of channels 1 and 2, respectively, as in Arnold's thesis. The set of templates generated by the CAD package for channels 1 and 2, with the nominal points emphasized, are illustrated in Figs. 4-2 and 4-3. A comparison of the templates generated by the CAD package to those given in Arnold's thesis shown in Figs. 4-4 through 4-9 reveal significant differences in the low frequency templates. These differences arise for two reasons. First, errors occurred on the calculations used by Arnold to form equivalent plants for plant cases 14, 15, and 24. For these cases, the gains were incorrect. The second reason for the difference is that the angle used to plot template points, as obtained from previous CAD packages, could be in error by 360° . This is the reason for the 360° degree width of Arnold's template for q_{22} at $\omega = 4.0 \text{ rad/sec}$ shown in Fig. 4-8. That the template width is incorrect can be validated by inspection of the Bode plot generated by the CAD package of the equivalent plant q_{22} shown in Fig. 4-10. This effect, which caused the 360° errors, can be seen by comparing the correct Bode angle plot obtained from the newly developed CAD package in Fig. 4-10 to the Bode angle plot obtained from MATLAB illustrated in Fig. 4-11. All plant cases must converge to the same angle at high frequencies, but the result from MATLAB does not reveal this. Only when the Bode angle is properly determined can the correct templates be generated.

Once the sets of templates are available, bounds on the NC can be generated. Since channel 2 was designed first by Arnold thus it is also examined first in this comparison. Bounds generated by the CAD package include stability bounds shown in Fig. 4-12, tracking bounds shown in Fig. 4-13, disturbance bounds shown in Fig. 4-14, and gamma bounds shown in Fig. 4-15. Composite bounds, shown in Fig. 4-16, are then generated based on the stability, disturbance, and tracking bounds. It is seen by comparing the composite bounds of Fig. 4-16 to those used by Arnold, shown in Fig. 4-17, that the disturbance bounds

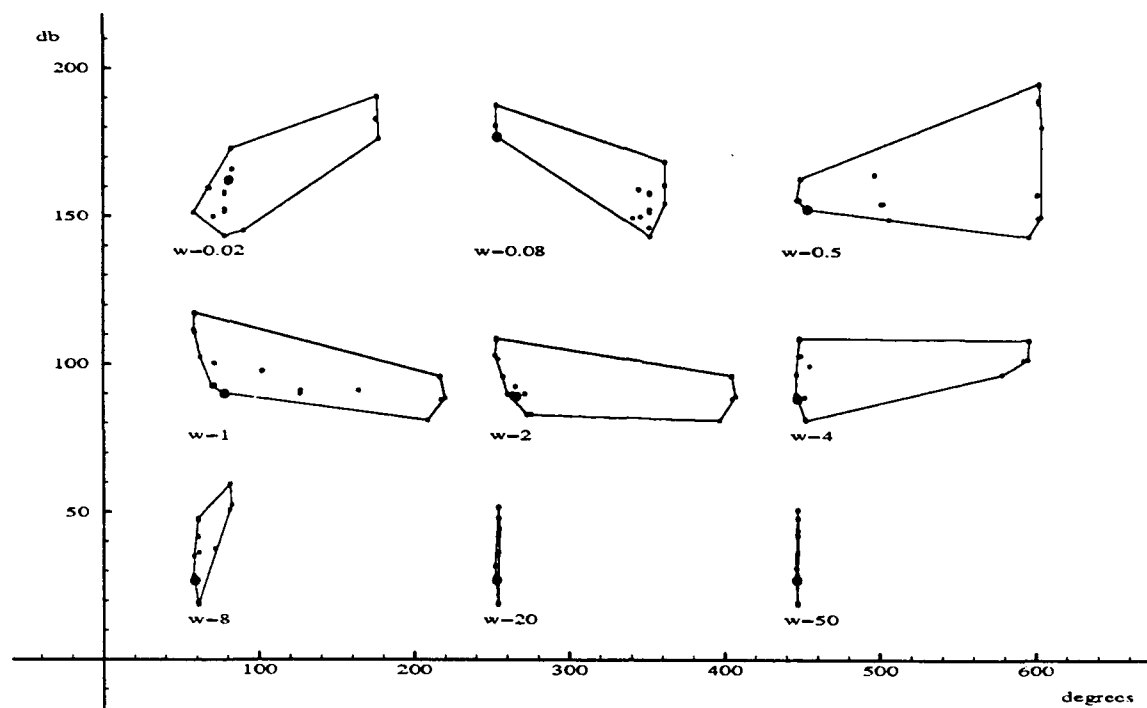


Fig. 4-2 Templates for channel 1

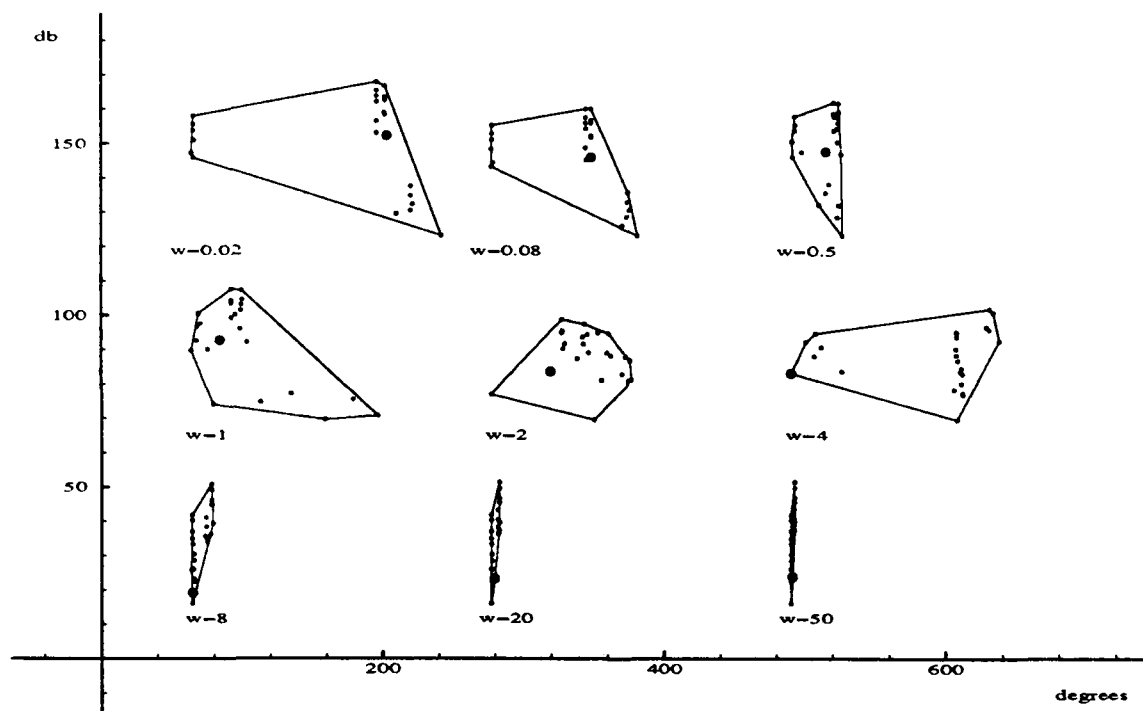


Fig. 4-3 Templates for channel 2

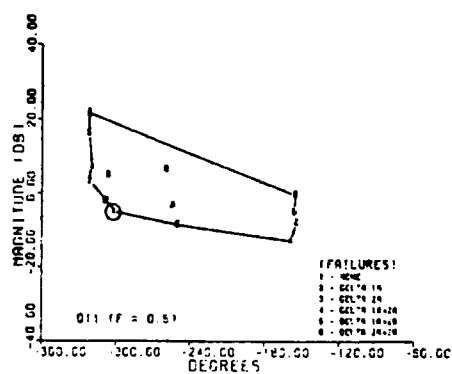


Fig. 4-4 Template for q_{11} , 0.5 rad/sec

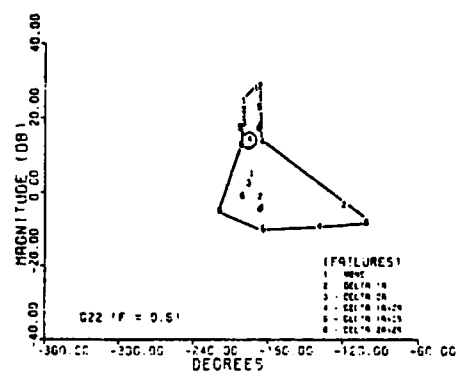


Fig. 4-5 Template for q_{22} , 0.5 rad/sec

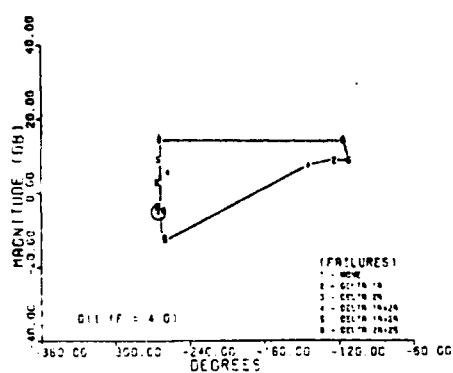


Fig. 4-6 Template for q_{11} , 4 rad/sec

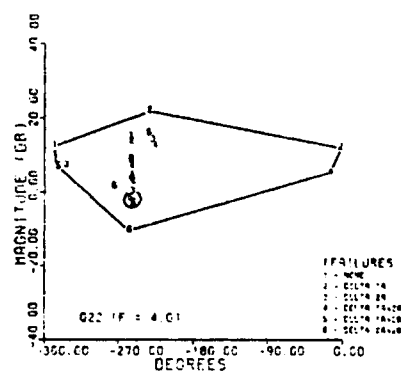


Fig. 4-7 Template for q_{22} , 4 rad/sec

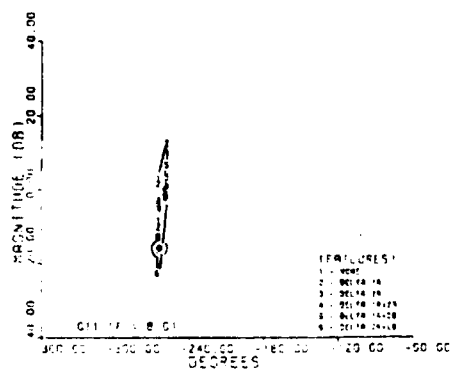


Fig. 4-8 Template for q_{11} , 8 rad/sec

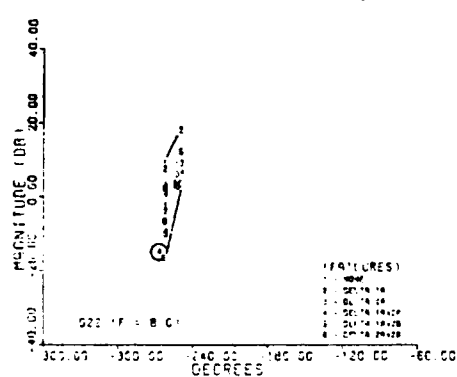


Fig. 4-9 Template for q_{22} , 8 rad/sec

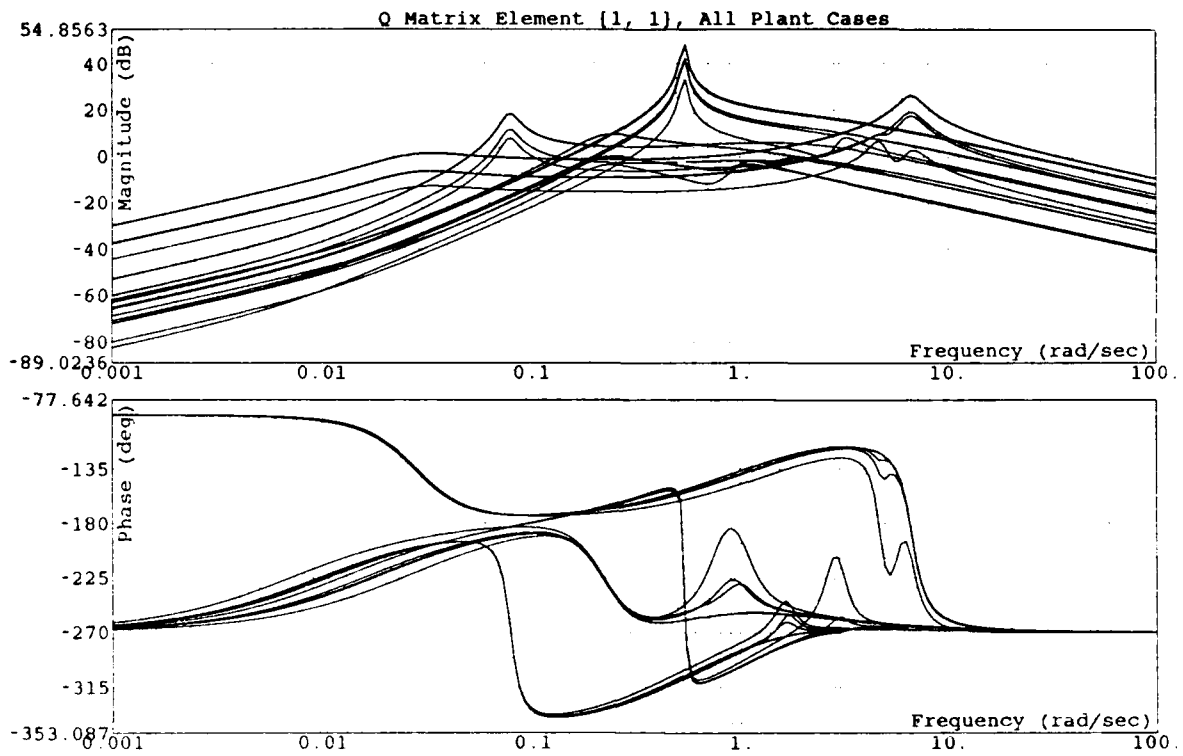


Fig. 4-10 Bode plot of q_{11} for all plant cases

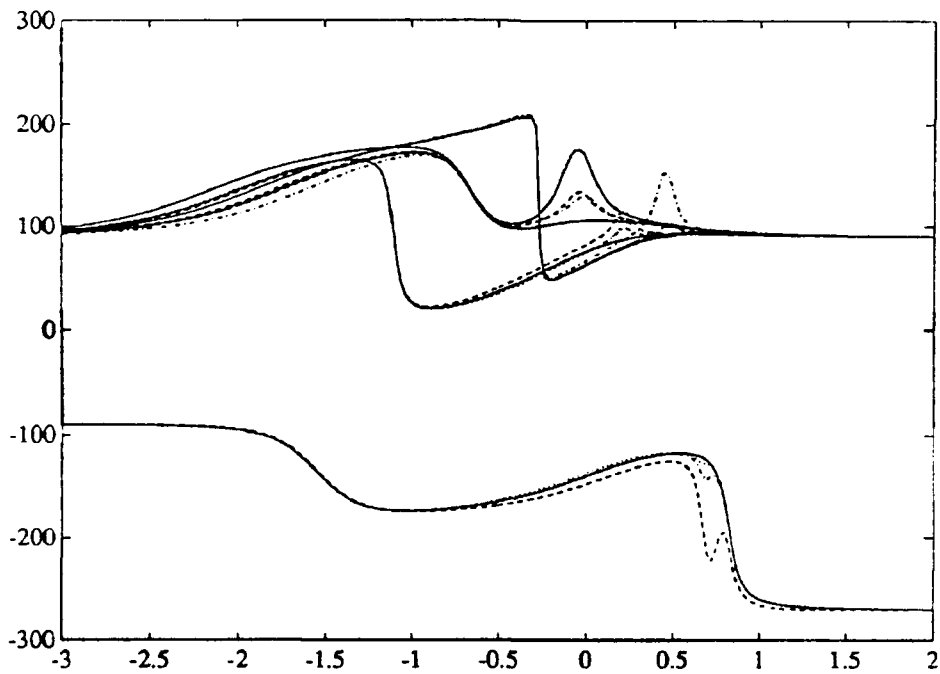


Fig. 4-11 Matlab Bode angle plot comparison

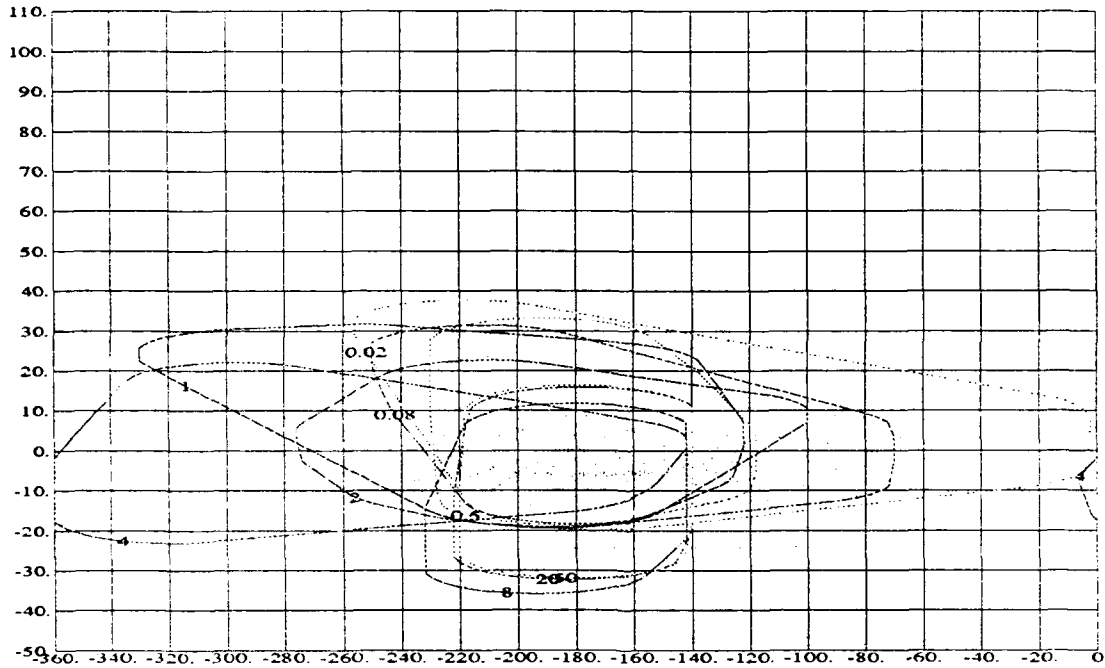


Fig. 4-12 Stability bounds for channel 2

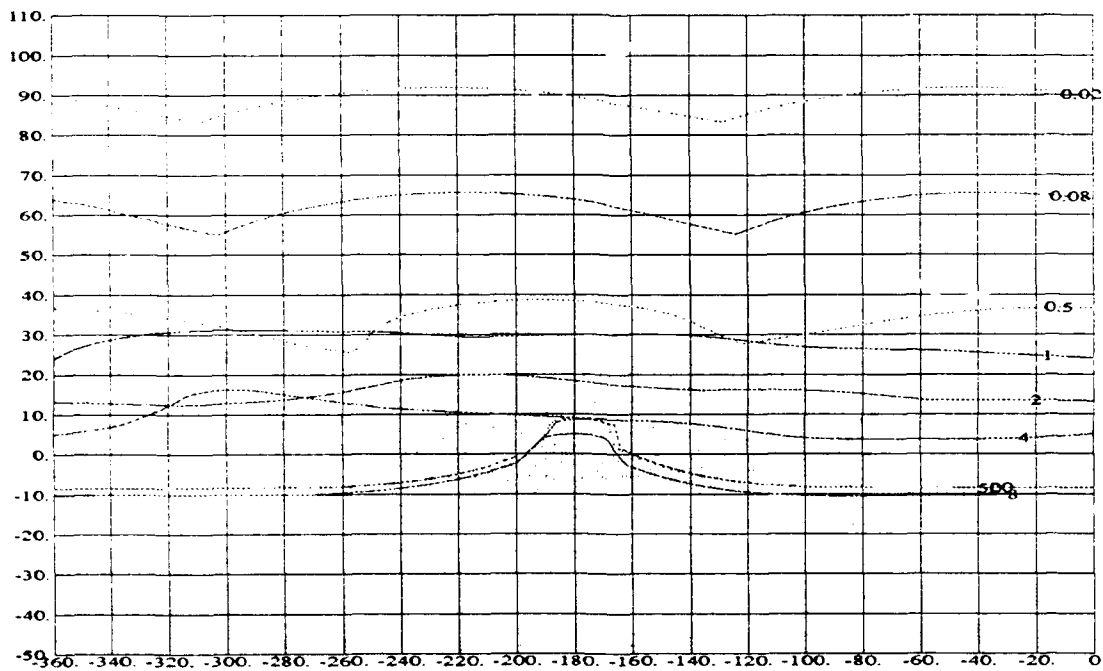


Fig. 4-13 Allocated tracking bounds for channel 2

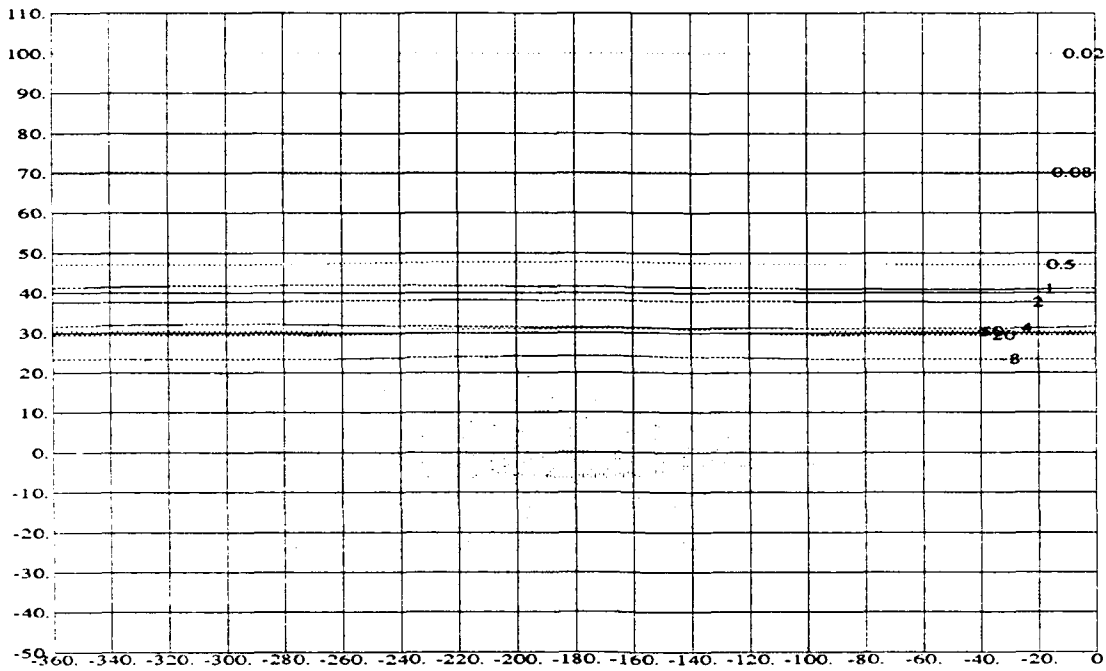


Fig. 4-14 Disturbance bounds for channel 2

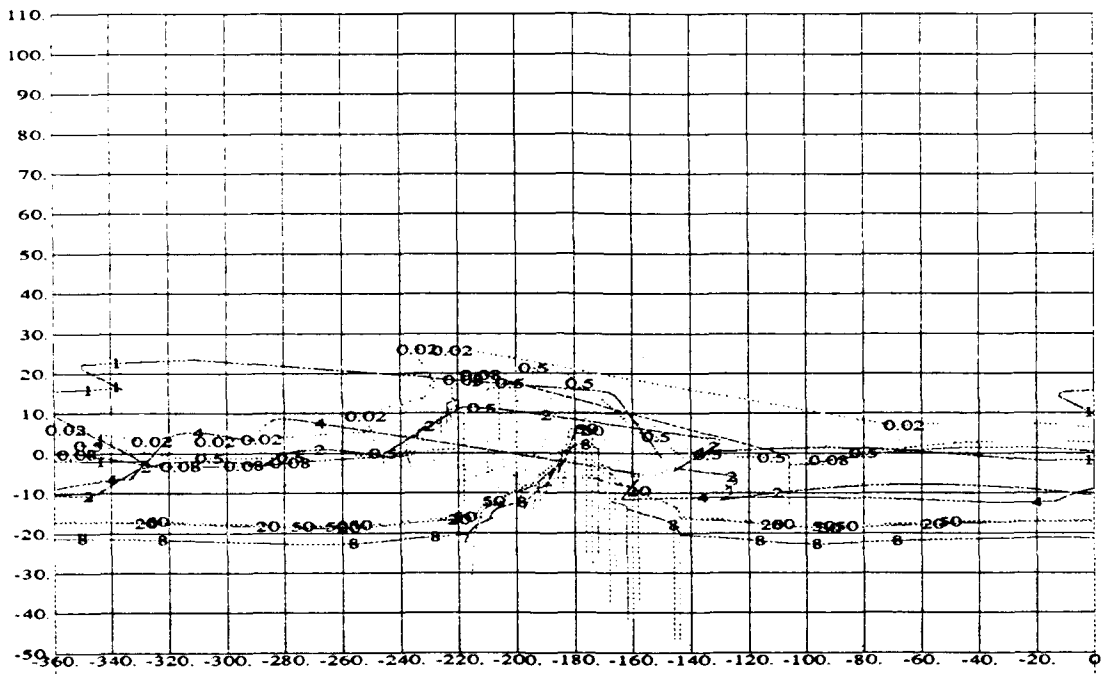


Fig. 4-15 Gamma bounds for channel 2

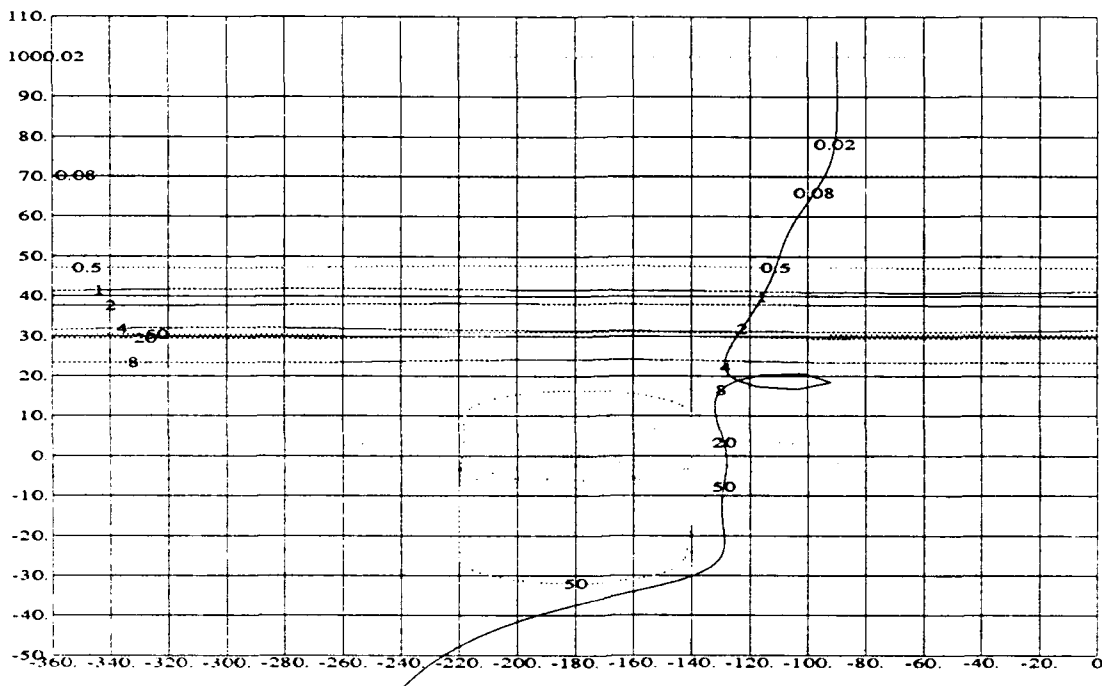


Fig. 4-16 Composite bounds with OLTF for channel 2

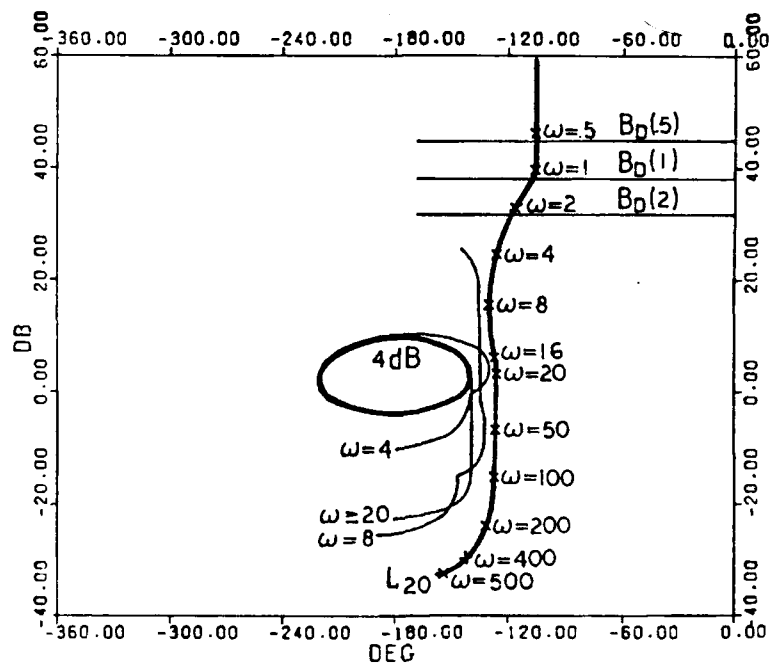


Fig. 4-17 Channel 2 OLTF from Arnold's thesis

dominate the composite bounds in both cases and that the disturbance bounds generated by the CAD package are less restrictive. Keeping in mind items 1 and 2 of Sec. 4.1, Arnold's $B_{D_{21}}(j\omega_i)$ bounds compare favorably with those generated by the CAD package. The difference arises due to the manner in which the disturbance bound on the loop transmission is computed.

In the CAD package the limit is implemented for the (i,j) MISO loop as:

$$|1 + q_{ii}g_i| \geq \frac{|q_{ii}|}{|b_{ij}|} \left(\sum_{k \neq i} \frac{|b_{kj}|}{|q_{ik}|} \right)_{\max} \quad (4-1)$$

The expression used by the CAD package is exact whereas in Arnold's thesis it is approximate, based on $|1 + L| \approx |L|$ in the low ω range, resulting in a more restrictive bound. For Arnold's case, when $|L_{20}| \gg 1$, the expression for the second channel, used by the CAD package, simplifies to:

$$|g_2 q_{22}| \geq \left| \frac{b_{11} q_{22}}{q_{21 \min} b_{21}} \right| \quad (4-2)$$

An additional discrepancy exists between the bounds used by Arnold and those generated by the CAD package. Arnold used only stability bounds for $\omega > 2 \text{ rad/sec}$, while the CAD package shows that tracking and disturbance bounds exist for all template frequencies. The disturbance bounds for L_{20} , as $\omega \rightarrow \infty$, never drop off the NC for Arnold's case because the restriction on $|1 + L_i|$, i.e.,

$$|1 + L_2| \geq \left| \frac{b_{11} q_{22}}{b_{21} q_{21 \min}} \right| \quad (4-3)$$

does not continue to become less restrictive for high frequencies as $\omega \rightarrow \infty$. This is true because all terms b_{11} , q_{22} , b_{21} , and q_{21} have an excess of poles over zeros of one, and therefore the magnitude of the right hand side of Eq. (4-3) entire quantity reaches a constant value at high frequencies. A limit exists, therefore, as to how much less restrictive the disturbance bounds become as the frequency for which the bounds are generated is increased. Control analysis considerations, however, permit the designer to disregard performance (tracking and disturbance) bounds at high frequencies since above some frequency ω_h only stability bounds are of concern (16). Once this open loop transmission has decreased to less than -12 dB, the effect of the open loop transmission on the time domain performance (transient response) of the closed loop

system is considered negligible. Therefore, the accepted practice is to consider only stability bounds for $\omega_i > \omega_h$. The CAD package generates and displays all bounds to allow the designer to apply engineering judgment in choosing which performance bounds to consider when designing the compensator.

Another significant difference between the bounds used by Arnold and those of the CAD package is evident in the plotting of tracking bounds. Because Arnold used a manual technique to plot the tracking bounds, he could never have plotted the tracking bound at $\omega = 0.02$ or at $\omega = 0.08$. Also, Arnold could not have plotted the tracking bounds at $\omega = 8$ or at $\omega = 20$ properly because he did not allocate a portion of δ_R to disturbance before checking for the existence of a tracking bound.

The open loop transmission on the NC with composite bounds (dominated by disturbance bounds) is shown in Fig. 4-16. As plotted, the performance bounds have all been violated. Also shown is the open loop transmission with gamma bounds in Fig. 4-18. It is seen that the loop transmission does not violate the gamma bounds for any of the bound frequencies. Accordingly, no right-half plane poles are introduced when Arnold applied the improved method for his channel 1 design. A Bode plot of the open loop

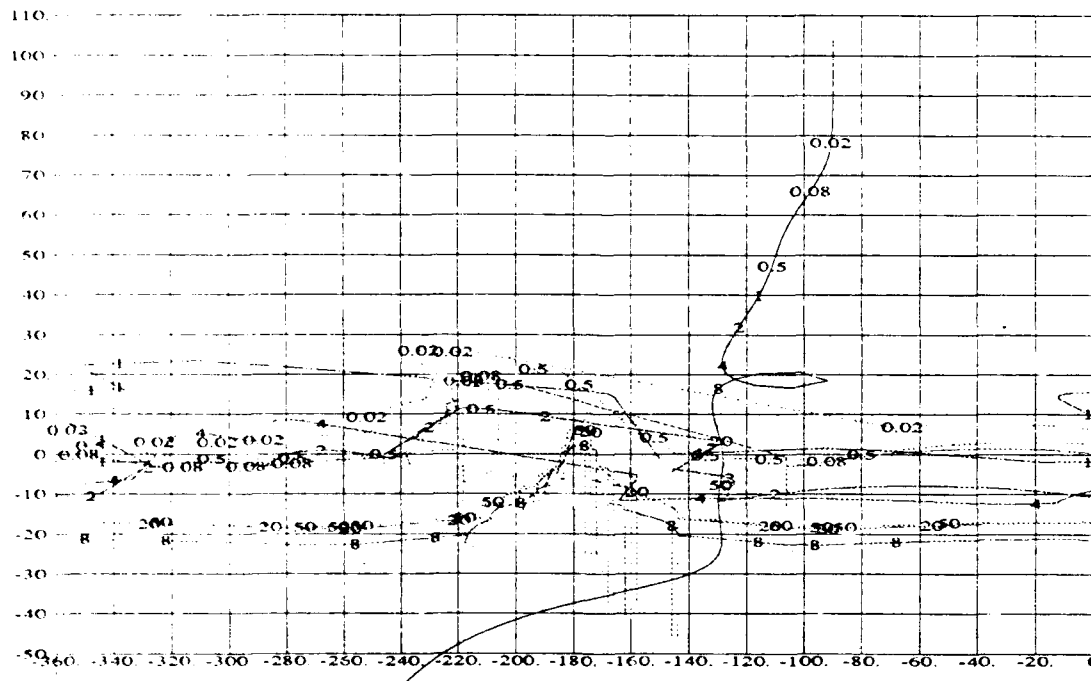


Fig. 4-18 Gamma bounds with OLTF for channel 2

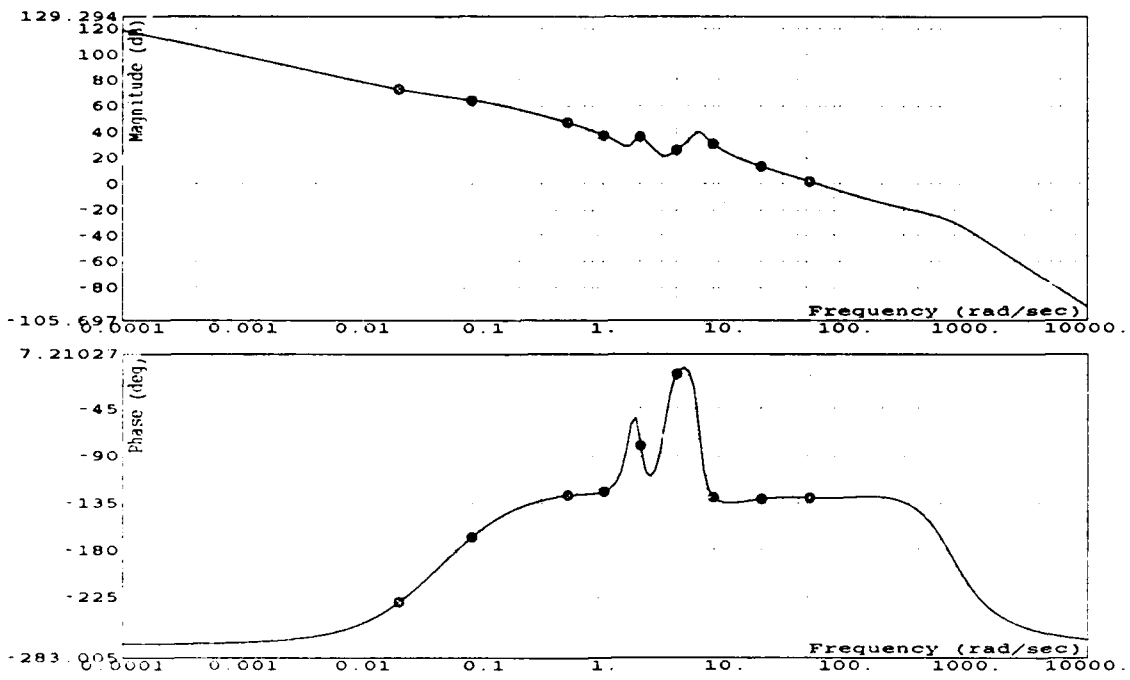


Fig. 4-19 Bode plot of channel 2 open loop transmission

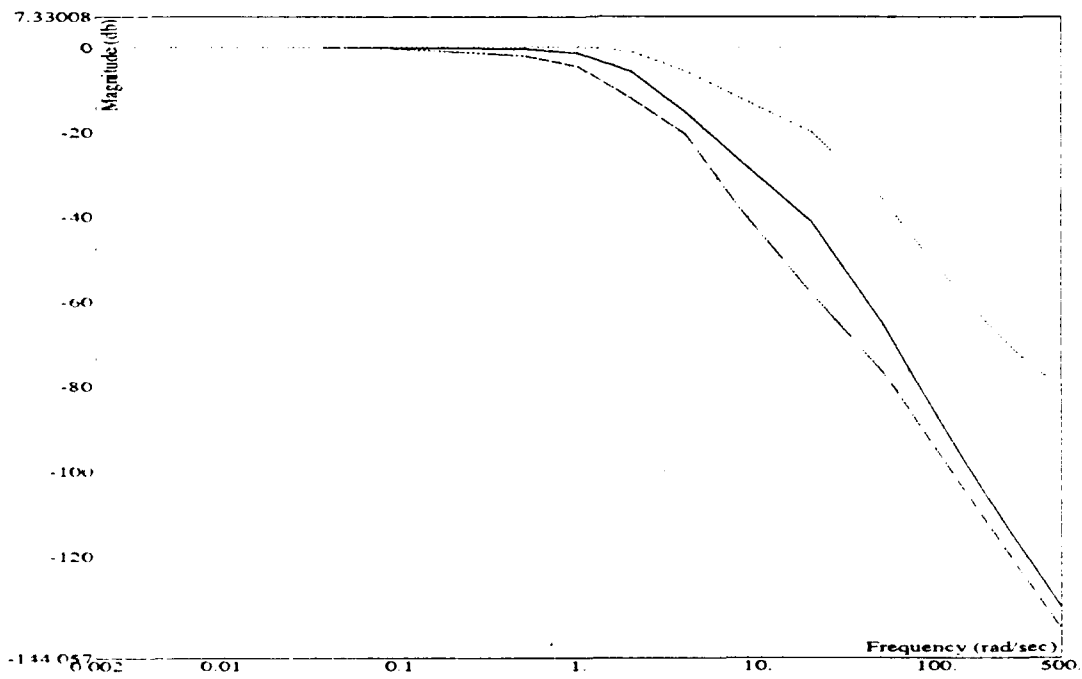


Fig. 4-20 Channel 2 nominal CLTF with filter bounds

transmission in Fig 4-19 shows a 0 dB crossover frequency of 27 rad/sec , which is about as high as acceptable for an aircraft flight control problem. There is little the designer can do, therefore, in terms of adding gain to satisfy the performance bounds on the NC. The bounds used for prefilter design are shown in Fig. 4-20. The prefilter from Arnold's thesis satisfies the tolerances on the nominal closed loop transmission up to 20 rad/sec , where b_{ij} is -20 dB. Since this is less than -12 dB, the prefilter design is considered good.

Arnold next accomplished the design of channel 1 by applying the improved method. He recognized that $\gamma_{ij} \ll 1$ for all plant cases resulted in the equivalent plant q_{11e} being essentially equal to q_{11} . The bounds are therefore generated by the CAD package of this thesis using the q_{ij} plants. The stability, tracking, and disturbance bounds are shown in Figs. 4-21, 4-22, and 4-23 respectively. Composite bounds, shown in Fig. 4-24, are then formed based on the stability, tracking, and disturbance bounds. The composite bounds of Fig. 4-24 are now compared to those given in Arnold's thesis shown in Fig. 4-25. The composite bounds of the CAD package as well as those given in Arnold's thesis are dominated by disturbance bounds.

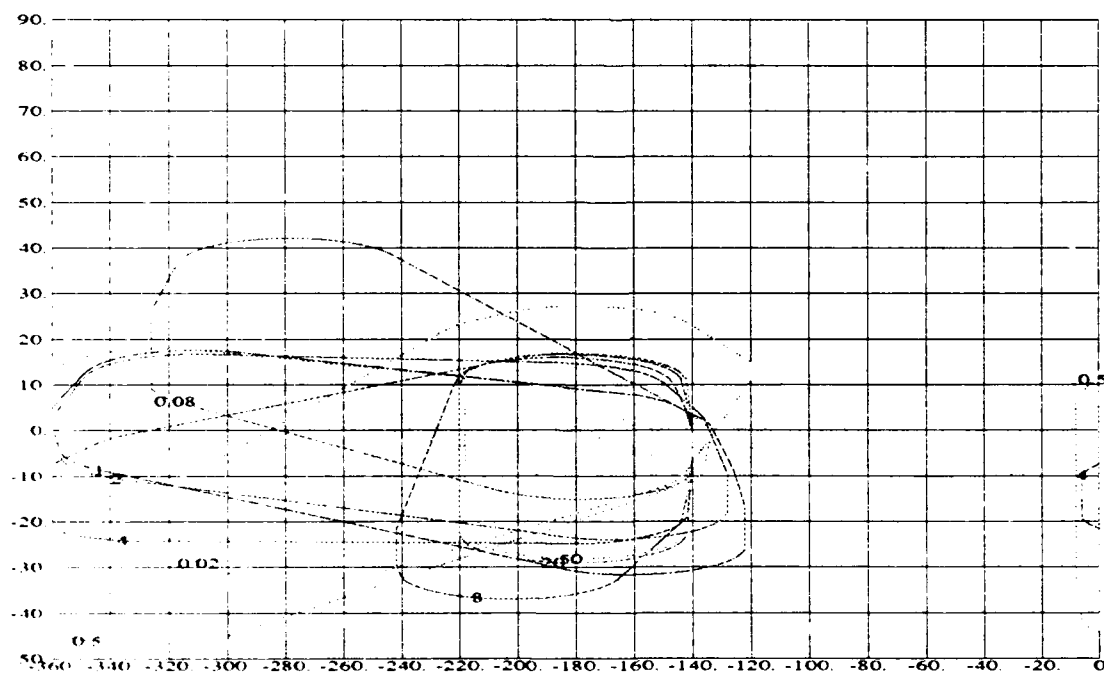


Fig. 4-21 Stability bounds for channel 1

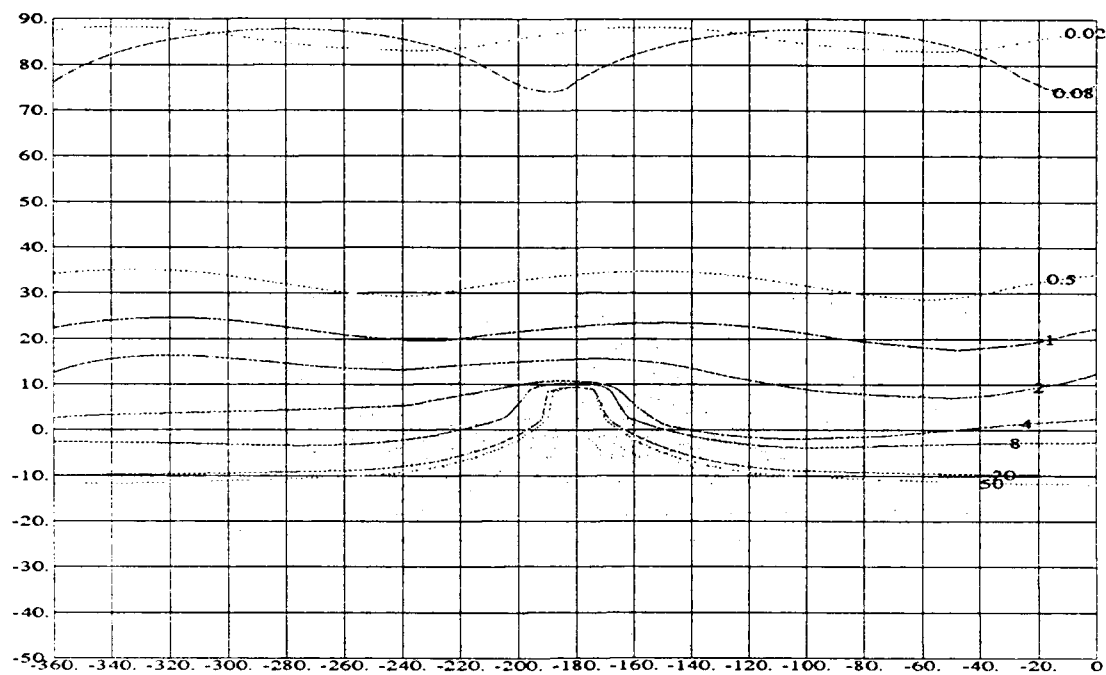


Fig. 4-22 Tracking bounds for channel 1

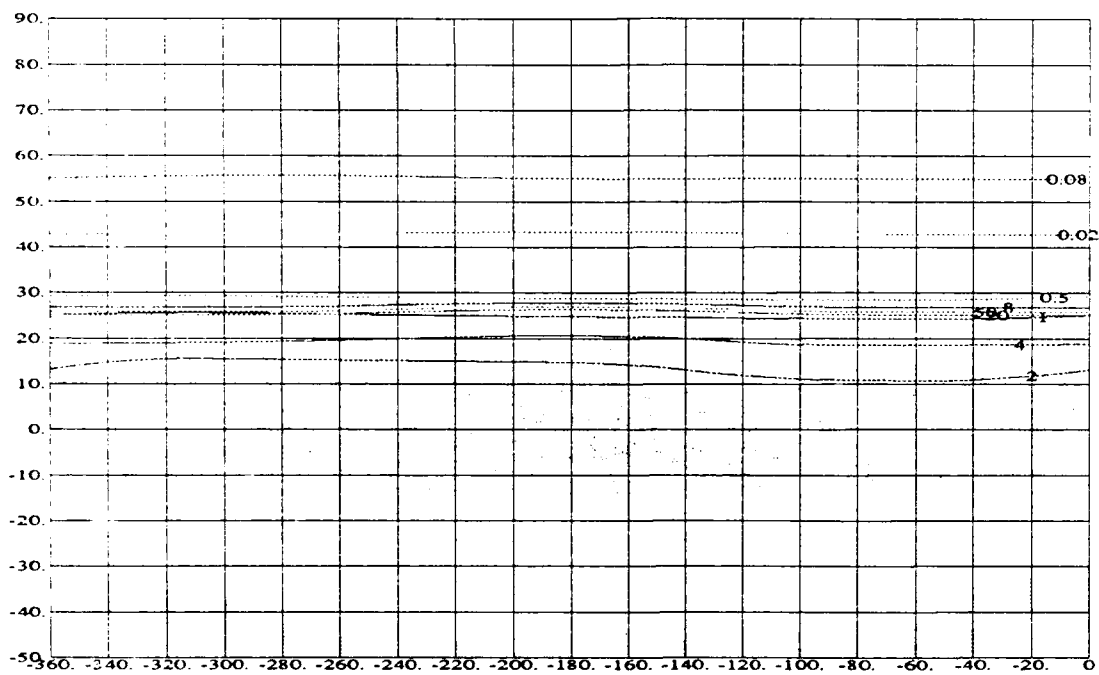


Fig. 4-23 Disturbance bounds for channel 1

The disturbance bounds on L_{10} generated by the CAD package, while slightly more restrictive, are in good agreement with those used by Arnold. The CAD package does, however generate disturbance bounds for all template frequencies while Arnold plotted disturbance bounds only for $\omega = 1 \text{ rad/sec}$ and $\omega = 2 \text{ rad/sec}$. Applying engineering judgment, Arnold chose to satisfy only stability bounds for frequencies greater than 2 rad/sec . The open loop transmission shown on the NC with composite bounds generated by the CAD package in Fig. 4-24 violates the performance bounds for frequencies greater than 1 rad/sec , which are dominated by the disturbance bounds. From the Bode plot of the loop transmission, Fig. 4-26, it is seen that the frequency at which the loop transmission crosses the 0 dB axis is 17 rad/sec . This frequency is below the highest tolerable crossover frequency for the aircraft flight control system of 30 rad/sec . (16). As with the open loop of channel 2, the gain cannot be increased much further in an attempt to meet the performance bounds without exceeding the highest tolerable crossover frequency. Arnold therefore could not have satisfied the disturbance bounds for frequencies above 1 rad/sec if they had been plotted.

The Bode plot of the nominal closed loop transmission with upper and lower filter bounds shown in Fig. 4-27 shows that the prefilter design satisfies the diagonal MISO loop performance specifications up to the frequency 60 rad/sec , which is much larger than needed, except for the region around 0.08 rad/sec , at which the channel between a'_{ij} and b'_{ji} is pinched off. This violation must be tolerated for the same reason that the violation in the disturbance bound violations must be tolerated: the gain cannot be increased without limit.

The closed loop transfer function matrix is then formed based on the compensator and prefilter transfer functions given in Arnold's thesis and the effective plants formed from the basic plant models and weighting matrix. Bode plots of the closed loop system response of the true MIMO system are plotted by the CAD package and are shown in Fig. 4-28 along with the performance tolerances. The violations in the disturbance bounds, in particular, manifest themselves in violation of the performance tolerances of the off-diagonal closed loop transmissions. The violation of the tracking bound at 0.08 rad/sec for channel 2 results in the notch at 0.08 rad/sec in the closed loop response of the (1,1) transfer function. The plot of closed loop

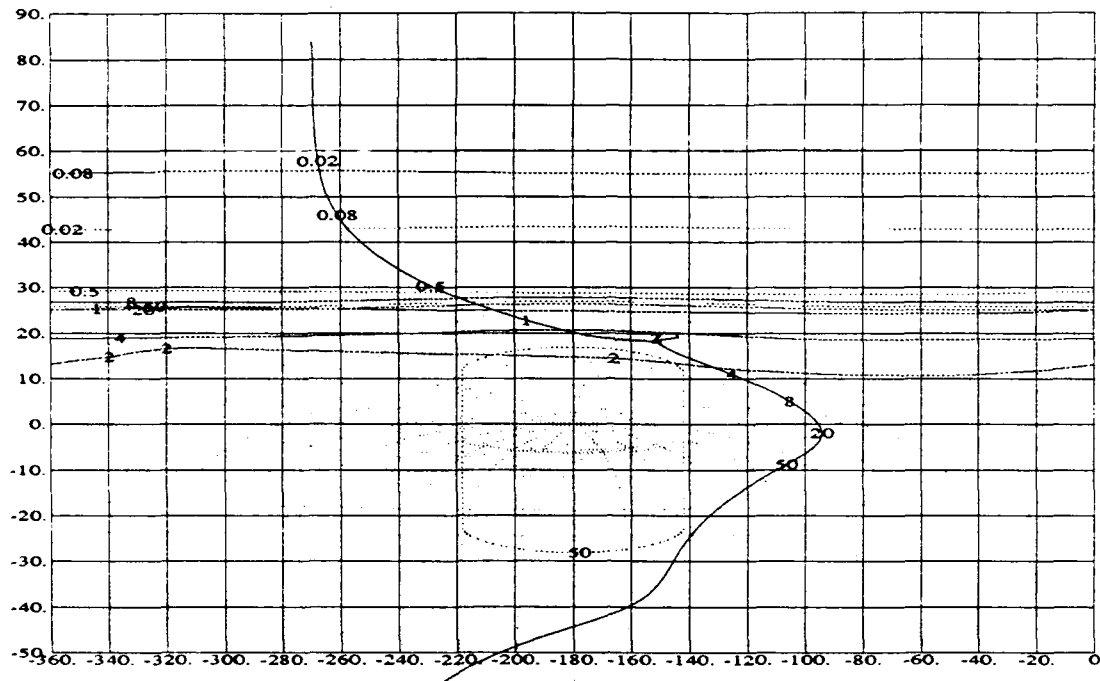


Fig. 4-24 Channel 1 OLTF with composite bounds

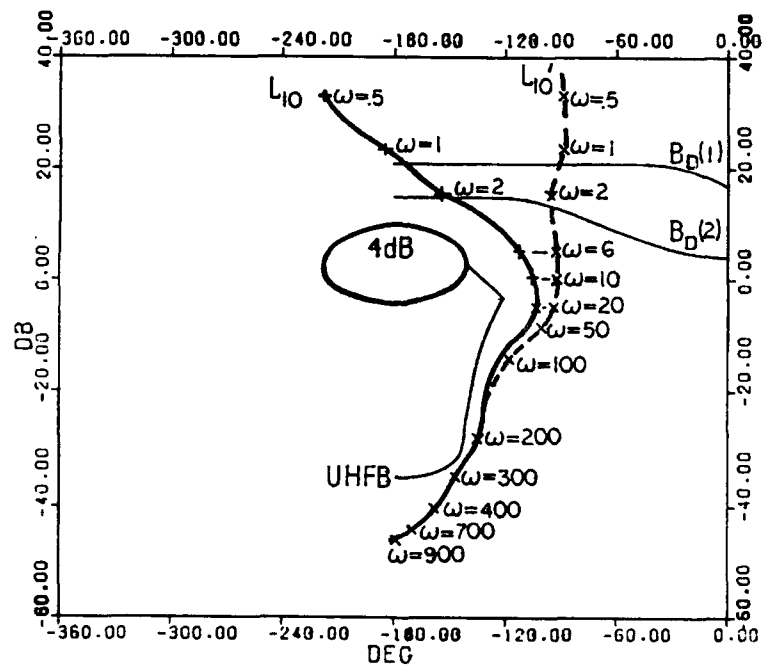


Fig. 4-25 Channel 1 OLTF from Arnold's thesis

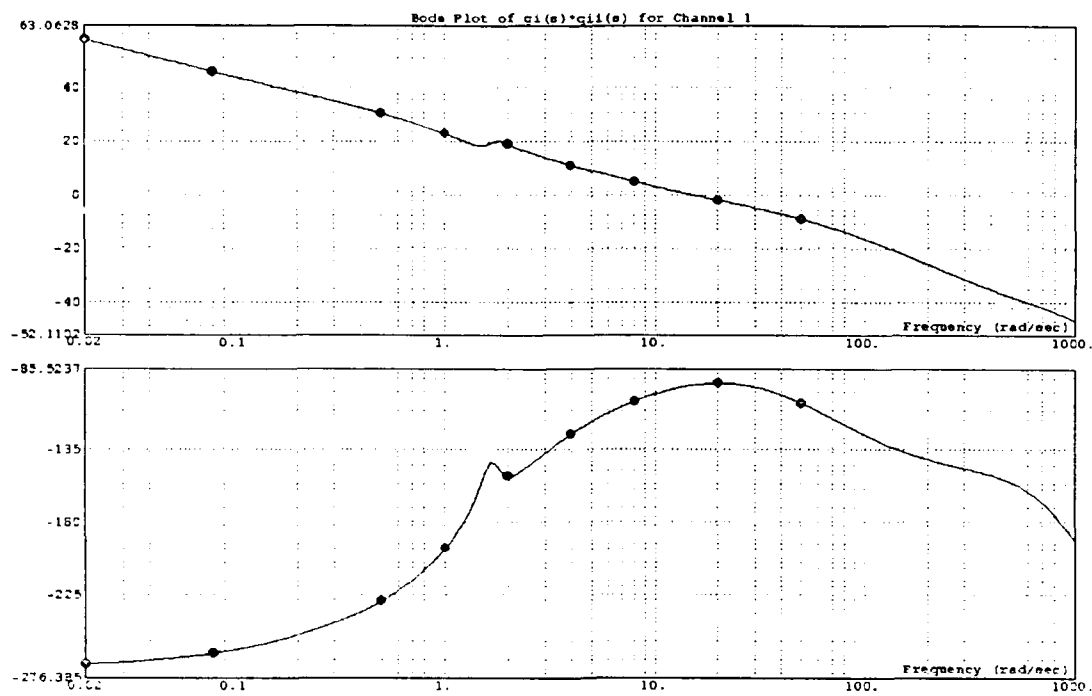


Fig. 4-26 Bode plot of channel 1 open loop transmission

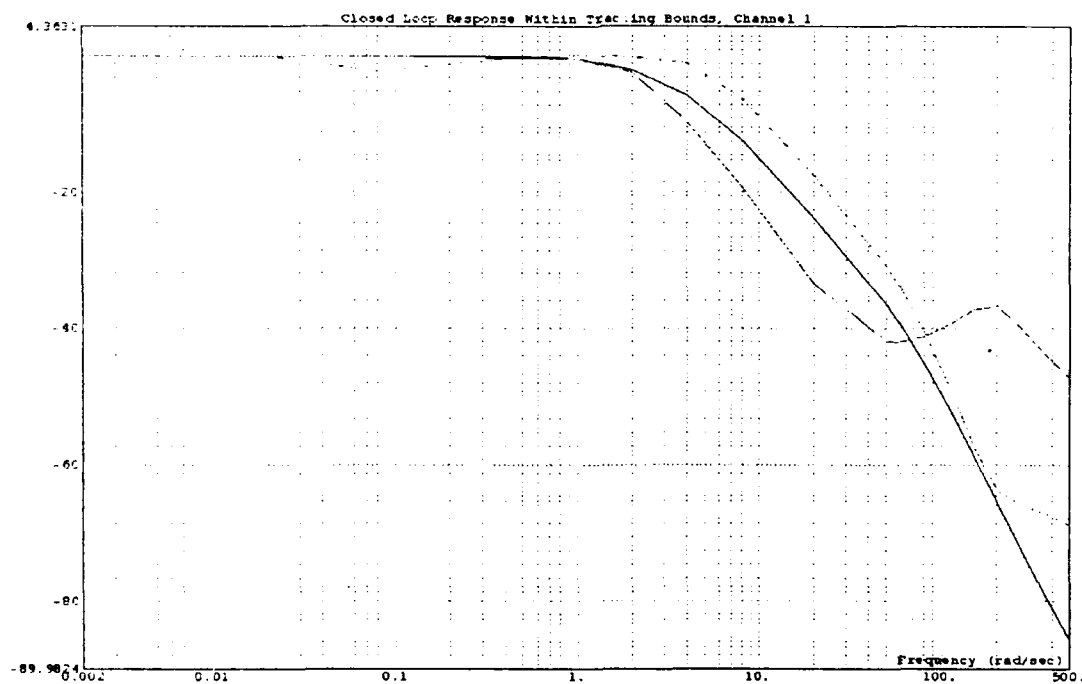


Fig. 4-27 Channel 1 nominal CLTF with filter bounds

transfer function responses, therefore, is shown to be a useful tool for visualizing the consequences of violating performance bounds on the NC during the design process.

The open loop transmissions of the 24 plant cases are plotted on the NC for channel 1 and channel 2 in Figs. 4-29 and 4-30, respectively, to verify that the compensator designs satisfy the stability specifications. From the Nichols plots, it can be seen by inspection that for channels 1 and 2 none of the open loop transmissions violate the 4 dB M_L contour on the Nichols plots of Figs. 4-29 and 4-30.

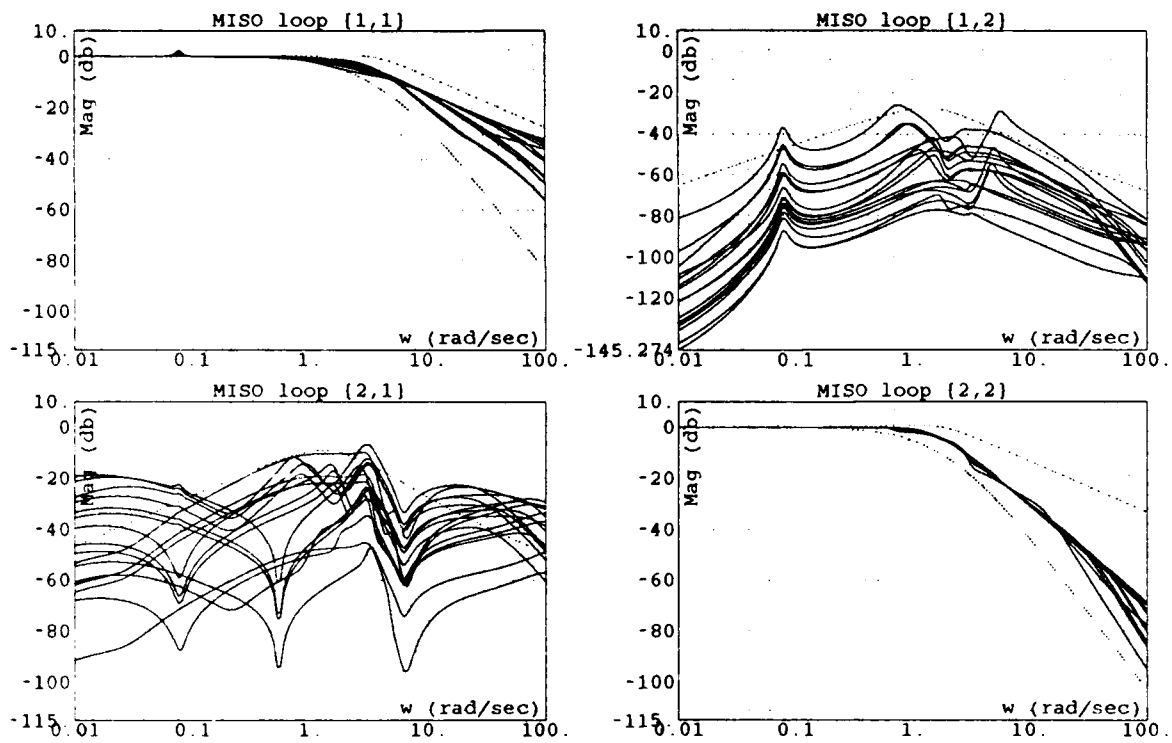


Fig. 4-28 Closed loop transmissions for Arnold

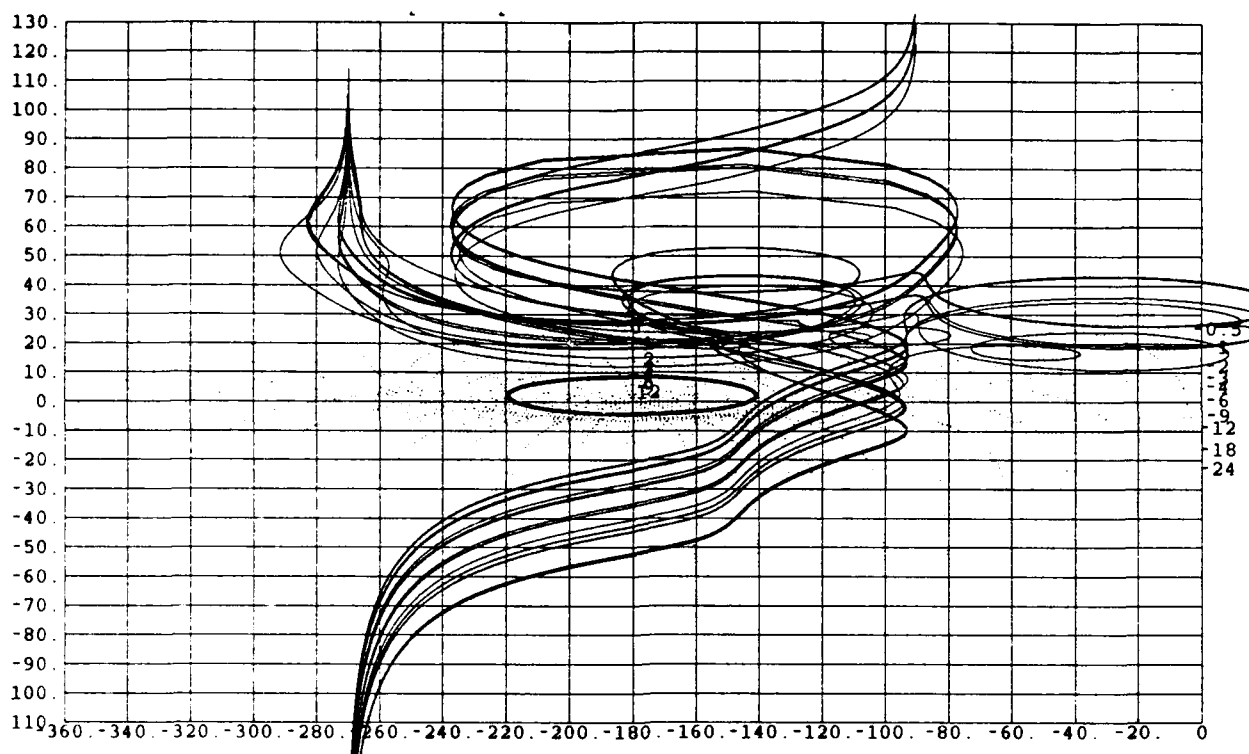


Fig. 4-29 Open loop transmissions for channel 1

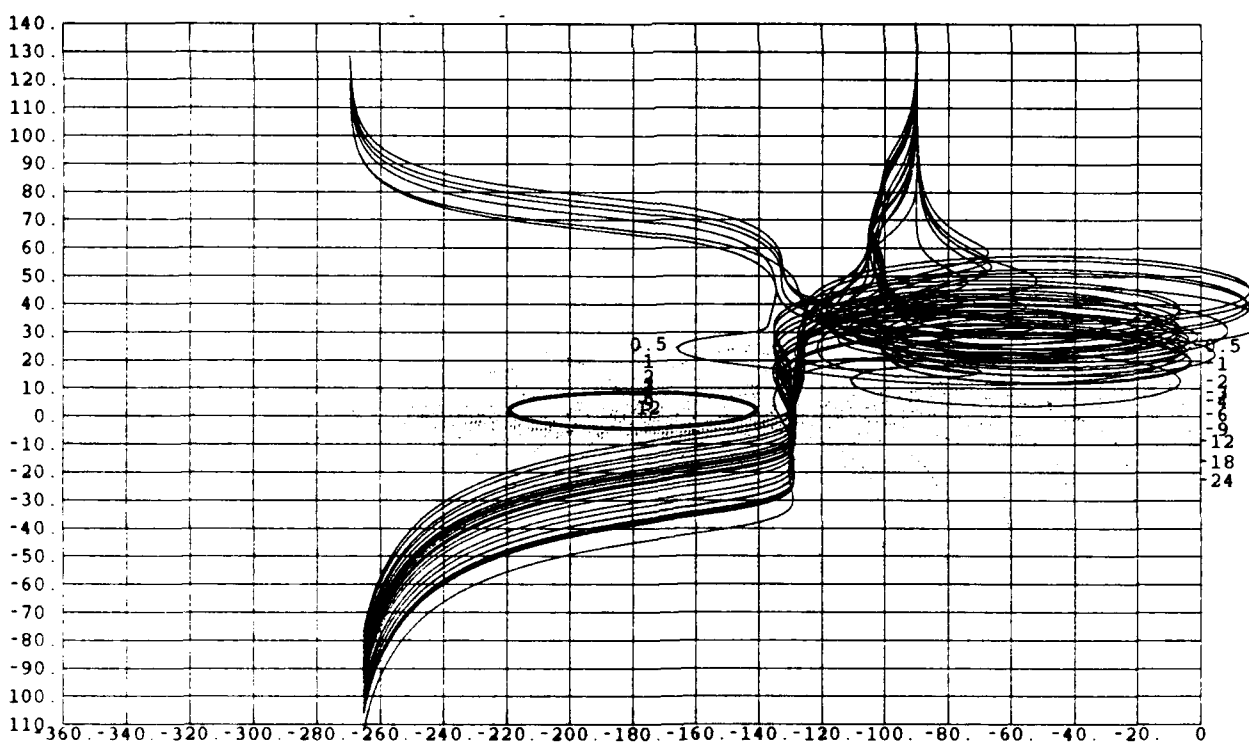


Fig. 4-30 Open loop transmissions for channel 2

4.3 Validation of Thesis Results of Robert Betzold

The implementation of the algorithms of the MIMO CAD package is also validated by comparing results obtained by using the CAD package to those shown in Betzold's thesis (5). In his thesis, Betzold applied MIMO QFT theory by utilizing the improved method to design the analog channel controllers for the C-135 aircraft. He also utilized diagonal prefilter and compensator matrices, \underline{F} and \underline{G} , respectively, for his 2×2 effective plant. Bank angle and sideslip are the aircraft parameters to be controlled. Since there is no sideslip command input, only one equivalent MISO and one SISO loop are considered in the thesis: roll due to roll command and sideslip due to roll command as shown in Figs. 4-31 and 4-32, respectively.

Betzold provides the equivalent plant matrix \underline{Q} for each of the three flight conditions considered in his design. These plant matrices are manually entered into the CAD package. Effective plant matrices are formed by working backwards from \underline{Q} to \underline{P}_e for the purpose of forming the closed loop system to illustrate the performance of the controller in the frequency domain. The diagonal elements q_{ij} of the matrix \underline{Q} are used directly to form the plant templates shown in Fig 4-33 for channel 1 and in Fig. 4-34 for channel 2.

Betzold began by designing the off-diagonal SISO loop of channel 2, see Fig. 4-32, to meet specifications on sideslip due to roll command. Plant case 2 is chosen as the nominal plant for channel 2 and is

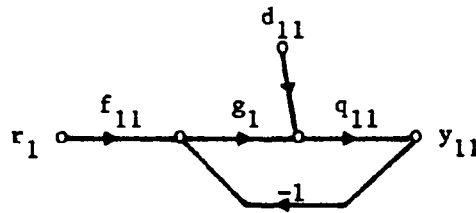


Fig. 4-31 (1,1) MISO loop from Betzold's thesis

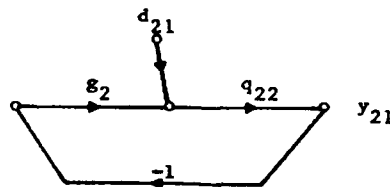


Fig. 4-32 (2,1) SISO loop from Betzold's thesis

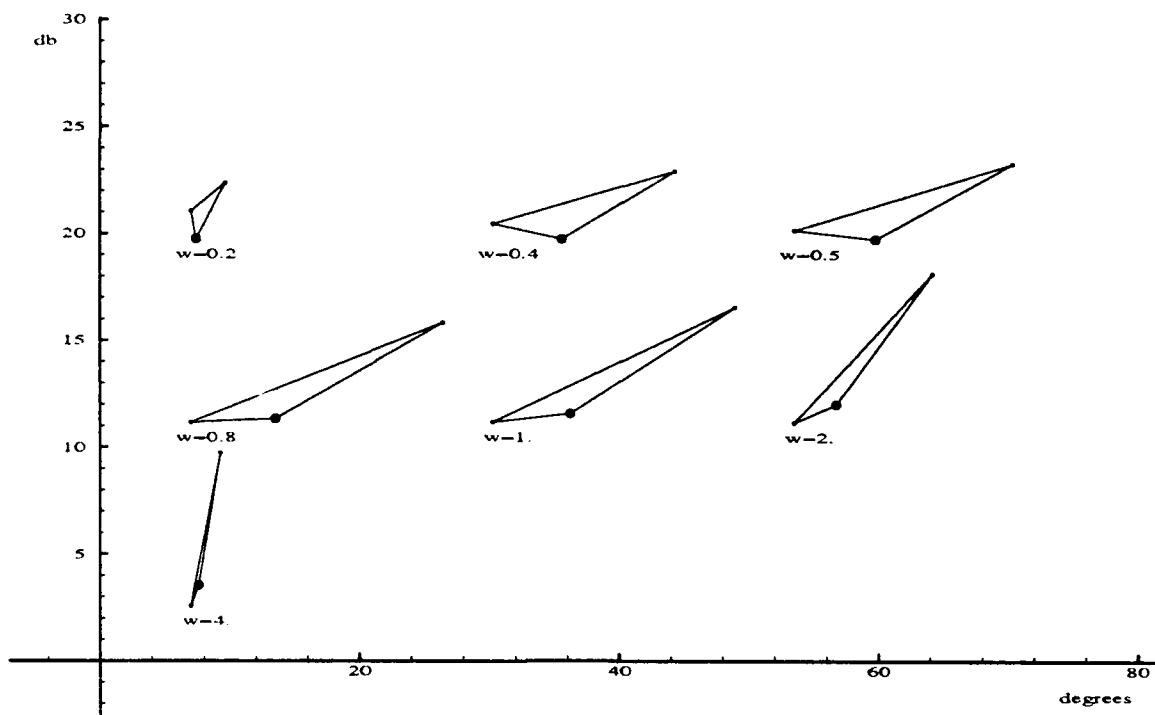


Fig. 4-33 Templates for Channel 1 of Betzold's thesis

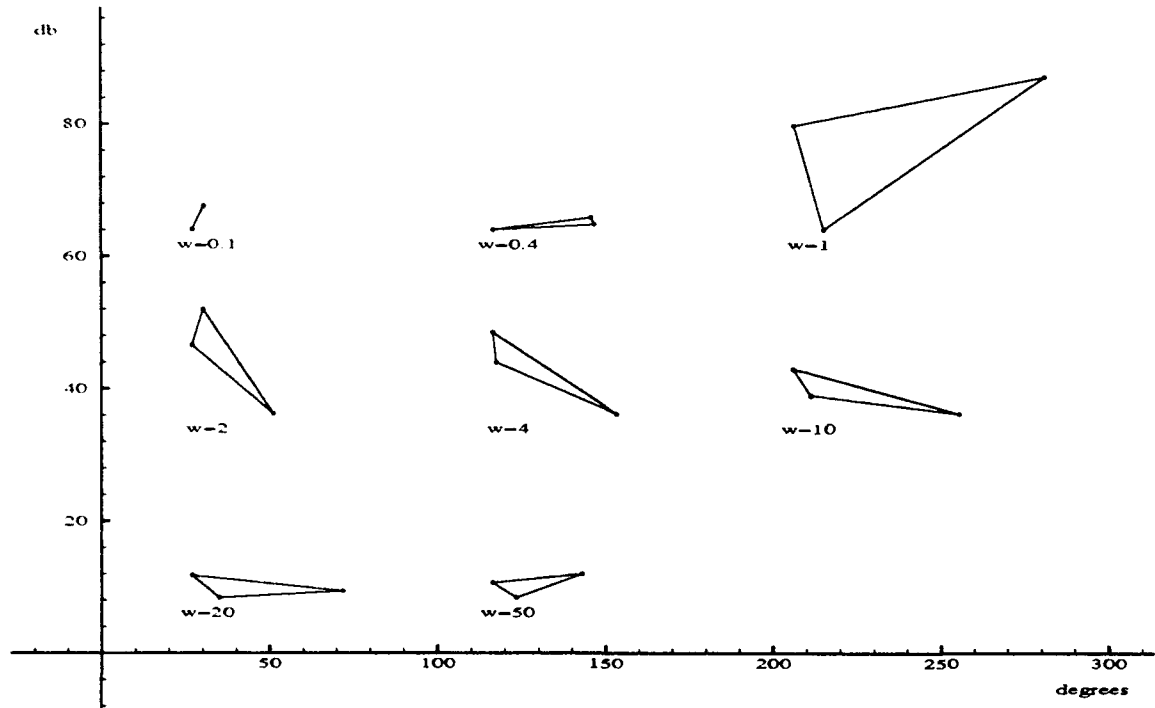


Fig. 4-34 Templates for channel 2 of Betzold's thesis

emphasized on the chart of templates shown in Fig. 4-34. For this channel, stability, disturbance, and gamma bounds are generated by the CAD package as shown in Fig. 4-35, Fig. 4-36, and Fig. 4-37 respectively. Tracking bounds are not generated since there is no sideslip command. Next, a set of composite bounds are generated by the CAD package based on the stability and disturbance bounds. The open loop transmission plotted on the NC along with the composite bounds is shown in Fig. 4-38. The plot shows that the open loop transmission of channel 2 easily satisfies all composite bounds generated by the CAD package. Comparing the composite bounds generated by the CAD package to those from Betzold's thesis shown in Fig. 4-39, the bounds are seen to be in close agreement.

Since Betzold was using the improved method, the open loop transmission is also plotted on the NC with the gamma bounds as shown in Fig. 4-37. The loop easily satisfies all gamma bounds. Accordingly, no new right-half plane poles are introduced into the equivalent plants formed by applying the improved method. Next, a Bode plot of the open loop transmission is generated showing an acceptable 0 dB crossover frequency of 20 rad/sec . No prefilter is designed for this channel since there is no sideslip input.

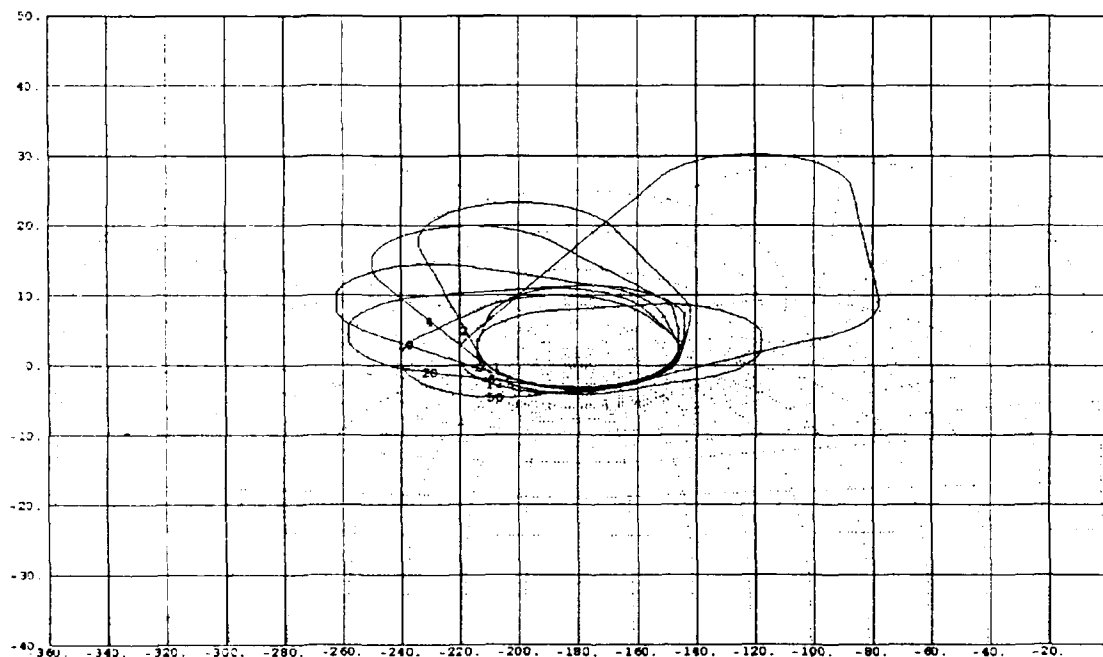


Fig. 4-35 Stability bounds for channel 2

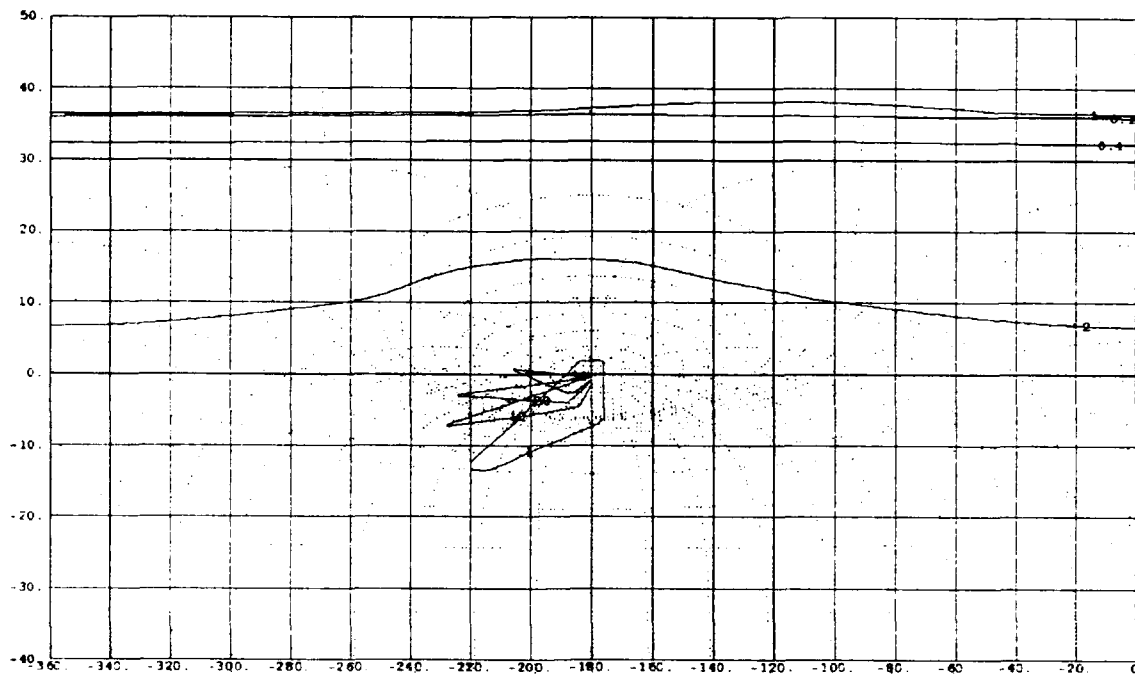


Fig. 4-36 Disturbance bounds for channel 2

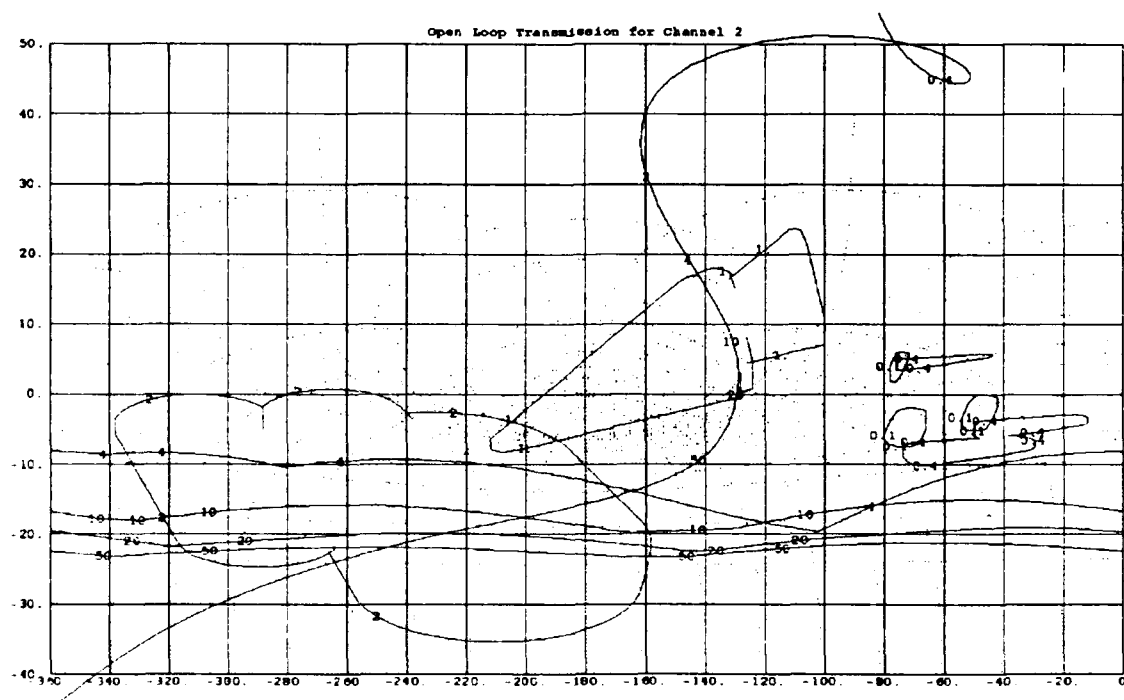


Fig. 4-37 Channel 2 OLTF with gamma bounds

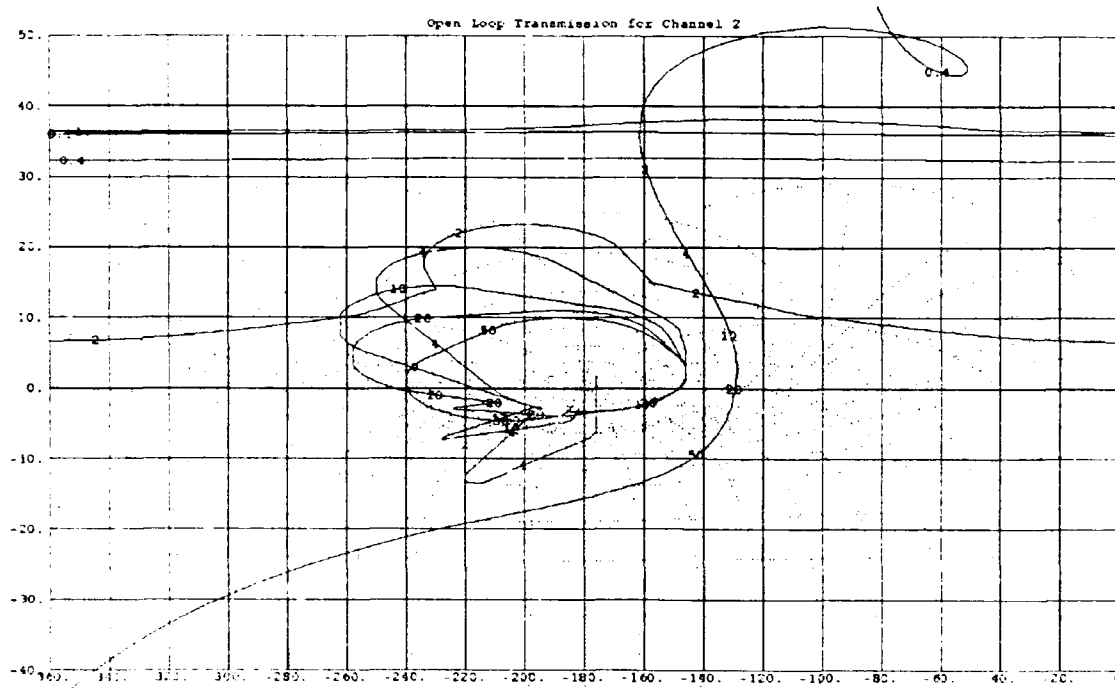


Fig. 4-38 Channel 2 OLTF with composite bounds

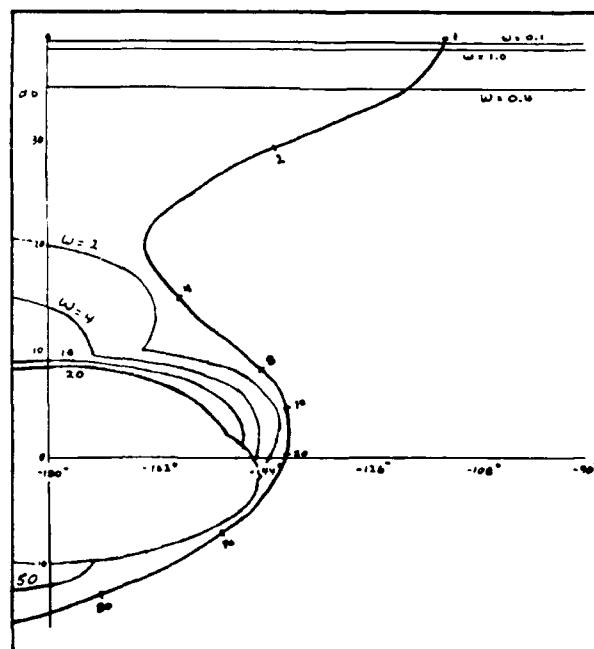


Fig. 4-39 Channel 2 OLTF from Betzold's thesis

Next, Betzold designed the compensator and prefilter for channel 1. Betzold applied the improved method to obtain a new set of equivalent plants q_{11}^* , which are manually substituted for q_{11} in the CAD package. A plant not among the plant cases is chosen as the nominal plant. Therefore no plant point is emphasized on the templates for the first channel shown in Fig. 4-33. Once the templates are generated, the bounds are formed. For the roll channel, channel 1, only stability and tracking bounds are generated, and are shown in Figs. 4-40 and 4-41 respectively. No disturbance bounds are generated since there is no sideslip command input for channel 2. It can also be seen that the tracking bound is significantly more restrictive than those plotted by Betzold. The difference arises because Betzold did not allocate for disturbance when plotting the tracking bound.

The open loop transmission and composite bounds are then plotted on the NC by the CAD package as shown in Fig. 4-42. The open loop transmission violates every tracking bound on the NC. This contrasts with the open loop and tracking bounds in Betzold's thesis, shown in Fig. 4-43, which satisfies the tracking bounds. When the tracking bounds generated by the CAD package do not take disturbance into account, the tracking bounds as plotted on the NC in Fig. 4-44 are identical to those of Betzold's thesis; none of the bounds are violated by the open loop transmission. The consequences of not taking the effect of disturbance into account is apparent when the closed loop system is formed and the Bode plot of t_{ij} plotted.

The compensator for channel 1 is now re-designed to validate that the frequency domain performance tolerances a_{11} and b_{11} are satisfied when the open loop transmission L_{10} satisfies the bounds generated by the CAD package. First, a Bode plot of the open loop transmission for channel 1 using the compensator given in Betzold's thesis is examined. From the Bode plot in Fig. 4-45, it is seen that the 0 dB crossover frequency for the open loop is 1 rad/sec . More gain can be tolerated in channel 1 since this has a low cutoff frequency. When the CAD package plots the nominal closed loop transmission with filter bounds based on Betzold's compensator, shown in Fig. 4-46, the upper bound is below the lower bound. This is caused by the fact that the allocated tracking bounds are all violated by the open loop transmission. Figure 4-46 implies, therefore, that no solution exists for the prefilter design problem using the compensator given in

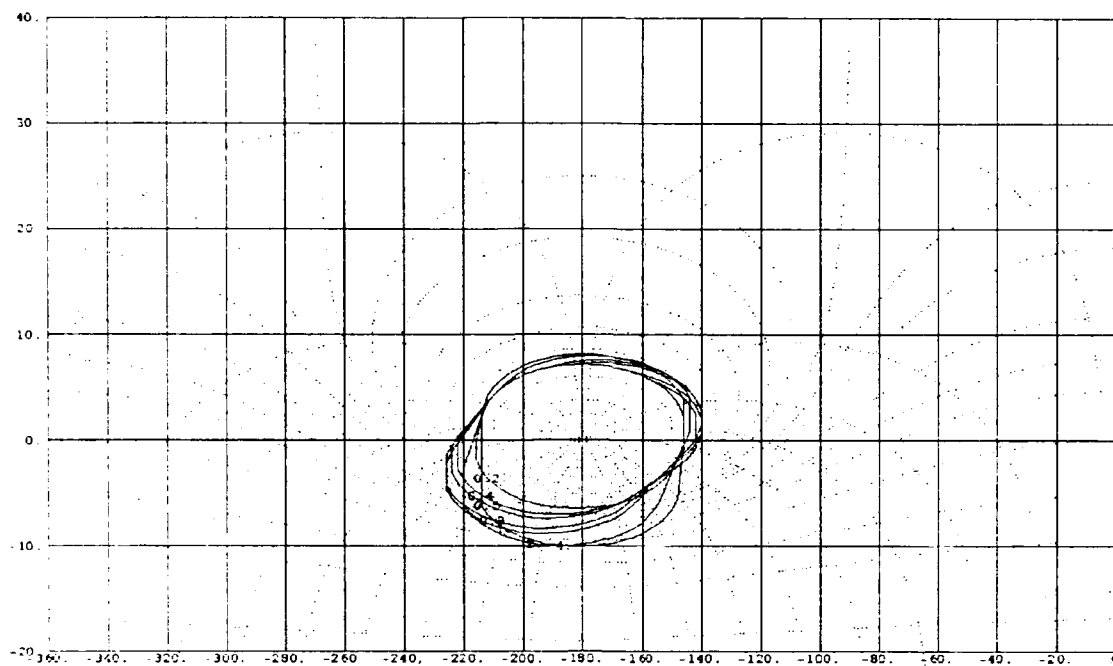


Fig. 4-40 Stability bounds for channel 1

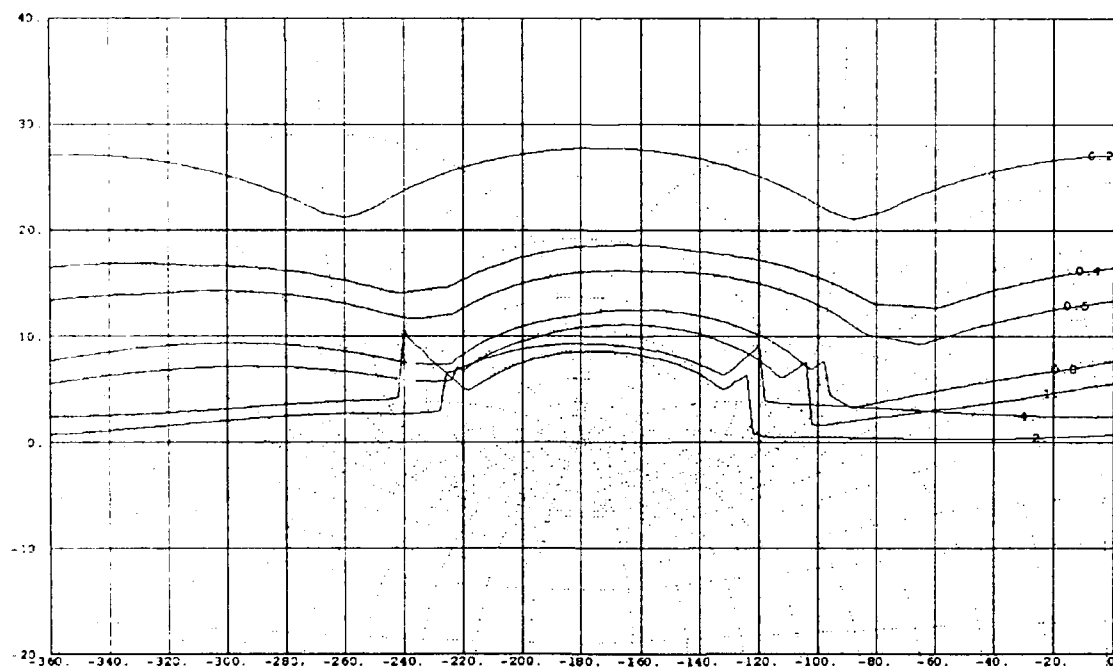


Fig. 4-41 Allocated tracking bounds for channel 1

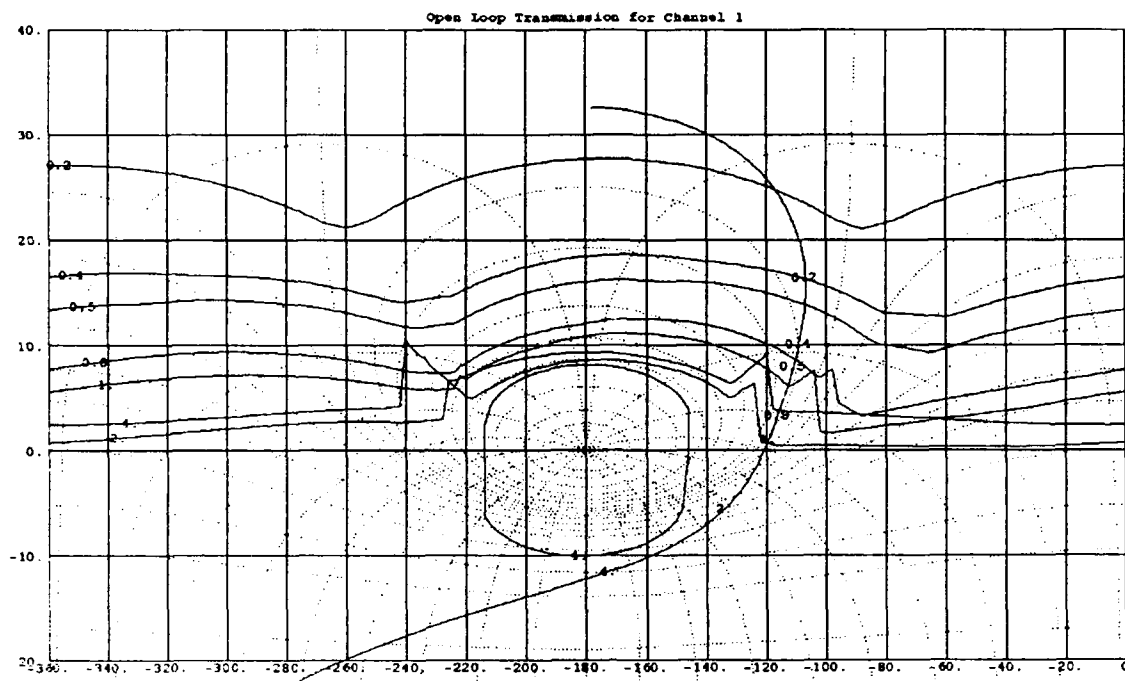


Fig. 4-42 Channel 1 OLTF with composite bounds

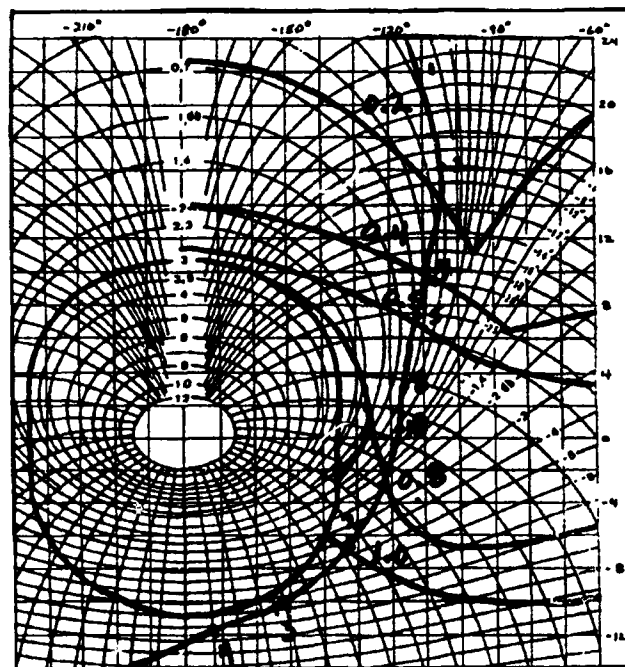


Fig. 4-43 Channel 1 OLTF from Betzold's thesis

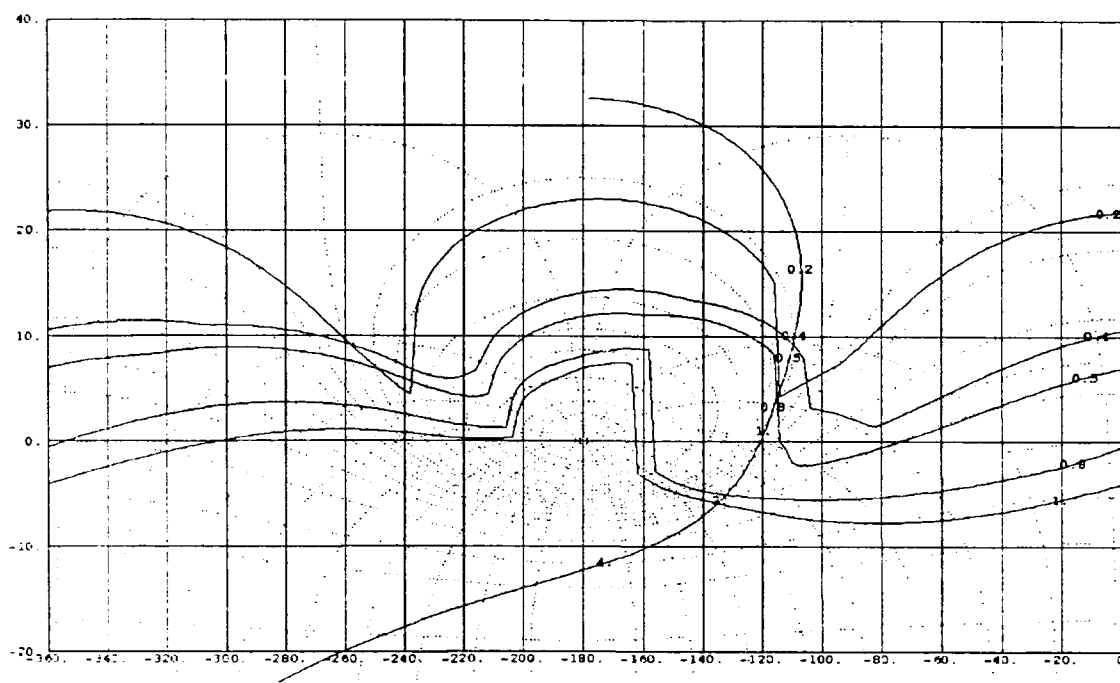


Fig. 4-44 OLTF with bounds - disturbance not allocated

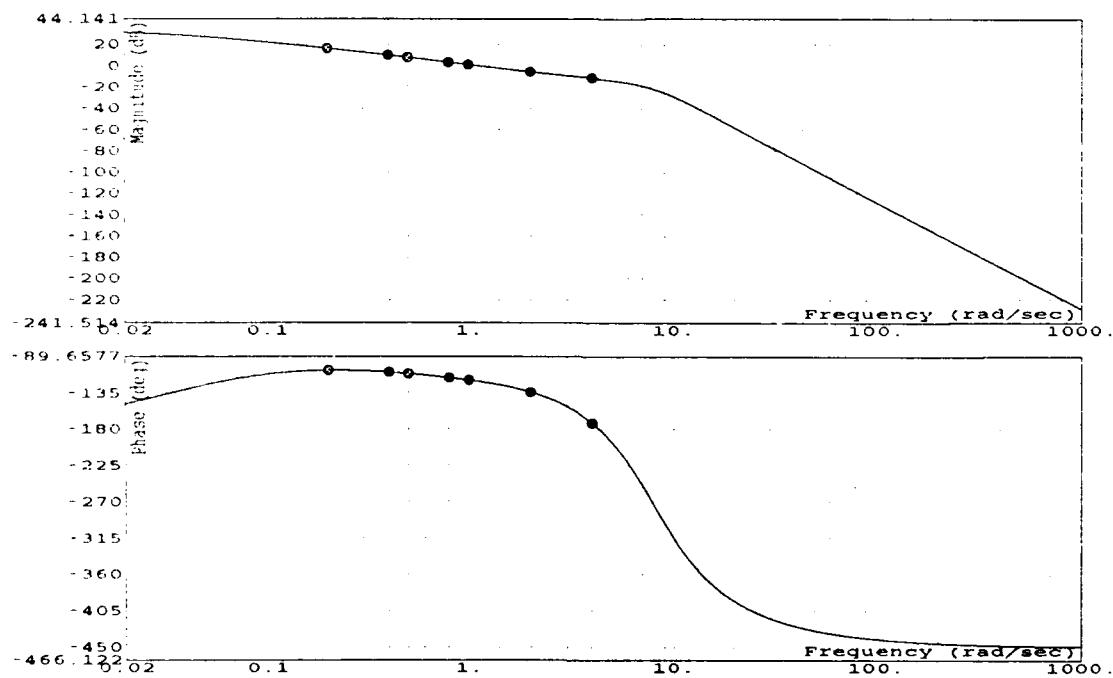


Fig. 4-45 Open loop Bode plot for channel 1

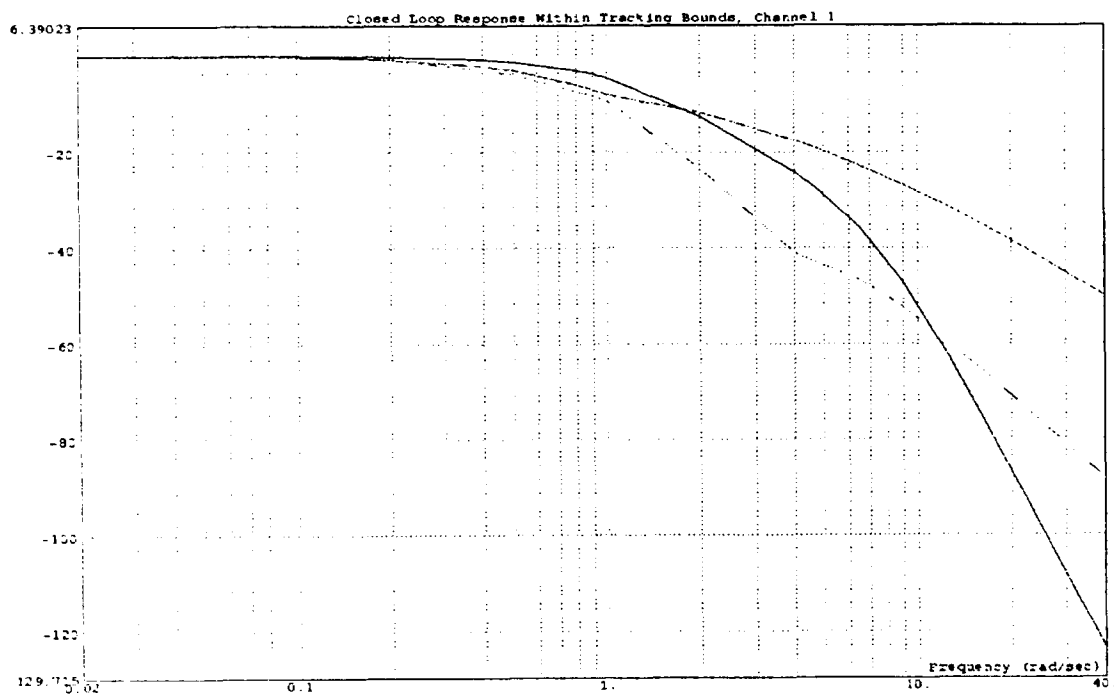


Fig. 4-46 Channel 1 nominal CLTF with filter bounds

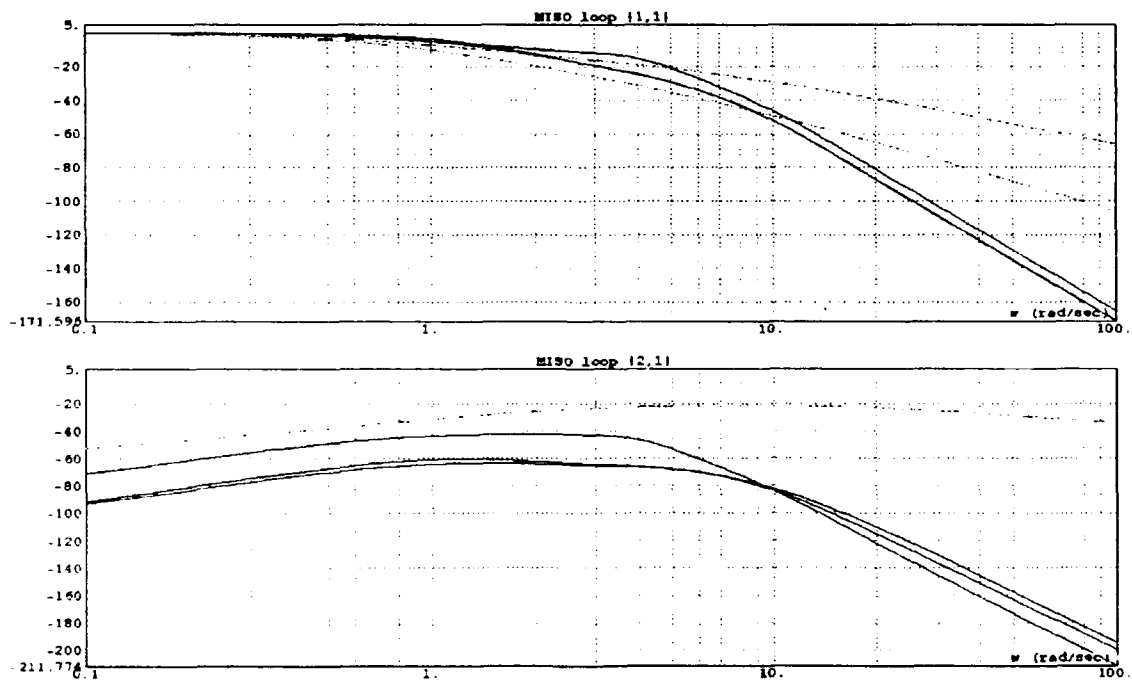


Fig. 4-47 Bode plots of closed loop transfer functions

Betzold's thesis. The closed loop system is then formed for each effective plant using the compensators and prefilter given in the thesis. Bode plots are then generated for the transfer function elements of interest, and are shown in Fig. 4-47 along with the performance tolerances. The frequency domain transmission of the roll channel, channel 1, violates the design specifications.

The compensator and prefilter of channel 1 is re-designed based on the allocated tracking bounds generated by the CAD package as an attempt to satisfy the requirements on the closed loop system. The loop transmission, based on a re-designed compensator, is shown on the NC in Fig. 4-48. The re-designed compensator transfer function is:

$$g_1 = \frac{2.03 \times 10^7 (s + 1.6)}{(s + 28 + j28.57)(s + 28 - j28.57)(s + 20 + j34.64)(s + 20 - j34.64)} \quad (4-9)$$

Next, the prefilter is re-designed based on the nominal closed loop transmission obtained when using the new compensator. The Bode plot with filter bounds of the nominal closed loop transmission, when using the re-designed prefilter, is shown in Fig. 4-49. The transfer function of the re-designed prefilter is:

$$f_{11} = \frac{1.35}{(s + 0.45)(s + 3)} \quad (4-10)$$

The closed loop system is then formed based on the re-designed compensator and prefilter of channel 1. A Bode plot of the transmission of the closed loop transfer function elements in Fig. 4-50 indicates that the performance tolerances are satisfied up to 40 rad/sec , violating a_{11} when the closed loop transmission is negligible at -80 dB. Clearly the design now satisfies the performance requirements in the frequency range of interest.

Finally, the open loop transmissions of the 3 plant cases are plotted on the NC for channel 1 and channel 2 in Figs. 4-51 and 4-52, respectively, to verify that the compensator designs satisfy the stability specifications. From the Nichols plots, it is seen by inspection that for channels 1 and 2 none of the open loop transmissions violate the 3 dB M_L contour on the Nichols plots of Figs. 4-51 and 4-52.

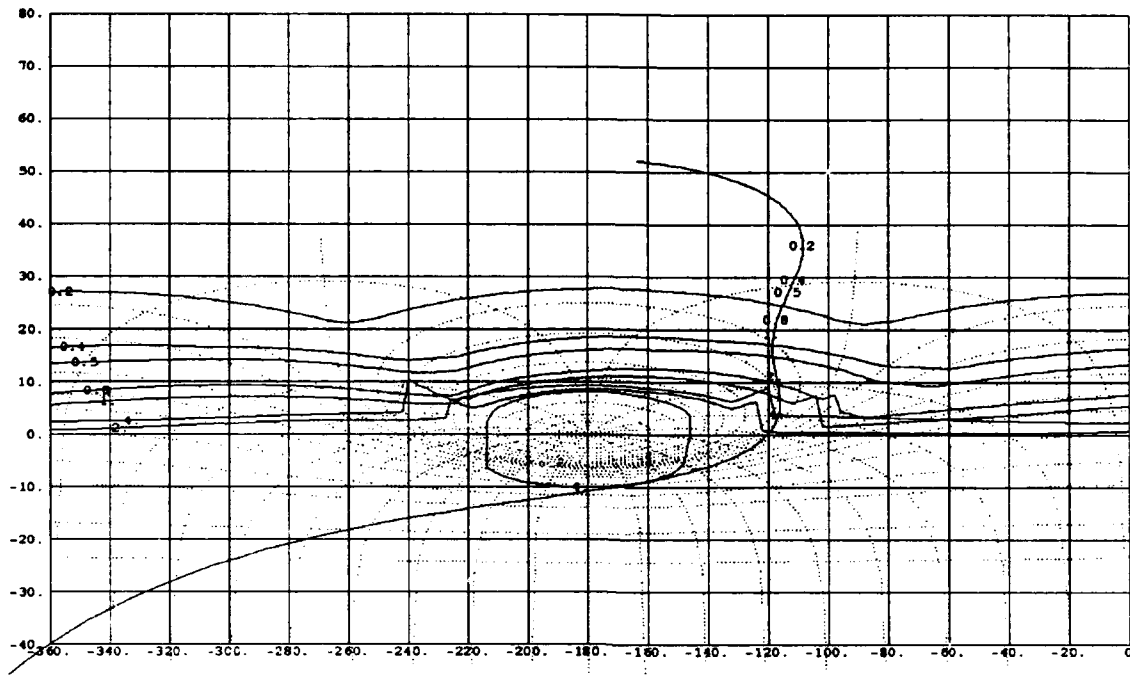


Fig. 4-48 OLTF with re-designed compensator

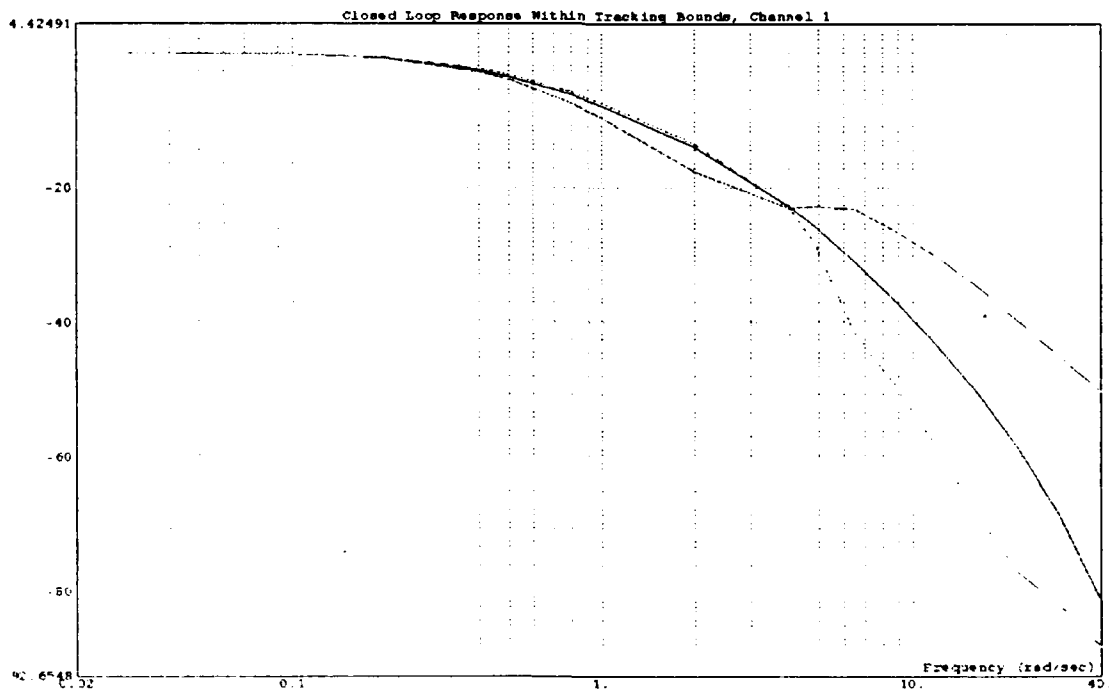


Fig. 4-49 Nominal closed loop for new channel 1 design

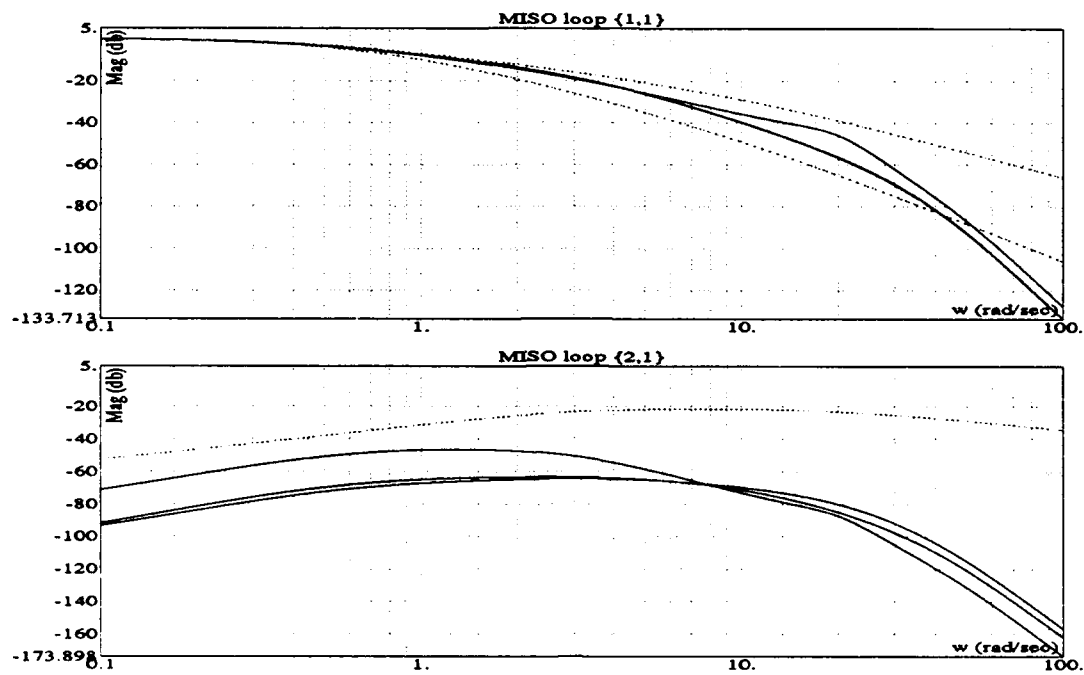


Fig. 4-50 Closed loop Bode plots for re-designed system

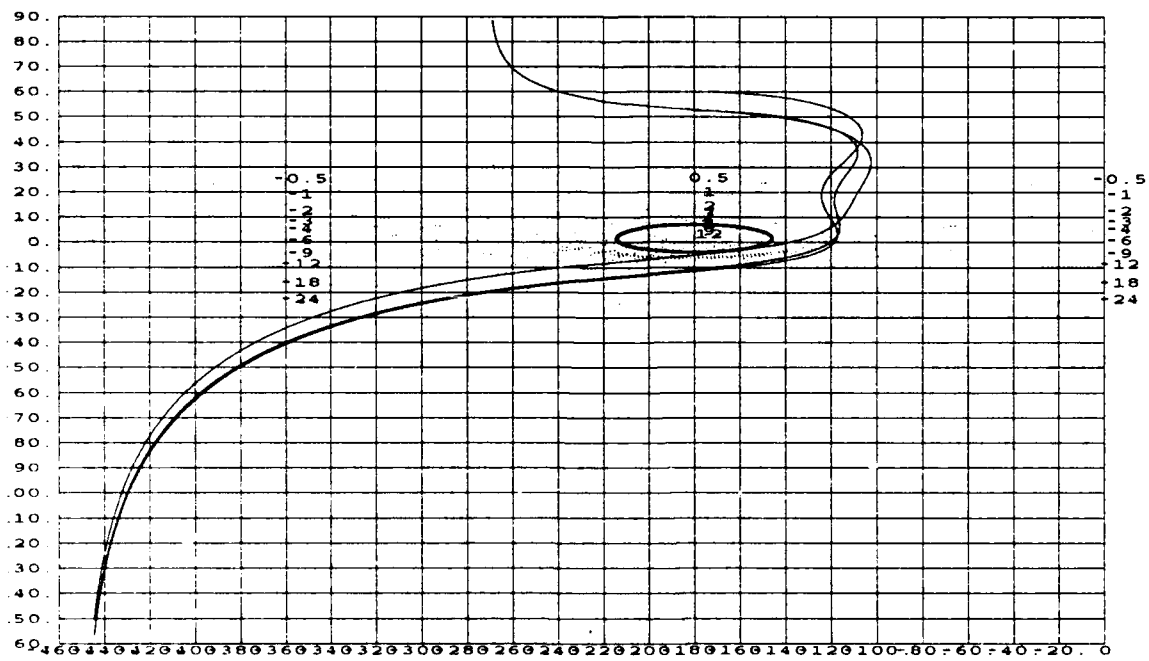
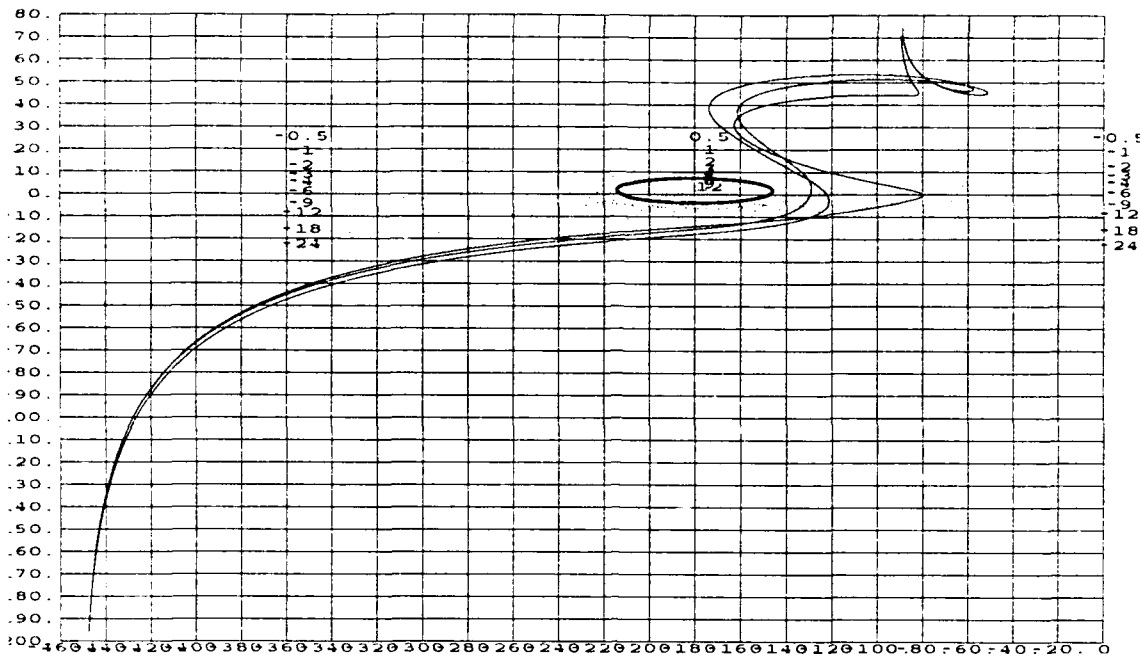


Fig. 4-51 Open loop transmissions for channel 1



4.4 Summary

This chapter has shown that the results obtained using the MIMO/QFT CAD software are in good agreement with results obtained by Betzold and Arnold in past thesis work. Cases where the results are not in agreement occurred due to the increased accuracy of software CAD routines and due to the more exact but more computationally intensive methods used by the CAD software. As noted in items 1 and 2 of Sec. 4.1, the accuracy of previous thesis work was limited by the absence of CAD software specialized for QFT. From this exercise, the CAD software has demonstrated that it is a very useful tool which overcomes these difficulties by reducing computational errors and the possibility of human error by automating the design process. The availability of this software should expedite the utilization of the QFT technique by multivariable control system designers.

5 Chapter 5

5.1 Accomplishments

The efforts of this thesis have provided the following accomplishments:

- Provides for the menu driven automated MIMO QFT CAD package developed
- Provides for the automated loading of contractor plant matrix data
- Provides for the implementation of a symbolic weighting matrix for gain scheduling
- Provides for the implementation of generalized polynomial matrix inverse using arbitrary precision calculations
- Provides for the automatic generation of templates
- Provides for the automatic generation of stability, tracking, disturbance, and composite bounds
- Provides for the automatic allocation to disturbance during generation of tracking bound
- Provides the capability of generating gamma bounds for use with the improved method on a 2×2 system
- The implementation of the improved method for 2×2 MIMO systems
- The implementation of compensator design procedure on the NC
- The implementation of prefilter design procedure on the Bode plot
- The implementation of frequency domain evaluation of closed loop system performance
- The implementation of frequency domain method to verify a satisfactory stability margin exists for the MISO equivalent loops

5.2 Conclusions

- A MIMO QFT CAD package is developed during this thesis effort which is capable of carrying a design from problem specifications and contractor plant models, through the design process, to frequency domain evaluation of the closed loop compensated system.
- The QFT/MIMO CAD package implementation is judged successful based on agreement with the results obtained from past MIMO QFT thesis work.

- The QFT/MIMO CAD package provides improved accuracy and eliminates potential sources of error.

5.3 Recommended Areas of Further Study

The following areas of further study and improvement of this CAD package are recommended:

- Extending the package to handle discrete control problems
- The implementation of a generalized improved method for $m \times m$ MIMO systems
- The implementation of the Binet-Cauchy theorem
- The automation of weighting matrix tuning process
- The implementation of generalized test for diagonal dominance for any $m \times m$ problem
- The improvement in robustness of polynomial root solver
- Extending the method of generating gamma bounds to any $m \times m$ problem
- The implementation of an option allowing the designer to renumber plant outputs
- The implementation of automatic loop shaping routines
- The development of an automated algorithm for optimizing b_{ij} specification of the off-diagonal MISO loops to reach equilibrium between the disturbance bounds and the tracking bounds on the NC when the b_{ij} specifications are not a-priori fixed
- The development of routines for time domain performance analysis of the closed loop system
- The addition of the option to export the finished design to Matlab and EASY5 for simulation

A Appendix A - Philip Arnold's Design

A.1 P_e Matrix Transfer Functions From CAD Package

A.1.1 Plant Case 1

Plant Case: 1 Element: {1, 1}

Roots of Numerator	Roots of Denominator
-----	-----
0	0.3633
-0.01750899094	-0.07683 + 0.2065 I
-0.1041	-0.07683 - 0.2065 I
-0.2741 + 1.909 I	-0.1041
-0.2741 - 1.909 I	-0.2741 + 1.909 I
-0.4616997602	-0.2741 - 1.909 I
-0.6835	-0.6835
	-1 3

Factored form gain multiplier: -2.17555

Plant Case: 1 Element: {1, 2}

Roots of Numerator	Roots of Denominator
-----	-----
	0.3633
	-0.07683 + 0.2065 I
	-0.07683 - 0.2065 I
	-0.1041
	-0.2741 + 1.909 I
	-0.2741 - 1.909 I
	-0.6835
	-1.3

Factored form gain multiplier: 0

Plant Case: 1 Element: {2, 1}

Roots of Numerator	Roots of Denominator
-----	-----
	0.3633
	-0.07683 + 0.2065 I
	-0.07683 - 0.2065 I
	-0.1041
	-0.2741 + 1.909 I
	-0.2741 - 1.909 I
	-0.6835
	-1.3

Factored form gain multiplier: 0

Plant Case: 1 Element: {2, 2}

Roots of Numerator	Roots of Denominator
-----	-----
0.3633	0.3633
0	-0.07683 + 0.2065 I
-0.07683 + 0.2065 I	-0.07683 - 0.2065 I
-0.07683 - 0.2065 I	-0.1041
-0.2236638493 + 1.029339632 I	-0.2741 + 1.909 I
-0.2236638493 - 1.029339632 I	-0.2741 - 1.909 I
-1.3	-0.6835
	-1.3

Factored form gain multiplier: -5.549

A.1.2 Plant Case 2

Plant Case: 2 Element: {1, 1}

Roots of Numerator	Roots of Denominator
-----	-----
0	0.3633
-0.01677417266	-0.07683 + 0.2065 I
-0.1041	-0.07683 - 0.2065 I
-0.2741 + 1.909 I	-0.1041
-0.2741 - 1.909 I	-0.2741 + 1.909 I
-0.4668627603	-0.2741 - 1.909 I
-0.6835	-0.6835
	-1.3

Factored form gain multiplier: -1.05755

Plant Case: 2 Element: {1, 2}

Roots of Numerator	Roots of Denominator
-----	-----
0	0.3633
-0.01822	-0.07683 + 0.2065 I
-0.1041	-0.07683 - 0.2065 I
-0.2741 + 1.909 I	-0.1041
-0.2741 - 1.909 I	-0.2741 + 1.909 I
-0.4568	-0.2741 - 1.909 I
-0.6835	-0.6835
	-1.3

Factored form gain multiplier: 0.2795

Plant Case: 2 Element: {2, 1}

Roots of Numerator	Roots of Denominator
-----	-----
0.3633	0.3633
0	-0.07683 + 0.2065 I
-0.07683 + 0.2065 I	-0.07683 - 0.2065 I
-0.07683 - 0.2065 I	-0.1041
-0.3017 + 1.562 I	-0.2741 + 1.909 I
-0.3017 - 1.562 I	-0.2741 - 1.909 I
-1.3	-0.6835
	-1.3

Factored form gain multiplier: 2.142

Plant Case: 2 Element: {2, 2}

Roots of Numerator	Roots of Denominator
-----	-----
0.3633	0.3633
0	-0.07683 + 0.2065 I
-0.07683 + 0.2065 I	-0.07683 - 0.2065 I
-0.07683 - 0.2065 I	-0.1041
-0.2153286826 + 0.9546662645 I	-0.2741 + 1.909 I
-0.2153286826 - 0.9546662645 I	-0.2741 - 1.909 I
-1.3	-0.6835
	-1.3

Factored form gain multiplier: -5.0135

A.1.3 Plant Case 3

Plant Case: 3 Element: {1, 1}

Roots of Numerator	Roots of Denominator
-----	-----
0	0.3633
-0.01786739384	-0.07683 + 0.2065 I
-0.1041	-0.07683 - 0.2065 I
-0.2741 + 1.909 I	-0.1041
-0.2741 - 1.909 I	-0.2741 + 1.909 I
-0.4592182832	-0.2741 - 1.909 I
-0.6835	-0.6835
	-1.3

Factored form gain multiplier: -2.205775

Plant Case: 3 Element: {1, 2}

Roots of Numerator	Roots of Denominator
-----	-----
0	0.3633
-0.06537	-0.07683 + 0.2065 I
-0.1041	-0.07683 - 0.2065 I
-0.2589	-0.1041
-0.2741 + 1.909 I	-0.2741 + 1.909 I
-0.2741 - 1.909 I	-0.2741 - 1.909 I
-0.6835	-0.6835
	-1.3

Factored form gain multiplier: -0.1209

Plant Case: 3 Element: {2, 1}

Roots of Numerator	Roots of Denominator
-----	-----
0.3633	0.3633
0	-0.07683 + 0.2065 I
-0.07683 + 0.2065 I	-0.07683 - 0.2065 I
-0.07683 - 0.2065 I	-0.1041
-0.205 + 0.853 I	-0.2741 + 1.909 I
-0.205 - 0.853 I	-0.2741 - 1.909 I
-1.3	-0.6835
	-1.3

Factored form gain multiplier: 0.55975

Plant Case: 3 Element: {2, 2}

Roots of Numerator	Roots of Denominator
-----	-----
0.3633	0.3633
0	-0.07683 + 0.2065 I
-0.07683 + 0.2065 I	-0.07683 - 0.2065 I
-0.07683 - 0.2065 I	-0.1041
-0.2362887311 + 1.132993767 I	-0.2741 + 1.909 I
-0.2362887311 - 1.132993767 I	-0.2741 - 1.909 I
-1.3	-0.6835
	-1.3

Factored form gain multiplier: -3.31

A.1.4 Plant Case 4

Plant Case: 4 Element: {1, 1}

Roots of Numerator	Roots of Denominator
-----	-----
0	0.3633
-0.01750899094	-0.07683 + 0.2065 I
-0.1041	-0.07683 - 0.2065 I
-0.2741 + 1.909 I	-0.1041
-0.2741 - 1.909 I	-0.2741 + 1.909 I
-0.4616997602	-0.2741 - 1.909 I
-0.6835	-0.6835
	-1.3

Factored form gain multiplier: -1.087775

Plant Case: 4 Element: {1, 2}

Roots of Numerator	Roots of Denominator
-----	-----
0	0.3633
-0.003009051506	-0.07683 + 0.2065 I
-0.1041	-0.07683 - 0.2065 I
-0.2741 + 1.909 I	-0.1041
-0.2741 - 1.909 I	-0.2741 + 1.909 I
-0.5869269321	-0.2741 - 1.909 I
-0.6835	-0.6835
	-1.3

Factored form gain multiplier: 0.1586

Plant Case: 4 Element: {2, 1}

Roots of Numerator	Roots of Denominator
-----	-----
0.3633	0.3633
0	-0.07683 + 0.2065 I
-0.07683 + 0.2065 I	-0.07683 - 0.2065 I
-0.07683 - 0.2065 I	-0.1041
-0.2816656426 + 1.444520055 I	-0.2741 + 1.909 I
-0.2816656426 - 1.444520055 I	-0.2741 - 1.909 I
-1.3	-0.6835
	-1.3

Factored form gain multiplier: 2.70175

Plant Case: 4 Element: {2, 2}

Roots of Numerator	Roots of Denominator
-----	-----
0.3633	0.3633
0	-0.07683 + 0.2065 I
-0.07683 + 0.2065 I	-0.07683 - 0.2065 I
-0.07683 - 0.2065 I	-0.1041
-0.2236638493 + 1.029339632 I	-0.2741 + 1.909 I
-0.2236638493 - 1.029339632 I	-0.2741 - 1.909 I
-1.3	-0.6835
	-1.3

Factored form gain multiplier: -2.7745

A.1.5 Plant Case 5

Plant Case: 5 Element: {1, 1}

Roots of Numerator	Roots of Denominator
-----	-----
0	0.3633
-0.01750899094	-0.07683 + 0.2065 I
-0.1041	-0.07683 - 0.2065 I
-0.2741 + 1.909 I	-0.1041
-0.2741 - 1.909 I	-0.2741 + 1.909 I
-0.4616997602	-0.2741 - 1.909 I
-0.6835	-0.6835
	-1.3

Factored form gain multiplier: -1.087775

Plant Case: 5 Element: {1, 2}

Roots of Numerator	Roots of Denominator
-----	-----
0	0.3633
-0.0271399588	-0.07683 + 0.2065 I
-0.1041	-0.07683 - 0.2065 I
-0.2741 + 1.909 I	-0.1041
-0.2741 - 1.909 I	-0.2741 + 1.909 I
-0.4023613724	-0.2741 - 1.909 I
-0.6835	-0.6835
	-1.3

Factored form gain multiplier: 0.4004

Plant Case: 5 Element: {2, 1}

Roots of Numerator	Roots of Denominator
-----	-----
0.3633	0.3633
0	-0.07683 + 0.2065 I
-0.07683 + 0.2065 I	-0.07683 - 0.2065 I
-0.07683 - 0.2065 I	-0.1041
-0.3359094012 + 1.743875067 I	-0.2741 + 1.909 I
-0.3359094012 - 1.743875067 I	-0.2741 - 1.909 I
-1.3	-0.6835
	-1.3

Factored form gain multiplier: 1.58225

Plant Case: 5 Element: {2, 2}

Roots of Numerator	Roots of Denominator
-----	-----
0.3633	0.3633
0	-0.07683 + 0.2065 I
-0.07683 + 0.2065 I	-0.07683 - 0.2065 I
-0.07683 - 0.2065 I	-0.1041
-0.2236638493 + 1.029339632 I	-0.2741 + 1.909 I
-0.2236638493 - 1.029339632 I	-0.2741 - 1.909 I
-1.3	-0.6835
	-1.3

Factored form gain multiplier: -2.7745

A.1.6 Plant Case 6

Plant Case: 6 Element: {1, 1}

Roots of Numerator	Roots of Denominator
-----	-----
0	0.3633
-0.01822	-0.07683 + 0.2065 I
-0.1041	-0.07683 - 0.2065 I
-0.2741 + 1.909 I	-0.1041
-0.2741 - 1.909 I	-0.2741 + 1.909 I
-0.4568	-0.2741 - 1.909 I
-0.6835	-0.6835
	-1.3

Factored form gain multiplier: -2.236

Plant Case: 6 Element: {1, 2}

Roots of Numerator	Roots of Denominator
-----	-----
	0.3633
	-0.07683 + 0.2065 I
	-0.07683 - 0.2065 I
	-0.1041
	-0.2741 + 1.909 I
	-0.2741 - 1.909 I
	-0.6835
	-1.3

Factored form gain multiplier: 0

Plant Case: 6 Element: {2, 1}

Roots of Numerator	Roots of Denominator
-----	-----
	0.3633
	-0.07683 + 0.2065 I
	-0.07683 - 0.2065 I
	-0.1041
	-0.2741 + 1.909 I
	-0.2741 - 1.909 I
	-0.6835
	-1.3

Factored form gain multiplier: 0

Plant Case: 6 Element: {2, 2}

Roots of Numerator	Roots of Denominator
-----	-----
0.3633	0.3633
0	-0.07683 + 0.2065 I
-0.07683 + 0.2065 I	-0.07683 - 0.2065 I
-0.07683 - 0.2065 I	-0.1041
-0.3017 + 1.562 I	-0.2741 + 1.909 I
-0.3017 - 1.562 I	-0.2741 - 1.909 I
-1.3	-0.6835
	-1.3

Factored form gain multiplier: -1.071

A.1.7 Plant Case 7

Plant Case: 7 Element: {1, 1}

Roots of Numerator	Roots of Denominator
-----	-----
0.07795	1.167
0	0.07795
-0.009939645444	-0.006472 + 0.07803 I
-0.211 + 1.953 I	-0.006472 - 0.07803 I
-0.211 - 1.953 I	-0.211 + 1.953 I
-0.5620045698	-0.211 - 1.953 I
-0.8265	-0.8265
	-2.028

Factored form gain multiplier: -5.91495

Plant Case: 7 Element: {1, 2}

Roots of Numerator	Roots of Denominator
-----	-----
	1.167
	0.07795
	-0.006472 + 0.07803 I
	-0.006472 - 0.07803 I
	-0.211 + 1.953 I
	-0.211 - 1.953 I
	-0.8265
	-2.028

Factored form gain multiplier: 0

Plant Case: 7 Element: {2, 1}

Roots of Numerator	Roots of Denominator
-----	-----
	1.167
	0.07795
	-0.006472 + 0.07803 I
	-0.006472 - 0.07803 I
	-0.211 + 1.953 I
	-0.211 - 1.953 I
	-0.8265
	-2.028

Factored form gain multiplier: 0

Plant Case: 7 Element: {2, 2}

Roots of Numerator	Roots of Denominator
-----	-----
1.167	1.167
0	0.07795
-0.006472 + 0.07803 I	-0.006472 + 0.07803 I
-0.006472 - 0.07803 I	-0.006472 - 0.07803 I
-0.2231060935 + 1.697351372 I	-0.211 + 1.953 I
-0.2231060935 - 1.697351372 I	-0.211 - 1.953 I
-2.028	-0.8265
	-2.028

Factored form gain multiplier: -20.842

A.1.8 Plant Case 8

Plant Case: 8 Element: {1, 1}

Roots of Numerator	Roots of Denominator
-----	-----
0.07795	1.167
0	0.07795
-0.009845163158	-0.006472 + 0.07803 I
-0.211 + 1.953 I	-0.006472 - 0.07803 I
-0.211 - 1.953 I	-0.211 + 1.953 I
-0.5735955769	-0.211 - 1.953 I
-0.8265	-0.8265
	-2.028

Factored form gain multiplier: -2.98395

Plant Case: 8 Element: {1, 2}

Roots of Numerator	Roots of Denominator
-----	-----
0.07795	1.167
0	0.07795
-0.01004	-0.006472 + 0.07803 I
-0.211 + 1.953 I	-0.006472 - 0.07803 I
-0.211 - 1.953 I	-0.211 + 1.953 I
-0.5502	-0.211 - 1.953 I
-0.8265	-0.8265
	-2.028

Factored form gain multiplier: 0.73275

Plant Case: 8 Element: {2, 1}

Roots of Numerator	Roots of Denominator
-----	-----
1.167	1.167
0	0.07795
-0.006472 + 0.07803 I	-0.006472 + 0.07803 I
-0.006472 - 0.07803 I	-0.006472 - 0.07803 I
-0.2442 + 2.101 I	-0.211 + 1.953 I
-0.2442 - 2.101 I	-0.211 - 1.953 I
-2.028	-0.8265
	-2.028

Factored form gain multiplier: 6.792

Plant Case: 8 Element: {2, 2}

Roots of Numerator	Roots of Denominator
-----	-----
1.167	1.167
0	0.07795
-0.006472 + 0.07803 I	-0.006472 + 0.07803 I
-0.006472 - 0.07803 I	-0.006472 - 0.07803 I
-0.2212351442 + 1.656795028 I	-0.211 + 1.953 I
-0.2212351442 - 1.656795028 I	-0.211 - 1.953 I
-2.028	-0.8265
	-2.028

Factored form gain multiplier: -19.144

A.1.9 Plant Case 9

Plant Case: 9 Element: {1, 1}

Roots of Numerator	Roots of Denominator
-----	-----
0.07795	1.167
0	0.07795
-0.009989054852	-0.006472 + 0.07803 I
-0.211 + 1.953 I	-0.006472 - 0.07803 I
-0.211 - 1.953 I	-0.211 + 1.953 I
-0.5561293643	-0.211 - 1.953 I
-0.8265	-0.8265
	-2.028

Factored form gain multiplier: -5.888475

Plant Case: 9 Element: {1, 2}

Roots of Numerator	Roots of Denominator
-----	-----
0.07795	1.167
0	0.07795
-0.006697	-0.006472 + 0.07803 I
-0.211 + 1.953 I	-0.006472 - 0.07803 I
-0.211 - 1.953 I	-0.211 + 1.953 I
-0.8265	-0.211 - 1.953 I
-1.861	-0.8265
	-2.028

Factored form gain multiplier: 0.1059

Plant Case: 9 Element: {2, 1}

Roots of Numerator	Roots of Denominator
-----	-----
1.167	1.167
0	0.07795
-0.006472 + 0.07803 I	-0.006472 + 0.07803 I
-0.006472 - 0.07803 I	-0.006472 - 0.07803 I
-0.219 + 1.607 I	-0.211 + 1.953 I
-0.219 - 1.607 I	-0.211 - 1.953 I
-2.028	-0.8265
	-2.028

Factored form gain multiplier: 2.18075

Plant Case: 9 Element: {2, 2}

Roots of Numerator	Roots of Denominator
-----	-----
1.167	1.167
0	0.07795
-0.006472 + 0.07803 I	-0.006472 + 0.07803 I
-0.006472 - 0.07803 I	-0.006472 - 0.07803 I
-0.2260615727 + 1.759509227 I	-0.211 + 1.953 I
-0.2260615727 - 1.759509227 I	-0.211 - 1.953 I
-2.028	-0.8265
	-2.028

Factored form gain multiplier: -12.119

A.1.10 Plant Case 10

Plant Case: 10 Element: {1, 1}

Roots of Numerator	Roots of Denominator
-----	-----
0.07795	1.167
0	0.07795
-0.009939645444	-0.006472 + 0.07803 I
-0.211 + 1.953 I	-0.006472 - 0.07803 I
-0.211 - 1.953 I	-0.211 + 1.953 I
-0.5620045698	-0.211 - 1.953 I
-0.8265	-0.8265
	-2.028

Factored form gain multiplier: -2.957475

Plant Case: 10 Element: {1, 2}

Roots of Numerator	Roots of Denominator
-----	-----
0.07795	1.167
0	0.07795
-0.008933835362	-0.006472 + 0.07803 I
-0.211 + 1.953 I	-0.006472 - 0.07803 I
-0.211 - 1.953 I	-0.211 + 1.953 I
-0.716404473	-0.211 - 1.953 I
-0.8265	-0.8265
	-2.028

Factored form gain multiplier: 0.83865

Plant Case: 10 Element: {2, 1}

Roots of Numerator	Roots of Denominator
-----	-----
1.167	1.167
0	0.07795
-0.006472 + 0.07803 I	-0.006472 + 0.07803 I
-0.006472 - 0.07803 I	-0.006472 - 0.07803 I
-0.2380753559 + 1.992266599 I	-0.211 + 1.953 I
-0.2380753559 - 1.992266599 I	-0.211 - 1.953 I
-2.028	-0.8265
	-2.028

Factored form gain multiplier: 8.97275

Plant Case: 10 Element: {2, 2}

Roots of Numerator	Roots of Denominator
-----	-----
1.167	1.167
0	0.07795
-0.006472 + 0.07803 I	-0.006472 + 0.07803 I
-0.006472 - 0.07803 I	-0.006472 - 0.07803 I
-0.2231060935 + 1.697351372 I	-0.211 + 1.953 I
-0.2231060935 - 1.697351372 I	-0.211 - 1.953 I
-2.028	-0.8265
	-2.028

Factored form gain multiplier: -10.421

A.1.11 Plant Case 11

Plant Case: 11 Element: {1, 1}

Roots of Numerator	Roots of Denominator
-----	-----
0.07795	1.167
0	0.07795
-0.009939645444	-0.006472 + 0.07803 I
-0.211 + 1.953 I	-0.006472 - 0.07803 I
-0.211 - 1.953 I	-0.211 + 1.953 I
-0.5620045698	-0.211 - 1.953 I
-0.8265	-0.8265
	-2.028

Factored form gain multiplier: -2.957475

Plant Case: 11 Element: {1, 2}

Roots of Numerator	Roots of Denominator
-----	-----
0.07795	1.167
0	0.07795
-0.01334841556	-0.006472 + 0.07803 I
-0.211 + 1.953 I	-0.006472 - 0.07803 I
-0.211 - 1.953 I	-0.211 + 1.953 I
-0.3260098802	-0.211 - 1.953 I
-0.8265	-0.8265
	-2.028

Factored form gain multiplier: 0.62685

Plant Case: 11 Element: {2, 1}

Roots of Numerator	Roots of Denominator
-----	-----
1.167	1.167
0	0.07795
-0.006472 + 0.07803 I	-0.006472 + 0.07803 I
-0.006472 - 0.07803 I	-0.006472 - 0.07803 I
-0.2561175712 + 2.297831558 I	-0.211 + 1.953 I
-0.2561175712 - 2.297831558 I	-0.211 - 1.953 I
-2.028	-0.8265
	-2.028

Factored form gain multiplier: 4.61125

Plant Case: 11 Element: {2, 2}

Roots of Numerator	Roots of Denominator
-----	-----
1.167	1.167
0	0.07795
-0.006472 + 0.07803 I	-0.006472 + 0.07803 I
-0.006472 - 0.07803 I	-0.006472 - 0.07803 I
-0.2231060935 + 1.697351372 I	-0.211 + 1.953 I
-0.2231060935 - 1.697351372 I	-0.211 - 1.953 I
-2.028	-0.8265
	-2.028

Factored form gain multiplier: -10.421

A.1.12 Plant Case 12

Plant Case: 12 Element: {1, 1}

Roots of Numerator	Roots of Denominator
-----	-----
0.07795	1.167
0	0.07795
-0.01004	-0.006472 + 0.07803 I
-0.211 + 1.953 I	-0.006472 - 0.07803 I
-0.211 - 1.953 I	-0.211 + 1.953 I
-0.5502	-0.211 - 1.953 I
-0.8265	-0.8265
	-2.028

Factored form gain multiplier: -5.862

Plant Case: 12 Element: {1, 2}

Roots of Numerator	Roots of Denominator
-----	-----
	1.167
	0.07795
	-0.006472 + 0.07803 I
	-0.006472 - 0.07803 I
	-0.211 + 1.953 I
	-0.211 - 1.953 I
	-0.8265
	-2.028

Factored form gain multiplier: 0

Plant Case: 12 Element: {2, 1}

Roots of Numerator	Roots of Denominator
-----	-----
	1.167
	0.07795
	-0.006472 + 0.07803 I
	-0.006472 - 0.07803 I
	-0.211 + 1.953 I
	-0.211 - 1.953 I
	-0.8265
	-2.028

Factored form gain multiplier: 0

Plant Case: 12 Element: {2, 2}

Roots of Numerator	Roots of Denominator
-----	-----
1.167	1.167
0	0.07795
-0.006472 + 0.07803 I	-0.006472 + 0.07803 I
-0.006472 - 0.07803 I	-0.006472 - 0.07803 I
-0.2442 + 2.101 I	-0.211 + 1.953 I
-0.2442 - 2.101 I	-0.211 - 1.953 I
-2.028	-0.8265
	-2.028

Factored form gain multiplier: -3.396

A.1.13 Plant Case 13

Plant Case: 13 Element: {1, 1}

Roots of Numerator	Roots of Denominator
-----	-----
0	0.9645
-0.01261453256	-0.007553 + 0.5384 I
-0.02719	-0.007553 - 0.5384 I
-0.391 + 2.962 I	-0.02719
-0.391 - 2.962 I	-0.391 + 2.962 I
-1.518569941	-0.391 - 2.962 I
-2.697	-2.697
	-3.223

Factored form gain multiplier: -25.678

Plant Case: 13 Element: {1, 2}

Roots of Numerator	Roots of Denominator
-----	-----
	0.9645
	-0.007553 + 0.5384 I
	-0.007553 - 0.5384 I
	-0.02719
	-0.391 + 2.962 I
	-0.391 - 2.962 I
	-2.697
	-3.223

Factored form gain multiplier: 0

Plant Case: 13 Element: {2, 1}

Roots of Numerator	Roots of Denominator
-----	-----
	0.9645
	-0.007553 + 0.5384 I
	-0.007553 - 0.5384 I
	-0.02719
	-0.391 + 2.962 I
	-0.391 - 2.962 I
	-2.697
	-3.223

Factored form gain multiplier: 0

Plant Case: 13 Element: {2, 2}

Roots of Numerator	Roots of Denominator
-----	-----
0.9645	0.9645
0	-0.007553 + 0.5384 I
-0.007553 + 0.5384 I	-0.007553 - 0.5384 I
-0.007553 - 0.5384 I	-0.02719
-0.3582378099 + 3.06754481 I	-0.391 + 2.962 I
-0.3582378099 - 3.06754481 I	-0.391 - 2.962 I
-3.223	-2.697
	-3.223

Factored form gain multiplier: -63.74

A.1.14 Plant Case 14

Plant Case: 14 Element: {1, 1}

Roots of Numerator	Roots of Denominator
-----	-----
0	0.9645
-0.01260976464	-0.007553 + 0.5384 I
-0.02719	-0.007553 - 0.5384 I
-0.391 + 2.962 I	-0.02719
-0.391 - 2.962 I	-0.391 + 2.962 I
-1.526123846	-0.391 - 2.962 I
-2.697	-2.697
	-3.223

Factored form gain multiplier: -13.648

Plant Case: 14 Element: {1, 2}

Roots of Numerator	Roots of Denominator
-----	-----
0	0.9645
-0.01262	-0.007553 + 0.5384 I
-0.02719	-0.007553 - 0.5384 I
-0.391 + 2.962 I	-0.02719
-0.391 - 2.962 I	-0.391 + 2.962 I
-1.51	-0.391 - 2.962 I
-2.697	-2.697
	-3.223

Factored form gain multiplier: 3.0075

Plant Case: 14 Element: {2, 1}

Roots of Numerator	Roots of Denominator
-----	-----
0.9645	0.9645
0	-0.007553 + 0.5384 I
-0.007553 + 0.5384 I	-0.007553 - 0.5384 I
-0.007553 - 0.5384 I	-0.02719
-0.3749 + 3.578 I	-0.391 + 2.962 I
-0.3749 - 3.578 I	-0.391 - 2.962 I
-3.223	-2.697
	-3.223

Factored form gain multiplier: 25.36

Plant Case: 14 Element: {2, 2}

Roots of Numerator	Roots of Denominator
-----	-----
0.9645	0.9645
0	-0.007553 + 0.5384 I
-0.007553 + 0.5384 I	-0.007553 - 0.5384 I
-0.007553 - 0.5384 I	-0.02719
-0.3563974216 + 3.005846427 I	-0.391 + 2.962 I
-0.3563974216 - 3.005846427 I	-0.391 - 2.962 I
-3.223	-2.697
	-3.223

Factored form gain multiplier: -57.4

A.1.15 Plant Case 15

Plant Case: 15 Element: {1, 1}

Roots of Numerator	Roots of Denominator
-----	-----
0	0.9645
-0.01261716956	-0.007553 + 0.5384 I
-0.02719	-0.007553 - 0.5384 I
-0.391 + 2.962 I	-0.02719
-0.391 - 2.962 I	-0.391 + 2.962 I
-1.514424371	-0.391 - 2.962 I
-2.697	-2.697
	-3.223

Factored form gain multiplier: -24.869

Plant Case: 15 Element: {1, 2}

Roots of Numerator	Roots of Denominator
-----	-----
0	0.9645
-0.01254	-0.007553 + 0.5384 I
-0.02719	-0.007553 - 0.5384 I
-0.391 + 2.962 I	-0.02719
-0.391 - 2.962 I	-0.391 + 2.962 I
-1.646	-0.391 - 2.962 I
-2.697	-2.697
	-3.223

Factored form gain multiplier: 3.236

Plant Case: 15 Element: {2, 1}

Roots of Numerator	Roots of Denominator
-----	-----
0.9645	0.9645
0	-0.007553 + 0.5384 I
-0.007553 + 0.5384 I	-0.007553 - 0.5384 I
-0.007553 - 0.5384 I	-0.02719
-0.3541 + 2.927 I	-0.391 + 2.962 I
-0.3541 - 2.927 I	-0.391 - 2.962 I
-3.223	-2.697
	-3.223

Factored form gain multiplier: 6.3825

Plant Case: 15 Element: {2, 2}

Roots of Numerator	Roots of Denominator
-----	-----
0.9645	0.9645
0	-0.007553 + 0.5384 I
-0.007553 + 0.5384 I	-0.007553 - 0.5384 I
-0.007553 - 0.5384 I	-0.02719
-0.3610024863 + 3.157962895 I	-0.391 + 2.962 I
-0.3610024863 - 3.157962895 I	-0.391 - 2.962 I
-3.223	-2.697
	-3.223

Factored form gain multiplier: -38.21

A.1.16 Plant Case 16

Plant Case: 16 Element: {1, 1}

Roots of Numerator	Roots of Denominator
-----	-----
0	0.9645
-0.01261453256	-0.007553 + 0.5384 I
-0.02719	-0.007553 - 0.5384 I
-0.391 + 2.962 I	-0.02719
-0.391 - 2.962 I	-0.391 + 2.962 I
-1.5185699-1	-0.391 - 2.962 I
-2.697	-2.697
	-3.223

Factored form gain multiplier: -12.839

Plant Case: 16 Element: {1, 2}

Roots of Numerator	Roots of Denominator
-----	-----
0	0.9645
-0.01257680361	-0.007553 + 0.5384 I
-0.02719	-0.007553 - 0.5384 I
-0.391 + 2.962 I	-0.02719
-0.391 - 2.962 I	-0.391 + 2.962 I
-1.580490401	-0.391 - 2.962 I
-2.697	-2.697
	-3.223

Factored form gain multiplier: 6.2435

Plant Case: 16 Element: {2, 1}

Roots of Numerator	Roots of Denominator
-----	-----
0.9645	0.9645
0	-0.007553 + 0.5384 I
-0.007553 + 0.5384 I	-0.007553 - 0.5384 I
-0.007553 - 0.5384 I	-0.02719
-0.3707177207 + 3.456973615 I	-0.391 + 2.962 I
-0.3707177207 - 3.456973615 I	-0.391 - 2.962 I
-3.223	-2.697
	-3.223

Factored form gain multiplier: 31.7425

Plant Case: 16 Element: {2, 2}

Roots of Numerator	Roots of Denominator
-----	-----
0.9645	0.9645
0	-0.007553 + 0.5384 I
-0.007553 + 0.5384 I	-0.007553 - 0.5384 I
-0.007553 - 0.5384 I	-0.02719
-0.3582378099 + 3.06754481 I	-0.391 + 2.962 I
-0.3582378099 - 3.06754481 I	-0.391 - 2.962 I
-3.223	-2.697
	-3.223

Factored form gain multiplier: -31.87

A.1.17 Plant Case 17

Plant Case: 17 Element: {1, 1}

Roots of Numerator	Roots of Denominator
-----	-----
0	0.9645
-0.01261453256	-0.007553 + 0.5384 I
-0.02719	-0.007553 - 0.5384 I
-0.391 + 2.962 I	-0.02719
-0.391 - 2.962 I	-0.391 + 2.962 I
-1.518569941	-0.391 - 2.962 I
-2.697	-2.697
	-3.223

Factored form gain multiplier: -12.839

Plant Case: 17 Element: {1, 2}

Roots of Numerator	Roots of Denominator
-----	-----
0	0.9645
-0.01207934927	-0.007553 + 0.5384 I
-0.02719	-0.007553 - 0.5384 I
-0.391 + 2.962 I	-0.02719
-0.391 - 2.962 I	-0.391 + 2.962 I
-2.697	-0.391 - 2.962 I
-3.435429579	-2.697
	-3.223

Factored form gain multiplier: -0.2285

Plant Case: 17 Element: {2, 1}

Roots of Numerator	Roots of Denominator
-----	-----
0.9645	0.9645
0	-0.007553 + 0.5384 I
-0.007553 + 0.5384 I	-0.007553 - 0.5384 I
-0.007553 - 0.5384 I	-0.02719
-0.381895442 + 3.771752842 I	-0.391 + 2.962 I
-0.381895442 - 3.771752842 I	-0.391 - 2.962 I
-3.223	-2.697
	-3.223

Factored form gain multiplier: 18.9775

Plant Case: 17 Element: {2, 2}

Roots of Numerator	Roots of Denominator
-----	-----
0.9645	0.9645
0	-0.007553 + 0.5384 I
-0.007553 + 0.5384 I	-0.007553 - 0.5384 I
-0.007553 - 0.5384 I	-0.02719
-0.3582378099 + 3.06754481 I	-0.391 + 2.962 I
-0.3582378099 - 3.06754481 I	-0.391 - 2.962 I
-3.223	-2.697
	-3.223

Factored form gain multiplier: -31.87

A.1.18 Plant Case 18

Plant Case: 18 Element: {1, 1}

Roots of Numerator	Roots of Denominator
-----	-----
0	0.9645
-0.01262	-0.007553 + 0.5384 I
-0.02719	-0.007553 - 0.5384 I
-0.391 + 2.962 I	-0.02719
-0.391 - 2.962 I	-0.391 + 2.962 I
-1.51	-0.391 - 2.962 I
-2.697	-2.697
	-3.223

Factored form gain multiplier: -24.06

Plant Case: 18 Element: {1, 2}

Roots of Numerator	Roots of Denominator
-----	-----
	0.9645
	-0.007553 + 0.5384 I
	-0.007553 - 0.5384 I
	-0.02719
	-0.391 + 2.962 I
	-0.391 - 2.962 I
	-2.697
	-3.223

Factored form gain multiplier: 0

Plant Case: 18 Element: {2, 1}

Roots of Numerator	Roots of Denominator
-----	-----
	0.9645
	-0.007553 + 0.5384 I
	-0.007553 - 0.5384 I
	-0.02719
	-0.391 + 2.962 I
	-0.391 - 2.962 I
	-2.697
	-3.223

Factored form gain multiplier: 0

Plant Case: 18 Element: {2, 2}

Roots of Numerator	Roots of Denominator
-----	-----
0.9645	0.9645
0	-0.007553 + 0.5384 I
-0.007553 + 0.5384 I	-0.007553 - 0.5384 I
-0.007553 - 0.5384 I	-0.02719
-0.3749 + 3.578 I	-0.391 + 2.962 I
-0.3749 - 3.578 I	-0.391 - 2.962 I
-3.223	-2.697
	-3.223

Factored form gain multiplier: -12.68

A.1.19 Plant Case 19

Plant Case: 19 Element: {1, 1}

Roots of Numerator	Roots of Denominator
-----	-----
0	-0.01516 + 0.02343 I
-0.03008318398	-0.01516 - 0.02343 I
-0.03448	-0.03448
-0.4996 + 3.129 I	-0.4996 + 3.129 I
-0.4996 - 3.129 I	-0.4996 - 3.129 I
-1.079585586	-0.8012 + 6.592 I
-2.171	-0.8012 - 6.592 I
	-2.171

Factored form gain multiplier: -34.3625

Plant Case: 19 Element: {1, 2}

Roots of Numerator	Roots of Denominator
-----	-----
	-0.01516 + 0.02343 I
	-0.01516 - 0.02343 I
	-0.03448
	-0.4996 + 3.129 I
	-0.4996 - 3.129 I
	-0.8012 + 6.592 I
	-0.8012 - 6.592 I
	-2.171

Factored form gain multiplier: 0

Plant Case: 19 Element: {2, 1}

Roots of Numerator	Roots of Denominator
-----	-----
	-0.01516 + 0.02343 I
	-0.01516 - 0.02343 I
	-0.03448
	-0.4996 + 3.129 I
	-0.4996 - 3.129 I
	-0.8012 + 6.592 I
	-0.8012 - 6.592 I
	-2.171

Factored form gain multiplier: 0

Plant Case: 19 Element: {2, 2}

Roots of Numerator	Roots of Denominator
-----	-----
0	-0.01516 + 0.02343 I
-0.01516 + 0.02343 I	-0.01516 - 0.02343 I
-0.01516 - 0.02343 I	-0.03448
-0.3943568208 + 4.656189818 I	-0.4996 + 3.129 I
-0.3943568208 - 4.656189818 I	-0.4996 - 3.129 I
-0.8012 + 6.592 I	-0.8012 + 6.592 I
-0.8012 - 6.592 I	-0.8012 - 6.592 I
	-2.171

Factored form gain multiplier: -25.818

A.1.20 Plant Case 20

Plant Case: 20 Element: {1, 1}

Roots of Numerator	Roots of Denominator
-----	-----
0	-0.01516 + 0.02343 I
-0.03019996745	-0.01516 - 0.02343 I
-0.03448	-0.03448
-0.4996 + 3.129 I	-0.4996 + 3.129 I
-0.4996 - 3.129 I	-0.4996 - 3.129 I
-1.063589349	-0.8012 + 6.592 I
-2.171	-0.8012 - 6.592 I
	-2.171

Factored form gain multiplier: -17.9125

Plant Case: 20 Element: {1, 2}

Roots of Numerator	Roots of Denominator
-----	-----
0	-0.01516 + 0.02343 I
-0.02996	-0.01516 - 0.02343 I
-0.03448	-0.03448
-0.4996 + 3.129 I	-0.4996 + 3.129 I
-0.4996 - 3.129 I	-0.4996 - 3.129 I
-1.097	-0.8012 + 6.592 I
-2.171	-0.8012 - 6.592 I
	-2.171

Factored form gain multiplier: 4.1125

Plant Case: 20 Element: {2, 1}

Roots of Numerator	Roots of Denominator
-----	-----
0	-0.01516 + 0.02343 I
-0.01516 + 0.02343 I	-0.01516 - 0.02343 I
-0.01516 - 0.02343 I	-0.03448
-0.3774 + 4.319155473 I	-0.4996 + 3.129 I
-0.3774 - 4.319155473 I	-0.4996 - 3.129 I
-0.8012 + 6.592 I	-0.8012 + 6.592 I
-0.8012 - 6.592 I	-0.8012 - 6.592 I
	-2.171

Factored form gain multiplier: 23.3

Plant Case: 20 Element: {2, 2}

Roots of Numerator	Roots of Denominator
-----	-----
0	-0.01516 + 0.02343 I
-0.01516 + 0.02343 I	-0.01516 - 0.02343 I
-0.01516 - 0.02343 I	-0.03448
-0.399297224 + 4.749877372 I	-0.4996 + 3.129 I
-0.399297224 - 4.749877372 I	-0.4996 - 3.129 I
-0.8012 + 6.592 I	-0.8012 + 6.592 I
-0.8012 - 6.592 I	-0.8012 - 6.592 I
	-2.171

Factored form gain multiplier: -19.993

A.1.21 Plant Case 21

Plant Case: 21 Element: {1, 1}

Roots of Numerator	Roots of Denominator
-----	-----
0	-0.01516 + 0.02343 I
-0.03002242458	-0.01516 - 0.02343 I
-0.03448	-0.03448
-0.4996 + 3.129 I	-0.4996 + 3.129 I
-0.4996 - 3.129 I	-0.4996 - 3.129 I
-1.088103978	-0.8012 + 6.592 I
-2.171	-0.8012 - 6.592 I
	-2.171

Factored form gain multiplier: -33.63125

Plant Case: 21 Element: {1, 2}

Roots of Numerator	Roots of Denominator
-----	-----
0	-0.01516 + 0.02343 I
-0.03448	-0.01516 - 0.02343 I
-0.03459	-0.03448
-0.4996 + 3.129 I	-0.4996 + 3.129 I
-0.4996 - 3.129 I	-0.4996 - 3.129 I
-0.6861	-0.8012 + 6.592 I
-2.171	-0.8012 - 6.592 I
	-2.171

Factored form gain multiplier: 2.925

Plant Case: 21 Element: {2, 1}

Roots of Numerator	Roots of Denominator
-----	-----
0	-0.01516 + 0.02343 I
-0.01516 + 0.02343 I	-0.01516 - 0.02343 I
-0.01516 - 0.02343 I	-0.03448
-0.4083 + 4.916 I	-0.4996 + 3.129 I
-0.4083 - 4.916 I	-0.4996 - 3.129 I
-0.8012 + 6.592 I	-0.8012 + 6.592 I
-0.8012 - 6.592 I	-0.8012 - 6.592 I
	-2.171

Factored form gain multiplier: 1.771

Plant Case: 21 Element: {2, 2}

Roots of Numerator	Roots of Denominator
-----	-----
0	-0.01516 + 0.02343 I
-0.01516 + 0.02343 I	-0.01516 - 0.02343 I
-0.01516 - 0.02343 I	-0.03448
-0.3890844027 + 4.554074665 I	-0.4996 + 3.129 I
-0.3890844027 - 4.554074665 I	-0.4996 - 3.129 I
-0.8012 + 6.592 I	-0.8012 + 6.592 I
-0.8012 - 6.592 I	-0.8012 - 6.592 I
	-2.171

Factored form gain multiplier: -18.734

A.1.22 Plant Case 22

Plant Case: 22 Element: {1, 1}

Roots of Numerator	Roots of Denominator
-----	-----
0	-0.01516 + 0.02343 I
-0.03008318398	-0.01516 - 0.02343 I
-0.03448	-0.03448
-0.4996 + 3.129 I	-0.4996 + 3.129 I
-0.4996 - 3.129 I	-0.4996 - 3.129 I
-1.079585586	-0.8012 + 6.592 I
-2.171	-0.8012 - 6.592 I
	-2.171

Factored form gain multiplier: -17.18125

Plant Case: 22 Element: {1, 2}

Roots of Numerator	Roots of Denominator
-----	-----
0	-0.01516 + 0.02343 I
-0.03136799809	-0.01516 - 0.02343 I
-0.03448	-0.03448
-0.4996 + 3.129 I	-0.4996 + 3.129 I
-0.4996 - 3.129 I	-0.4996 - 3.129 I
-0.9267337781	-0.8012 + 6.592 I
-2.171	-0.8012 - 6.592 I
	-2.171

Factored form gain multiplier: 7.0375

Plant Case: 22 Element: {2, 1}

Roots of Numerator	Roots of Denominator
-----	-----
0	-0.01516 + 0.02343 I
-0.01516 + 0.02343 I	-0.01516 - 0.02343 I
-0.01516 - 0.02343 I	-0.03448
-0.379582757 + 4.364003618 I	-0.4996 + 3.129 I
-0.379582757 - 4.364003618 I	-0.4996 - 3.129 I
-0.8012 + 6.592 I	-0.8012 + 6.592 I
-0.8012 - 6.592 I	-0.8012 - 6.592 I
	-2.171

Factored form gain multiplier: 25.071

Plant Case: 22 Element: {2, 2}

Roots of Numerator	Roots of Denominator
-----	-----
0	-0.01516 + 0.02343 I
-0.01516 + 0.02343 I	-0.01516 - 0.02343 I
-0.01516 - 0.02343 I	-0.03448
-0.3943568208 + 4.656189818 I	-0.4996 + 3.129 I
-0.3943568208 - 4.656189818 I	-0.4996 - 3.129 I
-0.8012 + 6.592 I	-0.8012 + 6.592 I
-0.8012 - 6.592 I	-0.8012 - 6.592 I
	-2.171

Factored form gain multiplier: -12.909

A.1.23 Plant Case 23

Plant Case: 23 Element: {1, 1}

Roots of Numerator	Roots of Denominator
-----	-----
0	-0.01516 + 0.02343 I
-0.03008318398	-0.01516 - 0.02343 I
-0.03448	-0.03448
-0.4996 + 3.129 I	-0.4996 + 3.129 I
-0.4996 - 3.129 I	-0.4996 - 3.129 I
-1.079585586	-0.8012 + 6.592 I
-2.171	-0.8012 - 6.592 I
	-2.171

Factored form gain multiplier: -17.18125

Plant Case: 23 Element: {1, 2}

Roots of Numerator	Roots of Denominator
-----	-----
0	-0.01516 + 0.02343 I
-0.02634744696	-0.01516 - 0.02343 I
-0.03448	-0.03448
-0.4996 + 3.129 I	-0.4996 + 3.129 I
-0.4996 - 3.129 I	-0.4996 - 3.129 I
-2.101319711	-0.8012 + 6.592 I
-2.171	-0.8012 - 6.592 I
	-2.171

Factored form gain multiplier: 1.1875

Plant Case: 23 Element: {2, 1}

Roots of Numerator	Roots of Denominator
-----	-----
0	-0.01516 + 0.02343 I
-0.01516 + 0.02343 I	-0.01516 - 0.02343 I
-0.01516 - 0.02343 I	-0.03448
-0.3748581309 + 4.266333269 I	-0.4996 + 3.129 I
-0.3748581309 - 4.266333269 I	-0.4996 - 3.129 I
-0.8012 + 6.592 I	-0.8012 + 6.592 I
-0.8012 - 6.592 I	-0.8012 - 6.592 I
	-2.171

Factored form gain multiplier: 21.529

Plant Case: 23 Element: {2, 2}

Roots of Numerator	Roots of Denominator
-----	-----
0	-0.01516 + 0.02343 I
-0.01516 + 0.02343 I	-0.01516 - 0.02343 I
-0.01516 - 0.02343 I	-0.03448
-0.3943568208 + 4.656189818 I	-0.4996 + 3.129 I
-0.3943568208 - 4.656189818 I	-0.4996 - 3.129 I
-0.8012 + 6.592 I	-0.8012 + 6.592 I
-0.8012 - 6.592 I	-0.8012 - 6.592 I
	-2.171

Factored form gain multiplier: -12.909

A.1.24 Plant Case 24

Plant Case: 24 Element: {1, 1}

Roots of Numerator	Roots of Denominator
-----	-----
0	-0.01516 + 0.02343 I
-0.02996	-0.01516 - 0.02343 I
-0.03448	-0.03448
-0.4996 + 3.129 I	-0.4996 + 3.129 I
-0.4996 - 3.129 I	-0.4996 - 3.129 I
-1.097	-0.8012 + 6.592 I
-2.171	-0.8012 - 6.592 I
	-2.171

Factored form gain multiplier: -32.9

Plant Case: 24 Element: {1, 2}

Roots of Numerator	Roots of Denominator
-----	-----
	-0.01516 + 0.02343 I
	-0.01516 - 0.02343 I
	-0.03448
	-0.4996 + 3.129 I
	-0.4996 - 3.129 I
	-0.8012 + 6.592 I
	-0.8012 - 6.592 I
	-2.171

Factored form gain multiplier: 0

Plant Case: 24 Element: {2, 1}

Roots of Numerator	Roots of Denominator
-----	-----
	-0.01516 + 0.02343 I
	-0.01516 - 0.02343 I
	-0.03448
	-0.4996 + 3.129 I
	-0.4996 - 3.129 I
	-0.8012 + 6.592 I
	-0.8012 - 6.592 I
	-2.171

Factored form gain multiplier: 0

Plant Case: 24 Element: {2, 2}

Roots of Numerator	Roots of Denominator
-----	-----
0	-0.01516 + 0.02343 I
-0.01516 + 0.02343 I	-0.01516 - 0.02343 I
-0.01516 - 0.02343 I	-0.03448
-0.3774 + 4.319155473 I	-0.4996 + 3.129 I
-0.3774 - 4.319155473 I	-0.4996 - 3.129 I
-0.8012 + 6.592 I	-0.8012 + 6.592 I
-0.8012 - 6.592 I	-0.8012 - 6.592 I
	-2.171

Factored form gain multiplier: -11.65

A.2 P_e Determinants From CAD Package

Plant Case: 1

Roots of Numerator of Det[Pe]	Roots of Denominator of Det[Pe]
-----	-----
0	0.3633
0	-0.07682999737 + 0.2065 I
-0.01750899094	-0.07682999737 - 0.2065 I
-0.2236638493 + 1.029339632 I	-0.1041
-0.2236638493 - 1.029339632 I	-0.2741 + 1.909 I
-0.4616997602	-0.2741 - 1.909 I
	-0.6835
	-1.3

Plant Case: 2

Roots of Numerator of Det[Pe]	Roots of Denominator of Det[Pe]
-----	-----
0	0.3633
0	-0.07682999737 + 0.2065 I
-0.01617592182	-0.07682999737 - 0.2065 I
-0.2031816462 + 0.8466260833 I	-0.1041
-0.2031816462 - 0.8466260833 I	-0.2741 + 1.909 I
-0.4708634843	-0.2741 - 1.909 I
	-0.6835
	-1.3

Plant Case: 3

Roots of Numerator of Det[Pe]	Roots of Denominator of Det[Pe]
-----	-----
0	0.3633
0	-0.07682999737 + 0.2065 I
-0.01800469395	-0.07682999737 - 0.2065 I
-0.2357205606 + 1.130855201 I	-0.1041
-0.2357205606 - 1.130855201 I	-0.2741 + 1.909 I
-0.4582391881	-0.2741 - 1.909 I
	-0.6835
	-1.3

Plant Case: 4

Roots of Numerator of Det[Pe]

0
0
-0.02559309899
-0.2255463507 + 0.9379562951 I
-0.2255463507 - 0.9379562951 I
-0.4123328591

Roots of Denominator of Det[Pe]

0.3633
-0.07682999737 + 0.2065 I
-0.07682999737 - 0.2065 I
-0.1041
-0.2741 + 1.909 I
-0.2741 - 1.909 I
-0.6835
-1.3

Plant Case: 5

Roots of Numerator of Det[Pe]

0
0
-0.007096831889
-0.1695335828 + 0.7432415914 I
-0.1695335828 - 0.7432415914 I
-0.5339345123

Roots of Denominator of Det[Pe]

0.3633
-0.07682999737 + 0.2065 I
-0.07682999737 - 0.2065 I
-0.1041
-0.2741 + 1.909 I
-0.2741 - 1.909 I
-0.6835
-1.3

Plant Case: 6

Roots of Numerator of Det[Pe]

0
0
-0.01822
-0.3017 + 1.562 I
-0.3017 - 1.562 I
-0.4568

Roots of Denominator of Det[Pe]

0.3633
-0.07682999737 + 0.2065 I
-0.07682999737 - 0.2065 I
-0.1041
-0.2741 + 1.909 I
-0.2741 - 1.909 I
-0.6835
-1.3

Plant Case: 7

Roots of Numerator of Det[Pe]

0
0
-0.009939645444
-0.2231060935 + 1.697351372 I
-0.2231060935 - 1.697351372 I
-0.5620045698

Roots of Denominator of Det[Pe]

1.167
0.07795
-0.006472 + 0.07803 I
-0.006472 - 0.07803 I
-0.211 + 1.953 I
-0.211 - 1.953 I
-0.8265
-2.028

Plant Case: 8

Roots of Numerator of Det[Pe]

0
0
-0.009815072143
-0.2183048925 + 1.608183851 I
-0.2183048925 - 1.608183851 I
-0.5773169868

Roots of Denominator of Det[Pe]

1.167
0.07795
-0.006472 + 0.07803 I
-0.006472 - 0.07803 I
-0.211 + 1.953 I
-0.211 - 1.953 I
-0.8265
-2.028

Plant Case: 9

Roots of Numerator of Det[Pe]

0
0
-0.01001950949
-0.2257480147 + 1.760063131 I
-0.2257480147 - 1.760063131 I
-0.5525460655

Roots of Denominator of Det[Pe]

1.167
0.07795
-0.006472 + 0.07803 I
-0.006472 - 0.07803 I
-0.211 + 1.953 I
-0.211 - 1.953 I
-0.8265
-2.028

Plant Case: 10

Roots of Numerator of Det[Pe]

0
0
-0.01069676636
-0.231887918 + 1.587406074 I
-0.231887918 - 1.587406074 I
-0.4844613815

Roots of Denominator of Det[Pe]

1.167
0.07795
-0.006472 + 0.07803 I
-0.006472 - 0.07803 I
-0.211 + 1.953 I
-0.211 - 1.953 I
-0.8265
-2.028

Plant Case: 11

Roots of Numerator of Det[Pe]

0
0
-0.009569120179
-0.2083665407 + 1.62577185 I
-0.2083665407 - 1.62577185 I
-0.6090927582

Roots of Denominator of Det[Pe]

1.167
0.07795
-0.006472 + 0.07803 I
-0.006472 - 0.07803 I
-0.211 + 1.953 I
-0.211 - 1.953 I
-0.8265
-2.028

Plant Case: 12

Roots of Numerator of Det[Pe]

0
0
-0.01004
-0.2442 + 2.101 I
-0.2442 - 2.101 I
-0.5502

Roots of Denominator of Det[Pe]

1.167
0.07795
-0.006472 + 0.07803 I
-0.006472 - 0.07803 I
-0.211 + 1.953 I
-0.211 - 1.953 I
-0.8265
-2.028

Plant Case: 13

Roots of Numerator of Det[Pe]

0
0
-0.01261453256
-0.3582378099 + 3.06754481 I
-0.3582378099 - 3.06754481 I
-1.518569941

Roots of Denominator of Det[Pe]

0.9645
-0.007553 + 0.5384 I
-0.007553 - 0.5384 I
-0.02719
-0.391 + 2.962 I
-0.391 - 2.962 I
-2.697
-3.223

Plant Case: 14

Roots of Numerator of Det[Pe]

0
0
-0.01260815216
-0.354043529 + 2.937631878 I
-0.354043529 - 2.937631878 I
-1.528579891

Roots of Denominator of Det[Pe]

0.9645
-0.007553 + 0.5384 I
-0.007553 - 0.5384 I
-0.02719
-0.391 + 2.962 I
-0.391 - 2.962 I
-2.697
-3.223

Plant Case: 15

Roots of Numerator of Det[Pe]

0
0
-0.01261877154
-0.3609727016 + 3.162975977 I
-0.3609727016 - 3.162975977 I
-1.511867408

Roots of Denominator of Det[Pe]

0.9645
-0.007553 + 0.5384 I
-0.007553 - 0.5384 I
-0.02719
-0.391 + 2.962 I
-0.391 - 2.962 I
-2.697
-3.223

Plant Case: 16

Roots of Numerator of Det[Pe]

0
0
-0.01268136836
-0.3638212458 + 2.642435984 I
-0.3638212458 - 2.642435984 I
-1.425766242

Roots of Denominator of Det[Pe]

0.9645
-0.007553 + 0.5384 I
-0.007553 - 0.5384 I
-0.02719
-0.391 + 2.962 I
-0.391 - 2.962 I
-2.697
-3.223

Plant Case: 17

Roots of Numerator of Det[Pe]

0
0
-0.01259578413
-0.3541334715 + 3.077600345 I
-0.3541334715 - 3.077600345 I
-1.54738922

Roots of Denominator of Det[Pe]

0.9645
-0.007553 + 0.5384 I
-0.007553 - 0.5384 I
-0.02719
-0.391 + 2.962 I
-0.391 - 2.962 I
-2.697
-3.223

Plant Case: 18

Roots of Numerator of Det[Pe]

0
0
-0.01262
-0.3749 + 3.578 I
-0.3749 - 3.578 I
-1.51

Roots of Denominator of Det[Pe]

0.9645
-0.007553 + 0.5384 I
-0.007553 - 0.5384 I
-0.02719
-0.391 + 2.962 I
-0.391 - 2.962 I
-2.697
-3.223

Plant Case: 19

Roots of Numerator of Det[Pe]

0
0
-0.03008318398
-0.3943568208 + 4.656189818 I
-0.3943568208 - 4.656189818 I
-1.079585586

Roots of Denominator of Det[Pe]

-0.01516 + 0.02343 I
-0.01516 - 0.02343 I
-0.03448
-0.4996 + 3.129 I
-0.4996 - 3.129 I
-0.8012 + 6.592 I
-0.8012 - 6.592 I
-2.170999975

Plant Case: 20

Roots of Numerator of Det[Pe]

0
0
-0.03027103524
-0.4059826056 + 4.898011078 I
-0.4059826056 - 4.898011078 I
-1.054028453

Roots of Denominator of Det[Pe]

-0.01516 + 0.02343 I
-0.01516 - 0.02343 I
-0.03448
-0.4996 + 3.129 I
-0.4996 - 3.129 I
-0.8012 + 6.592 I
-0.8012 - 6.592 I
-2.170999975

Plant Case: 21

Roots of Numerator of Det[Pe]

0
0
-0.0299951359
-0.3886587722 + 4.551009274 I
-0.3886587722 - 4.551009274 I
-1.091958693

Roots of Denominator of Det[Pe]

-0.01516 + 0.02343 I
-0.01516 - 0.02343 I
-0.03448
-0.4996 + 3.129 I
-0.4996 - 3.129 I
-0.8012 + 6.592 I
-0.8012 - 6.592 I
-2.170999975

Plant Case: 22

Roots of Numerator of Det[Pe]

0
0
-0.0281768207
-0.5658911377 + 5.6216463 I
-0.5658911377 - 5.6216463 I
-1.442976725

Roots of Denominator of Det[Pe]

-0.01516 + 0.02343 I
-0.01516 - 0.02343 I
-0.03448
-0.4996 + 3.129 I
-0.4996 - 3.129 I
-0.8012 + 6.592 I
-0.8012 - 6.592 I
-2.170999975

Plant Case: 23

Roots of Numerator of Det[Pe]

0
0
-0.03096598996
-0.3853668983 + 4.706629116 I
-0.3853668983 - 4.706629116 I
-0.9691322627

Roots of Denominator of Det[Pe]

-0.01516 + 0.02343 I
-0.01516 - 0.02343 I
-0.03448
-0.4996 + 3.129 I
-0.4996 - 3.129 I
-0.8012 + 6.592 I
-0.8012 - 6.592 I
-2.171

Plant Case: 24

Roots of Numerator of Det[Pe]

0
0
-0.02996
-0.3774 + 4.319155473 I
-0.3774 - 4.319155473 I
-1.097

Roots of Denominator of Det[Pe]

-0.01516 + 0.02343 I
-0.01516 - 0.02343 I
-0.03448
-0.4996 + 3.129 I
-0.4996 - 3.129 I
-0.8012 + 6.592 I
-0.8012 - 6.592 I
-2.170999975

A.3 Q Matrix from CAD Package

A.3.1 Plant Case 1

Plant Case: 1 Element: {1, 1}

Roots of Numerator	Roots of Denominator
-----	-----
0	0.3633
-0.01750899094	-0.07683 + 0.2065 I
-0.4616997502	-0.07683 - 0.2065 I
	-1.3

Factored form gain multiplier: -2.17555

Plant Case: 1 Element: {1, 2}

Roots of Numerator	Roots of Denominator
-----	-----

Factored form gain multiplier: Infinity

Plant Case: 1 Element: {2, 1}

Roots of Numerator	Roots of Denominator
-----	-----

Factored form gain multiplier: Infinity

Plant Case: 1 Element: {2, 2}

Roots of Numerator	Roots of Denominator
-----	-----
0	-0.1041
-0.2236638493 + 1.029339632 I	-0.2741 + 1.909 I
-0.2236638493 - 1.029339632 I	-0.2741 - 1.909 I
	-0.6835

Factored form gain multiplier: -5.549

A.3.2 Plant Case 2

Plant Case: 2 Element: {1, 1}

Roots of Numerator	Roots of Denominator
-----	-----
0	0.3633
-0.01617592182	-0.07683 + 0.2065 I
-0.2031816462 + 0.8466260833 I	-0.07683 - 0.2065 I
-0.2031816462 - 0.8466260833 I	-0.2153286826 + 0.9546662645 I
-0.4708634843	-0.2153286826 - 0.9546662645 I
	-1.3

Factored form gain multiplier: -0.9381346215

Plant Case: 2 Element: {1, 2}

Roots of Numerator	Roots of Denominator
-----	-----
0	-0.01822
-0.01617592182	-0.1041
-0.2031816462 + 0.8466260833 I	-0.2741 + 1.909 I
-0.2031816462 - 0.8466260833 I	-0.2741 - 1.909 I
-0.4708634843	-0.4568
	-0.6835

Factored form gain multiplier: -16.82768488

Plant Case: 2 Element: {2, 1}

Roots of Numerator	Roots of Denominator
-----	-----
0	0.3633
-0.01617592182	-0.07683 + 0.2065 I
-0.2031816462 + 0.8466260833 I	-0.07683 - 0.2065 I
-0.2031816462 - 0.8466260833 I	-0.3017 + 1.562 I
-0.4708634843	-0.3017 - 1.562 I
	-1.3

Factored form gain multiplier: -2.195769339

Plant Case: 2 Element: {2, 2}

Roots of Numerator	Roots of Denominator
-----	-----
0	-0.01677417266
-0.01617592182	-0.1041
-0.2031816462 + 0.8466260833 I	-0.2741 + 1.909 I
-0.2031816462 - 0.8466260833 I	-0.2741 - 1.909 I
-0.4708634843	-0.4668627603
	-0.6835

Factored form gain multiplier: -4.447390596

A.3.3 Plant Case 3

Plant Case: 3 Element: {1, 1}

Roots of Numerator	Roots of Denominator
-----	-----
0	0.3633
-0.01800469395	-0.07683 + 0.2065 I
-0.2357205606 + 1.130855201 I	-0.07683 - 0.2065 I
-0.2357205606 - 1.130855201 I	-0.2362887311 + 1.132993767 I
-0.4582391881	-0.2362887311 - 1.132993767 I
	-1.3

Factored form gain multiplier: -2.226220249

Plant Case: 3 Element: {1, 2}

Roots of Numerator	Roots of Denominator
-----	-----
0	-0.06537
-0.01800469395	-0.1041
-0.2357205606 + 1.130855201 I	-0.2589
-0.2357205606 - 1.130855201 I	-0.2741 + 1.909 I
-0.4582391881	-0.2741 - 1.909 I
	-0.6835

Factored form gain multiplier: 60.9494543

Plant Case: 3 Element: {2, 1}

Roots of Numerator	Roots of Denominator
-----	-----
0	0.3633
-0.01800469395	-0.07683 + 0.2065 I
-0.2357205606 + 1.130855201 I	-0.07683 - 0.2065 I
-0.2357205606 - 1.130855201 I	-0.205 + 0.853 I
-0.4582391881	-0.205 - 0.853 I
	-1.3

Factored form gain multiplier: -13.16442881

Plant Case: 3 Element: {2, 2}

Roots of Numerator	Roots of Denominator
-----	-----
0	-0.01786739384
-0.01800469395	-0.1041
-0.2357205606 + 1.130855201 I	-0.2741 + 1.909 I
-0.2357205606 - 1.130855201 I	-0.2741 - 1.909 I
-0.4582391881	-0.4592182832
	-0.6835

Factored form gain multiplier: -3.340680271

A.3.4 Plant Case 4

Plant Case: 4 Element: {1, 1}

Roots of Numerator	Roots of Denominator
-----	-----
0	0.3633
-0.02559309899	-0.07683 + 0.2065 I
-0.2255463507 + 0.9379562951 I	-0.07683 - 0.2065 I
-0.2255463507 - 0.9379562951 I	-0.2236638493 + 1.029339632 I
-0.4123328591	-0.2236638493 - 1.029339632 I
	-1.3

Factored form gain multiplier: -0.9333336412

Plant Case: 4 Element: {1, 2}

Roots of Numerator	Roots of Denominator
-----	-----
0	-0.003009051506
-0.02559309899	-0.1041
-0.2255463507 + 0.9379562951 I	-0.2741 + 1.909 I
-0.2255463507 - 0.9379562951 I	-0.2741 - 1.909 I
-0.4123328591	-0.5869269321
	-0.6835

Factored form gain multiplier: -16.32745389

Plant Case: 4 Element: {2, 1}

Roots of Numerator

0
-0.02559309899
-0.2255463507 + 0.9379562951 I
-0.2255463507 - 0.9379562951 I
-0.4123328591

Roots of Denominator

0.3633
-0.07683 + 0.2065 I
-0.07683 - 0.2065 I
-0.2816656426 + 1.444520055 I
-0.2816656426 - 1.444520055 I
-1.3

Factored form gain multiplier: -0.9584655085

Plant Case: 4 Element: {2, 2}

Roots of Numerator

0
-0.02559309899
-0.2255463507 + 0.9379562951 I
-0.2255463507 - 0.9379562951 I
-0.4123328591

Roots of Denominator

-0.01750899094
-0.1041
-0.2741 + 1.909 I
-0.2741 - 1.909 I
-0.4616997602
-0.6835

Factored form gain multiplier: -2.380578877

A.3.5 Plant Case 5

Plant Case: 5 Element: {1, 1}

Roots of Numerator	Roots of Denominator
-----	-----
0	0.3633
-0.007096831889	-0.07683 + 0.2065 I
-0.1695335828 + 0.7432415914 I	-0.07683 - 0.2065 I
-0.1695335828 - 0.7432415914 I	-0.2236638493 + 1.029339632 I
-0.5339345123	-0.2236638493 - 1.029339632 I
	-1.3

Factored form gain multiplier: -0.8594337133

Plant Case: 5 Element: {1, 2}

Roots of Numerator	Roots of Denominator
-----	-----
0	-0.0271399588
-0.007096831889	-0.1041
-0.1695335828 + 0.7432415914 I	-0.2741 + 1.909 I
-0.1695335828 - 0.7432415914 I	-0.2741 - 1.909 I
-0.5339345123	-0.4023613724
	-0.6835

Factored form gain multiplier: -5.955291802

Plant Case: 5 Element: {2, 1}

Roots of Numerator

0
-0.007096831889
-0.1695335828 + 0.7432415914 I
-0.1695335828 - 0.7432415914 I
-0.5339345123

Roots of Denominator

0.3633
-0.07683 + 0.2065 I
-0.07683 - 0.2065 I
-0.3359094012 + 1.743875067 I
-0.3359094012 - 1.743875067 I
-1.3

Factored form gain multiplier: -1.507030392

Plant Case: 5 Element: {2, 2}

Roots of Numerator

0
-0.007096831889
-0.1695335828 + 0.7432415914 I
-0.1695335828 - 0.7432415914 I
-0.5339345123

Roots of Denominator

-0.01750899094
-0.1041
-0.2741 + 1.909 I
-0.2741 - 1.909 I
-0.4616997602
-0.6835

Factored form gain multiplier: -2.192088288

A.3.6 Plant Case 6

Plant Case: 6 Element: {1, 1}

Roots of Numerator	Roots of Denominator
-----	-----
0	0.3633
-0.01822	-0.07683 + 0.2065 I
-0.4568	-0.07683 - 0.2065 I
	-1.3

Factored form gain multiplier: -2.236

Plant Case: 6 Element: {1, 2}

Roots of Numerator	Roots of Denominator
-----	-----

Factored form gain multiplier: Infinity

Plant Case: 6 Element: {2, 1}

Roots of Numerator	Roots of Denominator
-----	-----

Factored form gain multiplier: Infinity

Plant Case: 6 Element: {2, 2}

Roots of Numerator	Roots of Denominator
-----	-----
0	-0.1041
-0.3017 + 1.562 I	-0.2741 + 1.909 I
-0.3017 - 1.562 I	-0.2741 - 1.909 I
	-0.6835

Factored form gain multiplier: -1.071

A.3.7 Plant Case 7

Plant Case: 7 Element: {1, 1}

Roots of Numerator	Roots of Denominator
-----	-----
0	1.167
-0.009939645444	-0.006472 + 0.07803 I
-0.5620045698	-0.006472 - 0.07803 I
	-2.028

Factored form gain multiplier: -5.91495

Plant Case: 7 Element: {1, 2}

Roots of Numerator	Roots of Denominator
-----	-----

Factored form gain multiplier: Infinity

Plant Case: 7 Element: {2, 1}

Roots of Numerator	Roots of Denominator
-----	-----

Factored form gain multiplier: Infinity

Plant Case: 7 Element: {2, 2}

Roots of Numerator	Roots of Denominator
-----	-----
0	0.07795
-0.2231060935 + 1.697351372 I	-0.211 + 1.953 I
-0.2231060935 - 1.697351372 I	-0.211 - 1.953 I
	-0.8265

Factored form gain multiplier: -20.842

A.3.8 Plant Case 8

Plant Case: 8 Element: {1, 1}

Roots of Numerator	Roots of Denominator
-----	-----
0	1.167
-0.009815072143	-0.006472 + 0.07803 I
-0.2183048925 + 1.608183851 I	-0.006472 - 0.07803 I
-0.2183048925 - 1.608183851 I	-0.2212351442 + 1.656795028 I
-0.5773169868	-0.2212351442 - 1.656795028 I
	-2.028

Factored form gain multiplier: -2.723981446

Plant Case: 8 Element: {1, 2}

Roots of Numerator	Roots of Denominator
-----	-----
0	0.07795
-0.009815072143	-0.01004
-0.2183048925 + 1.608183851 I	-0.211 + 1.953 I
-0.2183048925 - 1.608183851 I	-0.211 - 1.953 I
-0.5773169868	-0.5502
	-0.8265

Factored form gain multiplier: -71.16738424

Plant Case: 8 Element: {2, 1}

Roots of Numerator	Roots of Denominator
-----	-----
0	1.167
-0.009815072143	-0.006472 + 0.07803 I
-0.2183048925 + 1.608183851 I	-0.006472 - 0.07803 I
-0.2183048925 - 1.608183851 I	-0.2442 + 2.101 I
-0.5773169868	-0.2442 - 2.101 I
	-2.028

Factored form gain multiplier: -7.677841696

Plant Case: 8 Element: {2, 2}

Roots of Numerator	Roots of Denominator
-----	-----
0	0.07795
-0.009815072143	-0.009845163158
-0.2183048925 + 1.608183851 I	-0.211 + 1.953 I
-0.2183048925 - 1.608183851 I	-0.211 - 1.953 I
-0.5773169868	-0.5735955769
	-0.8265

Factored form gain multiplier: -17.4761309

A.3.9 Plant Case 9

Plant Case: 9 Element: {1, 1}

Roots of Numerator	Roots of Denominator
-----	-----
0	1.167
-0.01001950949	-0.006472 + 0.07803 I
-0.2257480147 + 1.760063131 I	-0.006472 - 0.07803 I
-0.2257480147 - 1.760063131 I	-0.2260615727 + 1.759509227 I
-0.5525460655	-0.2260615727 - 1.759509227 I
	-2.028

Factored form gain multiplier: -5.869418855

Plant Case: 9 Element: {1, 2}

Roots of Numerator	Roots of Denominator
-----	-----
0	0.07795
-0.01001950949	-0.006697
-0.2257480147 + 1.760063131 I	-0.211 + 1.953 I
-0.2257480147 - 1.760063131 I	-0.211 - 1.953 I
-0.5525460655	-0.8265
	-1.861

Factored form gain multiplier: -671.6854306

Plant Case: 9 Element: {2, 1}

Roots of Numerator

0
-0.01001950949
-0.2257480147 + 1.760063131 I
-0.2257480147 - 1.760063131 I
-0.5525460655

Roots of Denominator

1.167
-0.006472 + 0.07803 I
-0.006472 - 0.07803 I
-0.219 + 1.607 I
-0.219 - 1.607 I
-2.028

Factored form gain multiplier: -32.61790077

Plant Case: 9 Element: {2, 2}

Roots of Numerator

0
-0.01001950949
-0.2257480147 + 1.760063131 I
-0.2257480147 - 1.760063131 I
-0.5525460655

Roots of Denominator

0.07795
-0.009989054852
-0.211 + 1.953 I
-0.211 - 1.953 I
-0.5561293643
-0.8265

Factored form gain multiplier: -12.07978078

A.3.10 Plant Case 10

Plant Case: 10 Element: {1, 1}

Roots of Numerator	Roots of Denominator
-----	-----
0	1.167
-0.01069676636	-0.006472 + 0.07803 I
-0.231887918 + 1.587406074 I	-0.006472 - 0.07803 I
-0.231887918 - 1.587406074 I	-0.2231060935 + 1.697351372 I
-0.4844613815	-0.2231060935 - 1.697351372 I
	-2.028

Factored form gain multiplier: -2.235375702

Plant Case: 10 Element: {1, 2}

Roots of Numerator	Roots of Denominator
-----	-----
0	0.07795
-0.01069676636	-0.008933835362
-0.231887918 + 1.587406074 I	-0.211 + 1.953 I
-0.231887918 - 1.587406074 I	-0.211 - 1.953 I
-0.4844613815	-0.716404473
	-0.8265

Factored form gain multiplier: -27.77660548

Plant Case: 10 Element: {2, 1}

Roots of Numerator	Roots of Denominator
-----	-----
0	1.167
-0.01069676636	-0.006472 + 0.07803 I
-0.231887918 + 1.587406074 I	-0.006472 - 0.07803 I
-0.231887918 - 1.587406074 I	-0.2380753559 + 1.992266599 I
-0.4844613815	-0.2380753559 - 1.992266599 I
	-2.028

Factored form gain multiplier: -2.596177336

Plant Case: 10 Element: {2, 2}

Roots of Numerator	Roots of Denominator
-----	-----
0	0.07795
-0.01069676636	-0.009939645444
-0.231887918 + 1.587406074 I	-0.211 + 1.953 I
-0.231887918 - 1.587406074 I	-0.211 - 1.953 I
-0.4844613815	-0.5620045698
	-0.8265

Factored form gain multiplier: -7.87660088

A.3.11 Plant Case 11

Plant Case: 11 Element: {1, 1}

Roots of Numerator	Roots of Denominator
-----	-----
0	1.167
-0.009569120179	-0.006472 + 0.07803 I
-0.2083665407 + 1.62577185 I	-0.006472 - 0.07803 I
-0.2083665407 - 1.62577185 I	-0.2231060935 + 1.697351372 I
-0.6090927582	-0.2231060935 - 1.697351372 I
	-2.028

Factored form gain multiplier: -2.680096431

Plant Case: 11 Element: {1, 2}

Roots of Numerator	Roots of Denominator
-----	-----
0	0.07795
-0.009569120179	-0.01334841556
-0.2083665407 + 1.62577185 I	-0.211 + 1.953 I
-0.2083665407 - 1.62577185 I	-0.211 - 1.953 I
-0.6090927582	-0.3260098802
	-0.8265

Factored form gain multiplier: -44.55497314

Plant Case: 11 Element: {2, 1}

Roots of Numerator

0
-0.009569120179
-0.2083665407 + 1.62577185 I
-0.2083665407 - 1.62577185 I
-0.6090927582

Roots of Denominator

1.167
-0.006472 + 0.07803 I
-0.006472 - 0.07803 I
-0.2561175712 + 2.297831558 I
-0.2561175712 - 2.297831558 I
-2.028

Factored form gain multiplier: -6.056770922

Plant Case: 11 Element: {2, 2}

Roots of Numerator

0
-0.009569120179
-0.2083665407 + 1.62577185 I
-0.2083665407 - 1.62577185 I
-0.6090927582

Roots of Denominator

0.07795
-0.009939645444
-0.211 + 1.953 I
-0.211 - 1.953 I
-0.5620045698
-0.8265

Factored form gain multiplier: -9.443625022

A.3.12 Plant Case 12

Plant Case: 12 Element: {1, 1}

Roots of Numerator	Roots of Denominator
-----	-----
0	1.167
-0.01004	-0.006472 + 0.07803 I
-0.5502	-0.006472 - 0.07803 I
	-2.028

Factored form gain multiplier: -5.862

Plant Case: 12 Element: {1, 2}

Roots of Numerator	Roots of Denominator
-----	-----

Factored form gain multiplier: Infinity

Plant Case: 12 Element: {2, 1}

Roots of Numerator	Roots of Denominator
-----	-----

Factored form gain multiplier: Infinity

Plant Case: 12 Element: {2, 2}

Roots of Numerator	Roots of Denominator
-----	-----
0	0.07795
-0.2442 + 2.101 I	-0.211 + 1.953 I
-0.2442 - 2.101 I	-0.211 - 1.953 I
	-0.8265

Factored form gain multiplier: -3.396

A.3.13 Plant Case 13

Plant Case: 13 Element: {1, 1}

Roots of Numerator	Roots of Denominator
-----	-----
0	0.9645
-0.01261453256	-0.007553 + 0.5384 I
-1.518569941	-0.007553 - 0.5384 I
	-3.223

Factored form gain multiplier: -25.678

Plant Case: 13 Element: {1, 2}

Roots of Numerator	Roots of Denominator
-----	-----

Factored form gain multiplier: Infinity

Plant Case: 13 Element: {2, 1}

Roots of Numerator	Roots of Denominator
-----	-----

Factored form gain multiplier: Infinity

Plant Case: 13 Element: {2, 2}

Roots of Numerator	Roots of Denominator
-----	-----
0	-0.02719
-0.3582378099 + 3.06754481 I	-0.391 + 2.962 I
-0.3582378099 - 3.06754481 I	-0.391 - 2.962 I
	-2.697

Factored form gain multiplier: -63.74

A.3.14 Plant Case 14

Plant Case: 14 Element: {1, 1}

Roots of Numerator	Roots of Denominator
-----	-----
0	0.9645
-0.01260815216	-0.007553 + 0.5384 I
-0.354043529 + 2.937631878 I	-0.007553 - 0.5384 I
-0.354043529 - 2.937631878 I	-0.3563974216 + 3.005846427 I
-1.528579891	-0.3563974216 - 3.005846427 I
	-3.223

Factored form gain multiplier: -12.31925087

Plant Case: 14 Element: {1, 2}

Roots of Numerator	Roots of Denominator
-----	-----
0	-0.01262
-0.01260815216	-0.02719
-0.354043529 + 2.937631878 I	-0.391 + 2.962 I
-0.354043529 - 2.937631878 I	-0.391 - 2.962 I
-1.528579891	-1.51
	-2.697

Factored form gain multiplier: -235.120532

Plant Case: 14 Element: {2, 1}

Roots of Numerator	Roots of Denominator
-----	-----
0	0.9645
-0.01260815216	-0.007553 + 0.5384 I
-0.354043529 + 2.937631878 I	-0.007553 - 0.5384 I
-0.354043529 - 2.937631878 I	-0.3749 + 3.578 I
-1.528579891	-0.3749 - 3.578 I
	-3.223

Factored form gain multiplier: -27.88347792

Plant Case: 14 Element: {2, 2}

Roots of Numerator	Roots of Denominator
-----	-----
0	-0.01260976464
-0.01260815216	-0.02719
-0.354043529 + 2.937631878 I	-0.391 + 2.962 I
-0.354043529 - 2.937631878 I	-0.391 - 2.962 I
-1.528579891	-1.526123846
	-2.697

Factored form gain multiplier: -51.81162075

A.3.15 Plant Case 15

Plant Case: 15 Element: {1, 1}

Roots of Numerator	Roots of Denominator
-----	-----
0	0.9645
-0.01261877154	-0.007553 + 0.5384 I
-0.3609727016 + 3.162975977 I	-0.007553 - 0.5384 I
-0.3609727016 - 3.162975977 I	-0.3610024863 + 3.157962895 I
-1.511867408	-0.3610024863 - 3.157962895 I
	-3.223

Factored form gain multiplier: -24.32846689

Plant Case: 15 Element: {1, 2}

Roots of Numerator	Roots of Denominator
-----	-----
0	-0.01254
-0.01261877154	-0.02719
-0.3609727016 + 3.162975977 I	-0.391 + 2.962 I
-0.3609727016 - 3.162975977 I	-0.391 - 2.962 I
-1.511867408	-1.646
	-2.697

Factored form gain multiplier: -287.2653646

Plant Case: 15 Element: {2, 1}

Roots of Numerator	Roots of Denominator
-----	-----
0	0.9645
-0.01261877154	-0.007553 + 0.5384 I
-0.3609727016 + 3.162975977 I	-0.007553 - 0.5384 I
-0.3609727016 - 3.162975977 I	-0.3541 + 2.927 I
-1.511867408	-0.3541 - 2.927 I
	-3.223

Factored form gain multiplier: -145.646803

Plant Case: 15 Element: {2, 2}

Roots of Numerator	Roots of Denominator
-----	-----
0	-0.01261716956
-0.01261877154	-0.02719
-0.3609727016 + 3.162975977 I	-0.391 + 2.962 I
-0.3609727016 - 3.162975977 I	-0.391 - 2.962 I
-1.511867408	-1.514424371
	-2.697

Factored form gain multiplier: -37.37949737

A.3.16 Plant Case 16

Plant Case: 16 Element: {1, 1}

Roots of Numerator	Roots of Denominator
-----	-----
0	0.9645
-0.01268136836	-0.007553 + 0.5384 I
-0.3638212458 + 2.642435984 I	-0.007553 - 0.5384 I
-0.3638212458 - 2.642435984 I	-0.3582378099 + 3.06754481 I
-1.425766242	-0.3582378099 - 3.06754481 I
	-3.223

Factored form gain multiplier: -6.620477918

Plant Case: 16 Element: {1, 2}

Roots of Numerator	Roots of Denominator
-----	-----
0	-0.01257680361
-0.01268136836	-0.02719
-0.3638212458 + 2.642435984 I	-0.391 + 2.962 I
-0.3638212458 - 2.642435984 I	-0.391 - 2.962 I
-1.425766242	-1.580490401
	-2.697

Factored form gain multiplier: -33.79428706

Plant Case: 16 Element: {2, 1}

Roots of Numerator	Roots of Denominator
-----	-----
0	0.9645
-0.01268136836	-0.007553 + 0.5384 I
-0.3638212458 + 2.642435984 I	-0.007553 - 0.5384 I
-0.3638212458 - 2.642435984 I	-0.3707177207 + 3.456973615 I
-1.425766242	-0.3707177207 - 3.456973615 I
	-3.223

Factored form gain multiplier: -6.647070371

Plant Case: 16 Element: {2, 2}

Roots of Numerator	Roots of Denominator
-----	-----
0	-0.01261453256
-0.01268136836	-0.02719
-0.3638212458 + 2.642435984 I	-0.391 + 2.962 I
-0.3638212458 - 2.642435984 I	-0.391 - 2.962 I
-1.425766242	-1.518569941
	-2.697

Factored form gain multiplier: -16.43388358

A.3.17 Plant Case 17

Plant Case: 17 Element: {1, 1}

Roots of Numerator	Roots of Denominator
-----	-----
0	0.9645
-0.01259578413	-0.007553 + 0.5384 I
-0.3541334715 + 3.077600345 I	-0.007553 - 0.5384 I
-0.3541334715 - 3.077600345 I	-0.3582378099 + 3.06754481 I
-1.54738922	-0.3582378099 - 3.06754481 I
	-3.223

Factored form gain multiplier: -12.97506397

Plant Case: 17 Element: {1, 2}

Roots of Numerator	Roots of Denominator
-----	-----
0	-0.01207934927
-0.01259578413	-0.02719
-0.3541334715 + 3.077600345 I	-0.391 + 2.962 I
-0.3541334715 - 3.077600345 I	-0.391 - 2.962 I
-1.54738922	-2.697
	-3.435429579

Factored form gain multiplier: 1809.694918

Plant Case: 17 Element: {2, 1}

Roots of Numerator

0
-0.01259578413
-0.3541334715 + 3.077600345 I
-0.3541334715 - 3.077600345 I
-1.54738922

Roots of Denominator

0.9645
-0.007553 + 0.5384 I
-0.007553 - 0.5384 I
-0.381895442 + 3.771752842 I
-0.381895442 - 3.771752842 I
-3.223

Factored form gain multiplier: -21.78976624

Plant Case: 17 Element: {2, 2}

Roots of Numerator

0
-0.01259578413
-0.3541334715 + 3.077600345 I
-0.3541334715 - 3.077600345 I
-1.54738922

Roots of Denominator

-0.01261453256
-0.02719
-0.391 + 2.962 I
-0.391 - 2.962 I
-1.518569941
-2.697

Factored form gain multiplier: -32.20774895

A.3.18 Plant Case 18

Plant Case: 18 Element: {1, 1}

Roots of Numerator	Roots of Denominator
-----	-----
0	0.9645
-0.01262	-0.007553 + 0.5384 I
-1.51	-0.007553 - 0.5384 I
	-3.223

Factored form gain multiplier: -24.06

Plant Case: 18 Element: {1, 2}

Roots of Numerator	Roots of Denominator
-----	-----

Factored form gain multiplier: Infinity

Plant Case: 18 Element: {2, 1}

Roots of Numerator	Roots of Denominator
-----	-----

Factored form gain multiplier: Infinity

Plant Case: 18 Element: {2, 2}

Roots of Numerator	Roots of Denominator
-----	-----
0	-0.02719
-0.3749 + 3.578 I	-0.391 + 2.962 I
-0.3749 - 3.578 I	-0.391 - 2.962 I
	-2.697

Factored form gain multiplier: -12.68

A.3.19 Plant Case 19

Plant Case: 19 Element: {1, 1}

Roots of Numerator	Roots of Denominator
-----	-----
0	-0.01516 + 0.02343 I
-0.03008318398	-0.01516 - 0.02343 I
-1.079585586	-0.8012 + 6.592 I
	-0.8012 - 6.592 I

Factored form gain multiplier: -34.3625

Plant Case: 19 Element: {1, 2}

Roots of Numerator	Roots of Denominator
-----	-----

Factored form gain multiplier: Infinity

Plant Case: 19 Element: {2, 1}

Roots of Numerator	Roots of Denominator
-----	-----

Factored form gain multiplier: Infinity

Plant Case: 19 Element: {2, 2}

Roots of Numerator	Roots of Denominator
-----	-----
0	-0.03448
-0.3943568208 + 4.656189818 I	-0.4996 + 3.129 I
-0.3943568208 - 4.656189818 I	-0.4996 - 3.129 I
	-2.171

Factored form gain multiplier: -25.818

A.3.20 Plant Case 20

Plant Case: 20 Element: {1, 1}

Roots of Numerator	Roots of Denominator
-----	-----
0	-0.01516 + 0.02343 I
-0.03027103524	-0.01516 - 0.02343 I
-0.4059826056 + 4.898011078 I	-0.399297224 + 4.749877372 I
-0.4059826056 - 4.898011078 I	-0.399297224 - 4.749877372 I
-1.054028453	-0.8012 + 6.592 I
	-0.8012 - 6.592 I

Factored form gain multiplier: -13.11976004

Plant Case: 20 Element: {1, 2}

Roots of Numerator	Roots of Denominator
-----	-----
0	-0.02996
-0.03027103524	-0.03448
-0.4059826056 + 4.898011078 I	-0.4996 + 3.129 I
-0.4059826056 - 4.898011078 I	-0.4996 - 3.129 I
-1.054028453	-1.097
	-2.171

Factored form gain multiplier: -63.78197264

Plant Case: 20 Element: {2, 1}

Roots of Numerator	Roots of Denominator
-----	-----
0	-0.01516 + 0.02343 I
-0.03027103524	-0.01516 - 0.02343 I
-0.4059826056 + 4.898011078 I	-0.3774 + 4.319155473 I
-0.4059826056 - 4.898011078 I	-0.3774 - 4.319155473 I
-1.054028453	-0.8012 + 6.592 I
	-0.8012 - 6.592 I

Factored form gain multiplier: -11.25765504

Plant Case: 20 Element: {2, 2}

Roots of Numerator	Roots of Denominator
-----	-----
0	-0.03019996745
-0.03027103524	-0.03448
-0.4059826056 + 4.898011078 I	-0.4996 + 3.129 I
-0.4059826056 - 4.898011078 I	-0.4996 - 3.129 I
-1.054028453	-1.063589349
	-2.171

Factored form gain multiplier: -14.64359316

A.3.21 Plant Case 21

Plant Case: 21 Element: {1, 1}

Roots of Numerator	Roots of Denominator
-----	-----
0	-0.01516 + 0.02343 I
-0.0299951359	-0.01516 - 0.02343 I
-0.3886587722 + 4.551009274 I	-0.3890844027 + 4.554074665 I
-0.3886587722 - 4.551009274 I	-0.3890844027 - 4.554074665 I
-1.091958693	-0.8012 + 6.592 I
	-0.8012 - 6.592 I

Factored form gain multiplier: -33.35473804

Plant Case: 21 Element: {1, 2}

Roots of Numerator	Roots of Denominator
-----	-----
0	-0.03448
-0.0299951359	-0.03459
-0.3886587722 + 4.551009274 I	-0.4996 + 3.129 I
-0.3886587722 - 4.551009274 I	-0.4996 - 3.129 I
-1.091958693	-0.6861
	-2.171

Factored form gain multiplier: -213.6299701

Plant Case: 21 Element: {2, 1}

Roots of Numerator	Roots of Denominator
-----	-----
0	-0.01516 + 0.02343 I
-0.0299951359	-0.01516 - 0.02343 I
-0.3886587722 + 4.551009274 I	-0.4083 + 4.916 I
-0.3886587722 - 4.551009274 I	-0.4083 - 4.916 I
-1.091958693	-0.8012 + 6.592 I
	-0.8012 - 6.592 I

Factored form gain multiplier: -352.8332369

Plant Case: 21 Element: {2, 2}

Roots of Numerator	Roots of Denominator
-----	-----
0	-0.03002242458
-0.0299951359	-0.03448
-0.3886587722 + 4.551009274 I	-0.4996 + 3.129 I
-0.3886587722 - 4.551009274 I	-0.4996 - 3.129 I
-1.091958693	-1.088103978
	-2.171

Factored form gain multiplier: -18.57997138

A.3.22 Plant Case 22

Plant Case: 22 Element: {1, 1}

Roots of Numerator	Roots of Denominator
-----	-----
0	-0.01516 + 0.02343 I
-0.0281768207	-0.01516 - 0.02343 I
-0.5658911377 + 5.6216463 I	-0.3943568208 + 4.656189818 I
-0.5658911377 - 5.6216463 I	-0.3943568208 - 4.656189818 I
-1.442976725	-0.8012 + 6.592 I
	-0.8012 - 6.592 I

Factored form gain multiplier: -3.513486231

Plant Case: 22 Element: {1, 2}

Roots of Numerator	Roots of Denominator
-----	-----
0	-0.03136799809
-0.0281768207	-0.03448
-0.5658911377 + 5.6216463 I	-0.4996 + 3.129 I
-0.5658911377 - 5.6216463 I	-0.4996 - 3.129 I
-1.442976725	-0.9267337781
	-2.171

Factored form gain multiplier: -6.444844583

Plant Case: 22 Element: {2, 1}

Roots of Numerator

0
-0.0281768207
-0.5658911377 + 5.6216463 I
-0.5658911377 - 5.6216463 I
-1.442976725

Roots of Denominator

-0.01516 + 0.02343 I
-0.01516 - 0.02343 I
-0.379582757 + 4.364003618 I
-0.379582757 - 4.364003618 I
-0.8012 + 6.592 I
-0.8012 - 6.592 I

Factored form gain multiplier: -1.809085946

Plant Case: 22 Element: {2, 2}

Roots of Numerator

0
-0.0281768207
-0.5658911377 + 5.6216463 I
-0.5658911377 - 5.6216463 I
-1.442976725

Roots of Denominator

-0.03008318398
-0.03448
-0.4996 + 3.129 I
-0.4996 - 3.129 I
-1.079585586
-2.171

Factored form gain multiplier: -2.639830848

A.3.23 Plant Case 23

Plant Case: 23 Element: {1, 1}

Roots of Numerator	Roots of Denominator
-----	-----
0	-0.01516 + 0.02343 I
-0.03096598996	-0.01516 - 0.02343 I
-0.3853668983 + 4.706629116 I	-0.3943568208 + 4.656189818 I
-0.3853668983 - 4.706629116 I	-0.3943568208 - 4.656189818 I
-0.9691322627	-0.8012 + 6.592 I
	-0.8012 - 6.592 I

Factored form gain multiplier: -15.20079547

Plant Case: 23 Element: {1, 2}

Roots of Numerator	Roots of Denominator
-----	-----
0	-0.02634744696
-0.03096598996	-0.03448
-0.3853668983 + 4.706629116 I	-0.4996 + 3.129 I
-0.3853668983 - 4.706629116 I	-0.4996 - 3.129 I
-0.9691322627	-2.101319711
	-2.171

Factored form gain multiplier: -165.2438474

Plant Case: 23 Element: {2, 1}

Roots of Numerator

0
-0.03096598996
-0.3853668983 + 4.706629116 I
-0.3853668983 - 4.706629116 I
-0.9691322627

Roots of Denominator

-0.01516 + 0.02343 I
-0.01516 - 0.02343 I
-0.3748581309 + 4.266333269 I
-0.3748581309 - 4.266333269 I
-0.8012 + 6.592 I
-0.8012 - 6.592 I

Factored form gain multiplier: -9.114546368

Plant Case: 23 Element: {2, 2}

Roots of Numerator

0
-0.03096598996
-0.3853668983 + 4.706629116 I
-0.3853668983 - 4.706629116 I
-0.9691322627

Roots of Denominator

-0.03008318398
-0.03448
-0.4996 + 3.129 I
-0.4996 - 3.129 I
-1.079585586
-2.171

Factored form gain multiplier: -11.42100073

A.3.24 Plant Case 24

Plant Case: 24 Element: {1, 1}

Roots of Numerator	Roots of Denominator
-----	-----
0	-0.01516 + 0.02343 I
-0.02996	-0.01516 - 0.02343 I
-1.097	-0.8012 + 6.592 I
	-0.8012 - 6.592 I

Factored form gain multiplier: -32.9

Plant Case: 24 Element: {1, 2}

Roots of Numerator	Roots of Denominator
-----	-----

Factored form gain multiplier: Infinity

Plant Case: 24 Element: {2, 1}

Roots of Numerator	Roots of Denominator
-----	-----

Factored form gain multiplier: Infinity

Plant Case: 24 Element: {2, 2}

Roots of Numerator	Roots of Denominator
-----	-----
0	-0.03448
-0.3774 + 4.319155473 I	-0.4996 + 3.129 I
-0.3774 - 4.319155473 I	-0.4996 - 3.129 I
	-2.171

Factored form gain multiplier: -11.65

B Appendix B - Robert Betzold's Design

B.1 P_e Matrix Transfer Functions From CAD Package

B.1.1 Plant Case 1

Plant Case: 1 Element: {1, 1}

Roots of Numerator	Roots of Denominator
-----	-----
-0.087 + 0.7945 I	-0.009303144518 + 0.8902165661 I
-0.087 - 0.7945 I	-0.009303144518 - 0.8902165661 I
-22.3459	-0.009359976213
	-0.6203193063
	-22.34857028

Factored form gain multiplier: 0.7278

Plant Case: 1 Element: {1, 2}

Roots of Numerator	Roots of Denominator
-----	-----
2.038	-0.009303144518 + 0.8902165661 I
-1.631	-0.009303144518 - 0.8902165661 I
-22.3459	-0.009359976213
	-0.6203193063
	-22.34857028

Factored form gain multiplier: 0.3288683694

Plant Case: 1 Element: {2, 1}

Roots of Numerator	Roots of Denominator
-----	-----
-0.0603	-0.009303144518 + 0.8902165661 I
-2.438	-0.009303144518 - 0.8902165661 I
-22.3459	-0.009359976213
	-0.6203193063
	-22.34857028

Factored form gain multiplier: 0.02317192691

Plant Case: 1 Element: {2, 2}

Roots of Numerator	Roots of Denominator
-----	-----
0.0157	-0.009303144518 + 0.8902165661 I
-0.5238	-0.009303144518 - 0.8902165661 I
-22.3459	-0.009359976213
-22.77	-0.6203193063
	-22.34857028

Factored form gain multiplier: 0.023

B.1.2 Plant Case 2

Plant Case: 2 Element: {1, 1}

Roots of Numerator	Roots of Denominator
-----	-----
-0.137 + 1.017 I	0.001342491142 + 1.024203412 I
-0.137 - 1.017 I	0.001342491142 - 1.024203412 I
-30.297	0.0002242280203
	-0.892504982
	-30.27768085

Factored form gain multiplier: 0.7088

Plant Case: 2 Element: {1, 2}

Roots of Numerator	Roots of Denominator
-----	-----
2.93	0.001342491142 + 1.024203412 I
-2.178	0.001342491142 - 1.024203412 I
-30.297	0.0002242280203
	-0.892504982
	-30.27768085

Factored form gain multiplier: 0.3608436364

Plant Case: 2 Element: {2, 1}

Roots of Numerator	Roots of Denominator
-----	-----
1.58	0.001342491142 + 1.024203412 I
-0.095	0.001342491142 - 1.024203412 I
-30.297	0.0002242280203
	-0.892504982
	-30.27768085

Factored form gain multiplier: -0.04083621399

Plant Case: 2 Element: {2, 2}

Roots of Numerator	Roots of Denominator
-----	-----
0.032	0.001342491142 + 1.024203412 I
-0.7228	0.001342491142 - 1.024203412 I
-29.46	0.0002242280203
-30.297	-0.892504982
	-30.27768085

Factored form gain multiplier: 0.028

B.1.3 Plant Case 3

Plant Case: 3 Element: {1, 1}

Roots of Numerator	Roots of Denominator
-----	-----
-0.0006	0
-0.006	-0.01371701971 + 0.008810265786 I
-0.153 + 0.5226 I	-0.01371701971 - 0.008810265786 I
-0.153 - 0.5226 I	-0.02524080608 - 0.7384883801 I
-4.12	-0.02524080608 + 0.7384883801 I
	-1.135459827
	-4.114539658

Factored form gain multiplier: 1.434

Plant Case: 3 Element: {1, 2}

Roots of Numerator	Roots of Denominator
-----	-----
1.78	0
-0.0006	-0.01371701971 + 0.008810265786 I
-0.006	-0.01371701971 - 0.008810265786 I
-0.932	-0.02524080608 - 0.7384883801 I
-4.12	-0.02524080608 + 0.7384883801 I
	-1.135459827
	-4.114539658

Factored form gain multiplier: 0.1352158809

Plant Case: 3 Element: {2, 1}

Roots of Numerator

67.97

C

-0.006

-0.093

-4.12

Roots of Denominator

0

-0.01371701971 + 0.008810265786 I

-0.01371701971 - 0.008810265786 I

-0.02524080608 - 0.7384883801 I

-0.02524080608 + 0.7384883801 I

-1.135459827

-4.114539658

Factored form gain multiplier: -0.00456

Plant Case: 3 Element: {2, 2}

Roots of Numerator

0.04

0

-0.0006

-1.26

-3.79

-4.12

Roots of Denominator

0

-0.01371701971 + 0.008810265786 I

-0.01371701971 - 0.008810265786 I

-0.02524080608 - 0.7384883801 I

-0.02524080608 + 0.7384883801 I

-1.135459827

-4.114539658

Factored form gain multiplier: 0.038

B.2 P_e Determinants From CAD Package

Plant Case: 1

Roots of Numerator of Det[Pe]

-22.34582333

-22.34597894

Roots of Denominator of Det[Pe]

-0.009303144518 + 0.8902165661 I

-0.009303144518 - 0.8902165661 I

-0.009359976213

-0.6203193063

-22.34857028

Plant Case: 2

Roots of Numerator of Det[Pe]

-30.2969961

-30.2970039

Roots of Denominator of Det[Pe]

0.001342491142 + 1.024203427 I

0.001342491142 - 1.024203427 I

0.0002242280203

-0.892504982

-30.27768085

Plant Case: 3

Roots of Numerator of Det[Pe]

-0.0006

-0.006

-4.119999964

-4.120000036

Roots of Denominator of Det[Pe]

0

-0.01371701971 + 0.008810265786 I

-0.01371701971 - 0.008810265786 I

-0.02524080608 - 0.7384883801 I

-0.02524080608 + 0.7384883801 I

-1.135459827

-4.114539658

B.3 Q Matrix Transfer Functions From CAD Package

B.3.1 Plant Case 1

Plant Case: 1 Element: {1, 1}

Roots of Numerator	Roots of Denominator
-----	-----
-22.3459	0.0157
	-0.5238
	-22.77

Factored form gain multiplier: 0.7278

Plant Case: 1 Element: {1, 2}

Roots of Numerator	Roots of Denominator
-----	-----
-22.3459	2.038
	-1.631

Factored form gain multiplier: -0.0509

Plant Case: 1 Element: {2, 1}

Roots of Numerator	Roots of Denominator
-----	-----
-22.3459	-0.0603
	-2.438

Factored form gain multiplier: -0.7224

Plant Case: 1 Element: {2, 2}

Roots of Numerator	Roots of Denominator
-----	-----
-22.3459	-0.087 + 0.7945 I
	-0.087 - 0.7945 I

Factored form gain multiplier: 0.023

B.3.2 Plant Case 2

Plant Case: 2 Element: {1, 1}

Roots of Numerator	Roots of Denominator
-----	-----
-30.297	0.032
	-0.7228
	-29.46

Factored form gain multiplier: 0.7088

Plant Case: 2 Element: {1, 2}

Roots of Numerator	Roots of Denominator
-----	-----
-30.297	2.93
	-2.178

Factored form gain multiplier: -0.055

Plant Case: 2 Element: {2, 1}

Roots of Numerator	Roots of Denominator
-----	-----
-30.297	1.58
	-0.095

Factored form gain multiplier: 0.486

Plant Case: 2 Element: {2, 2}

Roots of Numerator	Roots of Denominator
-----	-----
-30.297	-0.137 + 1.017 I
	-0.137 - 1.017 I

Factored form gain multiplier: 0.028

B.3.3 Plant Case 3

Plant Case: 3 Element: {1, 1}

Roots of Numerator	Roots of Denominator
-----	-----
-0.006	0.04
-4.1199931	0
	-1.26
	-3.79

Factored form gain multiplier: 1.434

Plant Case: 3 Element: {1, 2}

Roots of Numerator	Roots of Denominator
-----	-----
-4.1199931	1.78
	-0.932

Factored form gain multiplier: -0.403

Plant Case: 3 Element: {2, 1}

Roots of Numerator	Roots of Denominator
-----	-----
-0.0006	67.97
-4.1199931	0
	-0.093

Factored form gain multiplier: 11.95

Plant Case: 3 Element: {2, 2}

Roots of Numerator	Roots of Denominator
-----	-----
-4.1199931	-0.153 + 0.5226 I
	-0.153 - 0.5226 I

Factored form gain multiplier: 0.038

B.4 Q Matrix from CAD Package

B.4.1 Plant Case 1

Plant Case: 1 Element: {1, 1}

Roots of Numerator	Roots of Denominator
-----	-----
-22.3459	0.0157
	-0.5238
	-22.77

Factored form gain multiplier: 0.7278

Plant Case: 1 Element: {1, 2}

Roots of Numerator	Roots of Denominator
-----	-----
-22.3459	2.038
	-1.631

Factored form gain multiplier: -0.0509

Plant Case: 1 Element: {2, 1}

Roots of Numerator	Roots of Denominator
-----	-----
-22.3459	-0.0603
	-2.438

Factored form gain multiplier: -0.7224

Plant Case: 1 Element: {2, 2}

Roots of Numerator	Roots of Denominator
-----	-----
-22.3459	-0.087 + 0.7945 I
	-0.087 - 0.7945 I

Factored form gain multiplier: 0.023

B.4.2 Plant Case 2

Plant Case: 2 Element: {1, 1}

Roots of Numerator	Roots of Denominator
-----	-----
-30.297	0.032
	-0.7228
	-29.46

Factored form gain multiplier: 0.7088

Plant Case: 2 Element: {1, 2}

Roots of Numerator	Roots of Denominator
-----	-----
-30.297	2.93
	-2.178

Factored form gain multiplier: -0.055

Plant Case: 2 Element: {2, 1}

Roots of Numerator	Roots of Denominator
-----	-----
-30.297	1.58
	-0.095

Factored form gain multiplier: 0.486

Plant Case: 2 Element: {2, 2}

Roots of Numerator	Roots of Denominator
-----	-----
-30.297	-0.137 + 1.017 I
	-0.137 - 1.017 I

Factored form gain multiplier: 0.028

B.4.3 Plant Case 3

Plant Case: 3 Element: {1, 1}

Roots of Numerator	Roots of Denominator
-----	-----
-0.006	0.04
-4.1199931	0
	-1.26
	-3.79

Factored form gain multiplier: 1.434

Plant Case: 3 Element: {1, 2}

Roots of Numerator	Roots of Denominator
-----	-----
-4.1199931	1.78
	-0.932

Factored form gain multiplier: -0.403

Plant Case: 3 Element: {2, 1}

Roots of Numerator	Roots of Denominator
-----	-----
-0.0006	67.97
-4.1199931	0
	-0.093

Factored form gain multiplier: 11.95

Plant Case: 3 Element: {2, 2}

Roots of Numerator	Roots of Denominator
-----	-----
-4.1199931	-0.153 + 0.5226 I
	-0.153 - 0.5226 I

Factored form gain multiplier: 0.038

Bibliography

1. Ammeraal, Leendert. *Programming Principles in Computer Graphics*. New York: John Wiley & Sons.
2. Arnold, Philip B. *Flight Control System Reconfiguration Design Using Quantitative Feedback Theory*. MS thesis, AFIT/GE/ENG/84D-15. School of Engineering, Air Force Institute of Technology (AU), Wright-Patterson AFB OH, December, 1984.
3. Bailey, F. N. and M. Kallel. "Loop Gain-Phase Shaping Techniques for Robust Coordinated Motion Control", *Proceedings of the American Control Conference*, June 1991.
4. Bailey, F. N. and others. "Two Algorithms for Frequency Domain Design of Robust Control Systems", *International Journal of Control*, Vol. 48(No. 5):pp 1787-1806, (1988).
5. Betzold, W. *Multiple Input - Multiple Output Flight Control Design With Highly Uncertain Parameters; Application to the C-135 Aircraft*. MS thesis, AFIT/GE/EE/83D-11. School of Engineering, Air Force Institute of Technology (AU), Wright-Patterson AFB OH, December, 1983.
6. Boyle and others. *Matrix Eigensystem Routines-Eispack Guide, (Second Edition)*. Springer Verlag, Berlin, Heidelberg, New York, 1976.
7. Bunch and others. *LINPACK User's Guide*. Siam, Philadelphia, 1979.
8. Chait, Yossi. "Multi-Input Multi-Output Computer-Aided Control Design Using QFT", *International Journal of Robust Control*, to be published.
9. Cole, Sandra R. H. *A Computer-Aided Design Package For Quantitative Feedback Theory*. MS thesis, AFIT/GE/ENG/86D-56. School of Engineering, Air Force Institute of Technology (AU), Wright-Patterson AFB OH, December, 1986.
10. Ctrl-C User's Guide, Systems Control Technology, Inc., Palo Alto, CA 94303.
11. D'Azzo, John J. and Constantine H. Houpis. *Linear Control System Analysis and Design: Conventional and Modern*. New York: McGraw-Hill Book Company, 1988.
12. EASY5 User's Manual, The Boeing Company, Seattle, WA 20491.
13. Horowitz, Issac. Founder of QFT. Personal Interviews and Correspondence. Air Force Institute of Technology, Wright-Patterson AFB OH, June 1991 through May 1992.
14. Horowitz, Issac. "Improved Design Technique For Uncertain Multiple-Input-Multiple-Output Feedback Systems," *International Journal of Control*, Vol. 36 (No. 6):pp 977-988 (1982).
15. Horowitz, Issac, and A. Gera, "Blending of Uncertain Nonminimal-Phase Plants for Elimination or Reduction of Nonminimal Phase Property," *International Journal of System Science*, Vol. 10(No. 9), 1979.
16. Houpis, Constantine H. Professor of Electrical Engineering. Personal Interviews. Air Force Institute of Technology, Wright-Patterson AFB OH, June 1991 through May 1992.

17. Houpis, Constantine H. *Quantitative Feedback Theory*. AFWAL-TR-86-3107. Dayton OH: AFWAL/FIGL, January 1987.
18. Lacey, Donald. *A Robust Digital Flight Control System For an Unmanned Research Vehicle Using Discrete Quantitative Feedback Theory*. MS thesis, AFIT/GE/ENG/91D-33. School of Engineering, Air Force Institute of Technology (AU), Wright-Patterson AFB OH, December, 1991.
19. MACSYMA Reference Manual, Symbolics, Inc., Burlington, MA 01803.
20. MATRIXx User's Guide, Integrated Systems, Inc., Santa Clara, CA 95054.
21. Miller, Russel B. *Multi-Input Multi-Output Flight Control System Design For the YF-16 Using Nonlinear QFT and Pilot Compensation*. MS thesis, AFIT/GE/ENG/90D-42. School of Engineering, Air Force Institute of Technology (AU), Wright-Patterson AFB OH, December, 1990.
22. Multiple Input Single Output (MISO) QFT-CAD User Manual, Oded Yaniv, Tel-Aviv University, Tel-Aviv 69 978, Israel.
23. Press, William H. and others. *Numeric Recipes in C*. New York: Cambridge University Press, 1988.
24. Pro-Matlab User's Guide, The MathWorks, Inc., South Natick, MA 01760.
25. Rasmussen, Steven J. Student. Personal Interviews. Air Force Institute of Technology, Wright-Patterson AFB, OH, June 1991.
26. Siegel, Charles. *Teach Yourself... C*. Portland: Management Information Source, Inc., 1989.
27. Thompson, David F. Optimal and Sub-Optimal Loop Shaping in Quantitative Feedback Theory. PhD dissertation. Purdue University, West Lafayette, IN, 1990.
28. Tremblay, Jean Paul, and others. *Introduction to Computer Science*. New York: McGraw-Hill Book Company, 1989.
29. Wolfram, Stephen and others. *Mathematica: a System For Doing Mathematics by Computer*. Redwood City: Addison-Wesley Publishing Company, 1991.

Vita

Richard R. Sating was born on December 27, 1964 in Cleveland, Ohio. He graduated from Lakewood High School in Cleveland, Ohio in 1982. He then attended The Ohio State University where he received continued his Bachelor of Science degree in Electrical Engineering in December 1987. Following graduation, he began working in quality control at PPG Industries. In June of 1990, he entered the School of Engineering at the Air Force Institute of Technology where he will continue working full time following graduation with a Master of Science degree in Electrical Engineering.

Permanent Address: P.O. Box 79171
 Lakewood, Ohio 44107

REPORT DOCUMENTATION PAGE

Form Approved
OMB No. 0704-0188

Public reporting burden for this collection of information is estimated to average 1 hour per response, including the time for reviewing instructions, searching existing data sources, gathering and maintaining the data needed, and completing and reviewing the collection of information. Send comments regarding this burden estimate or any other aspect of this collection of information, including suggestions for reducing this burden, to Washington Headquarters Services, Directorate for Information Operations and Reports, 1215 Jefferson Davis Highway, Suite 1204, Arlington, VA 22202-4302, and to the Office of Management and Budget, Paperwork Reduction Project (0704-0188), Washington, DC 20503.

1. AGENCY USE ONLY (Leave blank)		2. REPORT DATE June 1992	3. REPORT TYPE AND DATES COVERED Master's Thesis	
4. TITLE AND SUBTITLE DEVELOPMENT OF AN ANALOG MIMO QUANTITATIVE FEEDBACK THEORY (QFT) CAD PACKAGE			5. FUNDING NUMBERS	
6. AUTHOR(S) Richard Robert Sating				
7. PERFORMING ORGANIZATION NAME(S) AND ADDRESS(ES) Air Force Institute of Technology WPAFB, OH 45433-6583			8. PERFORMING ORGANIZATION REPORT NUMBER AFIT/GE/ENG/92J-04	
9. SPONSORING / MONITORING AGENCY NAME(S) AND ADDRESS(ES) Capt Stuart N. Sheldon Control Systems Development Branch Wright Laboratory Wright-Patterson AFB, OH 45433			10. SPONSORING / MONITORING AGENCY REPORT NUMBER	
11. SUPPLEMENTARY NOTES				
12a. DISTRIBUTION / AVAILABILITY STATEMENT Approved for Public Release; Distribution Unlimited			12b. DISTRIBUTION CODE	
13. ABSTRACT (Maximum 200 words) This thesis describes the development of an analog MIMO Quantitative Feedback Theory (QFT) CAD package for the automation of the multivariable control design process. The CAD package is capable of carrying a design from problem setup through the design process to a frequency domain analysis of the compensated MIMO system. The package automates the selection of the weighting matrix, formation of the square effective plants, the polynomial matrix inverse required to form the equivalent plants, generation of stability, tracking, disturbance, gamma, and composite bounds, loop shaping, design of the prefilter elements, and the frequency domain analysis of the completed design. Disturbance allocation is automatically performed while generating tracking bounds. The package allows gain scheduling to be used in the weighting matrix. The improved method may be applied for the case of a 2x2 effective plant. The package is implemented using Mathematica for use on the Sun Workstations.				
14. SUBJECT TERMS QFT, Quantitative Feedback Theory, CAD, Computer Aided Design, Multivariable Control, MIMO Control System Design			15. NUMBER OF PAGES 245	
			16. PRICE CODE	
17. SECURITY CLASSIFICATION OF REPORT Unclassified	18. SECURITY CLASSIFICATION OF THIS PAGE Unclassified	19. SECURITY CLASSIFICATION OF ABSTRACT Unclassified	20. LIMITATION OF ABSTRACT UL	